frontiers | Research Topics

Pathological reactions of cytotoxic lymphoid cells as universal therapeutic targets in cancer and autoimmune disease

Edited by
Elizaveta Fasler-Kan, Vadim V. Sumbayev and Bernhard F. Gibbs

Published in
Frontiers in Medicine

ISSN 1664-8714
ISBN 978-2-8325-2373-5
DOI 10.3389/978-2-8325-2373-5

About Frontiers

Frontiers is more than just an open access publisher of scholarly articles: it is a pioneering approach to the world of academia, radically improving the way scholarly research is managed. The grand vision of Frontiers is a world where all people have an equal opportunity to seek, share and generate knowledge. Frontiers provides immediate and permanent online open access to all its publications, but this alone is not enough to realize our grand goals.

Frontiers journal series

The Frontiers journal series is a multi-tier and interdisciplinary set of open-access, online journals, promising a paradigm shift from the current review, selection and dissemination processes in academic publishing. All Frontiers journals are driven by researchers for researchers; therefore, they constitute a service to the scholarly community. At the same time, the *Frontiers journal series* operates on a revolutionary invention, the tiered publishing system, initially addressing specific communities of scholars, and gradually climbing up to broader public understanding, thus serving the interests of the lay society, too.

Dedication to quality

Each Frontiers article is a landmark of the highest quality, thanks to genuinely collaborative interactions between authors and review editors, who include some of the world's best academicians. Research must be certified by peers before entering a stream of knowledge that may eventually reach the public - and shape society; therefore, Frontiers only applies the most rigorous and unbiased reviews. Frontiers revolutionizes research publishing by freely delivering the most outstanding research, evaluated with no bias from both the academic and social point of view. By applying the most advanced information technologies, Frontiers is catapulting scholarly publishing into a new generation.

What are Frontiers Research Topics?

Frontiers Research Topics are very popular trademarks of the *Frontiers journals series*: they are collections of at least ten articles, all centered on a particular subject. With their unique mix of varied contributions from Original Research to Review Articles, Frontiers Research Topics unify the most influential researchers, the latest key findings and historical advances in a hot research area.

Find out more on how to host your own Frontiers Research Topic or contribute to one as an author by contacting the Frontiers editorial office: frontiersin.org/about/contact

Pathological reactions of cytotoxic lymphoid cells as universal therapeutic targets in cancer and autoimmune disease

Topic editors

Elizaveta Fasler-Kan — University Hospital of Bern, Switzerland
Vadim V. Sumbayev — University of Kent, United Kingdom
Bernhard F. Gibbs — University of Oldenburg, Germany

Citation

Fasler-Kan, E., Sumbayev, V. V., Gibbs, B. F., eds. (2023). *Pathological reactions of cytotoxic lymphoid cells as universal therapeutic targets in cancer and autoimmune disease*. Lausanne: Frontiers Media SA. doi: 10.3389/978-2-8325-2373-5

Table of contents

frontiers | Frontiers in Medicine

TYPE Editorial
PUBLISHED 25 April 2023
DOI 10.3389/fmed.2023.1186318

OPEN ACCESS

EDITED AND REVIEWED BY
Dmitri Pchejetski,
University of East Anglia, United Kingdom

*CORRESPONDENCE
Vadim V. Sumbayev
✉ V.Sumbayev@kent.ac.uk
Bernhard F. Gibbs
✉ bernhard.gibbs@uni-oldenburg.de
Elizaveta Fasler-Kan
✉ elizaveta.fasler@insel.ch

RECEIVED 14 March 2023
ACCEPTED 10 April 2023
PUBLISHED 25 April 2023

CITATION
Sumbayev VV, Gibbs BF and Fasler-Kan E (2023) Editorial: Pathological reactions of cytotoxic lymphoid cells as universal therapeutic targets in cancer and autoimmune disease. *Front. Med.* 10:1186318. doi: 10.3389/fmed.2023.1186318

Editorial: Pathological reactions of cytotoxic lymphoid cells as universal therapeutic targets in cancer and autoimmune disease

Vadim V. Sumbayev[1]*, Bernhard F. Gibbs[2]* and Elizaveta Fasler-Kan[3,4]*

[1]Medway School of Pharmacy, Universities of Kent and Greenwich, Chatham Maritime, United Kingdom, [2]Department of Human Medicine, University of Oldenburg, Oldenburg, Germany, [3]Department of Pediatric Surgery, Children's Hospital, Inselspital Bern, University of Bern, Bern, Switzerland, [4]Department of Biomedical Research, University of Bern, Bern, Switzerland

KEYWORDS

immune evasion, cancer, autoimmune disease, T cells, immune checkpoints

Editorial on the Research Topic
Pathological reactions of cytotoxic lymphoid cells as universal therapeutic targets in cancer and autoimmune disease

Malignant transformation of human cells is associated with the activation of immunosuppressive biochemical pathways. Cytotoxic lymphoid cells, mainly T lymphocytes and natural killer (NK) cells are capable of attacking and eliminating malignant cells. However, cancer cells operate effective immune evasion machinery, which includes immune checkpoint proteins and small molecular weight compounds as well as biochemical pathways responsible for their expression, production and secretion. These immune evasion networks create an immunosuppressive milieu and allow cancer cells to escape immune attack, thus leading to disease progression (1).

Immune evasion networks include programmed cell death protein (PD-1)/ programmed death ligand (PD-L1), Tim-3 (T cell immunoglobulin and mucin domain-containing protein 3)/galectin-9, V domain Ig-containing suppressor of T cell activation (VISTA), T-cell immunoreceptor with Ig and ITIM domain (TIGIT), for example, as well as signaling cascades involving transforming growth factor beta type 1 (TGF-β)-Smad-3 and interferon beta or gamma (IFN-β or IFN-γ) pathways (2–6). However, recent evidence demonstrated that certain small molecular weight compounds are also effectively involved in suppression of T cell function and thus evasion of anti-cancer immunity. Recently, concern has been expressed regarding the role of L-kynurenine (LKU) and its metabolites in suppression of cytotoxic lymphoid cell functions during cancer progression. LKU is an amino acid which is formed during L-tryptophan (L-Trp) catabolism in kynurenine pathway (7). A number of malignant tumors express indoleamine 2,3-dioxygenase 1 (IDO1) which supports LKU production by tumor cells (7).

These immune checkpoint proteins and pathways cooperate, thus potentiating their immune evasion effects. For example, galectin-9 induces granzyme B activation in cytotoxic T cells (5, 8) and cooperates with other immune checkpoint proteins, particularly VISTA or PD-L1, which block their intracellular anti-apoptotic machinery, resulting in programmed death of these T cells. Additionally, VISTA, Tim-3 and PD-L1

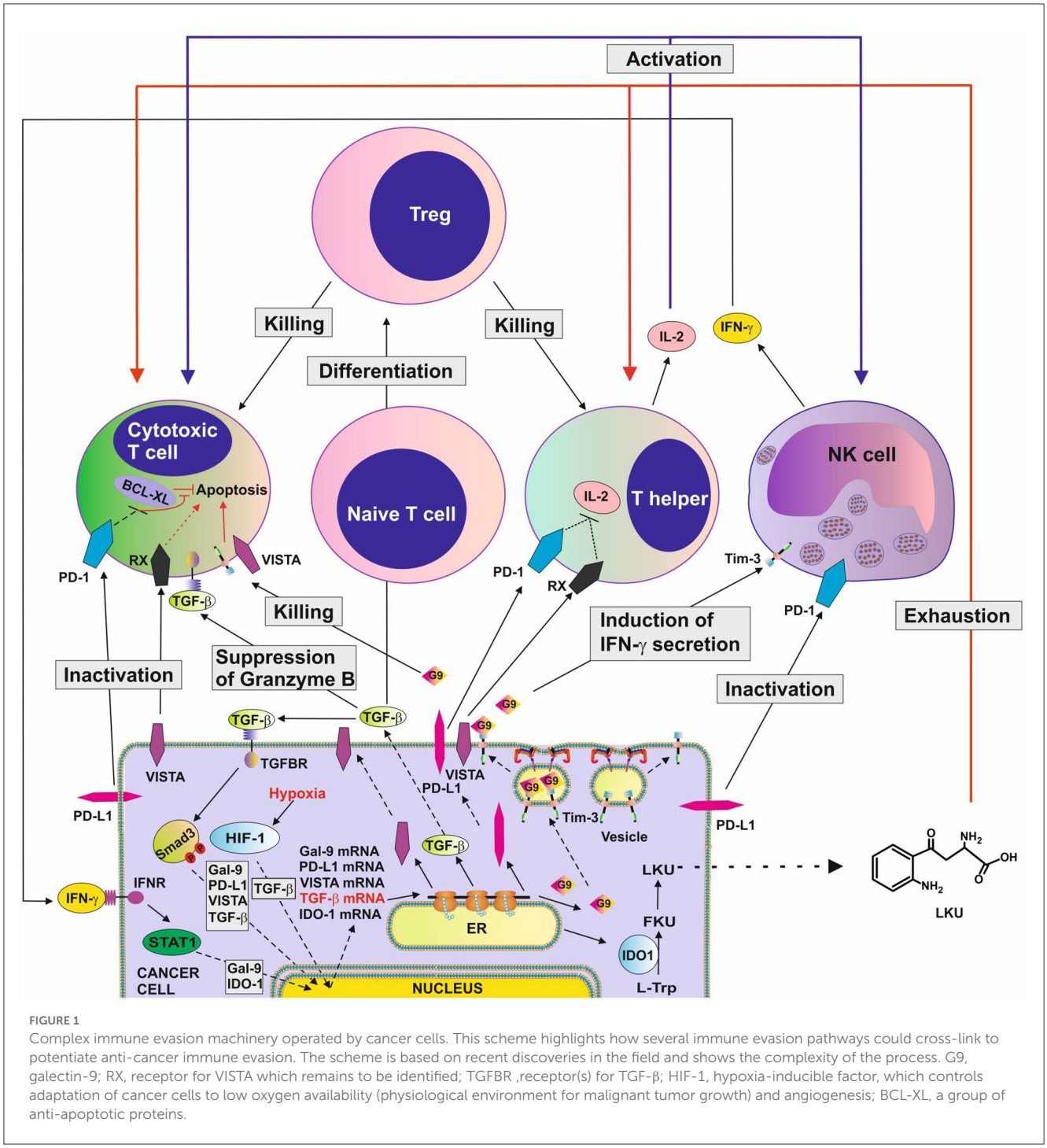

FIGURE 1
Complex immune evasion machinery operated by cancer cells. This scheme highlights how several immune evasion pathways could cross-link to potentiate anti-cancer immune evasion. The scheme is based on recent discoveries in the field and shows the complexity of the process. G9, galectin-9; RX, receptor for VISTA which remains to be identified; TGFBR ,receptor(s) for TGF-β; HIF-1, hypoxia-inducible factor, which controls adaptation of cancer cells to low oxygen availability (physiological environment for malignant tumor growth) and angiogenesis; BCL-XL, a group of anti-apoptotic proteins.

block the production of IL-2 by helper T cells thus preventing the activation of cytotoxic T cells (3, 8, 9). The TGF-β/Smad3 pathway can, on the one hand, upregulate expression of immune checkpoint proteins and, on the other hand, induce the differentiation of naïve T cells into Tregs which downregulate T cell-mediated attack of tumor cells. Examples of the various cross-links between immune checkpoint and immune evasion pathways are summarized in Figure 1.

Conversely to the detrimental role of immune evasion pathways in cancer, overactivation of immune responses leads to multiple autoimmune disorders such as rheumatoid arthritis, psoriasis, multiple sclerosis, affecting a large number of individuals worldwide. Autoreactive T cells are considered as key regulatory and effector cells in these autoimmune diseases (10). Therefore, pharmacological correction of immune checkpoint pathways is desirable for these diseases, and may result in fundamentally novel and highly efficient therapeutic strategies.

The goal of this Research Topic is to provide and summarize recent advances in our understanding of the molecular and cellular mechanisms of anti-tumor immunity and autoimmune disease

and, importantly, biochemical regulation and pharmacological correction of these immune networks.

The work by Brauneck et al. highlights co-expression of TIGIT with PD-1, TIM-3 or CD39 in Vδ1 T cells in acute myeloid leukemia (AML) and myeloma. γδ T cells are a unique subpopulation of T cells which recognize cancer cells through T cell receptors but also *via* NK cell receptors and are not dependent on major histocompatibility complex-mediated antigen presentation.

The work by Schlichtner et al. reports the discovery that VISTA expression is regulated by the TGF-β-Smad3 pathway, and highlights that the differential nature of this effect is most likely associated with nuclear compartmentalisation.

The article by Geanes et al. describes the development of combinational antibody therapies for diffuse large B cell lymphomas. This study highlighted that bispecific antibodies, which target multiple B cell receptors expressed by lymphoma cells, potentially deliver improved defense against relapse of the disease and its resistance to immunotherapy.

The paper by Mandour et al. showed for the first time that inhibition of IL-12 heterodimers impairs the protective effect of Toll-like receptor (TLR) 9 stimulation in preventing early mouse plasmacytoma cell growth, highlighting the crucial anti-cancer role for IL-12-mediated innate immunity caused by infections.

The mini review written by Turner et al. discusses the role of CXCR5+CD8 cytotoxic T cells in cancer and autoimmunity, including potential repercussions during immune checkpoint blockade therapy. This review analyses CXCR5+CD8 T cells as potential immunotherapy targets or possible drivers of immune-mediated adverse events.

The mini review by Gurrea-Rubio and Fox highlights the dual role of cluster of differentiation (CD) 6, a type I transmembrane glycoprotein belonging to the highly conserved scavenger receptor cysteine-rich superfamily of proteins, as a target for anti-cancer therapy and treatment of autoimmune disease.

The article by Potashnikova et al. describes the study of cytotoxic T cells from patients with atherosclerosis which exhibit increased adhesiveness and distinct integrin expression patterns.

The paper by Thurau et al. describes a clinical trial where a new small molecule dihydroorotate dehydrogenase (DHODH)-inhibitor [KIO-100 (PP-001)] was used to target activated T cells with the purpose of intraocular treatment of autoimmune uveitis. DHODH is an enzyme catalyzing the fourth enzymatic step, which involves the ubiquinone-mediated oxidation of dihydroorotate to orotate in *de novo* pyrimidine biosynthesis.

The study by Sato et al. discovers that salivary gland conventional NK cells may enhance autoreactive responses in target organs by upregulating IFN-γ production, whereas salivary gland-resident NK cells protect target cells against T cell cytotoxicity.

And the article by Chen et al. describes the clinical factors associated with blood transfusion in lymphedema liposuction surgery, comparing autologous and allogeneic transfusion patterns in lymphedema patients.

In conclusion, this Research Topic includes 5 original research papers, 2 brief research reports, 1 phase I clinical trial study and 2 mini-reviews. The articles highlight the novel aspects of anti-cancer immune evasion machinery and pathological reactions of T cells in cancer and autoimmune disease, supporting the concept of complex biochemical networks regulating cytotoxic immune responses.

Author contributions

VS, BG, and EF-K wrote the manuscript and created the figure. All authors contributed to the article and approved the submitted version.

Conflict of interest

The authors declare that the research was conducted in the absence of any commercial or financial relationships that could be construed as a potential conflict of interest.

Publisher's note

References

1. Abboud K, Umoru G, Esmail A, Abudayyeh A, Murakami N, Al-Shamsi HO, et al. Immune checkpoint inhibitors for solid tumors in the adjuvant setting: current progress, future directions, and role in transplant oncology. *Cancers*. (2023) 15:1433. doi: 10.3390/cancers15051433

2. Brauneck F, Fischer B, Witt M, Muschhammer J, Oelrich J, da Costa Avelar PH, et al. TIGIT blockade repolarizes AML-associated TIGIT+ M2 macrophages to an M1 phenotype and increases CD47-mediated phagocytosis. *J Immunother Cancer*. (2022) 10:e004794. doi: 10.1136/jitc-2022-004794

3. Selnø ATH, Schlichtner S, Yasinska IM, Sakhnevych SS, Fiedler W, Wellbrock J, et al. Transforming growth factor beta type 1 (TGF-β) and hypoxia-inducible factor 1 (HIF-1) transcription complex as master regulators of the immunosuppressive protein galectin-9 expression in human cancer and embryonic cells. *Aging (Albany NY)*. (2020) 12:23478–96. doi: 10.18632/aging.202343

4. Wu Q, Jiang L, Li SC, He QJ, Yang B, Cao J Small molecule inhibitors targeting the PD-1/PD-L1 signaling pathway. Acta pharmacologica Sinica. (2021). 42:1–9. doi: 10.1038/s41401-020-0366-x

5. Yasinska IM, Meyer NH, Schlichtner S, Hussain R, Siligardi G, Casely-Hayford M. Ligand-receptor interactions of galectin-9 and VISTA suppress human T lymphocyte cytotoxic activity. *Front Immunol*. (2020)11:580557. doi: 10.3389/fimmu.2020.580557

6. Yang R, Sun L, Li CF, Wang YH, Yao J, Li H, et al. Galectin-9 interacts with PD-1 and TIM-3 to regulate T cell death and is a target for cancer immunotherapy. *Nat Commun*. (2021) 12:832. doi: 10.1038/s41467-021-21099-2

7. Mezrich JD, Fechner JH, Zhang X, Johnson BP, Burlingham WJ, Bradfield CA. An interaction between kynurenine and the aryl hydrocarbon receptor can generate regulatory T cells. *J Immunol*. (2010) 185:3190–8. doi: 10.4049/jimmunol.0903670

8. Schlichtner S, Yasinska IM, Lall GS, Berger SM, Ruggiero S, Cholewa D, et al. T lymphocytes induce human cancer cells derived from solid malignant tumors to secrete galectin-9 which facilitates immunosuppression in cooperation with other immune checkpoint proteins. *J Immunother Cancer*. (2023) 11:e005714. doi: 10.1136/jitc-2022-005714

9. Silva IG, Yasinska IM, Sakhnevych SS, Fiedler W, Wellbrock J, Bardelli M, et al. The Tim-3-galectin-9 Secretory Pathway is involved in the immune escape of human acute myeloid leukemia cells. *EBioMedicine*. (2017) 22:44–57. doi: 10.1016/j.ebiom.2017.07.018

10. Jäger A, Kuchroo VK. Effector and regulatory T-cell subsets in autoimmunity and tissue inflammation. *Scandinavian J Immunol*. (2010) 72:173–84. doi: 10.1111/j.1365-3083.2010.02432.x

frontiers in Medicine

ORIGINAL RESEARCH
published: 08 November 2021
doi: 10.3389/fmed.2021.763773

Bone Marrow-Resident Vδ1 T Cells Co-express TIGIT With PD-1, TIM-3 or CD39 in AML and Myeloma

Franziska Brauneck[1†], Pauline Weimer[1†], Julian Schulze zur Wiesch[2], Katja Weisel[1], Lisa Leypoldt[1], Gabi Vohwinkel[1], Britta Fritzsche[3], Carsten Bokemeyer[1], Jasmin Wellbrock[1†] and Walter Fiedler[1†]*

[1] Department of Oncology, Hematology and Bone Marrow Transplantation With Section Pneumology, Hubertus Wald University Cancer Center, University Medical Center Hamburg-Eppendorf, Hamburg, Germany, [2] Infectious Diseases Unit, I. Department of Medicine, University Medical Center Hamburg-Eppendorf, Hamburg, Germany, [3] University Cancer Center Hamburg (UCCH)-Biobank, Department of Oncology, Hematology and Bone Marrow Transplantation With Section Pneumology, Hubertus Wald University Cancer Center, University Medical Center Hamburg-Eppendorf, Hamburg, Germany

OPEN ACCESS

Edited by:
Bernhard F. Gibbs,
University of Oldenburg, Germany

Reviewed by:
Daria M. Potashnikova,
Lomonosov Moscow State University, Russia
Michael Danilenko,
Ben-Gurion University of the Negev, Israel

***Correspondence:**
Walter Fiedler
fiedler@uke.de

[†]These authors have contributed equally to this work

Specialty section:
This article was submitted to Pathology, a section of the journal Frontiers in Medicine

Received: 24 August 2021
Accepted: 04 October 2021
Published: 08 November 2021

Citation:
Brauneck F, Weimer P, Schulze zur Wiesch J, Weisel K, Leypoldt L, Vohwinkel G, Fritzsche B, Bokemeyer C, Wellbrock J and Fiedler W (2021) Bone Marrow-Resident Vδ1 T Cells Co-express TIGIT With PD-1, TIM-3 or CD39 in AML and Myeloma. Front. Med. 8:763773. doi: 10.3389/fmed.2021.763773

Background: γδ T cells represent a unique T cell subpopulation due to their ability to recognize cancer cells in a T cell receptor- (TCR) dependent manner, but also in a non-major histocompatibility complex- (MHC) restricted way via natural killer receptors (NKRs). Endowed with these features, they represent attractive effectors for immuno-therapeutic strategies with a better safety profile and a more favorable anti-tumor efficacy in comparison to conventional αβ T cells. Also, remarkable progress has been achieved re-activating exhausted T lymphocytes with inhibitors of co-regulatory receptors e.g., programmed cell death protein 1 (PD-1), T cell immunoreceptor with Ig and ITIM domains (TIGIT) and of the adenosine pathway (CD39, CD73). Regarding γδ T cells, little evidence is available. This study aimed to immunophenotypically characterize γδ T cells from patients with diagnosed acute myeloid leukemia (AML) in comparison to patients with multiple myeloma (MM) and healthy donors (HD).

Methods: The frequency, differentiation, activation, and exhaustion status of bone marrow- (BM) derived γδ T cells from patients with AML ($n = 10$) and MM ($n = 11$) were assessed in comparison to corresponding $CD4^+$ and $CD8^+$ T cells and peripheral blood- (PB) derived γδ T cells from HDs ($n = 16$) using multiparameter flow cytometry.

Results: BM-infiltrating Vδ1 T cells showed an increased terminally differentiated cell population (TEMRAs) in AML and MM in comparison to HDs with an aberrant subpopulation of $CD27^-CD45RA^{++}$ cells. TIGIT, PD-1, TIM-3, and CD39 were more frequently expressed by γδ T cells in comparison to the corresponding $CD4^+$ T cell population, with expression levels that were similar to that on $CD8^+$ effector cells in both hematologic malignancies. In comparison to Vδ2 T cells, the increased frequency of PD-1^+-, $TIGIT^+$-, TIM-3^+, and $CD39^+$ cells was specifically observed on Vδ1 T cells and related to the TEMRA Vδ1 population with a significant co-expression of PD-1 and TIM-3 together with TIGIT.

Conclusion: Our results revealed that BM-resident γδ T cells in AML and MM express TIGIT, PD-1, TIM-3 and CD39. As effector population for autologous and allogeneic strategies, inhibition of co-inhibitory receptors on especially Vδ1 γδ T cells may lead to re-invigoration that could further increase their cytotoxic potential.

Keywords: (Vδ1) γδ T cells, TIGIT, PD-1, CD39, AML, myeloma

INTRODUCTION

Although γδ T cells represent a relatively small subset within all T lymphocytes (1–5%) (1, 2), they have a unique property to recognize cancer cells in a T cell receptor- (TCR) dependent manner but also in a non- major histocompatibility complex- (MHC) restricted way via their expression of natural killer cell receptors (NKRs) (3). In immuno-oncology, γδ T cells represent a novel attractive effector population for immuno-therapeutic strategies such as chimeric antigen receptor T cells (CAR-T cells) or bispecific T cell engagers (BiTEs).

In humans, γδ T cells can be differentiated into two major subsets by their expression of the Vδ chain. Vδ2 cells constitute the major circulating γδ T cell population in the peripheral blood (PB) whereas the Vδ1 subpopulation is enriched in the peripheral tissue (4, 5). Both γδ subpopulations exhibit cytotoxic capacities mediated by TCR- and natural killer group 2D (NKG2D) receptor signaling via production of the effector cytokines interferon (IFN)-γ, tumor necrosis factor (TNF)-α and soluble mediators such as perforin or granzymes (5–7). Moreover, γδ T cells can induce dendritic cell (DC) maturation via secretion of TNF-α (8, 9). They also have an antigen-presenting capacity by MHC-II loading and expression (10). Recent data also demonstrate a phagocytic potential of γδ T cells through expression of the scavenger receptor CD36 which is dependent on the transcription factor CCAAT-enhancer-binding protein α (C/EBPα) (11).

In oncology, both the Vδ1 and Vδ2 T cells have been described to exert pleiotropic effector functions: as mentioned above the tumor-infiltrating IFNγ-producing γδ T cell fraction has shown cytotoxic effects in solid and hematological malignancies (7, 12, 13), whereas interleukin (IL)-17- and galectin 1-secreting γδ T cells promote tumor growth and the recruitment of immunosuppressive myeloid cells (14, 15). By analyzing molecular profiles of expression signatures of 18.000 tumors from 39 different malignancies, including AML and MM with overall survival data, Gentles et al. identified tumor-infiltrating γδ T cells as the leukocyte subset with the most significant favorable cancer-wide prognostic relevance (16).

First clinical observations of patients with refractory/relapsed AML transplanted with haploidentical γδ T cells showed that γδ T cells can induce clinical anti-tumor effects (17, 18). Furthermore, preclinical data provide support for this contention: AML cells were efficiently killed by Vδ2 T cells *in vitro* (3, 6, 19). In an AML xenograft model, Vδ2 T cells traffic to the BM and have been shown to slow the progression of the disease (6). Also, in MM it has been recently published that impairment of Vδ2 T cell functions (including decreased proliferation and cytotoxicity) was already detectable in monoclonal gammopathy of undetermined significance (MGUS) (20).

Compared to Vδ2 T cells, Vδ1 T cells account for a small proportion of γδ T cells (1). Although most of the studies investigating the antitumoral effects of γδ T cells focus on Vδ2 T cells, it is becoming increasingly evident that Vδ1 T cells play a critical role in the anti-tumor functionality (21, 22). Enhanced reconstitution of γδ T cells following allogeneic hematopoietic stem cell transplantation (aHSCT) was associated with improved survival in patients with AML (23). Cordova et al. demonstrated that Vδ1 tumor-infiltrating lymphocyte- (TIL-) derived cells outperformed Vδ2 TILs in *in vitro* tumor cytotoxicity assays in malignant melanoma (24). In AML, increased levels of cytomegalovirus- (CMV) specific Vδ1 cells were associated with a reduced relapse probability. *In vitro*, these Vδ1 cells demonstrated increased cytotoxicity against AML cells, which could be further enhanced following CMV reactivation (19, 25). Additionally, Knight et al. showed a significant cytotoxicity of Vδ1 T cells for MM by lysis against patients' $CD38^{+}CD138^{+}$ BM-derived plasma cells *in vitro* (26).

First phenotypic analyses of BM-derived Vδ2 T cells from AML patients showed an increased subpopulation with a memory phenotype that was associated with a reduced capacity for expansion and cytotoxicity (6).

This study is focused on programmed cell death protein-1 (PD-1), the novel receptor T cell Ig and ITIM domain (TIGIT), the T cell immunoglobulin and mucin domain-containing protein 3 (TIM-3) and the ectonucleotidases ectonucleoside triphosphate diphosphohydrolase-1 (CD39) and ecto-5'-nucleotidase (CD73). All of these checkpoints are involved in αβ T lymphocyte dysfunction in cancer (27–29). TIGIT, PD-1 and TIM-3 are co-inhibitory receptors highly expressed by exhausted T cells in chronic infections and cancer (27, 30, 31).

Abbreviations: ADO, adenosine; aHSCT, allogeneic hematopoietic stem cell transplantation; AML, Acute myeloid leukemia; ATP, adenosine triphosphate; BiTEs, bispecific T cell engagers; BM, bone marrow; CAR-T cells, chimeric antigen receptor T cells; CD39, ectonucleoside triphosphate diphosphohydrolase-1; CD73, ecto-5′-nucleotidase; CM, central memory cells; CMV, cytomegalovirus; EM, effector memory cells; DC, dendritic cells; FMO, Fluorescence minus one; HD, healthy donor; IFN-γ, Interferon-γ; IL-2, interleukin-2; IL-10, interleukin 10; IL-12, interleukin 12; MM, multiple myeloma; MCF, multiparametric flow cytometry; MFI, mean fluorescence intensity; MGUS, monoclonal gammopathy of undetermined significance; NA, naïve cells; NKG2D, natural killer group 2D; non-APL AML, non-acute promyelocytic leukemia; PB, peripheral blood; PVR, poliovirus receptor; PVRL2, poliovirus receptor-related 2; TEMRA, terminal differentiated effector memory cells; TIGIT, T cell immunoreceptor with Ig and ITIM domains; TIL, tumor-infiltrating lymphocytes; TIM-3, hepatitis A virus cellular receptor 2; TME, tumor microenvironment; TNF, tumor necrosis factor; tSNE, t-distributed stochastic neighbor embedding.

Inhibition of these receptors have shown increased proliferation and cytotoxic efficiency *in vitro* (27, 30–32). Recently, inhibition of the adenosine-generating enzymes CD39 and CD73 showed anti-tumor immunity through multiple mechanisms, including enhancement of T cell and natural killer- (NK) cell function (33, 34). It is well-acknowledged that multiple co-expression of inhibitory receptors and suppression of inflammatory cues by CD39 enzymatic overactivity are highly associated with the severity of T cell dysfunction (35, 36), thus representing an important feature of T cell exhaustion (37). Regarding the (co)-expression of these checkpoints on γδ T cells, little is known. Jin et al. showed for the first time that TIGIT is also expressed by regulatory Forkhead-Box-Protein P3 $(FOXP3)^+$ γδ T cells in AML (38). Moreover, it has been presented that tumor-infiltrating γδ T cells express the ectonucleotidases CD39 and CD73 and may be dysfunctional via the activation of adenosine-mediated pathways (39, 40).

Since circulating γδ T cells in the peripheral blood have been more elucidated, the present study provides an extensive immunophenotypic characterization of γδ T cells derived from the bone marrow of patients with untreated newly diagnosed acute myeloid leukemia or multiple myeloma. We focus on the comparison of the Vδ1- and Vδ2-cell phenotypes, including differentiation and expression of immune checkpoints and metabolic molecules that may dampen antitumor immunity in patients with acute myeloid leukemia in comparison to patients with myeloma and healthy volunteers.

MATERIALS AND METHODS

Patient Cohorts

Bone marrow-derived aspirates were collected from patients with newly diagnosed non-M3 AML ($n = 10$) and patients with multiple myeloma ($n = 11$) before the start of intensive chemotherapy treatment, and peripheral blood specimens from age-matched healthy donors (HD, $n = 16$) after written informed consent in accordance with the Declaration of Helsinki and approval by the local ethics board of the Ärztekammer Hamburg (PV3469 and PV5119). The median age of the AML patient cohort was 70 years (range 43–86), the median age of the MM patient cohort 61.5 years (range 55–86), and the median age of the healthy donors was 60 years (range 27–71) (**Supplementary Table 1**).

Multiparameter Flow Cytometry

For multiparametric flow cytometry analysis (MFC), cryopreserved BM mononuclear cells from patients with $CD117^+CD33^+$ AML, from patients with $CD38^+CD138^+$ MM and peripheral blood (PB) mononuclear cells from HDs were thawed and counted. After washing with PBS and FCR blocking (FcR blocking reagent, human, Miltenyi Biotec), mononuclear cells were stained with the LIVE/DEAD™ Fixable Near-IR dye (Thermo Fisher) according to the manufacturer's protocol for exclusion of dead cells. Afterwards, cells were washed and incubated for surface staining with appropriate fluorochrome-conjugated antibodies, including anti-CD3 (OKT3), anti-CD4 (RPA-T4), anti-CD8 (RPA-T8), anti-CD33 (P67.6), anti-CD117 (104D2), anti-CD38 (HIT2), anti-CD138 (MI15), anti-γδ TCR (B1), anti-Vδ1 TCR (REA173), anti-Vδ2 TCR (REA771), anti-CD45RA (HI100), anti-CD27 (O323), anti-CD19 (HIB19), anti-CD56 (HCD56), anti-PD-1 (EH12.2H7), anti-TIGIT (A15153G), anti-TIM-3 (F38-2E2), anti-CD39 (A1), anti-CD73 (AD2), and anti-HLA-DR (L243) for 20 min at room temperature in the dark. Subsequently, samples were fixed with 0.5% paraformaldehyde (Sigma Aldrich) and incubated for 15 min at 4°C in the dark. Antibodies were obtained from Biolegend, BD Biosciences or Miltenyi Biotec. Compensation controls were measured using single-stained Comp Beads (Anti-Mouse Ig,κ/Negative Control Compensation Particles Set, BD Biosciences). For live/dead compensation, Comp Beads stained with anti-CD19 (APC Cy-7, BioLegend) were applied. All samples were run on a BD FACSymphony A3 with FACS Diva version 8 (BD Biosciences).

T-Distributed Stochastic Neighbor Embedding Analyses

Individual donor FCS files were imported into FlowJo version 10.5.2. A subset of 3,000 cells were selected for each donor at random and merged into a single expression matrix prior to tSNE analysis. The following channels were removed from the expression matrix to only include protein markers in tSNE analysis: viability, CD19, CD56, AML lineage markers (CD33, CD117), MM lineage markers (CD38, CD138), offset, residual, and time. A total of 12,000 cells and 14 markers were used to create a tSNE map of the PB- and BM- derived γδ T cells from HDs and patients with AML and MM. A perplexity parameter of 30 and iteration number of 550 was used for applying the dimensionality reduction algorithm. The output was in the form of a matrix with two columns corresponding to tSNE dimension 1 and dimension 2. tSNE maps were generated by plotting each event by its tSNE dimensions in a dot-plot. Intensities for markers of interest were overlaid on the dot-plot to show the expression of those markers on different cell islands.

Statistical Analysis

All flow cytometric data were analyzed using FlowJo version 10.5.2. software (Treestar). Statistical analysis was carried out using Prism 7.0 software (GraphPad Software). Groups were tested for normal distribution with the Kolmogorov-Smirnov test. Non-normally distributed data were analyzed by the Mann-Whitney test for two unpaired groups, the Wilcoxon test for two paired groups, respectively. Pearson's correlation and Spearman's rank correlation coefficient were applied for bivariate correlation analysis. Frequencies in the text are described as medians unless stated otherwise (as indicated in the figure legend). *P*-values below 0.05 were considered significant, where *, **, and *** indicate *p*-values between 0.01–0.05, 0.001–0.01 and 0.0001–0.001, respectively.

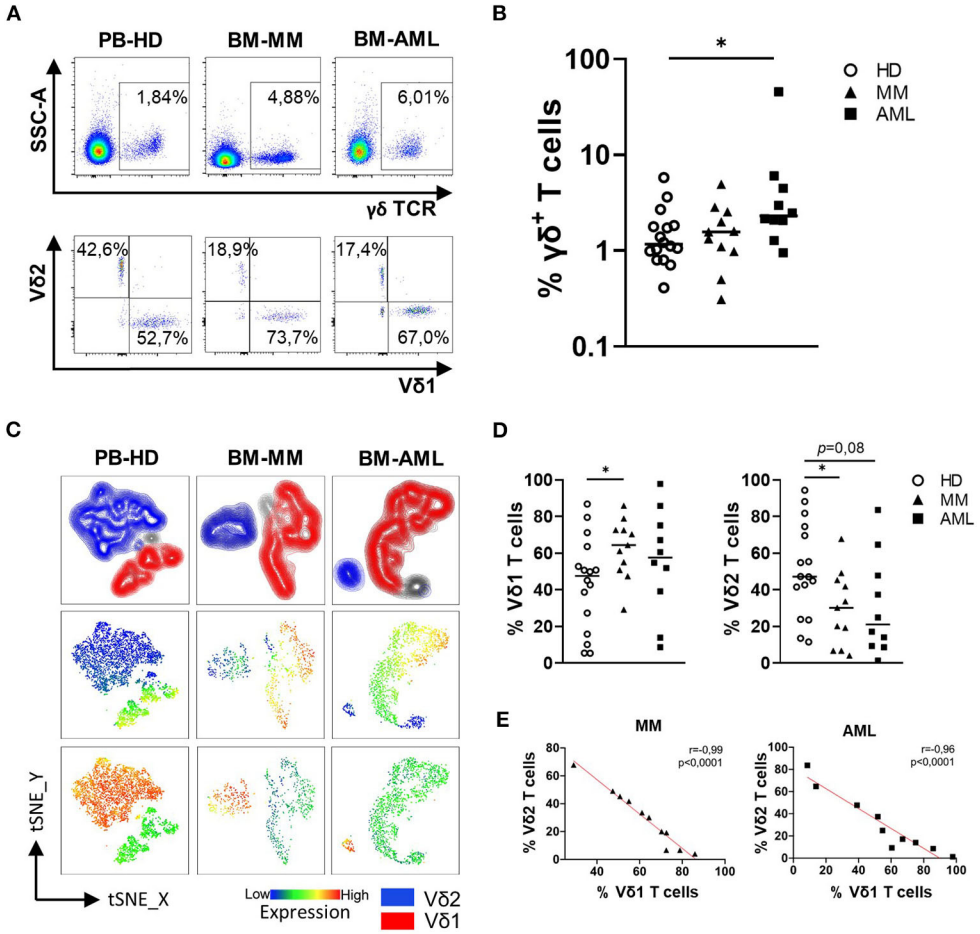

FIGURE 1 | The increased frequency of Vδ1 γδ T cells is associated with reduced infiltration of Vδ2 γδ T cells in AML and MM. Flow cytometric analysis of the co-expression of the γδ TCR and the Vδ1 and Vδ2 receptor on $CD3^+$ T cells was performed for bone marrow (BM) samples from patients with AML (AML, black rectangles, $n = 10$), MM patients (MM, black triangles, $n = 11$), and peripheral blood (PB)-derived mononuclear cells from healthy donors (HD, white circles, $n = 16$). **(A)** Representative flow cytometry data show γδ T cells, Vδ1, and Vδ2 γδ T cells. **(B)** Summary data illustrate the frequency of γδ T cells in HD, AML, and MM. *P*-values were obtained by the Mann-Whitney test. $^*P < 0.05$, $^{**}P < 0.01$, $^{***}P < 0.001$. **(C)** t-distributed stochastic neighbor embedding (tSNE) analysis delineate the distribution of Vδ1 and Vδ2 γδ T cells within the total γδ T cells in BM aspirates from four HDs (left graphs), four patients with MM (middle graphs), and four patients with AML (right graphs). **(D)** Summary data show the frequency of Vδ1 and Vδ2 T cell subpopulations. *P*-values were obtained by the Mann-Whitney test. $^*P < 0.05$, $^{**}P < 0.01$, $^{***}P < 0.001$. **(E)** Correlative analysis of the expression of the Vδ1 and Vδ2 receptors was performed for BM-derived aspirates of the MM and AML patients. Pearson's test was used to test for correlations.

RESULTS

BM-Derived Vδ1 T Cells of AML and MM Patients Show a Shift Toward Effector Memory- and Terminally Differentiated Memory Cells

γδ T cells were analyzed in the BM from patients with AML ($n = 10$) and MM ($n = 11$) in comparison to the PB from age-matched HDs ($n = 16$). For gating strategy see **Supplementary Figure 1**. The study included aspirates of patients with typical phenotypes namely $CD33^+CD117^+$ for AML and $CD38^+CD138^+$ for MM aspirates. This selection of patients enabled us to differentiate tumor cells from further immune cell populations in the BM. Our studies revealed a significantly increased frequency of γδ T cells in AML in comparison to HD. In contrast, this was not observed for MM (AML vs. HD $p = 0.014$; MM vs. HD $p = 0.707$, MM vs. AML $p = 0.085$; **Figures 1A,B**), implying differences in the immune response between both entities. Additional characterization of the γδ T cells was performed to investigate the immunophenotype of these cells in more detail. As illustrated in the t-distributed stochastic neighbor embedding (tSNE) analysis (**Figure 1C**), the distribution of Vδ1 and Vδ2 γδ T cells differed between HD, AML and MM: Vδ2 T cells were more prevalent in the PB in HDs compared to the BM compartment in AML and MM (**Figure 1D**). The fraction of BM-infiltrating Vδ1 T cells was significantly increased in MM patients relative to HDs ($p = 0.035$; **Figure 1D**), but not in patients with AML ($p = 0.220$; **Figure 1D**). Due to a shift of γδ subpopulations in the BM in

AML and MM patients compared to HDs, decreased levels of Vδ2 T cells were correlated with increased frequencies of Vδ1 T cells in BM of both malignancies (AML $r = -0.96$, $p < 0.0001$ and MM $r = -0.98$, $p < 0.001$; **Figure 1E**), indicating homing of Vδ1 T cells into the site of tumor development. To validate that these observations are not site-associated but malignancy-associated, we compared mononuclear cells derived from paired PB and BM aspirates of 9 AML patients. Our analyses revealed no differences regarding the total fraction of γδ T cells and the distribution of Vδ1 and Vδ2 γδ T cells between paired PB and BM (**Supplementary Figure 2A**).

Next, γδ T cells were subdivided into the following subpopulations regarding their differentiation status based on the expression of CD27 and CD45RA: Naïve (NA = $CD27^+CD45RA^+$), Central Memory (CM = $CD27^+CD45RA^-$), Effector Memory (EM = $CD27^-CD45RA^-$), Terminally Differentiated Memory Cells (TEMRA = $CD27^-CD45RA^+$), and a subset of TEMRA cells characterized

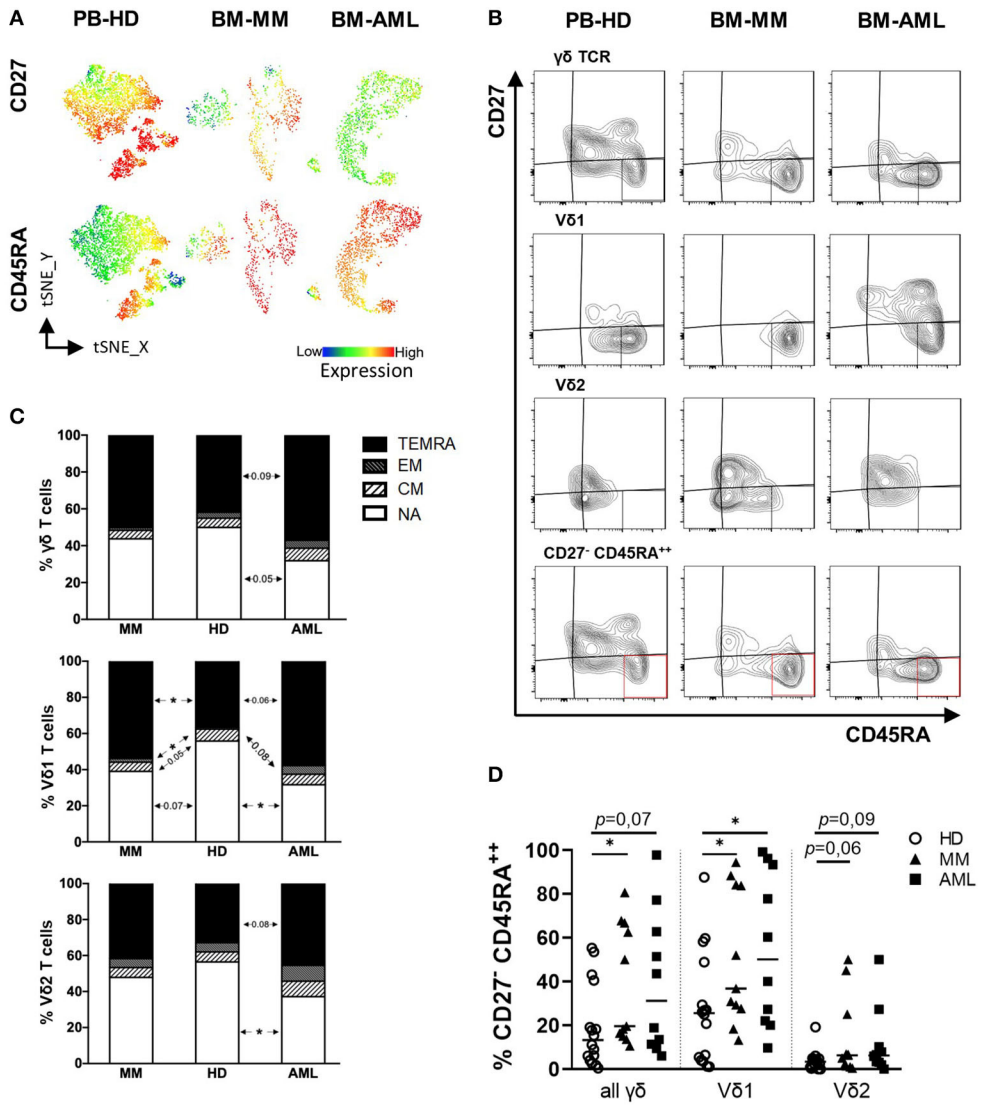

FIGURE 2 | Vδ1 γδ T cells from patients with AML and MM show a shift toward increased EM and TEMRA differentiation. γδ T cell differentiation was analyzed by expression of CD45RA and CD27 for healthy donors (HD, white circles, $n = 16$), patients with multiple myeloma (MM, black triangles, $n = 11$) and newly diagnosed AML patients (AML, black rectangles, $n = 10$). $CD27^+CD45RA^+$: naïve (NA); $CD27^+CD45RA^-$: central memory (CM); $CD27^-CD45RA^+$: effector memory (EM); $CD27^-CD45RA^+$: terminally differentiated (TEMRA). **(A)** T-distributed stochastic neighbor embedding (tSNE) analysis illustrate the differentiation status of Vδ1 and Vδ2 γδ T cells within the total γδ T cells in BM aspirates from four HDs (left graphs), four patients with MM (middle graphs), and four patients with AML (right graphs). **(B)** Representative flow cytometry data show the differentiation of γδ T cells. **(C)** Summary data are demonstrating the distribution of the differentiation status of γδ T cells. The upmost graph shows the subsets of all γδ T cells, followed by Vδ1 and Vδ2 cells only. **(D)** Displays the frequency of $CD27^-$ $CD45RA^{++}$ cells in all γδ T cells and Vδ1 and Vδ2 only. *P*-Values were obtained by the Mann-Whitney test. $^*P < 0.05$, $^{**}P < 0.01$, $^{***}P < 0.001$.

by $CD27^{-}CD45RA^{++}$ expression (for gating strategy see **Supplementary Figure 1**).

As in the previous analyses Vδ1 cells have been identified as the predominant γδ population in the BM of AML and MM patients, further tSNE analyses showed a prevailing expression of CD45RA in AML and MM mainly in the Vδ1 T cell population (**Figure 2A**). Further summary analyses revealed an increased frequency of Vδ1 T cells within the EM- and TEMRA

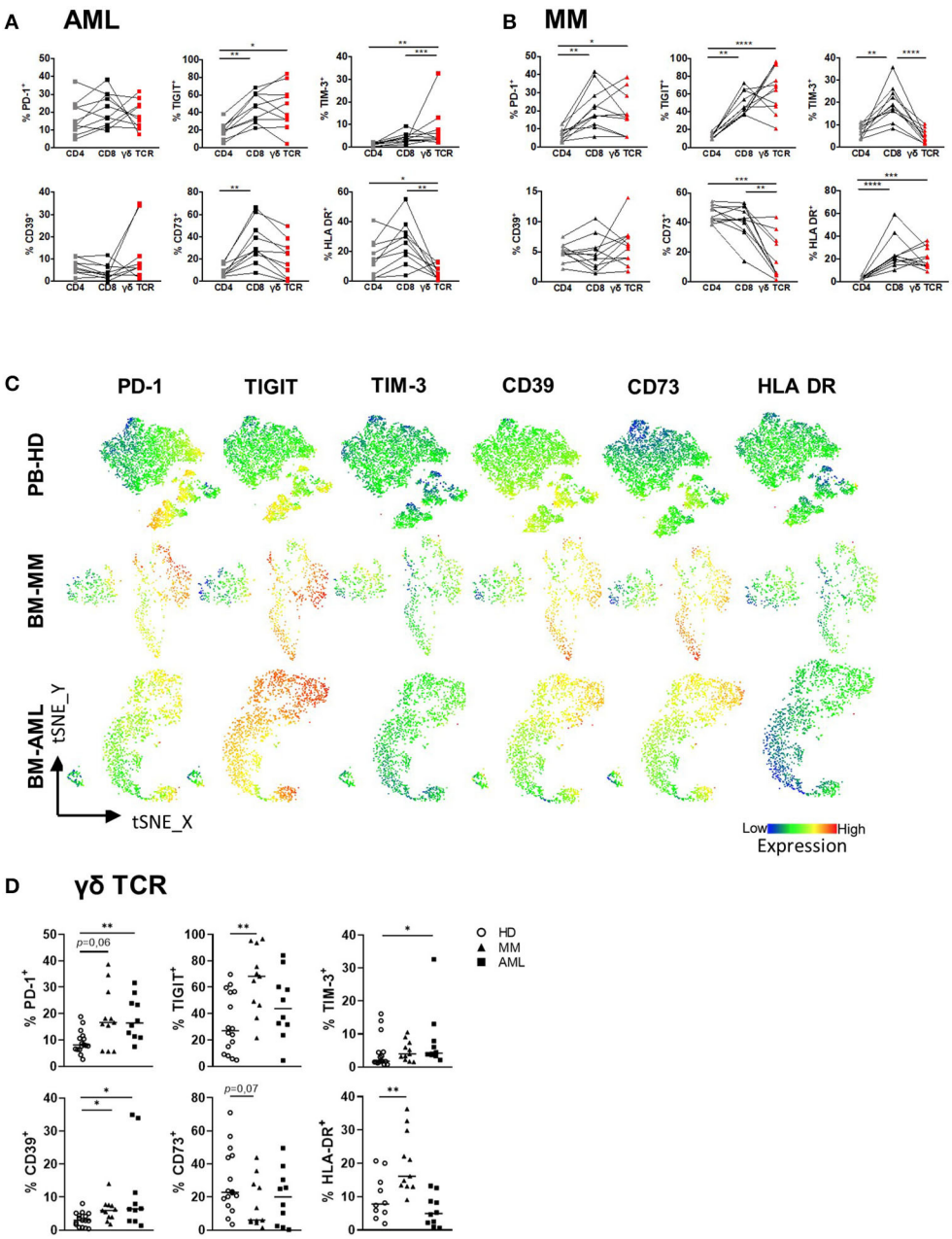

FIGURE 3 | PD-1, TIGIT, TIM-3, and CD39 are expressed by γδ T cells in AML and MM. The surface expression of PD-1, TIGIT, TIM-3, CD39, CD73, and HLA-DR was investigated on $CD4^{+}$, $CD8^{+}$, and γδ T cells by using multicolor flow analysis for healthy donors (HD, $n = 16$), patients with multiple myeloma (MM, $n = 11$), and newly diagnosed AML patients (AML, $n = 10$). **(A,B)** Summary data illustrating the frequency of PD-1, TIGIT, TIM-3, CD39, CD73, and HLA-DR on $CD4^{+}$ cells (gray squares/triangles), $CD8^{+}$ T cells (black squares/triangles), and γδ T cells (red squares/triangles). *P*-values were obtained by the ANOVA and Friedmann test. $^{*}P < 0.05$, $^{**}P < 0.01$, $^{***}P < 0.001$, $^{****}P < 0.0001$. **(C)** T-distributed stochastic neighbor embedding (tSNE) analysis demonstrate the distribution of PD-1, TIGIT, TIM-3, CD39, CD73, and HLA-DR on Vδ1 and Vδ2 γδ T cells within the total γδ T cells in BM aspirates from four HDs (upper graphs), four patients with MM (middle graphs), and four patients with AML (lower graphs). **(D)** Summary data show the expression of PD-1, TIGIT, TIM-3, HLA-DR, CD39, and CD73 on γδ T cells in HD (HD, white circle) vs. MM (black triangles) vs. AML (black rectangles). *P*-values were obtained by the Mann-Whitney test. $^{*}P < 0.05$, $^{**}P < 0.01$, $^{***}P < 0.001$.

compartment in AML and MM in comparison to HDs (HD vs. AML $p = 0.084$ and $p = 0.061$; HD vs. MM $p = 0.026$ and $p = 0.049$; **Figures 2B,C**). This shift of Vδ1 T cells was not observed for the total γδ T cell population (**Figures 2B,C**, upper panel) and also not within the Vδ2 subpopulation (**Figures 2B,C**, lower panel). Moreover, the $CD27^{-}CD45RA^{++}$ population which has been described as a dysfunctional subpopulation with limited proliferation capacity (41) was significantly increased within the BM-derived Vδ1 T cells in AML and MM in comparison to HDs (HD vs. AML $p = 0.036$; HD vs. MM $p = 0.026$, respectively, **Figure 2D**).

Taken together, our data show an increased frequency of EM, TEMRA, and $CD27^{-}CD45RA^{++}$ Vδ1 T cells in the BM from patients with AML or MM diagnosis providing the rationale to further analyze this cell population.

BM-Derived γδ T Cells From Patients With AML and MM Express PD-1, TIGIT, TIM-3, and CD39

Several studies have identified the expression of co-regulatory receptors and ectonucleotidases as characteristic features of altered αβ T cell function (42), but little is known about their surface expression and functional relevance on γδ T cells. For comprehensive immunophenotyping of γδ T cells, we compared the expression of the co-inhibitory molecules PD-1, TIGIT, TIM-3, the ectonucleotidases CD39 and CD73 and the human leukocyte antigen DR isotype (HLA-DR, which is expressed by activated T cells) between BM-derived γδ T cells from patients with AML and MM with that from corresponding $CD4^{+}$ and $CD8^{+}$ αβ T cells from the same patients. For AML, our analyses revealed an increased expression of TIGIT and TIM-3 on γδ T cells and $CD8^{+}$ T cells in comparison to $CD4^{+}$ T cells (γδ T cells vs. CD4: for TIGIT $p = 0.01$, for TIM-3 $p < 0.001$, and CD8 vs. CD4: for TIGIT $p = 0.006$, for TIM-3 $p = 0.01$; **Figure 3A**). In MM, a higher frequency of PD-1, TIGIT, and HLA-DR was observed within the γδ T cell and also the $CD8^{+}$ T cell population in comparison to the corresponding $CD4^{+}$ T cells (γδ T cells vs. CD4: for PD-1 $p = 0.029$, for TIGIT $p < 0.0001$ and for HLA-DR $p = 0.0008$; and CD8 vs. CD4: for PD-1 $p = 0.0022$, for TIGIT $p = 0.002$ and for HLA-DR $p < 0.0001$; **Figure 3B**). In MM, the frequency of $CD73^{+}$ cells was significantly lower in the γδ T cell population in comparison to the $CD4^{+}$ and $CD8^{+}$ population ($p = 0.0005$ and $p = 0.007$ respectively; **Figure 3B**). Next, we compared the expression of the co-regulatory receptors in AML and MM with that from age-matched PB of HDs (for gating strategy see **Supplementary Figure 3**). Performing tSNE analyses, our data revealed intense regions of $PD\text{-}1^{+}$, $TIGIT^{+}$, $TIM\text{-}3^{+}$, and $CD39^{+}$ γδ T cells that differed in AML and MM from that in HDs (**Figure 3C**). Also, our comprehensive analyses showed an increased frequency of γδ T cells expressing PD-1 and CD39 in both neoplasias in comparison to HDs (**Figure 3D**). Furthermore, in AML $TIM\text{-}3^{+}$ γδ T cells were more frequent in comparison to HDs ($p = 0.035$, **Figure 3C**) whereas in MM, γδ T cells showed increased levels of $TIGIT^{+}$ –and $HLA\text{-}DR^{+}$ cells ($p = 0.002$ and $p = 0.006$, respectively; **Figure 3D**). Analyzing the median fluorescence intensity (MFI), the same results were detected (**Supplementary Figure 4A**).

Overall, γδ T cells exhibit higher frequencies of co-regulatory receptors in comparison with $CD4^{+}$ T cells, but similar to that expressed by $CD8^{+}$ T cells. In contrast to HDs, γδ T cells in the BM from patients with AML and MM showed an increased expression of the co-inhibitory molecules PD-1, TIGIT, TIM-3 or CD39.

Vδ1 T Cells Exhibit the Highest Frequency of Co-inhibitory Receptors in AML and MM

In our phenotypic comparisons of BM-derived γδ T cells, PD-1, TIGIT, TIM-3, and CD39 emerged as receptors expressed by γδ T cells in AML and MM. We thus analyzed receptor expression on different γδ T cell subpopulations.

In both malignancies, $TIGIT^{+}$ and $TIM\text{-}3^{+}$ cells were significantly more frequent among the Vδ1 subpopulation in comparison to the Vδ2 subpopulation (AML: $p = 0.006$, $p = 0.014$ and MM: $p = 0.001$, $p = 0.042$; **Figures 4A,B**). Additionally, the PD-1 expression was increased on the Vδ1 cells in AML ($p = 0.002$, **Figures 4A,B**). Apart from TIGIT, the MFIs of TIM-3- and PD-1 MFIs were also significantly increased on the Vδ1–in comparison to the Vδ2 cells (**Supplementary Figures 4B–D**). Again, we compared mononuclear cells derived from paired PB and BM aspirates of 9 AML patients, to exclude that our data are compartment- and not tumor-associated. The frequencies of $PD\text{-}1^{+}$, $TIGIT^{+}$, $TIM\text{-}3^{+}$, $CD39^{+}$, and $CD73^{+}$ (Vδ1) γδ T cells were similar in both compartments (**Supplementary Figure 2B**).

Regarding the differentiation status, CM γδ T cells showed higher frequencies of $PD\text{-}1^{+}$ cells, whereas EM and TEMRA γδ T cells exhibit increased amounts of TIGIT and TIM-3 (**Supplementary Figure 5**). As the Vδ1 population in AML and MM showed a significant shift toward TEMRA and $CD27^{-}CD45RA^{++}$ differentiation, we further compared the receptor expression on these differentiation subgroups between paired Vδ1 and Vδ2 cells. In AML and MM, the frequency of $TIGIT^{+}$ and $TIM\text{-}3^{+}$ cells was higher on the TEMRA Vδ1 than on the TEMRA Vδ2 T cell subset (**Supplementary Figure 6**). Within the TEMRA Vδ1 T cell population, the aberrant population of $CD27^{-}CD45RA^{++}$ T cells showed the highest frequency of $PD\text{-}1^{+}$-, $TIGIT^{+}$-, $TIM\text{-}3^{+}$-, and $CD39^{+}$ cells in AML (**Supplementary Figure 7**). In MM, this was only the case for TIM-3 expression (**Supplementary Figure 7**), whereas CD73 was completely downregulated in these cells (**Supplementary Figure 7**).

Taken together, in both malignancies in contrast to HDs, the co-inhibitory receptors PD-1, TIGIT, and TIM-3 were expressed by the Vδ1 T cell subpopulation in comparison to their corresponding Vδ2 T cell subpopulation.

PD-1, TIM-3, and CD39 Were Co-expressed With TIGIT on Vδ1 T Cells in AML and MM

Since we found that PD-1, TIGIT, TIM-3, and CD39 are more frequently expressed by the Vδ1 subpopulation in AML and MM,

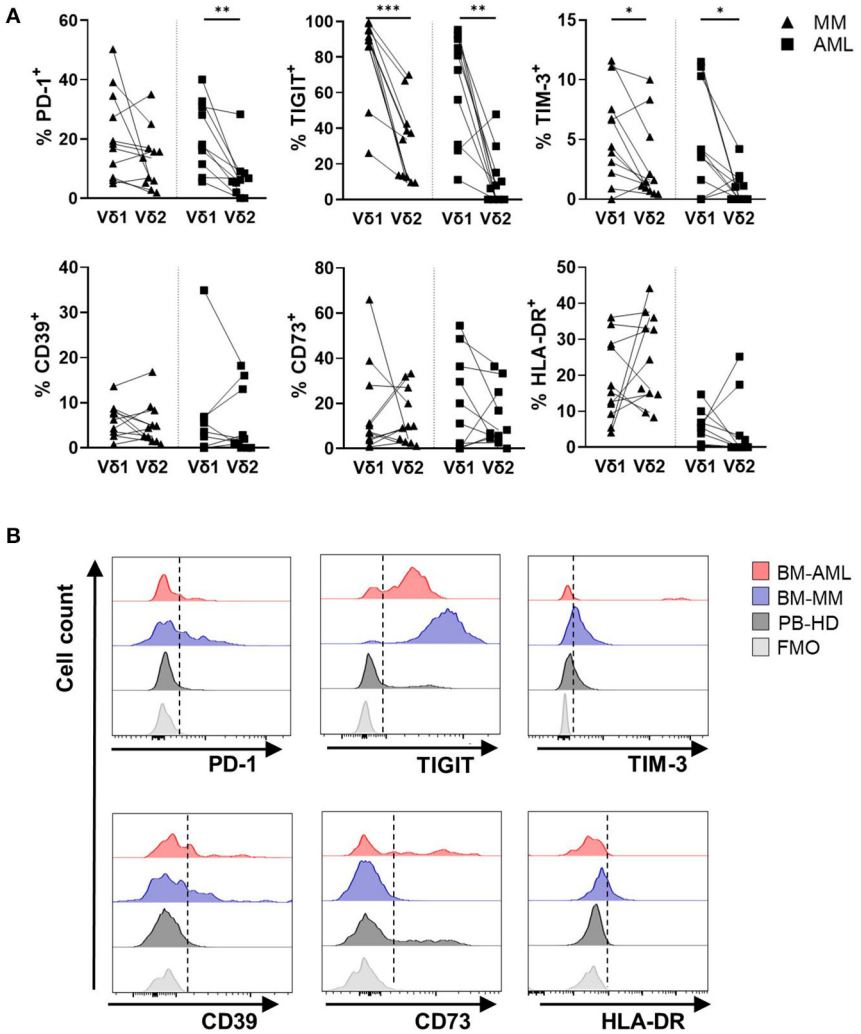

FIGURE 4 | Vδ1 γδ T cells highly express PD-1, TIGIT, TIM-3, but not CD39, CD73, and HLA-DR in AML and MM. The surface expression of PD-1, TIGIT, TIM-3, CD39, CD73, and HLA-DR was compared between Vδ1 and Vδ2 T cells in bone marrow (BM) aspirates from patients with multiple myeloma (MM, black triangles, $n = 11$) and newly diagnosed AML patients (AML, black rectangles, $n = 10$). **(A)** Summary data show the paired distribution of PD-1, TIGIT, TIM-3, CD39, CD73, and HLA-DR expression in Vδ1 and Vδ2 T cells per patient. *P*-values were obtained by the Wilcoxon matched-pairs signed-rank test. $^{*}P < 0.05$, $^{**}P < 0.01$, $^{***}P < 0.001$. **(B)** Representative flow cytometry histograms demonstrate the expression of PD-1, TIGIT, TIM-3, CD39, CD73, and HLA-DR on γδ T cells in healthy donors (HD, dark gray), multiple myeloma patients (MM, blue), and newly diagnosed AML patients (AML, red) in comparison to the fluorescence-minus-one control (FMO, gray).

the γδ T cells were further assessed with regard to a multiple co-expression of these co-regulatory molecules.

The frequency of γδ T cells co-expressing PD-1, TIM-3, and CD39 together with TIGIT was significantly higher in samples from AML and MM in comparison to HDs (AML vs. HD: $p = 0.006$, $p = 0.001$, $p = 0.08$ and MM vs. HD: $p = 0.004$, $p = 0.004$, $p = 0.017$; **Figure 5A**). This difference of co-expression in AML and MM was caused by the significant co-expression of PD-1 and TIM-3 on the TIGIT^{+} Vδ1 γδ T cells in comparison to their corresponding Vδ2 cells (AML: $p = 0.01$, $p = 0.008$ and MM: $p = 0.01$, $p = 0.042$; **Figure 5B**). In contrast to the increased co-expression of TIGIT and CD39 in all γδ T cells in AML and MM, the clustering of CD39 on Vδ1 in comparison to the corresponding Vδ2 γδ T cell subset was only nearly significant in MM, and not significant in AML. In addition, the majority of TIGIT^{+} Vδ1 γδ T cells did not express the ectoenzyme CD73 (**Figures 5A,B**). Again, this multiple co-expression of co-inhibitory molecules was in particular observed on the Vδ1 CD27^{-}CD45RA^{++} subset (**Supplementary Figure 8**).

In summary, the BM-infiltrating γδ T cells co-expressed PD-1, TIM-3, and CD39 with TIGIT in both hematological malignancies. Moreover, Vδ1 cells in AML and MM co-expressed PD-1 and TIM-3 with TIGIT more frequently than their corresponding Vδ2 T cells. For CD39, this was only the case in MM but not in AML CD39 was also significantly co-expressed with TIGIT on the Vδ1 T cells.

DISCUSSION

The present study provides a phenotypic analysis of the BM-resident γδ population in patients with AML and MM. Here,

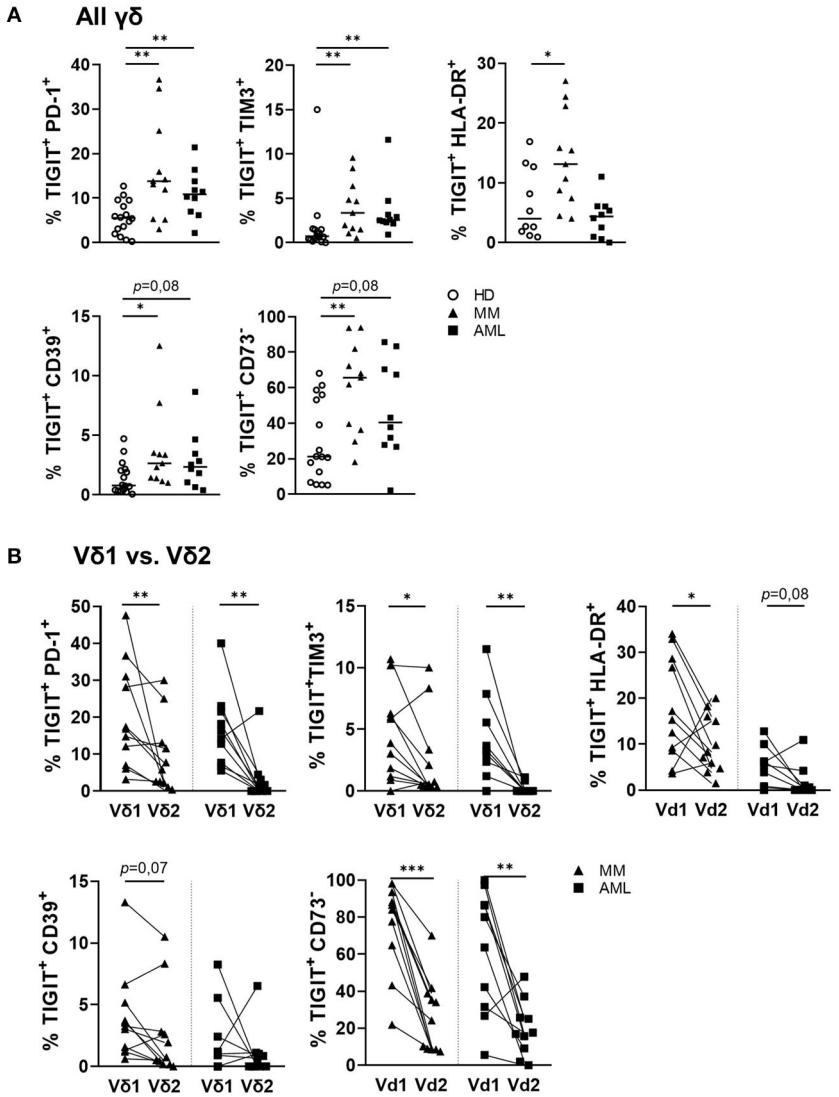

FIGURE 5 | PD-1 and TIM-3 are co-expressed with TIGIT on γδ T cells in AML and MM. The co-expression of PD-1, TIGIT, TIM-3, CD39, CD73, and HLA-DR was compared between γδ T cells from peripheral blood (PB) of healthy donors (HD, white circles, $n = 16$), and bone marrow (BM) aspirates from patients with multiple myeloma (MM, black triangles, $n = 11$), and newly diagnosed AML (AML, black rectangles, $n = 10$). **(A)** Summary data are illustrating the co-expression of PD-1, TIM-3, CD39, CD73, and the HLA-DR receptor with TIGIT on γδ T cells. *P*-values were obtained by the Mann-Whitney test. $^{*}P < 0.05$, $^{**}P < 0.01$, $^{***}P < 0.001$. **(B)** Summary data show the co-expression of PD-1, TIM-3, CD39, CD73, and HLA-DR with TIGIT on paired Vδ1 and Vδ2 γδ T cells from patients with MM (black triangles) and AML (black rectangles). *P*-values were obtained by the Wilcoxon matched-pairs signed-rank test. $^{*}P < 0.05$, $^{**}P < 0.01$, $^{***}P < 0.001$.

we demonstrate that Vδ1 T cells represent the predominant γδ T-cell population in the BM from these patients whereas Vδ2 T cells were dominant in the PB of HDs. The BM-infiltrating Vδ1 T cells in AML and MM showed an increased TEMRA cell compartment with an aberrant subpopulation of $CD27^{-}CD45RA^{++}$ cells in comparison to HDs. Expression analyses of corresponding immune effector cells derived from the BM revealed an increased expression of TIGIT, PD-1, TIM-3, and CD39 on γδ TCR cells in comparison to $CD4^{+}$ cells, which was similar to that on $CD8^{+}$ effector cells in both hematologic malignancies. In contrast to the Vδ2 T cells, the increased frequency of PD-1, TIGIT, TIM-3, and CD39 positive cells was mainly observed on Vδ1 T cells. This upregulated expression of co-regulatory receptors in AML and MM was related to the TEMRA γδ subpopulation and within this population, highest expression was found on the $CD27^{-}CD45RA^{++}$ cells. Furthermore, γδ T cells in AML and MM exhibited a further feature of exhaustion, manifested by an increased co-expression of multiple co-inhibitory molecules including PD-1, TIM-3, and CD39 together with TIGIT, which was caused by the increased co-expression on the Vδ1 T-cell population. In contrast, CD73 expression was downregulated by the $TIGIT^{+}$ γδ T cells in AML and MM. Regarding the co-expression of multiple co-inhibitory receptors, we observed similar frequencies of double positive

(TIGIT$^+$PD-1$^+$ / TIGIT$^+$TIM-3$^+$ or TIGIT$^+$CD39$^+$) cells in both cancer entities. In contrast, the single expression of TIGIT and HLA-DR was higher in MM, whereas TIM-3 was more frequently expressed by γδ T cells derived from patients with AML. These differences between both entities might be explained by variations in the immune response upon chronic stimulation.

γδ T cells are endowed with two independent recognition systems including the γδ TCR and NK cell receptors to identify tumor cells and initiate anti-cancer effector mechanisms, including cytokine production and cytotoxicity. Therefore, γδ T cells represent ideal effectors with a better safety profile and a more favorable anti-tumor efficacy in comparison to conventional αβ T cells because of their HLA-independent recognition of phosphoantigens that are characteristic for dysregulated metabolism in tumors (43, 44). Furthermore, the HLA- independent recognition system results in reduced graft vs. host disease and diminished target effects (44–47). Provided with these special features, γδ T cells represent attractive effector cells for adoptive T cell strategies. A recently designed γδ T cell construct with a GD2-targeted CAR showed potent responses against Disialoganglioside (GD2)$^+$ neuroblastoma (48, 49). Moreover, first clinical studies have been conducted to investigate the safety and efficacy of adoptive transfer of autologous or allogeneic γδ T cells in cancer patients including renal cell carcinoma, lung cancer, hepatocellular carcinoma, breast cancer, prostate cancer, and multiple myeloma (50). These studies confirmed that γδ T cell application is safe, with low levels of adverse events and that the clinical responses are ranging from partial to complete remissions (50). In AML, promising data have been recently presented by Ganesan et al. demonstrating increased *in vitro* and *in vivo* γδ T cell-mediated cytotoxicity by a bispecific engager molecule against T cell receptor gamma variable 9 (TRGV9) and CD123 (51). However, there is still potential for improvement including the engagement of co-regulatory checkpoint molecules.

In agreement with other studies, we found that in BM from AML and MM patients, the infiltration of tissue-resident Vδ1 T cells was increased, whereas the frequency of the circulating Vδ2 T cells was lower compared to that in the PB from HDs (3, 52). This inversion of the Vδ1/Vδ2 ratio in different tissues has been recently observed in solid cancer including melanoma, colorectal cancer, and non-small cell lung cancer as well (52). Although a clear correlation with γδ T cell infiltration and prognosis of cancer patients is still missing, some studies demonstrated that a reduction of Vδ2 T cells correlates with an advanced stage. In line with this, enhanced levels of Vδ2 T cells correlated with an early stage of melanoma, the absence of metastasis and a longer 5-year disease-free survival rate of colorectal cancer patients (52).

To exclude that the differences observed between HD-derived PB and patient-derived BM could be compartment-associated, we additionally compared paired BM and PB aspirates from nine AML patients on a random basis. We observed no difference in the frequency of the total γδ T cells, nor in the distribution of Vδ1 and Vδ2 T cells. Moreover, no variations of checkpoint expression on γδ T cells and subpopulations respectively, were observed in these nine AML patients. Similar with our findings, Rossol et al. compared Vδ1 T cells derived from the BM and PB from patients with HIV and observed no significant differences (53). Dean et al.'s studies confirmed these observations, revealing no significant differences of γδ T cells when they compared aspirates from the BM and PB derived from patients with an active hematopoietic malignancy or in remission (54). Our study has the limitation of a relatively small sample size of patients with newly diagnosed AML and MM. Therefore, the observations made in this study should be interpreted with caution until validated in a larger cohort.

Our analyses of the differentiation status revealed a shift toward increased TEMRA differentiation. Migration of TEMRAs into inflammatory sites to perform effector functions has also been observed for chronic infections such as CMV, but also for solid cancer including neuroblastoma, colorectal cancer, and melanoma (5). For AML patients, Gertner-Dardenne et al. first described an increased memory profile in γδ T cells derived from the PB and BM, but in contrast to our study, they observed a differentiation into CD27$^-$CD45RA$^-$ defined EMs (6). To our knowledge, our study is the first description of the differentiation status in the BM for MM. We also found a unique γδ T cell subpopulation in the BM niche from patients with AML and MM that is characterized by the CD27$^-$CD45RA^{++} phenotype. This aberrant subpopulation discovered by Odaira et al. is reported as a predominant subpopulation in different types of cancer and is characterized as "exhausted" subgroup defined by diminished proliferation capacity (41).

We and others have previously described an increased expression of TIGIT, PD-1, TIM-3, and CD39 on αβ T cells in AML and MM (31, 32, 55–57). Expression of these markers on αβ T cells was related to features of exhaustion manifested by transcriptional reprogramming, reduced effector cytokine production, decreased proliferation, and impaired lysis of tumor cells (32, 55, 58). Our comparative analyses of the co-regulatory marker expression on the corresponding CD4$^+$, CD8$^+$, and γδ T cells discovered that γδ T cells in the BM from patients with AML and MM exhibit a similar expression profile of TIGIT, PD-1, TIM-3, and CD39 to that on CD8$^+$ T cells. In MM, γδ T cells showed even higher frequencies of TIGIT$^+$ cells than the CD8$^+$ population. Moreover, this study illustrated the increased co-expression of PD-1 and TIM-3 together with TIGIT on γδ T cells in AML and MM for the first time, hypothesizing that these cells are functionally "exhausted."

Although the knowledge of checkpoint expression on γδ T cells is still sparse, our observations of an increased frequency of TIGIT$^+$ γδ T cells confirm the data of increased levels of TIGIT$^+$ γδ T cells in *de novo* AML patients published by Jin et al. In their study, upregulation of TIGIT on γδ T cells was associated with a lower overall survival rate for non-M3 AML (38). To our knowledge, there is no publication of the TIGIT expression on γδ T cells in MM.

PD-1 expression on human healthy γδ T cells has been reported upon antigen-stimulation (59). Additionally, the PD-L1/PD-1 signaling in γδ T cells prevented αβ T cell activation via checkpoint receptor ligation in pancreatic adenocarcinoma (60). In AML, pembrolizumab treatment in combination with zoledronate and interleukin-2 (IL-2) leads to increased

IFN-γ production in γδ T cells *in vitro* (61). Also, in MM PD-1 expression increased in γδ T cells after zoledronate stimulation in contrast to HD-derived γδ T cells, suggesting that MM-derived γδ T cells are intrinsically programmed to increase their threshold of refractoriness via PD-1 upregulation. Interestingly, this upregulation was observed especially in the central memory subset of the Vδ2 T cells, which in normal conditions is the subset with the highest proliferative capacity (20).

Similar to TIGIT and PD-1, receptors, TIM-3 expression and function on conventional αβ T cells has been profoundly studied, but characterization on γδ T cells is very limited. Schofield et al. reported an upregulation of TIM-3 on γδ T cells in childhood malaria. This was also mainly observed in the TEMRA population and was regulated by IL-18 and IL-12 (62). In colorectal cancer, the fraction of TIM-3$^+$ γδ T cells has been reported to be increased, which correlated with tumor-lymph-node-metastasis (TNM) staging. Moreover, TIM-3 signaling significantly inhibited the killing efficiency of Vδ2 T cells against colon cancer cells and reduced the secretion of perforin and granzyme B (63).

CD39$^+$ expression has been reported on tissue-resident γδ T cells (64). Moreover, CD39$^+$ γδ T cells suppressed immune responses via the adenosine pathway by recruitment of myeloid-derived suppressor cells in colorectal cancer (39). These CD39$^+$ γδ T cells also expressed FOXP3$^+$, a marker of regulatory αβ T cells but have more potent immunosuppressive activity than CD4$^+$ or CD8$^+$ regulatory T cells (Tregs) (39). Moreover, Casetti et al. reported that FOXP3$^+$ γδ T cells have the potential to inhibit the proliferation of anti-CD3/anti-CD28 stimulated PBMCs *in vitro* (65).

Despite Vδ1 and Vδ2 T cells both having cytotoxic capability, it has been shown that these two subsets express distinct chemokine receptors and cell adhesion molecules (1, 12, 15, 66, 67). Our data revealed that increased expression of TIGIT, PD-1, TIM-3, and CD39 was mainly confined to the Vδ1 T cell subpopulation in the BM from AML and MM patients. Recent studies found that the less studied Vδ1 T cells outperform Vδ2 T cells in most *in vitro* and first *in vivo* cancer models in terms of cytotoxicity and cell persistence after allogeneic cell transfer (68). Moreover, because of their different chemokine-receptor profile, Vδ1 T cells exhibit an increased ability of tissue penetration in comparison to Vδ2 T cells (69). Those results underline the functional relevance of the observed upregulation of multiple co-regulatory receptors on these cytotoxic effector Vδ1 T cells in AML and MM in this study.

Conclusion

This study identified γδ T cells, in particular Vδ1 T cells, in AML and MM as expressors of multiple inhibitory receptors including TIGIT, PD-1, TIM-3, and the potential tissue residency marker CD39. (Co-)expression of inhibitory receptors may reflect their exhaustion status and represent targetable structures on cytotoxic effector cells. Inhibition of TIGIT, PD-1, TIM-3, and CD39 especially on Vδ1 T cells alone or in combinatorial strategies should be further analyzed with regard to re-invigorating and boosting their cytotoxicity.

DATA AVAILABILITY STATEMENT

The original contributions presented in the study are included in the article/**Supplementary Material**, further inquiries can be directed to the corresponding author.

ETHICS STATEMENT

The studies involving human participants were reviewed and approved by Declaration of Helsinki and approval by the local ethics board of the Ärztekammer Hamburg (PV3469 and PV5119). The patients/participants provided their written informed consent to participate in this study.

AUTHOR CONTRIBUTIONS

FB designed the research study, analyzed the data, and wrote the manuscript. PW performed the experiments, analyzed the data, and reviewed the manuscript. KW, LL, and BF provided the myeloma aspirates and reviewed the manuscript. CB and JSzW reviewed the manuscript. JW and WF conceived the concept, oversaw the interpretation and presentation of the data, and reviewed the manuscript. All authors read and approved the final manuscript.

FUNDING

FB was supported by the Mildred Scheel Nachwuchszentrum Hamburg and the Hamburg Translational Research in Cancer program at the University Medical Center Hamburg-Eppendorf, Hamburg, Germany. JSzW was funded by the SFB1328 and by the DFG SFB841. The project was funded by the Roggenbuck Stiftung.

ACKNOWLEDGMENTS

We thank all our patients for their trust, understanding, and willingness to provide their bone marrow aspirates for our research. Moreover, we would like to thank the FACS Core Facility at the University Medical Center Hamburg-Eppendorf for making the technical implementation possible. Lastly, we would like to thank the Mildred-Scheel-Nachwuchszentrum for supporting our research.

SUPPLEMENTARY MATERIAL

The Supplementary Material for this article can be found online at: https://www.frontiersin.org/articles/10.3389/fmed.2021.763773/full#supplementary-material

REFERENCES

1. Pistoia V, Tumino N, Vacca P, Veneziani I, Moretta A, Locatelli F, et al. Human γδ T-cells: from surface receptors to the therapy of high-risk leukemias. *Front. Immunol.* (2018) 9:984. doi: 10.3389/fimmu.2018.00984
2. Benyamine A, Le Roy A, Mamessier E, Gertner-Dardenne J, Castanier C, Orlanducci F, et al. BTN3A molecules considerably improve Vγ9Vδ2T cells-based immunotherapy in acute myeloid leukemia. *Oncoimmunology.* (2016) 5:e1146843. doi: 10.1080/2162402X.2016.1146843
3. Gertner-Dardenne J, Fauriat C, Vey N, Olive D. Immunotherapy of acute myeloid leukemia based onγλd T cells. *Oncoimmunology.* (2012) 1:1614–6. doi: 10.4161/onci.21512
4. Kabelitz D, Kalyan S, Oberg HH, Wesch D. Human vδ2 versus non-vδ2 γδ t cells in antitumor immunity. *Oncoimmunology.* (2013) 2:2–7. doi: 10.4161/onci.23304
5. Khairallah C, Chu TH, Sheridan BS. Tissue adaptations of memory and tissue-resident gamma delta T cells. *Front Immunol.* (2018) 9:2636. doi: 10.3389/fimmu.2018.02636
6. Gertner-Dardenne J, Castellano R, Mamessier E, Garbit S, Kochbati E, Etienne A, et al. Human Vγ9Vδ2 T cells specifically recognize and kill acute myeloid leukemic blasts. *J Immunol.* (2012) 188:4701–8. doi: 10.4049/jimmunol.1103710
7. Poggi A, Zocchi MR. γδ T lymphocytes as a first line of immune defense: old and new ways of antigen recognition and implications for cancer immunotherapy. *Front Immunol.* (2014). 5:575. doi: 10.3389/fimmu.2014.00575
8. Leslie DS, Vincent MS, Spada FM, Das H, Sugita M, Morita CT, et al. CD1-mediated γ/δ T cell maturation of dendritic cells. *J Exp Med.* (2002) 196:1575–84. doi: 10.1084/jem.20021515
9. Ismaili J, Olislagers V, Poupot R, Fournié J-J, Goldman M. Human gamma delta T cells induce dendritic cell maturation. *Clin Immunol.* (2002) 103(3 Pt 1):296–302. doi: 10.1006/clim.2002.5218
10. Himoudi N, Morgenstern DA, Yan M, Vernay B, Saraiva L, Wu Y, et al. Human γδ T lymphocytes are licensed for professional antigen presentation by interaction with opsonized target cells. *J Immunol.* (2012) 188:1708–16. doi: 10.4049/jimmunol.1102654
11. Muto M, Baghdadi M, Maekawa R, Wada H, Seino K. Myeloid molecular characteristics of human γδ T cells support their acquisition of tumor antigen-presenting capacity. *Cancer Immunol Immunother.* (2015) 64:941–9. doi: 10.1007/s00262-015-1700-x
12. Lawand M, Déchanet-Merville J, Dieu-Nosjean MC. Key features of gamma-delta T-cell subsets in human diseases and their immunotherapeutic implications. *Front Immunol.* (2017) 8:761. doi: 10.3389/fimmu.2017.00761
13. Mattarollo SR, Kenna T, Nieda M, Nicol AJ. Chemotherapy and zoledronate sensitize solid tumour cells to Vγ9Vδ2 T cell cytotoxicity. *Cancer Immunol Immunother.* (2007) 56:1285–97. doi: 10.1007/s00262-007-0279-2
14. Coffelt SB, Kersten K, Doornebal CW, Weiden J, Vrijland K, Hau CS, et al. IL-17-producing γδ T cells and neutrophils conspire to promote breast cancer metastasis. *Nature.* (2015) 522:345–8. doi: 10.1038/nature14282
15. Park JH, Lee HK. Function of γδ T cells in tumor immunology and their application to cancer therapy. *Exp Mol Med.* (2021) 53:318–27. doi: 10.1038/s12276-021-00576-0
16. Gentles AJ, Newman AM, Liu CL, Bratman S V, Feng W, Kim D, et al. The prognostic landscape of genes and infiltrating immune cells across human cancers. *Nat Med.* (2015) 21:938–45. doi: 10.1038/nm.3909
17. Kunzmann V, Smetak M, Kimmel B, Weigang-Koehler K, Goebeler M, Birkmann J, et al. Tumor-promoting versus tumor-antagonizing roles of γδ T cells in cancer immunotherapy: results from a prospective phase I/II trial. *J Immunother.* (2012) 35:205–13. doi: 10.1097/CJI.0b013e318245bb1e
18. Wilhelm M, Smetak M, Schaefer-Eckart K, Kimmel B, Birkmann J, Einsele H, et al. Successful adoptive transfer and *in vivo* expansion of haploidentical γδ T cells. *J Transl Med.* (2014) 12:1–5. doi: 10.1186/1479-5876-12-45
19. Airoldi I, Bertaina A, Prigione I, Zorzoli A, Pagliara D, Cocco C, et al. γδ T-cell reconstitution after HLA-haploidentical hematopoietic transplantation depleted of TCR-αβ+/CD19+ lymphocytes. *Blood.* (2015) 125:2349–58. doi: 10.1182/blood-2014-09-599423
20. Castella B, Foglietta M, Riganti C, Massaia M. Vγ9Vδ2 T cells in the bone marrow of myeloma patients: a paradigm of microenvironment-induced immune suppression. *Front Immunol.* (2018) 9:1492. doi: 10.3389/fimmu.2018.01492
21. Lee HW, Chung YS, Kim TJ. Heterogeneity of human γδ t cells and their role in cancer immunity. *Immune Netw.* (2020) 20:1–15. doi: 10.4110/in.2020.20.e5
22. Presti E Lo, Pizzolato G, Corsale AM, Caccamo N, Sireci G, Dieli F, et al. γδ T cells and tumor microenvironment: from immunosurveillance to tumor evasion. *Front Immunol.* (2018). 9:1395. doi: 10.3389/fimmu.2018.01395
23. Godder KT, Henslee-Downey PJ, Mehta J, Park BS, Chiang KY, Abhyankar S, et al. Long term disease-free survival in acute leukemia patients recovering with increased γδ T cells after partially mismatched related donor bone marrow transplantation. *Bone Marrow Transplant.* (2007) 39:751–7. doi: 10.1038/sj.bmt.1705650
24. Cordova A, Toia F, la Mendola C, Orlando V, Meraviglia S, Rinaldi G, et al. Characterization of human γδ T lymphocytes infiltrating primary malignant melanomas. *PLoS ONE.* (2012) 7:e49878. doi: 10.1371/journal.pone.0049878
25. Scheper W, Van Dorp S, Kersting S, Pietersma F, Lindemans C, Hol S, et al. γδT cells elicited by CMV reactivation after allo-SCT cross-recognize CMV and leukemia. *Leukemia.* (2013) 27:1328–38. doi: 10.1038/leu.2012.374
26. Knight A, Mackinnon S, Lowdell MW. Human Vdelta1 gamma-delta T cells exert potent specific cytotoxicity against primary multiple myeloma cells. *Cytotherapy.* (2012) 14:1110–8. doi: 10.3109/14653249.2012.700766
27. Chauvin JM, Zarour HM. TIGIT in cancer immunotherapy. *J Immunother Cancer.* (2020) 8:e000957. doi: 10.1136/jitc-2020-000957
28. Chauvin JM, Pagliano O, Fourcade J, Sun Z, Wang H, Sander C, et al. TIGIT and PD-1 impair tumor antigen-specific CD8+ T cells in melanoma patients. *J Clin Invest.* (2015) 125:2046–58. doi: 10.1172/JCI80445
29. Anderson AC, Joller N, Kuchroo VK. L1 Anderson AC, *Joller, N. and Kuchroo VK.* (2016) Lag-3, Tim-3, and TIGIT: co-inhibitory receptors with specialized functions in immune regulation. Immunity, NIH public access 44, 989–1004.ag-3, Tim-3, and TIGIT: co-inhibitory receptors with specia. *Immunity.* (2016) 44:989–1004. doi: 10.1016/j.immuni.2016.05.001
30. Simon S, Labarriere N. PD-1 expression on tumor-specific T cells: friend or foe for immunotherapy? *Oncoimmunology.* (2018) 7:1–7. doi: 10.1080/2162402X.2017.1364828
31. Wolf Y, Anderson AC, Kuchroo VK. TIM3 comes of age as an inhibitory receptor. *Nat Rev Immunol.* (2020) 20:173–85. doi: 10.1038/s41577-019-0224-6
32. Kong Y, Zhu L, Schell TD, Zhang J, Claxton DF, Ehmann WC, et al. T-cell immunoglobulin and ITIM domain (TIGIT) associates with CD8+ T-cell exhaustion and poor clinical outcome in AML patients. *Clin Cancer Res.* (2016) 22:3057–66. doi: 10.1158/1078-0432.CCR-15-2626
33. Allard B, Longhi MS, Robson SC, Stagg J. The ectonucleotidases CD39 and CD73: Novel checkpoint inhibitor targets. *Immunol Rev.* (2017) 276:121–44. doi: 10.1111/imr.12528
34. Allard B, Allard D, Buisseret L, Stagg J. The adenosine pathway in immuno-oncology. *Nat Rev Clin Oncol.* (2020) 17:611–29. doi: 10.1038/s41571-020-0382-2
35. Scott AC, Dündar F, Zumbo P, Chandran SS, Klebanoff CA, Shakiba M, et al. TOX is a critical regulator of tumour-specific T cell differentiation. *Nature.* (2019) 571:270–4. doi: 10.1038/s41586-019-1324-y
36. Khan O, Giles JR, McDonald S, Manne S, Ngiow SF, Patel KP, et al. TOX transcriptionally and epigenetically programs CD8+ T cell exhaustion. *Nature.* (2019) 571:211–8. doi: 10.1038/s41586-019-1325-x
37. Jiang W, He Y, He W, Wu G, Zhou X, Sheng Q, et al. Exhausted CD8+T cells in the tumor immune microenvironment: new pathways to therapy. *Front Immunol.* (2021) 11:622509. doi: 10.3389/fimmu.2020.622509
38. Jin Z, Ye W, Lan T, Zhao Y, Liu X, Chen J, et al. Characteristic of TIGIT and DNAM-1 Expression on Foxp3+ γδ T cells in AML patients. *Biomed Res Int.* (2020) 2020:1–10. doi: 10.1155/2020/4612952
39. Hu G, Wu P, Cheng P, Zhang Z, Wang Z, Yu X, et al. Tumor-infiltrating CD39+ γδTregs are novel immunosuppressive T cells in human colorectal cancer. *Oncoimmunology.* (2017) 6:1–14. doi: 10.1080/2162402X.2016.1277305
40. Barjon C, Michaud HA, Fages A, Dejou C, Zampieri A, They L, et al. IL-21 promotes the development of a CD73-positive Vγ9Vδ2 T cell regulatory population. *Oncoimmunology.* (2018) 7:e1379642. doi: 10.1080/2162402X.2017.1379642
41. Odaira K, Kimura S, Fujieda N, Kobayashi Y, Kambara K, Takahashi T, et al. CD27-CD45+ γδ T cells can be divided into two populations, CD27-CD45int and CD27-CD45hi with little proliferation potential. *Biochem Biophys Res Commun.* (2016) 478:1298–303. doi: 10.1016/j.bbrc.2016.08.115

42. Wherry EJ, Kurachi M. Molecular and cellular insights into T cell exhaustion. *Nat Rev Immunol.* (2015) 15:486–99. doi: 10.1038/nri3862
43. Ou L, Wang H, Liu Q, Zhang J, Lu H, Luo L, et al. Dichotomous and stable gamma delta T-cell number and function in healthy individuals. *J Immunother Cancer.* (2021) 9:1–13. doi: 10.1136/jitc-2020-002274
44. Rafiq S, Hackett CS, Brentjens RJ. Engineering strategies to overcome the current roadblocks in CAR T cell therapy. *Nat Rev Clin Oncol.* (2020) 17:147–67. doi: 10.1038/s41571-019-0297-y
45. Biernacki MA, Sheth VS, Bleakley M. T cell optimization for graft-versusleukemia responses. *JCI Insight.* (2020) 5:1–17. doi: 10.1172/jci.insight.134939
46. Caldwell KJ, Gottschalk S, Talleur AC. Allogeneic CAR cell therapy—more than a pipe dream. *Front Immunol.* (2021) 11:618427. doi: 10.3389/fimmu.2020.618427
47. Rozenbaum M, Meir A, Aharony Y, Itzhaki O, Schachter J, Bank I, et al. Gamma-delta CAR-T cells show CAR-directed and independent activity against leukemia. *Front Immunol.* (2020) 11:1347. doi: 10.3389/fimmu.2020.01347
48. Capsomidis A, Benthall G, Van Acker HH, Fisher J, Kramer AM, Abeln Z, et al. Chimeric antigen receptor-engineered human gamma delta T cells: enhanced cytotoxicity with retention of cross presentation. *Mol Ther.* (2018) 26:354–65. doi: 10.1016/j.ymthe.2017.12.001
49. Fisher J, Abramowski P, Wisidagamage Don ND, Flutter B, Capsomidis A, Cheung GWK, et al. Avoidance of on-target off-tumor activation using a co-stimulation-only chimeric antigen receptor. *Mol Ther.* (2017) 25:1234–47. doi: 10.1016/j.ymthe.2017.03.002
50. Kabelitz D, Serrano R, Kouakanou L, Peters C, Kalyan S. Cancer immunotherapy with γδ T cells: many paths ahead of us. *Cell Mol Immunol.* (2020) 17:925–39. doi: 10.1038/s41423-020-0504-x
51. Ganesan R, Chennupati V, Ramachandran B, Hansen MR, Singh S, Grewal IS. Selective recruitment of γδ T cells by a bispecific antibody for the treatment of acute myeloid leukemia. *Leukemia.* (2021) doi: 10.1038/s41375-021-01122-7
52. Wesch D, Kabelitz D, Oberg HH. Tumor resistance mechanisms and their consequences on γδ T cell activation. *Immunol Rev.* (2020) 298:84–98. doi: 10.1111/imr.12925
53. Rossol R, Dobmeyer JM, Dobmeyer TS, Klein SA, Rossol S, Wesch D, et al. Increase in Vδ1+ γδ T cells in the peripheral blood and bone marrow as a selective feature of HIV-1 but not other virus infections. *Br J Haematol.* (1998) 100:728–34. doi: 10.1046/j.1365-2141.1998.00630.x
54. Dean J, McCarthy D, Lawler M, Doherty DG, O'Farrelly C, Golden-Mason L. Characterization of NKR + T-cell subsets in human bone marrow: implications for immunosurveillance of neoplasia. *Clin Immunol.* (2005) 114:42–51. doi: 10.1016/j.clim.2004.08.017
55. Brauneck F, Haag F, Woost R, Wildner N, Tolosa E, Rissiek A, et al. Increased frequency of TIGIT CD73-CD8 T cells with a TOX TCF-1low profile in patients with newly diagnosed and relapsed AML. *Oncoimmunology.* (2021) 10:1930391. doi: 10.1080/2162402X.2021.1930391
56. Hoffmann M, Pantazis N, Martin GE, Hickling S, Hurst J, Meyerowitz J, et al. Exhaustion of activated CD8 T cells predicts disease progression in primary HIV-1 infection. *PLoS Pathog.* (2016) 12:e1005661. doi: 10.1371/journal.ppat.1005661
57. Canale FP, Ramello MC, Núñez N, Furlan CLA, Bossio SN, Serrán MG, et al. CD39 expression defines cell exhaustion in tumor-infiltrating CD8+ T cells. *Cancer Res.* (2018) 78:115–28. doi: 10.1158/0008-5472.CAN-16-2684
58. Zeidan AM, Komrokji RS, Brunner AM. TIM-3 pathway dysregulation and targeting in cancer. *Expert Rev Anticancer Ther.* (2021) 21:523–34. doi: 10.1080/14737140.2021.1865814
59. Iwasaki M, Tanaka Y, Kobayashi H, Murata-Hirai K, Miyabe H, Sugie T, et al. Expression and function of PD-1 in human γδ T cells that recognize phosphoantigens. *Eur J Immunol.* (2011) 41:345–55. doi: 10.1002/eji.201040959
60. Daley D, Zambirinis CP, Seifert L, Akkad N, Mohan N, Werba G, et al. γδ T cells support pancreatic oncogenesis by restraining αβ T cell activation. *Cell.* (2016) 166:1485–1499.e15. doi: 10.1016/j.cell.2016.07.046
61. Hoeres T, Holzmann E, Smetak M, Birkmann J, Wilhelm M. PD-1 signaling modulates interferon-γ production by Gamma Delta (γδ) T-Cells in response to leukemia. *Oncoimmunology.* (2019) 8:1–11. doi: 10.1080/2162402X.2018.1550618
62. Schofield L, Ioannidis LJ, Karl S, Robinson LJ, Tan QY, Poole DP, et al. Synergistic effect of IL-12 and IL-18 induces TIM3 regulation of γδ T cell function and decreases the risk of clinical malaria in children living in Papua New Guinea. *BMC Med.* (2017) 15:114. doi: 10.1186/s12916-017-0883-8
63. Li X, Lu H, Gu Y, Zhang X, Zhang G, Shi T, et al. Tim-3 suppresses the killing effect of Vγ9Vδ2 T cells on colon cancer cells by reducing perforin and granzyme B expression. *Exp Cell Res.* (2020) 386:111719. doi: 10.1016/j.yexcr.2019.111719
64. Libera J, Wittner M, Kantowski M, Woost R, Eberhard JM, de Heer J, et al. Decreased frequency of intestinal CD39+ γδ+ T cells with tissue-resident memory phenotype in inflammatory bowel disease. *Front Immunol.* (2020) 11:567472. doi: 10.3389/fimmu.2020.567472
65. Casetti R, Agrati C, Wallace M, Sacchi A, Martini F, Martino A, et al. Cutting edge: TGF-β1 and IL-15 induce FOXP3 + γδ regulatory T cells in the presence of antigen stimulation. *J Immunol.* (2009) 183:3574–7. doi: 10.4049/jimmunol.0901334
66. Hayday AC. γδ T Cell update: adaptate orchestrators of immune surveillance. *J Immunol.* (2019) 203:311–20. doi: 10.4049/jimmunol.1800934
67. Zheng J, Liu Y, Lau YL, Tu W. γδ-T cells: an unpolished sword in human anti-infection immunity. *Cell Mol Immunol.* (2013) 10:50–7. doi: 10.1038/cmi.2012.43
68. Raverdeau M, Cunningham SP, Harmon C, Lynch L. γδ T cells in cancer: a small population of lymphocytes with big implications. *Clin Transl Immunol.* (2019) 8:1–15. doi: 10.1002/cti2.1080
69. Schilbach K, Frommer K, Meier S, Handgretinger R, Eyrich M. Immune response of human propagated gammadelta-T-cells to neuroblastoma recommend the Vdelta1+ subset for gammadelta-T-cell-based immunotherapy. *J Immunother.* (2008) 31:896–905. doi: 10.1097/CJI.0b013e31818955ad

Conflict of Interest: FB: Travel grant Daiichi Sankyo, Servier, Novartis; advisory board by Jazz. GmbH, Daiichi Sankyo. WF: Membership on an entity's board of directors or advisory Amgen, ARIAD/Incucyte, Pfizer, Novartis, Jazz Pharmaceuticals, Morphosys, Abbvie, Celgene; patents and royalities: Amgen; other support for meeting attendance Amgen, Gilead, Jazz Pharmaceuticals, Servier, Daiichi Sankyo; research funding Amgen, Pfizer. Travel grant, advisory board and research funding by Amgen Inc., travel grant and advisory board by TEVA GmbH, the advisory board: Ariad/Incucyte Inc., travel grant by Gilead Inc and Jazz. GmbH, research funding by Pfizer Inc. KW: Honoraria: AbbVie, Amgen, Adaptive Biotech, Celgene/BMS, GSK, Janssen, Karyopharm, Novartis, Roche, Takeda, Sanofi; Research funding: Amgen, Celgene, Janssen, Sanofi. LL: Non-financial support from GSK and from Abbvie. CB: Travel grant: Astra Zeneca, Bayer Healthcare, Berlin Chemie, Bristol Myers Squipp, Jansen Cilag, Merck Serono, Merck Sharp Dohme, Novartis, Roche Pharma, Sanofi Aventis; Advisory board: Astra Zeneca, Bayer Healthcare, Berlin Chemie, Bristol Myers Squipp, Jansen Cilag, Merck Serono, Merck Sharp Dohme, Novartis, Roche Pharma, Sanofi Aventis; Invited speaker: AOK Germany, med update, Merck Serono; Honoraria: AOK Germany, Astra Zeneca, Bayer Healthcare, Berlin Chemie, GSO Research Organisation, Jansen Cilag, med update, Merck Serono, Merck Sharp Dohme, Novartis, Roche Pharma, Sanofi Aventis.

The remaining authors declare that the research was conducted in the absence of any commercial or financial relationships that could be construed as a potential conflict of interest.

The handling editor declared a past co-authorship with the authors JW and WF.

Publisher's Note: All claims expressed in this article are solely those of the authors and do not necessarily represent those of their affiliated organizations, or those of the publisher, the editors and the reviewers. Any product that may be evaluated in this article, or claim that may be made by its manufacturer, is not guaranteed or endorsed by the publisher.

frontiers in Medicine

BRIEF RESEARCH REPORT
published: 10 February 2022
doi: 10.3389/fmed.2022.790995

Expression of the Immune Checkpoint Protein VISTA Is Differentially Regulated by the TGF-β1 – Smad3 Signaling Pathway in Rapidly Proliferating Human Cells and T Lymphocytes

Stephanie Schlichtner[1], Inna M. Yasinska[1], Sabrina Ruggiero[2], Steffen M. Berger[2], Nijas Aliu[3], Mateja Prunk[4], Janko Kos[4,5], N. Helge Meyer[6,7], Bernhard F. Gibbs[6], Elizaveta Fasler-Kan[2,8]* and Vadim V. Sumbayev[1]**

[1] Medway School of Pharmacy, Universities of Kent and Greenwich, Chatham Maritime, United Kingdom, [2] Department of Pediatric Surgery, Children's Hospital, Inselspital Bern, University of Bern, Bern, Switzerland, [3] Department of Human Genetics, Inselspital Bern, University of Bern, Bern, Switzerland, [4] Department of Biotechnology, JoŽef Stefan Institute, Ljubljana, Slovenia, [5] Faculty of Pharmacy, University of Ljubljana, Ljubljana, Slovenia, [6] Division of Experimental Allergology and Immunodermatology, Department of Human Medicine, University of Oldenburg, Oldenburg, Germany, [7] Division of General and Visceral Surgery, Department of Human Medicine, University of Oldenburg, Oldenburg, Germany, [8] Department of Biomedicine, University of Basel and University Hospital Basel, Basel, Switzerland

Immune checkpoint proteins play crucial roles in human embryonic development but are also used by cancer cells to escape immune surveillance. These proteins and biochemical pathways associated with them form a complex machinery capable of blocking the ability of cytotoxic immune lymphoid cells to attack cancer cells and, ultimately, to fully suppress anti-tumor immunity. One of the more recently discovered immune checkpoint proteins is V-domain Ig-containing suppressor of T cell activation (VISTA), which plays a crucial role in anti-cancer immune evasion pathways. The biochemical mechanisms underlying regulation of VISTA expression remain unknown. Here, we report for the first time that VISTA expression is controlled by the transforming growth factor beta type 1 (TGF-β)-Smad3 signaling pathway. However, in T lymphocytes, we found that VISTA expression was differentially regulated by TGF-β depending on their immune profile. Taken together, our results demonstrate the differential biochemical control of VISTA expression in human T cells and various types of rapidly proliferating cells, including cancer cells, fetal cells and keratinocytes.

Keywords: immune checkpoint, VISTA, anti-cancer immunity, T lymphocytes, galectin-9

OPEN ACCESS

Edited by:
Ihsan Ullah,
Khyber Medical University, Pakistan

Reviewed by:
Francesca Romana Mariotti,
Bambino Gesù Children's Hospital (IRCCS), Italy
Michele Bernasconi,
University Children's Hospital Bern, Switzerland
Oksana Kunduzova,
Institut National de la Santé et de la Recherche Médicale (INSERM), France
Dmitri Pchejetski,
University of East Anglia, United Kingdom
Michael Danilenko,
Ben-Gurion University of the Negev, Israel

***Correspondence:**
Vadim V. Sumbayev
V.Sumbayev@kent.ac.uk
Elizaveta Fasler-Kan
elizaveta.fasler@insel.ch
Bernhard F. Gibbs
bernhard.gibbs@uni-oldenburg.de

Specialty section:
This article was submitted to Pathology, a section of the journal Frontiers in Medicine

Received: *07 October 2021*
Accepted: *17 January 2022*
Published: *10 February 2022*

Citation:
Schlichtner S, Yasinska IM, Ruggiero S, Berger SM, Aliu N, Prunk M, Kos J, Meyer NH, Gibbs BF, Fasler-Kan E and Sumbayev VV (2022) Expression of the Immune Checkpoint Protein VISTA Is Differentially Regulated by the TGF-β1 – Smad3 Signaling Pathway in Rapidly Proliferating Human Cells and T Lymphocytes. Front. Med. 9:790995. doi: 10.3389/fmed.2022.790995

INTRODUCTION

Immune checkpoint proteins play crucial roles in determining the ability of human cancer cells to escape immune surveillance (1, 2). These proteins integrate into a complex machinery which is capable of blocking cytotoxic immune attacks on cancer cells by specialized human lymphoid cells and, in the long run, to fully suppress anti-tumor immunity (1, 2). These pathways can play

fundamental roles and were found to be implemented by human fetal cells in order to protect the embryo against rejection by the mother's immune system (3).

With some immune checkpoint proteins, such as programmed cell death protein 1 (PD-1) and its ligand (PD-L1), cytotoxic T-lymphocyte-associated protein 4 (CTLA4), T cell immunoglobulin and mucin domain containing protein 3 (Tim-3) and its ligand galectin-9, the biochemical mechanisms underlying their expression and regulation of their biological activities have been elucidated (1, 2, 4). Others were only discovered recently and thus such mechanisms remain poorly understood. However, this is a very important issue since identification of the optimal targets for immunotherapy of cancer crucially hinges on our understanding of the biochemistry of immune checkpoint pathways responsible for immune escape. One of such immune checkpoint proteins is V-domain Ig-containing suppressor of T cell activation (VISTA) which plays a crucial role in the suppression of human T cell responses during cancer progression (5–7). VISTA is expressed mainly in blood cells and plays a complex role in regulating immune responses (5–7). Myeloid cells show the highest levels of expression, but lymphoid cells, especially T lymphocytes also express this protein where it can be used as a receptor to suppress their anti-cancer activities (5–7). Interestingly, VISTA has been reported to display both receptor and ligand properties (5–7). However, its receptors (when it acts as a ligand) remain to be identified. One of the VISTA ligands is VSIG3 (V-set and immunoglobulin domain containing 3), which is a member of the immunoglobulin superfamily and is highly expressed in human brain and testis (8). Another VISTA ligand is galectin-9, which is a member of galectin family of proteins conserved throughout evolution (9). Galectin-9 contains two similar, but not identical, subunits bound through a peptide linker, which can be of different size (9, 10). There are three isoforms of galectin-9 which vary in linker size (10). Galectin-9 isoforms can interact with VISTA on the surface of cytotoxic T cells and induce programmed death most likely through prevention of granzyme B release from these cells. Granzyme B is a proteolytic enzyme used to induce apoptotic death of target cells, and its activation inside cytotoxic T cells, which fail to release it, is followed by their programmed death (9). Several types of human cancer cells are known to express VISTA too (11, 12). However, the mechanisms which regulate VISTA expression in human cells remain unknown. By analyzing the promoter region of human VISTA, we noticed that it contains response elements for Smad3 transcription factor which is activated by human transforming growth factor beta type 1 (TGF-β) through specific plasma membrane-associated receptors. Interestingly, we have recently reported that the TGF-β-Smad3 pathway is involved in regulating galectin-9 expression in human cancer and embryonic cells (3). TGF-β displays both autocrine and paracrine activities and is able to induce its own expression, which is also Smad3-dependent as is the expression of galectin-9 (3). Thus, in both cancer and embryonic cells, this pathway is self-controlling and self-sustaining. In this work we aimed to study whether the TGF-β-Smad3 pathway is also involved in VISTA expression.

We discovered for the first time that VISTA expression is controlled by the TGF-β-Smad3 signaling pathway. Interestingly, in T lymphocytes, VISTA is only upregulated by TGF-β if they do not display cytotoxic activity (lack granzyme B expression), while if T cells express this proteolytic enzyme and display cytotoxic activity, VISTA expression is decreased in the presence of TGF-β. We hypothesized that this phenomenon could be possibly triggered by differential nuclear compartmentalisation of VISTA encoding gene (VSIG).

MATERIALS AND METHODS

Materials

RPMI-1640 medium for cell culture, fetal bovine serum, supplements and basic laboratory chemicals were purchased from Sigma (Suffolk, UK). Microtiter plates for ELISA were obtained from Oxley Hughes Ltd (London, UK). Rabbit antibodies against VISTA, galectin-9, granzyme B, phospho-S423/S425-Smad3, Smad4 and TRIM33 as well as goat anti-rabbit horseradish peroxidase (HRP) labeled secondary antibody were purchased from Abcam (Cambridge, UK). Antibodies against β-actin were purchased from Proteintech (Manchester, UK). Goat anti-mouse and anti-rabbit fluorescently-labeled dye secondary antibodies were obtained from Li-COR (Lincoln, NE, USA). Mouse anti-Smad3 antibody, ELISA-based assay kits for the detection of VISTA, galectin-9 (both kits contain mouse capture antibodies against VISTA and galectin-9, respectively) and TGF-β as well as human recombinant TGF-β1 protein and mouse anti-Smad3 antibody were purchased from Bio-Techne (R&D Systems, Abingdon, UK). Anti-Tim-3 mouse monoclonal antibody was described before (13). All other chemicals employed in this study were of the highest grade of purity commercially available.

Cell Lines and Primary Human Samples

Cell lines used in this work were purchased from either the European Collection of Cell Cultures, American Tissue Culture Collection or CLS Cell Lines Service GmbH. Cell lines were accompanied by identification test certificates. Wilms Tumor cell line WT3ab was kindly provided by Dr. C. Stock (Children's Cancer Research Institute, Vienna, Austria) and cultured as it was previously described (14).

Jurkat T, MCF-7, THP-1, WT-3ab, HaCaT keratinocytes and K562 were cultured in RPMI 1640 media supplemented with 10% fetal bovine serum, penicillin (50 IU/ml), and streptomycin sulfate (50 μg/ml).

TALL-104 CD8-positive cytotoxic T lymphocytes, derived from human acute lymphoblastic leukemia (TALL), were cultured according to the ATCC instructions. Briefly, ATCC-formulated Iscove's Modified Dulbecco's Medium was used. To make the complete growth medium we added 100 units/ml recombinant human IL-2; 2.5 μg/ml human albumin; 0.5 μg/ml D-mannitol and fetal bovine serum to a final concentration of 20% (15). Medium was also supplemented with penicillin (50 IU/ml), and streptomycin sulfate (50 μg/ml).

Primary human AML mononuclear blasts (AML-PB001F, newly diagnosed/untreated) were also purchased from

AllCells (Alameda, CA, USA) and handled according to the manufacturer's recommendations. The studies were performed following ethical approval (REC reference: 16-SS-033).

Placental tissues (CVS, chorionic villus sampling) and amniotic fluids were collected after obtaining informed written consent from pregnant women at the University Hospital Bern, Inselspital. Fetal cells were handled and cultured as described before (3, 16).

Primary human T cells where isolated from buffy coat blood (purchased form the Deutsches Rotes Kreuz and following ethical approval from the Medizinische Ethikkommission der Carl von Ossietzky Universität Oldenburg) using Ficoll-density centrifugation. PBMCs were collected and T cells purified using a commercial CD3 T cell negative isolation kit (Biolegend) according to the manufacturer's protocol. 200,000 T cells per 200 µl were incubated for 16 h with and without TGF-β at a final concentration of 2 ng/ml in RPMI medium.

Western Blot Analysis

VISTA, granzyme B, galectin-9, Tim-3, phospho-S423/S425 Smad-3, Smad4 and TRIM33 were measured by Western blot and compared to the amounts of β-actin (protein loading control), as previously described (17).

Li-Cor goat secondary antibodies conjugated with infrared fluorescent dyes, were used as described in the manufacturer's protocol for visualization of specific proteins (Li-Cor Odyssey imaging system was employed). Western blot data were quantitatively analyzed using Odyssey software called Image Studio and values were subsequently normalized against those of β-actin.

Chromatin Immunoprecipitation (ChIP)

ChIP was performed as described recently (18). Resting Jurkat T cells and those treated for 24 h with 2 ng/ml TGF-β were subjected to the study. 5×10^6 cells were used for immunoprecipitation. Cross-linking was performed using 1.42% formaldehyde followed by quenching with 125 mM glycine for 5 min. Cells were then washed twice with PBS and subjected to ChIP in accordance with ChIP-IT high sensitivity kit (Active Motif) protocol. Immunoprecipitation was performed using mouse monoclonal anti-Smad3 antibody (R&D Systems, Abingdon, UK), and IgG isotype control antibody was used for a negative control IP. The Smad3 epitope recognized by this antibody does not overlap with DNA and co-activator binding sites of this protein. Immunoprecipitated DNA was then purified and subjected to quantitative real-time PCR (qRT-PCR) which was performed as outlined below. The following primers were designed using NCBI Primer-Blast primer designing tool: forward – 5′-GCCTACCACATACCAAGCCC-3′ and reverse: 5′-ATCGGCAGTTTAAAGCCCGT-3′. These primers allow to amplify the fragment of the promoter region of VSIG (VISTA gene), which surrounds Smad3-binding sites.

qRT-PCR Analysis

To detect VISTA mRNA levels, we used qRT-PCR (15). Total RNA was isolated using a GenElute™ mammalian total RNA preparation kit (Sigma-Aldrich) according to the manufacturer's protocol, followed by reverse transcriptase–polymerase chain reaction (RT-PCR) of a target protein mRNA (also performed according to the manufacturer's protocol). This was followed by qRT-PCR. The following primers were used. VISTA: forward – 5′-GATGCACCATCCAACTGTGT-3′, reverse – 5′-GCAGAGGATTCCTACGATGC-3′; actin: forward – 5′-TGACGGGGTCACCCACACTGTGCCCATCTA-3′, reverse – 5′-CTAGAAGCATTTGCGGTCGACGATGGAGGG-3′. Reactions were performed using a LightCycler® 480 qRT-PCR machine and SYBR Green I Master kit (Roche, Burgess Hill, UK). The assay was performed according to the manufacturer's protocol. Values representing VISTA mRNA levels were normalized against those of β-actin.

On-Cell Western Analysis

Cell surface levels of VISTA protein were analyzed using on-cell Western analysis performed using a Li-COR Odyssey imager and the assay was performed in line with manufacturer's recommendations as previously described (9).

Enzyme-Linked Immunosorbent Assays (ELISAs)

Secreted VISTA and TGF-β were measured in cell culture medium (VISTA was also measured in some of the cell lysates), by ELISA using R&D Systems kits (see Section Materials) according to manufacturer's protocols. To study recruitment of co-activators Smad4 and TRIM33 by Smad3 we used ELISA-based assay where we applied mouse anti-Smad3 antibody (R&D Systems) as capture. The plate was coated with this antibody (1:500) overnight followed by blocking with 1% BSA (dissolved in phosphate buffered saline, PBS). Then cell lysates were applied and incubated for 2 h followed by 5 times washing with TBS (50 mM Tris–HCl, 140 mM NaCl, pH 7.3) containing 0.1% Tween 20 (TBST). Rabbit anti-TRIM33 or anti-Smad4 antibodies were used (1:1000, 2h incubation) to detect these proteins interacted with Smad3. Finally, the plates were washed 5 times with TBST and horseradish peroxidase (HRP) labeled goat anti-rabbit antibody was applied for 1 h at room temperature. The plates were washed 5 times with TBST followed by visualization through the peroxidase reaction (ortho-phenylenediamine/H_2O_2). The reactions were quenched after 10 min with an equal volume of 1 M H_2SO_4 and the color development was measured in a microplate reader as the absorbance at 492 nm. Schematically both ELISA formats are illustrated in **Supplementary Figure 1**.

Statistical Analysis

Each experiment was performed at least three times and statistical analysis, was conducted using a two-tailed Student's *t*-test. Statistical probabilities (p) were expressed as * when $p < 0.05$; ** when $p < 0.01$ and *** when $p < 0.001$.

RESULTS

Firstly, we observed whether TGF-β could induce VISTA expression in human T cells, since this protein was found to mediate galectin-9-induced apoptosis in cytotoxic T lymphocytes (9). We used non-treated Jurkat T cells (CD4-positive), which express just traces of granzyme B protein (9, 16), as well as PMA-activated (activation was performed for 24 h using 100 nM PMA) Jurkat T cells which express granzyme B protein (9, 16). Cells were exposed for 24 h to 2 ng/ml TGF-β followed by detection of VISTA expression by Western blot analysis. We found that TGF-β significantly upregulated VISTA expression in resting Jurkat T cells (**Figure 1A**) while, in PMA-activated cells, VISTA levels were reduced by exposure to TGF-β compared to the non-treated cells (**Figure 1B**). In both cell types TGF-β induced phosphorylation of Smad3 transcription factor (**Supplementary Figure 2A**). We then tested cytotoxic CD8-positive TALL-104 cells. Similarly to granzyme B-expressing PMA-activated Jurkat T cells (**Figure 1B**), TGF-β (2 ng/ml for 24 h) reduced VISTA expression in TALL-104 cells (**Figure 1C**). However, Smad3 phosphorylation was upregulated by TGF-β (**Supplementary Figure 2B right panel**). The expression levels of granzyme B were downregulated by TGF-β in TALL-104 cells (**Supplementary Figure 2B, right panel**), which is in line with a previous observation reporting TGF-β-induced downregulation of granzyme B expression in cytotoxic T cells (19). Importantly, TALL-104 cells expressed Tim-3 and rather small amounts of galectin-9 (**Supplementary Figure 2B, left panel**). Expression of both proteins was not affected by TGF-β (**Supplementary Figure 2B, left panel**). We then isolated primary human T cells (all CD3 positive cells were isolated to allow for the presence of CD8-positive cytotoxic T cells, CD4-positive helper type T cells and CD4-positive cytotoxic cells). These cells were then exposed to 2 ng/ml TGF-β for 16 h (given the higher reactivity of primary T cells compared to T cell lines). Both VISTA and granzyme B expressions were lowered by TGF-β in these cells (**Figure 1D**). Primary human T cells expressed both Tim-3 and galectin-9 (**Supplementary Figure 2C**), but galectin-9 levels were very low (**Supplementary Figure 2C**). Smad3 phosphorylation was highly upregulated by TGF-β in primary T cells. We then tested human myeloid leukemia cells, which are known to express high levels of VISTA. We used the THP-1 cell line (monocytic leukemia) and more premature primary human acute myeloid leukemia (AML) blasts. In THP-1 cells, TGF-β is known to highly upregulate galectin-9 expression in a Smad3-dependent manner (a significant increase in Smad3 phosphorylation induced by TGF-β was also reported for these cells) (3, 20). Furthermore, THP-1 cells do not express detectable amounts of granzyme B protein and do not show detectable catalytic activity of this enzyme (9). However, TGF-β downregulated VISTA expression in THP-1 cells (**Figure 1E**). On the other hand, in primary AML blasts, VISTA expression was significantly upregulated by TGF-β (**Figure 1F**). Given the variation in the effects observed, we investigated whether TGF-β can induce VISTA expression in the cells, which in a resting state do not express this protein. We investigated MCF-7 human epithelial breast cancer cells, where TGF-β was reported to trigger the expression of galectin-9 (3) and discovered that TGF-β was unable to induce even traces of VISTA expression (**Figure 1G**). VISTA mRNA was also barely detectable in these cells by qRT-PCR (**Supplementary Figure 3**).

Interestingly, primary human embryonic cells express VISTA protein which is also present on their surface (16). The earlier the stage of pregnancy, the more TGF-β fetal cells produce (3). We compared primary human fetal cells taken at the amnion stage (*ca.* week 20) and chorion stage (weeks 13–14). In line with our previously reported results (3, 16), cells obtained at the chorion stage released significantly higher levels of TGF-β and expressed higher VISTA levels (**Figure 1H**). Also, we reported earlier that Smad3 phosphorylation levels are significantly higher in fetal cells obtained at chorion stage (3). Some solid tumor cells also express VISTA, which may be upregulated by TGF-β. We found that in human Wilms tumor (a type of pediatric kidney tumor) cells WT-3ab, which express VISTA, TGF-β significantly upregulated its expression (**Figure 1I**). These cells expressed small amounts of Tim-3 but higher amounts of galectin-9. Galectin-9 expression in these cells was upregulated by TGF-β, as in other cancer cells studied in the past (3), and this correlated with TGF-β-induced Smad3 phosphorylation (**Supplementary Figure 4**).

The same effect applied to non-malignant, rapidly proliferating, human keratinocytes (HaCaT). These cells express VISTA, and this expression was upregulated by 24 h exposure to 2 ng/ml TGF-β [**Figure 1J**; Smad3 activation in these cells takes place as well, though differently from the one reported for cancer and embryonic cells (3)]. Interestingly, in lymphoblasts isolated from human chronic myelogenous leukaemia (K562), which express traces of VISTA, this expression (unlike in MCF-7 cells where no VISTA protein expression is detected at all) can be induced by 24 h of exposure to 2 ng/ml TGF-β where this concentration appears to be the most effective (**Figure 1K**). Higher TGF-β concentrations (4 and 8 ng/ml) also induced VISTA expression, but the expression level was not higher compared to those observed with exposure to 2 ng/ml TGF-β. Resting K562 cells were reported to show undetectable amounts of phospho-Smad3, but this was highly upregulated by TGF-β (3).

Interestingly, most of the investigated cell types display glycosylated VISTA with a molecular weight of *ca.* 52 kDa [this phenomenon was discussed previously (9)], while others have some partially glycosylated (K562, **Figure 1K**) or non-glycosylated (molecular weight *ca.* 30 kDa; primary human embryonic cells, **Figure 1H**) VISTA. Since biologically functional VISTA is known to be glycosylated [52 kDa (9)], these results suggest that the glycosylation velocity of this protein may vary depending on the cell type. It is also possible that primary human embryonic cells store certain amounts of non-glycosylated VISTA, though the reason for this remains to be understood.

We then asked whether TGF-β-induced VISTA expression is Smad3-dependent or not. We used resting Jurkat T cells which we transfected with Smad3 siRNA (or random siRNA – negative control). Successful knockdown (in terms of biological effect) was monitored by Western blot analysis of intracellular levels of

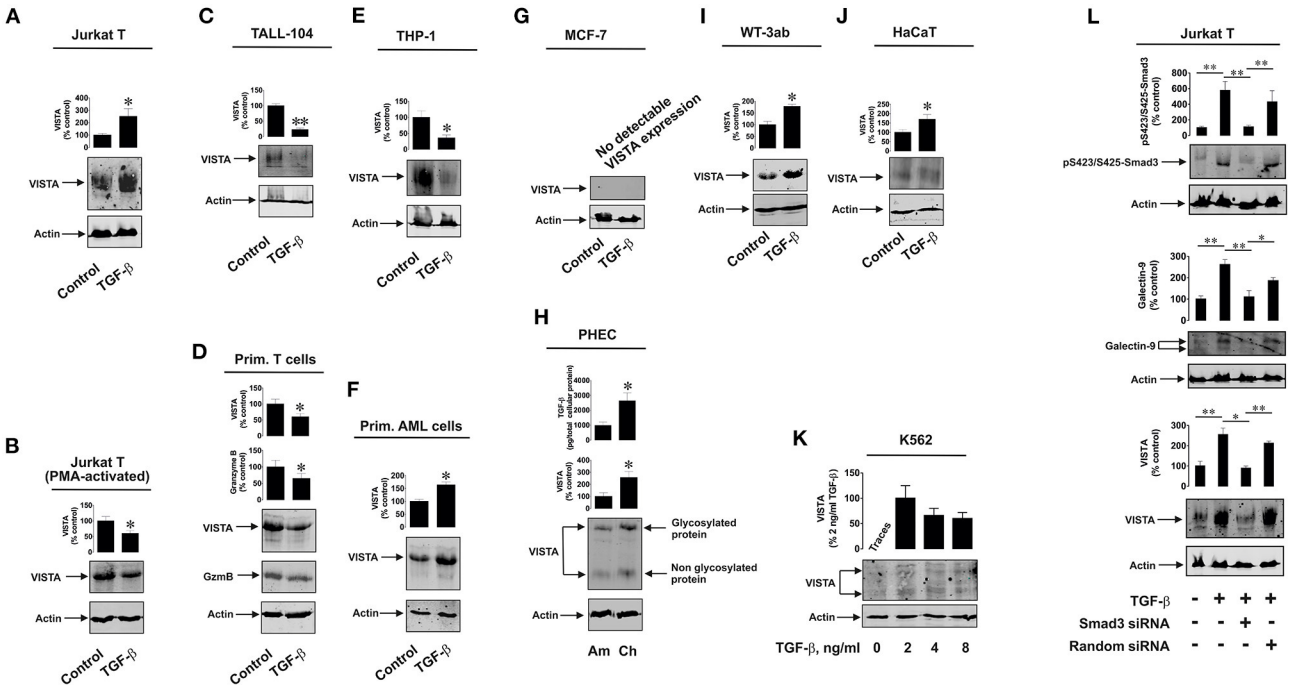

FIGURE 1 | Differential effects of TGF-β on VISTA expression in human T lymphocytes and various rapidly proliferating cell types. Resting Jurkat T cells **(A)** and those activated for 24 h with 100 nM PMA **(B)**, TALL-104 cytotoxic T cells **(C)**, primary human T lymphocytes **(D)**, THP-1 human AML cells **(E)** and primary human AML blasts **(F)** as well as MCF-7 breast cancer cells, **(G)** WT-3ab Wilms tumor cells **(I)**, non-malignant HaCaT keratinocytes **(J)** were exposed for 24 h (primary T cells – for 16 h) to 2 ng/ml TGF-β followed by Western blot detection of VISTA expression as outlined in Materials and Methods. In primary human T cells **(D)**, granzyme B protein expression was also analyzed by Western blot. Expression of VISTA and TGF-β secretion were tested in primary human embryonic cells **(H)** obtained during amnion (ca week 20) and chorion (weeks 13-14) stages. K562 cells **(K)** expressing barely detectable amounts of VISTA were exposed to 2, 4 or 8 ng/ml TGF-β for 24 h followed by Western blot analysis of VISTA expression. Finally, resting and Smad3 knockdown Jurkat T cells as well as those transfected with random siRNA (negative control siRNA) were exposed to 2 ng/ml TGF-β for 24 h followed by Western blot detection of phospho-Smad3, galectin-9 and VISTA **(L)**. Images are from one experiment representative of 4-7 which gave similar results. Quantitative data represent mean values ± SEM of 4-7 independent experiments. * $p < 0.05$ and ** $p < 0.01$ vs. control.

phosphorylated Smad3. Expressions of both VISTA and galectin-9 were induced by TGF-β and attenuated by Smad3 siRNA but not random siRNA (**Figure 1L**). This suggests that the process is Smad3-dependent.

We investigated whether the observed effects are taking place at mRNA level given the fact that TGF-β-regulated VISTA expression appeared to be Smad3 (transcription factor)-dependent. We used resting and TGF-β-treated (2 ng/ml for 24 h) Jurkat T (where TGF-β upregulates VISTA expression) and TALL-104 cells (where TGF-β treatment downregulated VISTA expression) and measured VISTA mRNA levels as outlined in Materials and Methods. We found that in Jurkat T cells TGF-β significantly upregulated VISTA mRNA levels while in TALL-104 we observed significant downregulation (**Figure 2A**). To verify that Smad3 binds VSIG (VISTA gene) directly we used ChIP qRT-PCR which confirmed that this process does take place and TGF-β significantly increased the fold of enrichment (**Figure 2B**) confirming that Smad3 can directly interact with the VSIG promoter region.

Importantly, we tested whether TGF-β impacted the cell surface presence and secretion of VISTA. We detected VISTA on the cell surface of resting and PMA-activated Jurkat T cells, TALL-104 and THP-1 cells with or without exposure to 2 ng/ml TGF-β for 24 h. The results suggested when the total amounts of VISTA were strongly downregulated (TALL-104 and THP-1 cells), VISTA surface presence was reduced. In other cases, TGF-β did not significantly impact VISTA cell surface presence (**Figure 2C**), suggesting that this growth factor mainly controls VISTA expression but not its distribution within the cell. We also measured both cell-associated and secreted protein using ELISA. We tested Jurkat T cells (**Figure 2D**), primary human T cells (**Figure 2E**), THP-1 cells (**Figure 2F**), primary human AML cells (**Figure 2G**), and HaCaT keratinocytes (**Figure 2H**). Other cell types reported in **Figure 1** did not secrete VISTA. The mean values ± SEM of cell-associated and secreted VISTA are shown in **Supplementary Table 1**. We observed that TGF-β only significantly affected VISTA secretion (upregulation) in AML cells, whereas total expression levels remained in line with our Western blot observations (**Figures 2D–H** and see also **Figures 1A–K** for comparison). This also suggests that TGF-β itself is unlikely to impact VISTA secretion in any of the cell types.

We then assessed if the differential effects observed could be due to involvement of different Smad3 co-activators – TRIM33 (tripartite motif-containing protein 33), also known

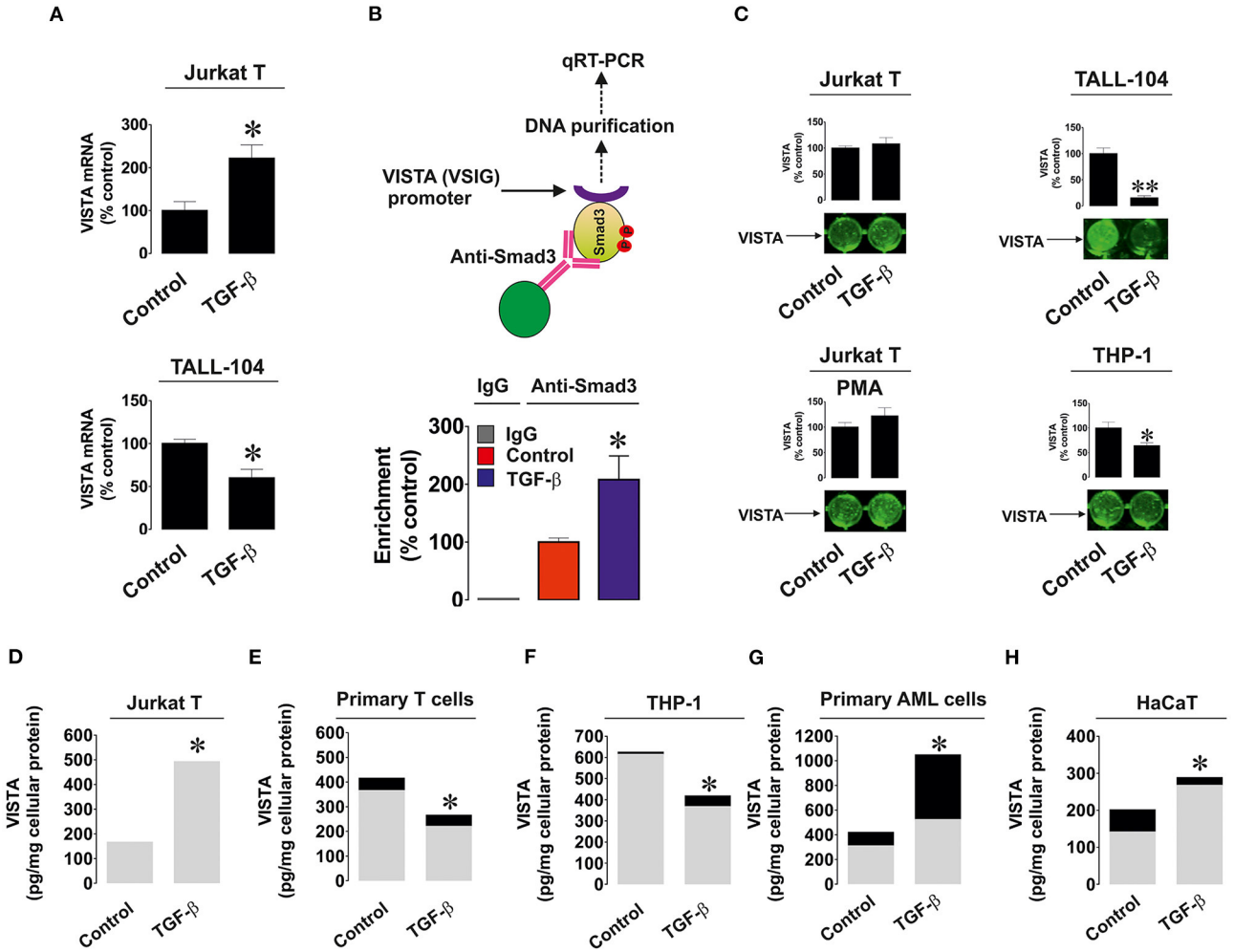

FIGURE 2 | Effects of TGF-β on expression and distribution of VISTA in various human cell types. **(A)** Jurkat T and TALL-104 cells were exposed to 2 ng/ml TGF-β for 24 h followed by total RNA isolation and detection of VISTA mRNA using qRT-PCR as outlined in Materials and Methods; **(B)** Resting Jurkat T cells and those treated for 24 h with 2 ng/ml TGF-β were subjected to ChIP followed by qRT-PCR as described in Methodology section in order to detect whether Smad3 binds to the VSIG promoter region; **(C)** Resting as well as PMA-activated Jurkat T cells, TALL-104 and THP-1 cells were exposed for 24 h to 2 ng/ml TGF-β followed by detection of cell surface-based VISTA by on-cell Western (see Materials and Methods for details); Jurkat T cells **(D)**, primary human T lymphocytes **(E)**, THP-1 AML cells **(F)**, primary AML blasts **(G)** and HaCaT keratinocytes **(H)** were exposed to 2 ng/ml TGF-β for 24 h followed by detection of cell-associated (gray color) and secreted (black color) VISTA levels. Images are from one experiment representative of 5 which gave similar results. Data are the mean values of 5 independent experiments. * $p < 0.05$ vs. control (total VISTA).

as transcriptional intermediary factor 1 gamma (TIF-1γ), and Smad4 (21). TRIM33 is known mainly to interact with Smad3 in order to induce expression of repressed genes (21), while Smad4 is used to trigger expression of non-repressed target genes. We tested resting Jurkat T cells (VISTA expression is upregulated by TGF-β), THP-1 (downregulation of VISTA expression by TGF-β), MCF-7 (no effect, since the cells do not express detectable amounts of VISTA) and HaCaT (where VISTA expression is upregulated by TGF-β). We also tested the recruitment of both co-activators by Smad3 using an ELISA-based assay (see Section Materials and Methods and **Supplementary Figure 1** for details). We found that there was no specific correlation between the effect of TGF-β on VISTA expression and the amounts of Smad4/TRIM33 accumulated in the cells or recruited by Smad3 (**Figure 3**). This suggests that the effects observed are unlikely to be due to the involvement of differential co-activators in different cell types.

DISCUSSION

VISTA has recently been reported to actively participate in the suppression of anti-cancer cytotoxic immune responses of T cells (5, 9). However, the mechanisms underlying the expression of this crucial immune checkpoint protein remain unknown. The promoter region of the VISTA gene, VSIR, contains several Smad response elements. As such, we hypothesized that the TGF-β-Smad3 pathway could be responsible for inducing

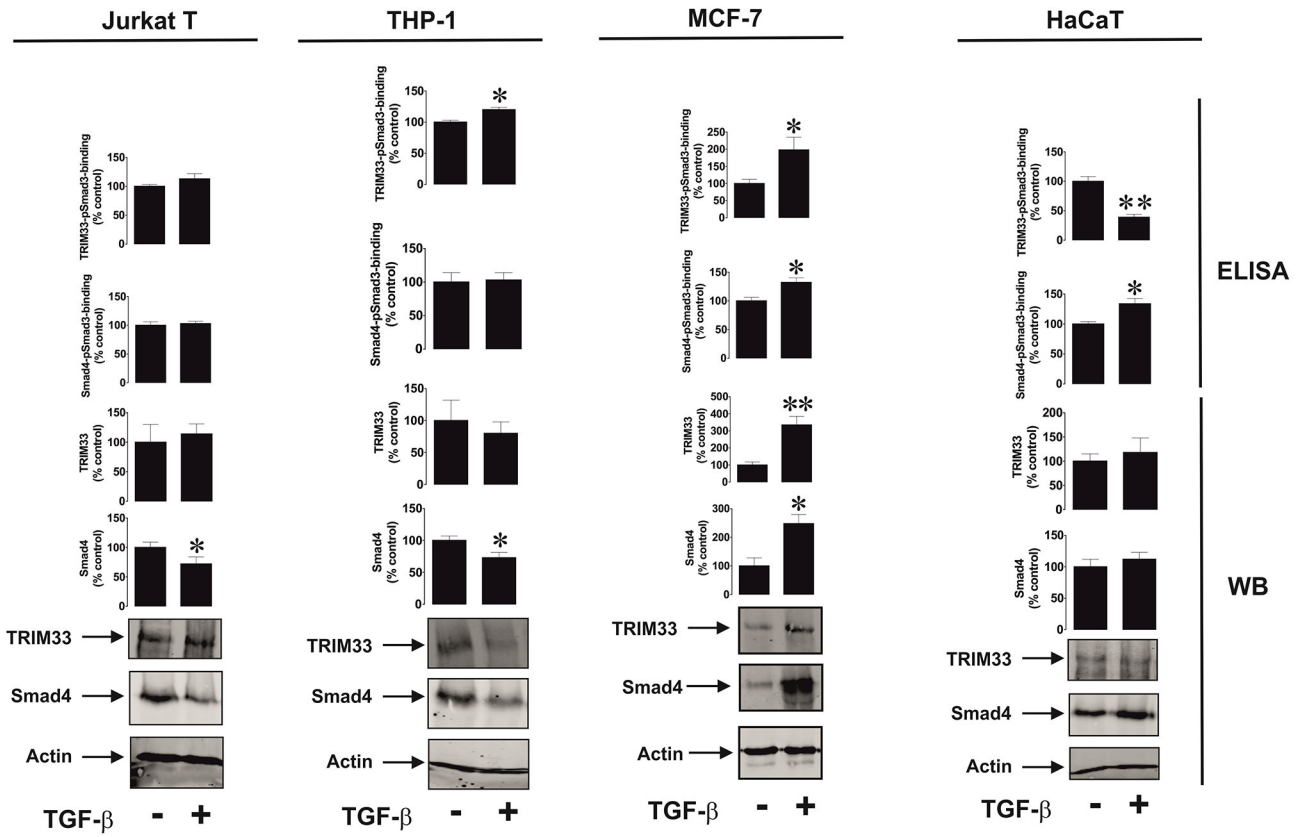

FIGURE 3 | Effects of TGF-β on Smad4 and TRIM-33 levels and phsopho-Smad3-Smad4 or phsopho-Smad3-TRIM33 interactions in a variety of rapidly proliferating human cells. Jurkat T, THP-1, MCF-7 and HaCaT cells were exposed to 2 ng/ml TGF-β for 24 h followed by Western blot detection of Smad4/TRIM-33 levels as well as ELISA-based analysis of phospho-Smad3-Smad4 or phospho-Smad3-TRIM33 interactions. Images are from 1 experiment representative of 4 which gave similar results. Quantitative data represent mean values ± SEM of 4 independent experiments. * $p < 0.05$ and ** $p < 0.01$ vs. control.

VISTA expression. The experiments showed that TGF-β-induced Smad3 activation led to an increase in VISTA expression in various cell types including resting CD4-positive Jurkat T cells, primary human AML blasts derived from myeloid cell precursors, primary human embryonic cells, Wilms tumor cells, chronic AML cells and HaCaT keratinocytes. In other cell types studied – PMA-activated, granzyme B expressing Jurkat T cells with cytotoxic activity, cytotoxic CD8-positive TALL-104 cells, primary CD3-positive human T lymphocytes (in both cell types, the overall granzyme B expression level is high) and monocytic AML THP-1 cells [which, unlike cytotoxic T cells, do not express detectable amounts of granzyme B protein (9)] – VISTA expression was reduced.

The biological reason for the observed downregulatory effects in various types of T cells described above is most likely their biological function associated with cytotoxic activity (granzyme B expression is used as a marker of their cytotoxic activity). As we have recently reported, galectin-9 interacts with VISTA on the surface of granzyme B-expressing T cells, which leads to leakage of granzyme B from intracellular granules, resulting in its activation (9). As such, these T cells may undergo programmed death mediated by VISTA. As seen in **Figure 1D** and **Supplementary Figure 2**, granzyme B expression is reduced by exposure of the cells to TGF-β, which is in line with previous observations (19). With monocytic AML cells, which do not express detectable amounts of granzyme B protein (9), this biological response has probably more complex reasons. THP-1 cells secrete high levels of galectin-9, especially when pre-treated with PMA or other triggers of exocytosis (such as latrotoxin, or Toll-like receptor (TLR) ligands) (20). They are also capable of secreting VISTA. Importantly, secretion of both proteins may be required to suppress cytotoxic immune attack conducted by T cells. However, a certain ratio of the amounts of galectin-9 and VISTA secreted is important to achieve the immunosuppressive effect, as we have recently shown (9). TGF-β induces galectin-9 expression in THP-1 cells but not its secretion (3). Upregulation of VISTA expression could potentially lead to increased level of its translocation onto the cell surface with possible shedding, leading to increased levels of soluble VISTA (the evidence of such an effect can be seen in **Figure 2F**). As a result, this kind of response could be required to sustain an effective ratio of secreted galectin-9 and VISTA proteins.

Importantly, TGF-β was only able to induce VISTA expression in cells which already express detectable amounts of this protein.

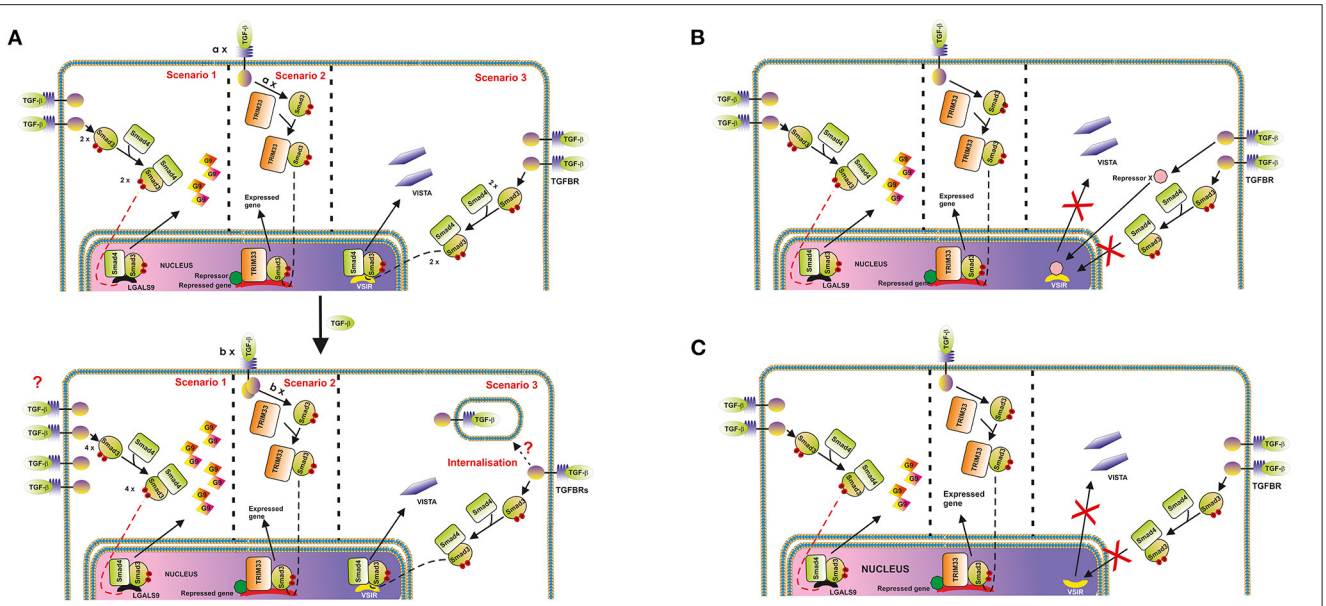

FIGURE 4 | Possible mechanisms underlying the differential regulation of protein (and in particular, VISTA) expression by the TGF-β-Smad3 pathway. **(A)** Changes in cell surface-based TGFBR levels. An example where galectin-9 expression is upregulated, and VISTA is downregulated is shown. The key message of this scheme is that the expression of target proteins could be differentially regulated by the TGF-β-Smad3 pathway, recruiting Smad4/TRIM33 co-activators. Differential responses are possibly determined by alterations of TGFBR levels on the surface of target cells. In the second scenario, "a" and "b" represent numbers of respective protein molecules. **(B)** Possibility of activation of a hypothetical protein-repressor of VSIG is depicted; **(C)** TGF-β-triggered changes in the localization of VSIG-containing locus during nuclear compartmentalisation in cell types where VISTA is downregulated by TGF-β (most likely scenario).

If cells did not express VISTA (MCF-7), no TGF-β-dependent induction was observed (as it can be seen from **Figure 1G**). Smad3 was obviously responsible for the process of TGF-β-induced VISTA expression. Knock-down of Smad3 expression by siRNA led to attenuation of TGF-β-induced VISTA expression in Jurkat T cells (**Figure 1L**). Further experiments demonstrated that the observed effects take place on both protein and mRNA levels. Furthermore, Smad3 was found to directly bind to the VSIG (VISTA gene) promoter region using ChIP followed by qRT-PCR (**Figures 2A,B**).

However, it is necessary to understand how such a differential effect of TGF-β on VISTA expression can be achieved biochemically. The activities of the Smad3 co-activators Smad4 and TRIM33 did not appear to determine any differences in response (**Figure 3**). Clearly, some cells use more Smad4 leading to reduction in its quantity, without substantially affecting the production and recruitment of TRIM33 by Smad3. This applies to resting Jurkat T cells and THP-1 cells, where the effects of TGF-β on VISTA expression were opposing. MCF-7 upregulate the amounts and usage of both co-activators, while VISTA expression was not induced in these cells. HaCaT cells, which respond to exposure to TGF-β by upregulation of VISTA expression, showed increased Smad3-Smad4 interaction activity and decreased TRIM33 recruitment induced by TGF-β (**Figure 3**).

These results suggest that the differential activities of Smad4 and TRIM33 are unlikely to contribute to achieving responses with TGF-β-induced changes in VISTA expression in various cell types. Importantly, VISTA expression is most likely to be activated by Smad3 in partnership with Smad4. TRIM33 is involved in Smad3-dependent de-repression of target genes (21). As shown in the **Figure 1G**, in MCF-7 cells, where VISTA gene VSIR is most likely repressed, TGF-β failed to induce its expression. The same is most likely to apply to galectin-9, where the TGF-β-Smad3 pathway was able to upregulate even very low expression levels of this protein (3).

Importantly, the receptors recognizing TGF-β could be internalized by the cell when complexed to its ligand (22–24). Furthermore, the amount of active TGF-β receptor (TGFBR) molecules on the cell surface could be increased in the presence of the ligand. This phenomenon was reported for several types of receptors including TGFBRs (22–24) and Toll-like receptors (TLRs) (25).

Thus, one could hypothesize that in cells where VISTA is upregulated, the respective number of active TGFBR molecules on the cell surface at each time point may either increase upon stimulation with TGF-β or remain unchanged. Conversely, in cells where VISTA is downregulated, the number of appropriate TGFBR molecules may be reduced. As such, the number of VISTA molecules produced will decrease. This proposed regulatory pathway is depicted in **Figure 4A**. However, TGF-β-induced Smad3 activation which took place regardless its effect on VISTA expression, which suggests that the strategy described above is unlikely to be involved.

On the other hand, one cannot rule out the involvement of repressing transcription factors like ATF1, which is known to

participate in TGF-β-induced Smad3-dependent downregulation of granzyme B expression (19). Specifically to ATF1, unlike the granzyme B gene promoter region, the promoter region of VSIR (a gene which encodes VISTA) does not have ATF1 response elements [CREB/ATF response elements ACGTAA or ACGTCC (19)]. If the cells express ATF1, and granzyme B, TGF-β will downregulate expression of this enzyme, however, with VISTA the effect is differential. This mechanism is shown in the **Figure 4B**.

In our view, the most likely molecular mechanism underlying the observed cell function-dependent differential impact of TGF-β on VISTA expression is associated with nuclear compartmentalisation (chromatin re-organization). This phenomenon has recently been investigated and thoroughly discussed as a fundamental molecular mechanism underlying regulation of gene expression (26). Importantly, this kind of regulation approach was reported for T cell development (26, 27). The loci containing genes, the expression of which needs to be downregulated or repressed can be re-located to the periphery of the nucleus, while active genes are normally biased toward the nuclear interior (26). As such, in the cells, which would benefit from downregulation of VISTA expression in response to the presence of TGF-β, respective loci may be re-localized accordingly, while other TGF-β-Smad3 inducible genes [like LGALS9 encoding galectin-9, which is upregulated by TGF-β in THP-1 cells (3) while VISTA is downregulated] can remain active. This kind of re-location to the periphery and possible association with nuclear lamina is sufficient to downregulate expression of respective genes (26). This regulatory strategy is presented in the **Figure 4C**.

The ability of T cell subsets that do not express granzyme B protein to respond to TGF-β by increasing VISTA expression may be the crucial biochemical mechanism used by granzyme B-negative T cell lymphoma/leukemia cells. Apoptotic T cells, which are always present in such cases, release TGF-β (15, 28). TGF-β could then induce VISTA expression which suppresses cytotoxic T lymphocytes trying to attack malignant T cells.

Taken together, our results have uncovered the biochemical phenomenon of differential control of VISTA expression in human T cells and various types of rapidly proliferating cells, including several types of cancer cells, fetal cells and keratinocytes. These results indicate the involvement of a complex molecular mechanism controlling expression of the critical immune checkpoint protein known as VISTA. Activation of this regulatory pathway could lead to differential outcomes which are most likely determined by the specific cell functions and type of interaction with immune and target cells.

DATA AVAILABILITY STATEMENT

The original contributions presented in the study are included in the article/**Supplementary Material**, further inquiries can be directed to the corresponding author/s.

ETHICS STATEMENT

The studies involving human participants were reviewed and approved by Research Ethics Committee (REC). Primary human AML mononuclear blasts (AML-PB001F, newly diagnosed/untreated) obtained from AllCells (Alameda, CA, USA) were used following ethical approval (REC reference: 16-SS-033). Primary human T cell work received ethical approval from the Medizinische Ethikkommission der Carl von Ossietzky Universität Oldenburg. Placental tissues and amniotic fluids were collected after obtaining informed written consent from pregnant women at the University Hospital Bern, Inselspital following ethical approval. The patients/participants provided their written informed consent to participate in this study.

AUTHOR CONTRIBUTIONS

SS performed majority of the experiments together with IY. EF-K, SR, MP, and JK contributed to performing the experiments on cytotoxic T cells. NM and BG performed isolation and experiments on primary human T cells. NA, EF-K, and SB completed the work with primary embryonic cells. VS designed the study and planned all the experiments together with EF-K and BG and analyzed the data. VS, EF-K, and BG wrote the manuscript. All authors contributed to the article and approved the submitted version.

ACKNOWLEDGMENTS

This work was partly supported by the Swiss Batzebär grant (to EF-K and SB). Also, this project was partly supported by Intramural Funding from the School of Medicine and Health Sciences, University of Oldenburg (FP 2017-013).

SUPPLEMENTARY MATERIAL

The Supplementary Material for this article can be found online at: https://www.frontiersin.org/articles/10.3389/fmed.2022.790995/full#supplementary-material

REFERENCES

1. Buckle I, Guillerey C. Inhibitory Receptors and Immune Checkpoints Regulating Natural Killer Cell Responses to Cancer. *Cancers.* (2021) 13:4263. doi: 10.3390/cancers13174263
2. Yoo MJ, Long B, Brady WJ, Holian A, Sudhir A, Gottlieb M. Immune checkpoint inhibitors: An emergency medicine focused review. *Am J Emerg Med.* (2021) 50:335–44. doi: 10.1016/j.ajem.2021.08.038
3. Selno ATH, Schlichtner S, Yasinska IM, Sakhnevych SS, Fiedler W, Wellbrock J, et al. Transforming growth factor beta type 1 (TGF-beta) and hypoxia-inducible factor 1 (HIF-1) transcription complex as master regulators of the immunosuppressive protein galectin-9 expression in human cancer and embryonic cells. *Aging.* (2020) 12:23478–96. doi: 10.18632/aging.202343
4. Yasinska IM, Goncalves Silva I, Sakhnevych S, Gibbs BF, Raap U, Fasler-Kan E, et al. Biochemical mechanisms implemented by human acute myeloid leukemia cells to suppress host immune surveillance. *Cell Mol Immunol.* (2018) 15:989–91. doi: 10.1038/s41423-018-0047-6

5. Lines JL, Pantazi E, Mak J, Sempere LF, Wang L, O'Connell S, et al. VISTA is an immune checkpoint molecule for human T cells. *Cancer Res.* (2014) 74:1924–32. doi: 10.1158/0008-5472.CAN-13-1504
6. Wang L, Rubinstein R, Lines JL, Wasiuk A, Ahonen C, Guo Y, et al. VISTA, a novel mouse Ig superfamily ligand that negatively regulates T cell responses. *J Exp Med.* (2011) 208:577–92. doi: 10.1084/jem.20100619
7. Lines JL, Sempere LF, Broughton T, Wang L, Noelle R. VISTA is a novel broad-spectrum negative checkpoint regulator for cancer immunotherapy. *Cancer Immunol Res.* (2014) 2:510–7. doi: 10.1158/2326-6066.CIR-14-0072
8. Xie X, Chen C, Chen W, Jiang J, Wang L, Li T, et al. Structural basis of VSIG3: the ligand for VISTA. *Front Immunol.* (2021) 12:625808. doi: 10.3389/fimmu.2021.625808
9. Yasinska IM, Meyer NH, Schlichtner S, Hussain R, Siligardi G, Casely-Hayford M, et al. Ligand-receptor interactions of galectin-9 and VISTA suppress human T lymphocyte cytotoxic activity. *Front Immunol.* (2020) 11:580557. doi: 10.3389/fimmu.2020.580557
10. Nagae M, Nishi N, Nakamura-Tsuruta S, Hirabayashi J, Wakatsuki S, Kato R. Structural analysis of the human galectin-9 N-terminal carbohydrate recognition domain reveals unexpected properties that differ from the mouse orthologue. *J Mol Biol.* (2008) 375:119–35. doi: 10.1016/j.jmb.2007.09.060
11. Im E, Sim DY, Lee HJ, Park JE, Park WY, Ko S, et al. Immune functions as a ligand or a receptor, cancer prognosis potential, clinical implication of VISTA in cancer immunotherapy. In: *Seminars in cancer biology.* (2021). doi: 10.1016/j.semcancer.2021.08.008
12. Popp FC, Capino I, Bartels J, Damanakis A, Li J, Datta RR, et al. Expression of immune checkpoint regulators IDO, VISTA, LAG3, and TIM3 in resected pancreatic ductal adenocarcinoma. *Cancers.* (2021) 13:2689. doi: 10.3390/cancers13112689
13. Prokhorov A, Gibbs BF, Bardelli M, Ruegg L, Fasler-Kan E, Varani L, et al. The immune receptor Tim-3 mediates activation of PI3 kinase/mTOR and HIF-1 pathways in human myeloid leukaemia cells. *Int J Biochem Cell Biol.* (2015) 59:11–20. doi: 10.1016/j.biocel.2014.11.017
14. Stock C, Ambros IM, Lion T, Zoubek A, Amann G, Gadner H, Ambros PF. Cancer Genetic changes of two Wilms tumors with anaplasia and a review of the literature suggesting a marker profile for therapy resistance. *Genet Cytogenet.* (2002) 135:128–38. doi: 10.1016/S0165-4608(01)00647-1
15. Yasinska IM, Sakhnevych SS, Pavlova L, Teo Hansen Selno A, Teuscher Abeleira AM, Benlaouer O, et al. The tim-3-galectin-9 pathway and its regulatory mechanisms in human breast cancer. *Front Immunol.* (2019) 10:1594. doi: 10.3389/fimmu.2019.01594
16. Schlichtner S, Meyer NH, Yasinska IM, Aliu N, Berger SM, Gibbs BF, et al. Functional role of galectin-9 in directing human innate immune reactions to Gram-negative bacteria and T cell apoptosis. *Int Immunolpharmacol.* (2021) 100:108155. doi: 10.1016/j.intimp.2021.108155
17. Goncalves Silva I, Gibbs BF, Bardelli M, Varani L, Sumbayev VV. Differential expression and biochemical activity of the immune receptor Tim-3 in healthy and malignant human myeloid cells. *Oncotarget.* (2015) 6:33823–33. doi: 10.18632/oncotarget.5257
18. Deng J, Li J, Sarde A, Lines JL, Lee YC, Qian DC, et al. Hypoxia-induced VISTA promotes the suppressive function of myeloid-derived suppressor cells in the tumor microenvironment cancer. *Immunol Res.* (2019) 7:1079–90. doi: 10.1158/2326-6066.CIR-18-0507
19. Thomas DA, Massague J. TGF-beta directly targets cytotoxic T cell functions during tumor evasion of immune surveillance. *Cancer Cell.* (2005) 8:369–80. doi: 10.1016/j.ccr.2005.10.012
20. Teo Hansen Selno A, Schlichtner S, Yasinska IM, Sakhnevych SS, Fiedler W, Wellbrock J, et al. High mobility group box 1 (HMGB1) induces toll-like receptor 4-mediated production of the immunosuppressive protein galectin-9 in human cancer cells. *Front Immunol.* (2021) 12:675731. doi: 10.3389/fimmu.2021.675731
21. Massague J, Xi Q. TGF-beta control of stem cell differentiation genes. *FEBS Lett.* (2012) 586:1953–8. doi: 10.1016/j.febslet.2012.03.023
22. Guglielmo GMDi, Le Roy C, Goodfellow AF, Wrana JL. Distinct endocytic pathways regulate TGF-β receptor signalling and turnover. *Nature Cell Biology.* (2003) 5:410–21. doi: 10.1038/ncb975
23. Mitchell H, Choudhury A, Pagano RE, Leof EB. Ligand-dependent and -independent transforming growth factor-β receptor recycling regulated by clathrin-mediated endocytosis and Rab11. *Molec Biol Cell.* (2004) 15:4166–78. doi: 10.1091/mbc.e04-03-0245
24. Miller DS, Bloxham RD, Jiang M, Gori I, Saunders RE, Das D, et al. The dynamics of TGF-beta signaling are dictated by receptor trafficking via the ESCRT machinery. *Cell Reports.* (2018) 25:1841–55.e5. doi: 10.1016/j.celrep.2018.10.056
25. Barton GM, Kagan JC. A cell biological view of Toll-like receptor function: regulation through compartmentalization. *Nat Rev Immunol.* (2009) 9:535–42. doi: 10.1038/nri2587
26. Meldi L, Brickner JH. Compartmentalization of the nucleus. *Trends Cell Biol.* (2011) 21:701–8. doi: 10.1016/j.tcb.2011.08.001
27. Spilianakis CG, Flavell RA. Long-range intrachromosomal interactions in the T helper type 2 cytokine locus. *Nat Immunol.* (2004) 5:1017–27. doi: 10.1038/ni1115
28. Chen W, Frank ME, Jin W, Wahl SM. TGF-beta released by apoptotic T cells contributes to an immunosuppressive milieu. *Immunity.* (2001) 14:715–25. doi: 10.1016/S1074-7613(01)00147-9

Conflict of Interest: The authors declare that the research was conducted in the absence of any commercial or financial relationships that could be construed as a potential conflict of interest.

Publisher's Note: All claims expressed in this article are solely those of the authors and do not necessarily represent those of their affiliated organizations, or those of the publisher, the editors and the reviewers. Any product that may be evaluated in this article, or claim that may be made by its manufacturer, is not guaranteed or endorsed by the publisher.

frontiers | Frontiers in Medicine

ORIGINAL RESEARCH
published: 05 April 2022
doi: 10.3389/fmed.2022.778230

Does Autologous Transfusion Decrease Allogeneic Transfusion in Liposuction Surgery of Lymphedema Patients?

Linfeng Chen[1†], *Kun Chang*[2†], *Yan Chen*[1], *Zhenhua Xu*[3] *and Wenbin Shen*[2*]

[1] Department of Blood Transfusion, Beijing Shijitan Hospital, Capital Medical University, Beijing, China, [2] Department of Lymph Surgery, Beijing Shijitan Hospital, Capital Medical University, Beijing, China, [3] HealSci Technology Co. Ltd., Beijing, China

Background and Objective: Liposuction is an effective treatment for fat disposition in lymphedema. Blood transfusion has been seldom investigated in lymphedema liposuction surgery. The purpose of the study was to analyze clinical factors associated with blood transfusion in liposuction surgery of lymphedema patients and compare the autologous and allogeneic transfusion patterns.

Methods: A total of 1,187 cases of liposuction due to lymphedema were recruited. Demographic, laboratory tests and operation information were collected. Patients were divided into a transfusion and a non-transfusion group. Different transfusion patterns were compared and analyzed.

Results: Between the two groups, there is a significant difference in postoperative hemoglobin levels, and as well as gender, age, surgery duration, body weight change, intraoperative transfusion volume and blood loss, hospital length of stay, and surgical site distribution. There is a significant difference in the comparison of hospital stay length, autologous transfusion volume, combined allogeneic volume, operative blood loss, intraoperative transfusion volume, and change in hemoglobin levels between predonation and acute normovolemic hemodilution (ANH) transfusion. In comparison with the allogeneic transfusion-only patients, the mean allogeneic transfusion volume in either ANH group, predonated transfusion group, or mixed group is statistically lower. Allogeneic transfusion volume in the predonated-only group is significantly lower than that of either the ANH-only group or the mixing ANH with predonation group. Ordinary least squares regression analysis suggests that autologous transfusion in the ANH-only mode is statistically associated with allogeneic transfusion.

Conclusions: This study described the blood transfusion in lymphedema liposuction surgery and compared autologous and allogeneic transfusion patterns in these patients. Autologous transfusion can reduce the transfusion volume of allogeneic blood and might be a beneficial mode of transfusion in these patients.

Keywords: autologous transfusion, allogeneic transfusion, lymphedema, liposuction surgery, transfusion patterns

OPEN ACCESS

Edited by:
Vadim V. Sumbayev,
University of Kent, United Kingdom

Reviewed by:
Faranak Behnaz,
Shahid Beheshti University of Medical Sciences, Iran
Okuno Takuya,
Kyoto University, Japan

***Correspondence:**
Wenbin Shen
swb_216@163.com

[†]These authors have contributed equally to this work

Specialty section:
This article was submitted to Pathology, a section of the journal Frontiers in Medicine

Received: *16 September 2021*
Accepted: *14 February 2022*
Published: *05 April 2022*

Citation:
Chen L, Chang K, Chen Y, Xu Z and Shen W (2022) Does Autologous Transfusion Decrease Allogeneic Transfusion in Liposuction Surgery of Lymphedema Patients? Front. Med. 9:778230. doi: 10.3389/fmed.2022.778230

INTRODUCTION

Lymphedema is a chronic condition in which fluids and fibers accumulate in bodies due to primary or secondary lymphatic obstructions (1). The manifestation of lymphedema includes swelling, pain, and skin hardening. Although it is an incurable disease, multiple therapies can help to release the symptom and improve the quality of life. The treatment for lymphedema can be mainly divided into nonsurgical techniques (2), such as exercise and bandage, and surgical techniques (3), such as anastomosis. In many cases, the deposited adipose tissue might not be reduced merely through bandaging or anastomosing the lymphatic duct. Therefore, liposuction is often needed to complement the reconstruction process (4).

Liposuction is a technique that can remove excess fat tissues with suction-pump devices. In plastic surgery, it is generally used to reduce localized adipose tissue within the abdomen, breast, upper limbs, and lower limbs (5). Blood loss and fluid management have always been a major issue in the process of liposuction (6). To minimize blood loss, Illouz (7) in the 1970s first introduced the concept of "wet liposuction" with a small amount of diluted hyaluronidase and normal saline injected subcutaneously. The wet technique is still accompanied by significant volumes of blood loss. Later, in the 1980s, dermatologists modified the process by pumping fluid containing saline and epinephrine into the area preoperatively (8). This produces tumescent and vasoconstriction effects, thus further lowering the blood loss.

Although tumescent technique has made it safer for surgeons to practice liposuction, hemodynamic stability and blood loss are still the main considerations during the operation that can influence aspirated volumes (9). Under some circumstances, especially when the aspirated volume exceeds 1,500 ml, blood transfusion is required to correct hypoxic symptom or coagulation abnormalities in the patients. To the best of the authors' knowledge, there are very few articles that investigate blood transfusion in liposuction surgery of lymphedema patients to date.

Therefore, this study was designed to describe and detect significant clinical factors associated with blood transfusion in lymphedema liposuction surgery. Meanwhile, different modes of transfusion (i.e., autologous or allogeneic) were analyzed to explore the best transfusion modes for liposuction surgery in lymphedema patients.

METHODS

Study Design, Participant, and Data Collection

A retrospective study design was adopted. Patients underwent liposuction in the Department of Lymphatic Surgery of Beijing Shijitan Hospital, Capital Medical University, from January 1, 2016 to August 31, 2019, were recruited as study population. Transfusion records and medical documents were retrospectively examined to extract the demographic characteristics (age, gender, and body weight), clinical data (diagnosis, admission date, and length of stay), laboratory test [pre- and postoperative prothrombin time (PT), activated partial thromboplastin time (APTT), fibrinogen (FIB), and hemoglobin (Hb)], and surgery-related information (intraoperative blood loss, autologous or allogeneic transfusion volume, transfusion component, operation duration, and surgical site). The collection was conducted by two independent investigators to ensure the exactness and correctness of data. The ethics of this study was discussed and approved by the local committee for the protection of patient's privacy at Beijing Shijitan Hospital.

Transfusion Implementation Protocol

According to the regulation enacted by Beijing Shijitan Hospital, patients are not allowed to transfuse allogeneic red blood cell (RBC) until intraoperative blood loss exceeds 600 ml under a normal preoperative hemoglobin level and coagulation function. The autologous transfusion is not dictated by this regulation. Plasma transfusion is performed when the intraoperative RBC transfusion volume is >4 U. For the postoperation management, the indication for transfusing RBC is hemoglobin <80 g/L in combination with high content of RBC in drainage fluid or occurrence of hypoxia symptoms. The indication of transfusing plasma is as follows: (1) drastic bleeding (been transfused with RBC at 40–80 mg/kg within 24 h); (2) bleeding (infiltration of blood out of the wound, large volume of drainage fluid, PT extension >3 s, APTT extension >1.5 times or international normalized radio, INR >2); (3) disseminated intravascular coagulation (DIC); and (4) complicated with hepatic diseases. Predonated autologous transfusion was conducted in accordance with the guideline of the American Association of Blood Banks (AABB) whose indication is preoperative Hb > 110 g/L, hematocrit > 0.33, normal coagulation time, and normal cardiopulmonary, hepatic and renal function. A total of 200–400 ml of whole blood was used for predisposition. Concerning the intraoperative acute normovolemic hemodilution (ANH), two venous routes were created after anesthesia. One route is used for blood collection at 200 ml every 5 min. Collection indication is hematocrit >25%, albumin >30 g/L, and Hb around 100 g/L. Collection volume ranged from 200 to 1,600 ml. The other route is used to transfuse the plasma exchange fluid.

Primary and Secondary Measurements

Our primary measurements were age, gender, surgical site, body weight change, surgery time, preoperative Hb level. These variables were used to assess their relationship with blood transfusion. The secondary measurement was transfusion volume and different transfusion modes. Correlation was evaluated between these variables.

Statistical Analysis

Statistical analyses were performed through the use of Python 3.6 software. Normality distribution was confirmed by Kolmogorov–Smirnov test with "scipy" package (version 1.2.0). To describe nonnormally distributed continuous data, median and percentiles (25th and 75th) were presented, whereas mean and standard deviation (SD) were calculated to represent normally distributed data (package "tableone," version 0.6.0). Nonparametric (Kruskal–Wallis test) and

TABLE 1 | Summary of patients' demographic and clinical information.

Items	Nontransfusion group	Transfusion group	*p*-value	Statistic
Gender			<0.001	Chi-square
Female, *n*, (%)	726 (94.3)	352 (84.4)		
Male, *n*, (%)	44 (5.7)	65 (15.6)		
Age, years, [median (range)]	54 (3, 81)	53 (12, 82)	0.04	Kruskal–Wallis
Length of stay, days, [median (range)]	7 (1, 30)	7 (5, 47)	<0.001	Kruskal–Wallis
Surgical site			<0.001	Chi-square
Upper limb, *n*, (%)	301 (43.0)	21 (4.3)		
Lower limb, *n*, (%)	384 (54.8)	456 (93.6)		
Others, *n*, (%)	15 (2.2)	10 (2.1)		
Intraoperative transfusion volume, ml, [median (range)]	0 (0, 0)	400 (200, 2200)	<0.001	Kruskal–Wallis
Intraoperative blood loss, ml, [median (range)]	400 (0, 1500)	800 (0, 2000)	<0.001	Kruskal-Wallis
Body weight change, Kg, [median (range)]	5.5 (0.0, 38)	11.1 (0, 35.4)	<0.001	Kruskal-Wallis
Surgery duration, min, (mean ± SD)	152.4 ± 78.2	235.0±96.8	<0.001	Two-Sample *t*-test
Preoperative Hb, g/L, *n*, (%)			0.789	Chi-square
<110	23 (3.1)	13 (3.6)		
≥110	715 (96.9)	345 (96.4)		
Postoperative Hb, g/L, *n*, (%)			<0.001	Chi-square
80–100	129 (17.8)	104 (29.0)		
<80	12 (1.7)	12 (3.3)		
≥100	584 (80.6)	243 (67.7)		

A total number of 1,187 patients underwent liposuction surgery were recruited. Data are expressed as mean ± SD or median and percentile unless otherwise stated. Body weight change equals preoperative minus postoperative. Surgery duration was transformed by Box-Cox into normal distribution and then tested.

parametric methods (*t*-test) were adopted depending on distribution and equal variance. Box-Cox method was tentatively used to transform deviated data into normal distribution. For categorical data, chi-square test was used to detect the difference. Correlation was determined using Pearson's or Spearman's analysis depending on data type (continuous or categorical) and distribution (normal or nonnormal). Ordinary least squares (OLS) regression analysis was utilized to further explore the factors that can statistically influence allogeneic transfusion. Allogeneic transfusion volume was regarded as dependent variable whereas different modes of autologous transfusion volumes were independent variables. Intraoperative blood loss was adjusted with the three modes of autologous transfusion (predonated only, ANH only, and mixed). Statistical significance was set at two-tailed $p < 0.05$.

RESULTS

Patient's Characteristics

From January 2016 to August 2019, there were 3,467 cases of lymphatic surgery, which include 856 cases of thoracic duct plasty, 671 cases of venous anastomosis, 614 cases of lymphangiography, 1,187 cases of liposuction, and 139 cases of other surgeries. The liposuction surgery had a higher rate of intraoperative blood transfusion (417/1187, 35.1%), which accounts for 96.4% of the entire perioperative blood transfusion volume of all surgeries. Other surgeries than liposuction had an intraoperative blood transfusion rate of 1–14%. Few patients had intraoperative plasma transfusion. According to the China's transfusion guideline, 1 U (150 ml) of RBC is defined as RBC products extracted from 200 ml whole blood. Based on whether to implement RBC transfusion or not, patients underwent liposuction were divided into transfusion and nontransfusion groups. The demographic and clinical characteristics of the two groups are shown in **Table 1**.

There is no statistical significance in the comparison of preoperative Hb concentrations between transfusion and nontransfusion groups. However, there is significant difference in postoperative Hb levels, and also gender, age, surgery duration, body weight change, intraoperative transfusion volume, intraoperative blood loss, hospital length of stay, and surgical site distribution. Intraoperative blood transfusion is statistically associated with longer surgical time ($p < 0.001$), larger body weight change ($p < 0.001$), and larger intraoperative blood loss ($p < 0.001$). Patients who received transfusion had a higher proportion of lower limb surgery compared with nontransfusion (93.6 vs. 54.8%, $p < 0.001$). Although the comparison of age is statistically significant, this significance is very borderline ($p = 0.04$) and the medians are quite approximate (53 vs. 54). The gender ratio is remarkably deviated, with female predominant to male in either transfusion or nontransfusion groups. Despite a less predominant gender constitution, male patient was more likely to transfuse than female patient (odds ratio = 3.05, $p < 0.001$).

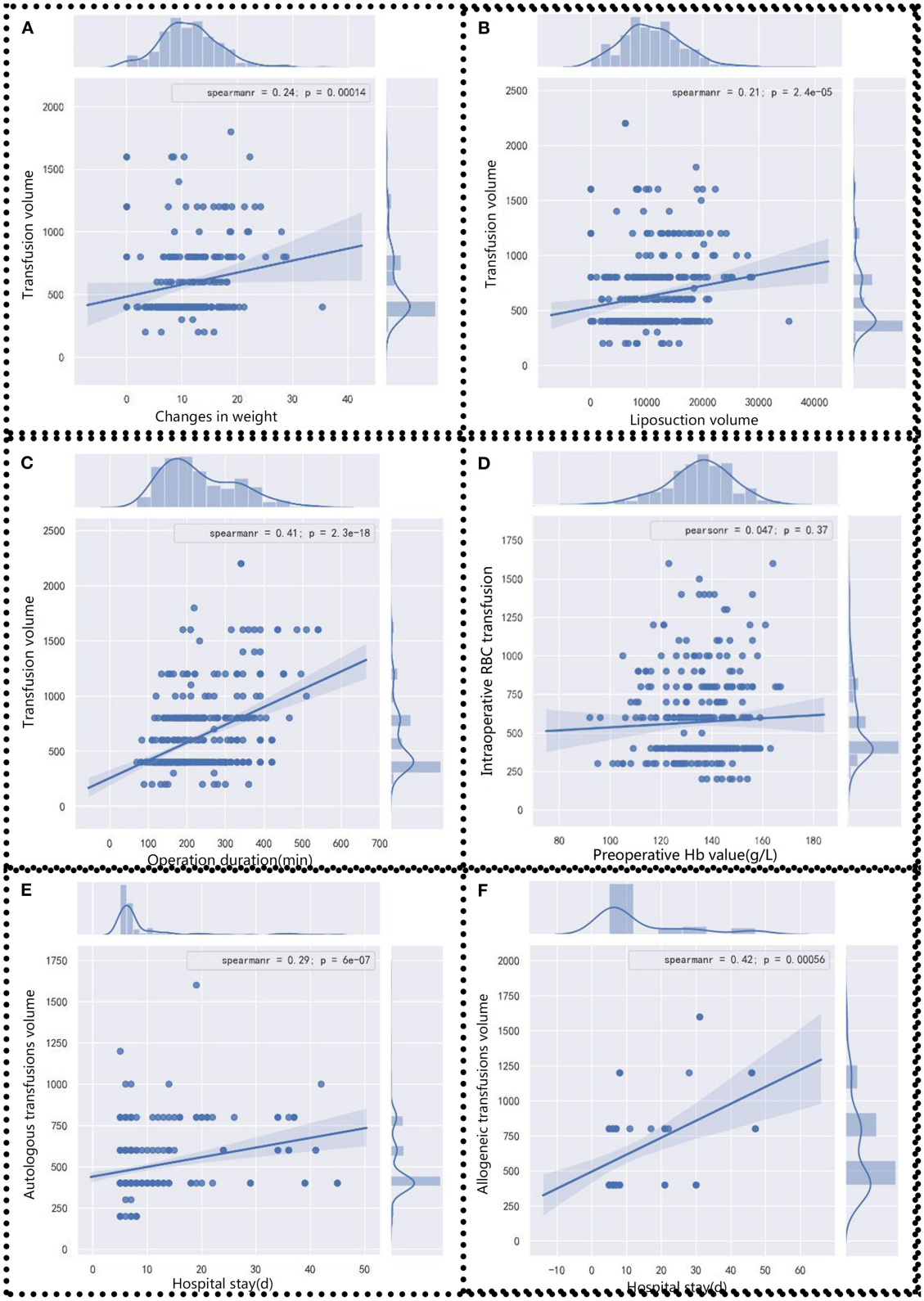

FIGURE 1 | Correlation analysis between clinical factors and blood transfusion volume. Blood transfusion volumes were analyzed with **(A)** body weight change, **(B)** liposuction volume, **(C)** operation duration, and **(D)** preoperative Hb value. **(E)** Autologous and **(F)** allogeneic transfusions volumes were analyzed with the length of stay. Pearson's or Spearman's analysis was chosen according to data distribution. Statistical significance was assigned at $p < 0.05$.

Correlation Between Intraoperative Blood Transfusion and Clinical Characteristics

To detect factors associated with intraoperative blood transfusion, several clinical factors that include body weight change, liposuction volume, surgery duration, preoperative Hb level, and length of hospital stay were analyzed through Pearson's or Spearman's correlation analysis. The body weight change value is positively correlated with blood transfusion volume ($r = 0.24$, $p < 0.05$) (**Figure 1A**). Similar correlations are also observed in intraoperative liposuction volume ($r = 0.21$, $p < 0.05$) (**Figure 1B**) and surgery duration ($r = 0.41$, $p = 2.3E\text{-}18$) (**Figure 1C**). There is statistical significance in preoperative Hb level ($r = 0.047$, $p = 0.37$) (**Figure 1D**). Although there appears to be a positive association between preoperative Hb and intraoperative RBC transfusion evidenced by the sloped line, the statistical association does not reach significant level, which suggests that there is no statistical significance in the comparison of association between the two variables. In other words, graph D does not implicate that the higher the preoperative Hb, the more the volume was. In terms of the length of stay with transfusion, the correlation is much stronger in allogeneic transfusion-only patients ($r = 0.42$) than in autologous transfusion-only patients ($r = 0.29$) (**Figures 1E,F**).

Analysis of Autologous and Allogeneic Transfusion

The current investigation focuses on the liposuction surgeries since 2016, when we began to launch autologous blood transfusions, which include predonated autologous transfusion and intraoperative ANH. The intraoperative blood loss and intraoperative autologous or allogeneic transfusion volumes each year are summarized in **Table 2**.

To compare the predonated autologous transfusion with intraoperative ANH transfusion, various indicators under the two scenarios were compared. As shown in **Table 3**, there was no statistical significance in gender ($p = 0.108$), age ($p = 0.283$), number of patients in combination with allogeneic transfusion ($p = 0.942$), blood coagulation index ($p = 0.128$ for PT, $p = 0.514$ for APTT, and $p = 0.356$ for FIB), and change in Hb level (in patients with combined transfusion with allogeneic) ($p = 0.146$). However, there was statistical significance in the comparison of length of hospital stay ($p = 0.017$), autologous transfusion volume ($p < 0.001$), combined allogeneic volume ($p = 0.006$), intraoperative blood loss ($p < 0.001$), intraoperative transfusion volume ($p = 0.001$), change in Hb level in transfusion patients ($p < 0.001$), and change in Hb level in patients with autologous transfusion only ($p < 0.001$).

These current results suggest that in patients with predonated autologous transfusion-only, the autologous transfusion volume, simultaneous allogeneic transfusion volume, and intraoperative transfusion volume are, respectively, lower than that of ANH-only patients. Although the median volume of intraoperative ANH transfusion is equal to that of predonated autologous transfusion, the range of intraoperative ANH transfusion volume is wider than that of predonated ones (200–1,600 vs. 200–800). In terms of the Hb levels, the decline of Hb is greater in the intraoperative ANH transfusion-only patients than in the predonated autologous transfusion-only patients. The range of length of hospital stay in the ANH-only patients is larger than that of predonated transfusion-only patients.

Impact of Autologous Transfusion on Allogeneic Transfusion

The allogeneic blood transfusion volumes were analyzed across different transfusion modes to determine whether autologous transfusion could reduce the consumption of allogeneic transfusion. We observed that the allogeneic transfusion volume in the autologous transfused patients was less than that of the allogeneic transfusion-only patients. As suggested in **Figure 2A**, in comparison with the allogeneic transfusion-only patients, the mean allogeneic transfusion volume in either ANH group, predonated transfusion group, or mixed group is statistically lower ($p < 0.001$).

Since the autologous blood transfusion could reduce the allogeneic transfusion volume in liposuction surgery, we further compared the three modes of autologous transfusion by Kruskal–Wallis test to determine which mode is best (**Figure 2A**). There were 270, 56, and 26 cases in the intraoperative ANH-only group, predonated transfusion-only group, and combined transfusion of ANH and predonation groups, respectively. There is no statistical significance across the three groups concerning the allogeneic blood consumption ($p = 0.103$) (**Figure 2A**). The mean value of allogeneic transfusion volume in intraoperative ANH-only patients and predonated transfusion-only patients is <150 ml, which indicates small demands for allogeneic transfusion in autologous transfusion patients.

To explore its impact on allogeneic transfusion, allogeneic volumes in combined modes were listed separately (**Figure 2B**).

TABLE 2 | Intraoperative blood loss and transfusion volumes in liposuction surgery.

Year	No. of surgery (*n*)	Intraoperative blood loss (ml)	Intraoperative blood transfusion (ml)	Autologous transfusion volume (ml)	Allogeneic transfusions volume (ml)	No. of predonated autologous transfusion only (*n*)	No. of intraoperative ANH only (*n*)
2016	275	804 ± 412	463 ± 347	18,400 (61.13%)	11,700 (38.87%)	1	34
2017	301	368 ± 367	296 ± 260	34,700 (71.55%)	13,800 (28.45%)	3	90
2018	374	471 ± 256	178 ± 264	38,100 (77.91%)	10,800 (22.09%)	2	101
2019	337	489 ± 295	259 ± 319	47,600 (77.52%)	13,800 (22.48%)	56	45

The volume of blood loss and transfusion that includes autologous and allogeneic transfusions was summarized. Data were detonated as mean ± SD or percentage.

TABLE 3 | Comparison of autologous transfusion mode between acute normovolemic hemodilution-only patients and predonated autologous transfusion-only patients.

Item	Acute normovolemic hemodilution-only patients ($n = 270$)	Predonated autologous transfusion-only patients ($n = 56$)	*p*-value	Statistics
Gender, *n* (%)			0.108	Chi-square
Male	45 (16.7%)	4 (7.1%)		
Female	225 (83.3%)	52 (92.9%)		
Age, *n* (%)			0.283	Chi-square
<40	60 (22.2%)	9 (16.1%)		
40–60	144 (53.3%)	28 (50.0%)		
>60	66 (24.4%)	19 (33.9%)		
Length of stay, days, [median (range)]	7.0 (5, 46)	7.0 (5, 21)	0.017	Kruskal–Wallis
Autologous transfusion volume, ml, [median (range)]	400.0 (200, 1600)	400.0 (200, 800)	<0.001	Kruskal–Wallis
Combination with allogeneic transfusion, n (%)			0.942	Chi-square
No	220 (81.5%)	46 (82.1%)		
Yes	50 (18.5%)	10 (17.9%)		
Combined allogeneic volume, ml, [median (range)]	400.0 (400, 1600)	400.0 (400.0, 400.0)	0.006	Kruskal–Wallis
Intraoperative blood loss, ml, [median (range)]	600.0 (0, 2000)	600.0 (10, 1000)	<0.001	Kruskal–Wallis
Intraoperative transfusion volume, ml, [median (range)]	400.0 (200, 2200)	400.0 (400, 800)	0.001	Kruskal–Wallis
Change in coagulation indicators				
Prothrombin time, PT, seconds, (mean ± SD)	1.5 ± 0.8	2.1 ± 0.6	0.128	Two-sample *t*-test
Activated partial thromboplastin time, APTT, seconds, (mean ± SD)	−3.6 ± 1.9	−3.2 ± 0.9	0.514	Two-sample *t*-test
Fibrinogen, FIB, seconds, (mean ± SD)	−0.4 ± 0.6	−0.7 ± 0.6	0.356	Two-sample *t*-test
Change in Hb levels in transfusion patients, g/L, (mean ± SD)	32.4 ± 14.0	23.8 ± 11.7	<0.001	Two-sample *t*-test
Change in Hb levels in autologous transfusion-only patients, g/L, (mean ± SD)	31.6±12.7	23.4 ± 9.8	<0.001	Two-sample *t*-test
Change in Hb levels in patients of combined transfusion with allogeneic, g/L, (mean ± SD)	36.6 ± 19.3	25.8 ± 18.9	0.146	Two-sample *t*-test

Change in Hb levels is calculated as preoperation minus postoperation, and change in coagulation indicators is calculated as postoperation minus preoperation. PT, APTT, FIB, and change in Hb level were transformed by Box-Cox into normal distribution and then compared through t-tests.

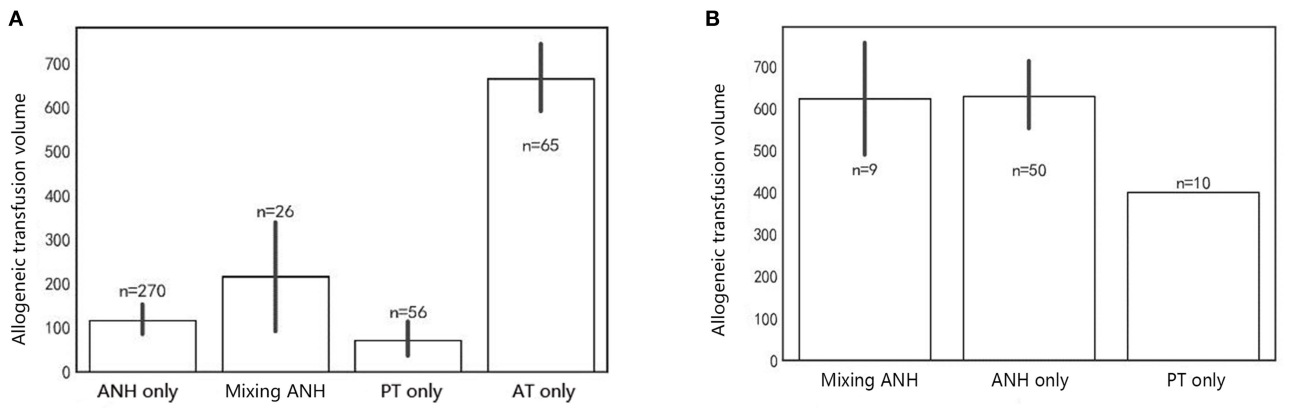

FIGURE 2 | Allogeneic blood transfusion volume of different situations. **(A)** Total allogeneic blood consumption across different modes. **(B)** Combined allogeneic blood consumption across different modes. Bar represents mean ± SD. ANH, Acute normovolemic hemodilution; Mixing ANH, mixing acute normovolemic hemodilution with predonation; PT, predonated transfusion; AT, allogeneic transfusion.

Under the circumstance of mixed transfusion, the combined allogeneic transfusion volume was statistically significantly different among the three groups (**Figure 2B**) ($p = 0.017$). *Post hoc* tests suggested that the allogeneic transfusion volume in the predonated-only group was insignificantly lower than that of the ANH-only group ($p = 0.06$) but significantly lower than that of the mixing ANH with predonation group ($p = 0.008$). These results implicate that the demand for allogeneic volume

TABLE 4 | Ordinary least squares regression analysis between autologous and allogeneic transfusion.

Item	Coefficient	Standard error	*t*	*P*-value	95% CI
Constant	283.425	61.589	4.602	0.000	159.780–407.070
Intraoperative blood loss	0.137	0.067	2.052	0.045	0.003–0.270
ANH only	147.393	36.251	4.066	0.000	74.616–220.170
Predonated only	9.835	49.900	0.197	0.845	−90.343–110.012
ANH + predonated	126.197	69.763	1.809	0.076	−13.858–266.253

Intraoperative blood loss and three modes of autologous transfusion volumes (ANH only, predonated only, and ANH + predonated transfusion) were the independent variables, and allogeneic transfusion volume was dependent variables. ANH: acute normovolemic hemodilution.

is small. The comparison between the ANH-only group and the mixing ANH with predonation group was of no statistical significance (p=0.78). The mean allogeneic transfusion volume in the predonated-only group is the lowest.

Ordinary least squares regression results showed that ANH-only group had a significant correlation with allogeneic transfusion and the other two modes had no significance (**Table 4**). The coefficient in the equation is the highest in the ANH-only group, followed by mixed transfusion mode, and predonated-only mode.

DISCUSSION

In this study, we found that transfusion group had a lower postoperative Hb levels, and blood transfusion was associated longer surgery time, larger body weight change, and larger operative blood loss. Intraoperative blood transfusion volume was correlated with body weight change, intraoperative liposuction, and surgery duration. Either autologous or allogeneic transfusion volume was positively associated with the length of stay. Between the ANH-only patients and predonated-only patients, there is significant difference in terms of the length of stay, autologous transfusion volume, mixed transfusion with allogeneic volume, intraoperative blood loss, intraoperative transfusion volume, and change in Hb levels. Predonated-only mode had the smallest demand for allogeneic transfusion compared with other two modes. OLS regression analysis suggests that autologous transfusion in the ANH-only mode is statistically associated with allogeneic transfusion.

To the best of our knowledge, this study has the largest sample size ever to describe blood transfusion in lymphedema liposuction surgery. Through PubMed search of English literature, we have found no article that investigates the blood transfusion in liposuction surgery for lymphedema patients. Thus, we venture the idea that our study is likely to be the first specific account of blood transfusion in lymphedema liposuctions. Previously, there seem to have been only two scattered investigations occasionally mentioning blood transfusion in lipoaspiration of lymphedema. Brorson et al. (10) described eight breast cancer-related lymphedema patients indicated for blood transfusion during liposuction. Wojnikow et al. (11) reported that a total of nine patients were subjected to lymphedema adipose suction receiving blood transfusion. However, their main focus was not on the blood transfusion itself, and they just utilized transfusion as an intermediate variable for the assessment of other treatments. The two articles simply brought up the occurrence of blood transfusion and have not specifically evaluated the effect of transfusion. Moreover, the small sample size <10 severely limits the ability to further extend their conclusion. From the most optimistic point of view, our study that comprises the largest sample size of 1,187 patients will lend invaluable academic credence to clinicians or scholars worldwide.

The operation of liposuction usually causes a substantial loss of fluid or blood from circulation or the third space. In this context, it poses a major risk for surgeons to aspire more than 2,000 ml of adipofibrosis tissue in one-stage surgery (12). A lack of circulating fluid is very dangerous for the perfusion of cardiopulmonary organs. Fortunately, availability of blood transfusion would effectively minimize the complication associated with the liposuction surgery (13). In our study, we found a positive significant association between liposuction volume and blood transfusion volume. This is consistent with clinical practice since the necessity of transfusion increases as the liposuction volume progresses. There is a literature recommending autologous transfusion in large-volume liposuctions (14). Compared with allogeneic blood, autologous blood is obviously safer in that it is associated with less morbidity and is logically free from blood-transmitted diseases (15). In our hospital, we began to pay more attention to autologous transfusion since 2013, and the percentage of autologous volume out of all transfusion volumes in liposuction surgery increased from 53.85 to 77.52%. We have observed that the demand for allogeneic blood was lower in patients with autologous transfusion than that in allogeneic transfusion-only patients, which implies that autologous transfusion would decrease the consumption of allogeneic blood. Similar conclusions have been drawn in the field of orthopedics that autologous transfusion is a cost-effective method to reduce the need for and quantity of allogeneic transfusion in elective total knee arthroplasty (16). Apart from the substitutability to consumption, another benefit of autotransfusion is the close-to-zero risk of infecting transfusion-transmitted disease such as AIDS or malaria (17). The blood-borne inflectional diseases can be tested before the operation to verify the status of infection, which is important for both surgeon and patients.

There are two main types of autotransfusion: the ANH, which is conducted during operation without preoperative

blood collection (18), and the predonated transfusion, which is prepared and collected preoperatively (19). In our study, we compared the two types of transfusion and found that predonation is associated with shorter hospital stay, lower blood loss, and smaller decrement of Hb change. This can be explained by that predonation usually begins 3–7 days before the surgery, which allows the body to have time to adjust to normal levels in advance and thus recover faster postoperatively (20). However, ANH does not have this advantage. Supporting evidence also emerges from our OLS analysis: by adjusting the intraoperative blood loss as a covariate, we discovered that the ANH, not predonation, has the correlation with allogeneic transfusion volume, which indicates that even taking into consideration of blood loss, ANH is still undesirably correlated with the use of allogeneic blood. In other words, in terms of reducing the allogeneic transfusion, ANH is not an ideal choice compared with predonation. Additionally, in the three modes of autotransfusion (predonation, ANH, and predonation + ANH) in our analysis, the predonation mode had the significantly lowest consumption for allogeneic blood than other two modes. This also further strengthens our idea in favor of predonated autotransfusion.

Another worthy point is that allogeneic blood transfusion is associated with immune modulations (21). Possible mechanisms of transfusion-associated immunomodulation are T-helper (Th) 2 activation and human leukocyte antigen (HLA) response (22). For instance, during allogeneic transfusion, Th2 cell is activated and the response of Th1 cell is thus decreased (23). Other mechanisms of immunomodulation might include the balance between T regulatory cell (Treg) and Th 17 cells: transfusion helped reverse the imbalance of Treg/Th17 ratios in hip fracture patients evidenced by the decrease and increased frequency of Tregs and Th17, respectively, after blood transfusion (24). In addition, in polytransfused sickle cell disease patients, high levels of $CXCR5^{+}PD1^{+}CD4^{+}$ T lymphocyte (TL) may be a biomarker for the inhibited functions of T cells (25). Multiple rounds of exposure to antigens in allogeneic blood transfusion trigger low degree of inflammatory stimulation, and the mononuclear cells cannot be presented. In addition, the elevated level of IL-10 in serum of transfused patients also accounts for suppression of immune response (26). Transfusion can cause acute lung injury *via* the modulation of HLA antibodies, evidenced by the fact that exclusion of plasma volume products can reduce the incidence of acute lung injury by nearly two-thirds (27). In gastric cancer, allogeneic blood transfusion is a deleterious prognostic factor on cancer-related mortality and recurrence (28). Blood restriction management has been proposed to minimize the use of allogeneic blood in gastric cancer. However, in the field of liposuction surgery, there is no such proposition. We herein make a radical supposition that autologous blood transfusion should be advocated in comparison with allogeneic transfusion in liposuction surgery, especially considering the modulated immune system that might not be good for lymphedema patients.

There are several drawbacks associated with the study. One limitation is that the sample size might not be sufficient to draw a solid conclusion. However, it is unclear what sample size is statistically required, since the current investigation is only a pilot cross-sectional analysis. Furthermore, our study lacks fundamental basic mechanistic research. There is a need for molecular studies to illustrate the biological role of transfusion in liposuction of lymphedema patients. Last but not least, the long-term effect of transfusion after discharge from hospital remains undetermined. Further study to examine the long-term role of blood transfusion would be needed.

CONCLUSIONS

This study described the blood transfusion in lymphedema liposuction surgery and compared autologous with allogeneic transfusion patterns in these patients. Autologous transfusion can reduce the transfusion volume of allogeneic blood.

DATA AVAILABILITY STATEMENT

The original contributions presented in the study are included in the article/supplementary material, further inquiries can be directed to the corresponding author.

ETHICS STATEMENT

The studies involving human participants were reviewed and approved by Scientific Research Ethics Committee of Beijing Shijitan Hospital, Capital Medical University. The affiliation of the Ethics Committee: National Health Commission of the People's Republic of China. The patients/participants provided their written informed consent to participate in this study. Written informed consent was obtained from the individual(s) for the publication of any potentially identifiable images or data included in this article.

AUTHOR CONTRIBUTIONS

LC contributed to the design of the study, statistical analyses, patient recruitment, execution of the patients' measurements, and manuscript preparation. YC and KC contributed to patient recruitment, execution of the patients' measurements, and manuscript preparation. ZX contributed to the statistical analyses and manuscript preparation. WS contributed to the design of the study and manuscript preparation. All authors contributed to the article and approved the submitted version.

REFERENCES

1. Shaitelman SF, Cromwell KD, Rasmussen JC, Stout NL, Armer JM, Lasinski BB, et al. Recent progress in the treatment and prevention of cancer-related lymphedema. *CA Cancer J Clin.* (2015) 65:55–81. doi: 10.3322/caac.21253
2. Zhang L, Fan A, Yan J, He Y, Zhang H, Zhang H, et al. Combining manual lymph drainage with physical exercise after modified radical mastectomy effectively prevents upper limb lymphedema. *Lymphat Res Biol.* (2016) 14:104–8. doi: 10.1089/lrb.2015.0036
3. Ogunleye AA, Nguyen DH, Lee GK. Surgical treatment of lymphedema. *JAMA Surg.* (2020) 155:522–3. doi: 10.1001/jamasurg.2020.0015
4. Stewart CJ, Munnoch DA. Liposuction as an effective treatment for lower extremity lymphoedema: a single surgeon's experience over nine years. *J Plast Reconstr Aesthet Surg.* (2018) 71:239–45. doi: 10.1016/j.bjps.2017.11.003
5. BM M, JE C, JM K. Optimizing patient outcomes and safety with liposuction. *Aesthet Surg J.* (2019) 39:66–82. doi: 10.1093/asj/sjy151
6. Cansancao AL, Condé-Green A, David JA, Cansancao B, Vidigal RA. Use of tranexamic acid to reduce blood loss in liposuction. *Plast Reconstr Surg.* (2018) 141:1132–5. doi: 10.1097/PRS.0000000000004282
7. Illouz YG. Body contouring by lipolysis: a 5-year experience with over 3000 cases. *Plast Reconstr Surg.* (1983) 72:591–7. doi: 10.1097/00006534-198311000-00001
8. Klein JA. The tumescent technique for liposuction surgery. *Am J Cosmetic Surg.* (1987) 4:263. doi: 10.1177/074880688700400403
9. Tierney EP, Kouba DJ, Hanke CW. Safety of tumescent and laser-assisted liposuction: review of the literature. *J Drugs Dermatol.* (2011) 10:1363–9.
10. Brorson H, Svensson H. Complete reduction of lymphoedema of the arm by liposuction after breast cancer. *Scand J Plast Reconstr Surg Hand Surg.* (1997) 31:137–43. doi: 10.3109/02844319709085480
11. Wojnikow S, Malm J, Brorson H. Use of a tourniquet with and without adrenaline reduces blood loss during liposuction for lymphoedema of the arm. *Scand J Plast Reconstr Surg Hand Surg.* (2007) 41:243–9. doi: 10.1080/02844310701546920
12. Trott SA, Beran SJ, Rohrich RJ, Kenkel JM, Adams WP. Jr, Klein KW. Safety considerations and fluid resuscitation in liposuction: an analysis of 53 consecutive patients. *Plast Reconstr Surg.* (1998) 102:2220–9. doi: 10.1097/00006534-199811000-00063
13. Choudry UH, Hyza P, Lane J, Petty P. The importance of preoperative hemoglobin evaluation in large volume liposuction: lessons learned from our 15-year experience. *Ann plast surg.* (2008) 61:230–4. doi: 10.1097/SAP.0b013e31815bf341
14. Klein J. Tumescent technique for local anesthesia improves safety in large-volume liposuction. *Plast Reconstr Surg.* (1993) 92:1085–98; discussion 1099–100. doi: 10.1097/00006534-199311000-00014
15. Zhou J, A. review of the application of autologous blood transfusion. *Braz J Med Biol Res.* (2016) 49:e5493. doi: 10.1590/1414-431x20165493
16. Pawaskar A, Salunke AA, Kekatpure A, Chen Y, Nambi GI, Tan J, et al. Do autologous blood transfusion systems reduce allogeneic blood transfusion in total knee arthroplasty? *Knee Surg Sports Traumatol Arthrosc.* (2017) 25:2957–66. doi: 10.1007/s00167-016-4116-z
17. Vassallo R, Goldman M, Germain M, Lozano M. Preoperative autologous blood donation: waning indications in an era of improved blood safety. *Transfus Med Rev.* (2015) 29:268–75. doi: 10.1016/j.tmrv.2015.04.001
18. Takekawa D, Saito J, Kinoshita H, Hashiba EI, Hirai N, Yamazaki Y, et al. Acute normovolemic hemodilution reduced allogeneic blood transfusion without increasing perioperative complications in patients undergoing free-flap reconstruction of the head and neck. *J Anesth.* (2020) 34:187–94. doi: 10.1007/s00540-019-02714-5
19. Dean CL, Wade J, Roback JD. Transfusion-transmitted infections: an update on product screening, diagnostic techniques, and the path ahead. *J Clin Microbiol.* (2018) 56:e00352–18. doi: 10.1128/JCM.00352-18
20. Ferraris VA, Ferraris SP, Saha SP, Hessel EA 2nd, Haan CK, Royston BD, et al. Perioperative blood transfusion and blood conservation in cardiac surgery: the society of thoracic surgeons and the society of cardiovascular anesthesiologists clinical practice guideline. *Ann Thorac Surg.* (2007) 83:S27–86. doi: 10.1016/j.athoracsur.2007.02.099
21. Zabala LM, Sutcliffe D and Faraoni D. Could we reduce the incidence of immune sensitization prior to heart transplant by reducing exposure to allogeneic blood transfusion? *Paediatr Anaesth.* (2021) 31:1028–30. doi: 10.1111/pan.14274
22. Zhu M, Zhu Z, Yang J, Hu K. and Li Y. Impact of perioperative blood transfusion on gene expression biomarkers in patients with gastrointestinal cancer. *Transfus Apher Sci.* (2018) 57:656–60. doi: 10.1016/j.transci.2018.07.022
23. Bal S, Heper Y, Kumaş L, Guvenc F, Budak F, Göral G, et al. Effect of storage period of red blood cell suspensions on helper T-cell subpopulations. *Blood transfusion.* (2018) 16:262–72. doi: 10.2450/2017.0238-16
24. Wang L, Chen W, Kang FB, Zhang YH, Qi LL. and Zhang YZ. Blood transfusion practices affect CD4(+) CD25(+) FOXP3(+) regulatory T cells/T helper-17 cells and the clinical outcome of geriatric patients with hip fracture. *Aging.* (2021) 13:21408–20. doi: 10.18632/aging.203479
25. Tamagne M, Pakdaman S, Bartolucci P, Habibi A, Galactéros F, Pirenne F, et al. Whole-blood phenotyping to assess alloimmunization status in transfused sickle cell disease patients. *Blood Adv.* (2021) 5:1278–82. doi: 10.1182/bloodadvances.2020003537
26. Kapur R, Kim M, Aslam R, McVey MJ, Tabuchi A, Luo A, et al. T regulatory cells and dendritic cells protect against transfusion-related acute lung injury via IL-10. *Blood.* (2017) 129:2557–69. doi: 10.1182/blood-2016-12-758185
27. Guo K. and Ma S. The immune system in transfusion-related acute lung injury prevention and therapy: update and perspective. *Front Mol Biosci.* (2021) 8:639976. doi: 10.3389/fmolb.2021.639976
28. Sun C, Wang Y, Yao H. and Hu Z. Allogeneic blood transfusion and the prognosis of gastric cancer patients: systematic review and meta-analysis. *Int J Surg.* (2015) 13:102–10. doi: 10.1016/j.ijsu.2014.11.044

Conflict of Interest: ZX was employed by HealSci Technology Co. Ltd.

The remaining authors declare that the research was conducted in the absence of any commercial or financial relationships that could be construed as a potential conflict of interest.

frontiers | Frontiers in Medicine

BRIEF RESEARCH REPORT
published: 13 July 2022
doi: 10.3389/fmed.2022.891916

CTLs From Patients With Atherosclerosis Show Elevated Adhesiveness and Distinct Integrin Expression Patterns on 2D Substrates

Daria M. Potashnikova[1,2†], *Aleena A. Saidova*[2†], *Anna V. Tvorogova*[2], *Alexandra S. Anisimova*[1,2], *Alexandra Yu Botsina*[2], *Elena Yu Vasilieva*[1,2‡] *and Leonid B. Margolis*[3*‡]

[1] *Laboratory of Atherothrombosis, Moscow State University of Medicine and Dentistry, Moscow, Russia,* [2] *Moscow Department of Healthcare, City Clinical Hospital Named After I.V. Davydovsky, Moscow, Russia,* [3] *Section on Intercellular Interactions, Eunice Kennedy Shriver National Institute of Child Health and Human Development, National Institutes of Health, Bethesda, MD, United States*

OPEN ACCESS

Edited by:
Elizaveta Fasler-Kan, Bern University Hospital, Switzerland

Reviewed by:
Maria Shutova, Université de Genève, Switzerland
Oksana Kunduzova, Institut National de la Santé et de la Recherche Médicale (INSERM), France

***Correspondence:**
Leonid B. Margolis
margolil@mail.nih.gov

†*These authors have contributed equally to this work*
‡*These authors share last authorship*

Specialty section:
This article was submitted to Pathology, a section of the journal Frontiers in Medicine

Received: *08 March 2022*
Accepted: *02 June 2022*
Published: *13 July 2022*

Citation:
Potashnikova DM, Saidova AA, Tvorogova AV, Anisimova AS, Botsina AY, Vasilieva EY and Margolis LB (2022) CTLs From Patients With Atherosclerosis Show Elevated Adhesiveness and Distinct Integrin Expression Patterns on 2D Substrates. Front. Med. 9:891916. doi: 10.3389/fmed.2022.891916

Atherosclerosis is the major cause of cardiovascular disease that is characterized by plaque formation in the blood vessel wall. Atherosclerotic plaques represent sites of chronic inflammation with diverse cell content that is shifted toward the prevalence of cytotoxic T-lymphocytes (CTLs) upon plaque progression. The studies of CTL recruitment to atherosclerotic plaques require adequate *in vitro* models accounting for CTL interactions with chemokine-ligands and extracellular matrix fibers *via* surface chemokine receptors and integrins. Here we applied such a model by investigating CTL adhesion and migration on six types of coated surfaces. We assessed adhesion and motility metrics, the expression of chemokine receptors, and integrins in CTLs of patients with atherosclerosis and healthy donors. Using fibronectin, platelet-poor plasma from patients with atherosclerosis, and conditioned medium from atherosclerotic plaques we revealed the role of substrate in CTL adhesiveness: fibronectin alone and fibronectin combined with platelet-poor plasma and conditioned medium elevated the CTL adhesiveness – in patients the elevation was significantly higher than in healthy donors ($p = 0.02$, mixed 2-way ANOVA model). This was in line with our finding that the expression levels of integrin-coding mRNAs were elevated in the presence of fibronectin ($p < 0.05$) and ITGB1, ITGA1, and ITGA4 were specifically upregulated in patients compared to healthy donors ($p < 0.01$). Our experimental model did not affect the expression levels of mRNAs CCR4, CCR5, and CX3CR1 coding the chemokine receptors that drive T-lymphocyte migration to plaques. Thus, we demonstrated the substrate-dependence of integrin expression and discriminated CTLs from patients and healthy donors by adhesion parameters and integrin expression levels.

Keywords: CTL, integrins, chemokines, atherosclerosis, T-lymphocyte adhesion, T-lymphocyte migration

INTRODUCTION

T-lymphocyte migration is a physiological process that occurs during normal maturation and also determines the immune response to a large number of stimuli in disease (1). As part of immune surveillance and inflammatory reaction of the organism different subtypes of T-lymphocytes are attracted to infected cells (2), tumors (3), and rheumatoid lesions (4) as well as to the vessel walls containing atherosclerotic plaques (5, 6). As the impact of T-cells on the pathogenesis of a variety of clinically important conditions becomes more evident, the focus of many studies is drawn to the specific mechanisms driving them to different organs and the phenotypic qualities of the attracted responder T-cell populations.

With atherosclerosis being a major cause of cardiovascular disease, and thus essentially accounting for the largest number of deaths and disabilities worldwide, the model of T-lymphocyte migration to atherosclerotic plaque calls for much attention. Atherosclerotic plaques that are often observed in the carotid artery wall and upon rapture trigger thrombosis, leading to myocardial infarction and stroke, present a site of chronic inflammation with heterogeneous immune cell content (7). Additional aberrant immune activation contributes to atherosclerosis progression (8–10) that is associated with activation and accumulation of T-lymphocytes in atherosclerotic plaques (11, 12). In the end T-lymphocytes and specifically CD8+ cytotoxic T-lymphocytes (CTLs) comprise the predominant population in advanced atherosclerotic plaques (12, 13) and although their functions are not completely clear, there is evidence of their role in plaque destabilization, confirmed on animal models (14).

The studies of cytotoxic T-lymphocyte migration to different sites employ various models including transwell and transgel (15, 16) as well as 2D assays (17), each of them have their advantages and limitations. The transwell assays focus on the chemotaxis analysis (a migration driven by a gradient of soluble chemokines, which occurs when an asymmetry in chemoattractant) to establish the role of chemokines, in CTL recruiting to tissues. The 2D models are used to explore haptokinesis (a migration along a surface, utilizing immobilized ligands such as chemokines or integrins, without any cue gradient to provide a directional bias) and subsequently the role of integrin adhesion in CTL migration. Usually, the cross-talk of the chemokine and integrin systems is not addressed in such models. Chemotaxis migration models in collagen (transgel) are considered more physiologic as they account for the presence of extracellular matrix and the integrin involvement in this process but do not allow to estimate of the differential effect of integrins on cell migration descriptors. Here we employ different 2D coatings to visualize the impact of extracellular matrix and the plaque-produced signaling molecules on CTLs of patients with atherosclerosis and healthy donors in the absence of specific antigen signaling. We assess the CTL adhesion properties and provide motility metrics along with the transcription level of the key migration-associated molecules–chemokine receptors and integrins. Together these findings will help to better understand the process of CTL migration into atherosclerotic plaques and gain new insight into the cellular mechanisms that drive it.

MATERIALS AND METHODS

Patient Plasma and Conditioned Medium Samples

The study involving blood plasma and a conditioned culture medium of human participants was performed according to the Declaration of Helsinki and approved by the Interuniversity Committee of Ethics (Prot#11 16.12.2021). The patients/participants provided their written informed consent to participate in this study.

Peripheral blood samples and atherosclerotic plaques were obtained from symptomatic patients admitted to the Neurology Department of Clinical City Hospital named after I.V. Davydovsky with cardiovascular disease, most often thrombosis and stroke. All patients had atherosclerosis of the carotid artery. Some of the patients were forwarded to endarterectomy shortly after admission. Blood plasma and conditioned culture media from cultured endarterectomies plaques were collected from the patients and stored as follows:

Peripheral blood was obtained from patients prior to endarterectomy, collected into ficoll-containing BD Vacutainer CPT tubes (BD, USA), and processed <20 min after withdrawal. Initial centrifugation was performed at 2,000 g for 20 min. The upper fraction 10 mm above the ring of mononuclear cells was transferred to new tubes, pipetted, and used to obtain platelet-poor plasma. Platelet-poor plasma was obtained by the standard method: two rounds of centrifugation at 3,000 g for 15 min. After each centrifugation, the supernatant was transferred to new tubes without disturbing the pellet and carefully pipetted to avoid foaming. Frozen aliquots of platelet-poor plasma were stored at −80°C and thawed to coat the plastic wells for T-cell seeding.

Endarterectomized plaques were processed <2 h after the operation. Plaque specimens were washed in a cell culture medium to remove the contaminating blood-derived mononuclear cells, dissected, placed on a wetted collagen sponge raft (Pfizer, USA) at the medium–air interface, and cultured in AIM V serum-free medium (Thermo Fisher Scientific, USA) at 37°C/5% CO_2 as described earlier (18). After 24 h of explant culture, the medium was changed. The plaque explants were then incubated for 72 h more, the culture medium was collected and centrifuged two times at 3,000 g for 15 min. After each centrifugation, the supernatant was transferred to new tubes without disturbing the pellet and carefully pipetted to avoid foaming. Frozen aliquots of conditioned culture medium were stored at −80°C and thawed to coat the plastic wells for T-cell seeding.

T-Lymphocyte Sorting

Six samples of venous blood (three from healthy donors and three from patients with atherosclerosis) were collected into BD Vacutainer CPT tubes (BD, USA). Characteristics of healthy donors and patients are presented in **Supplementary Table 1**.

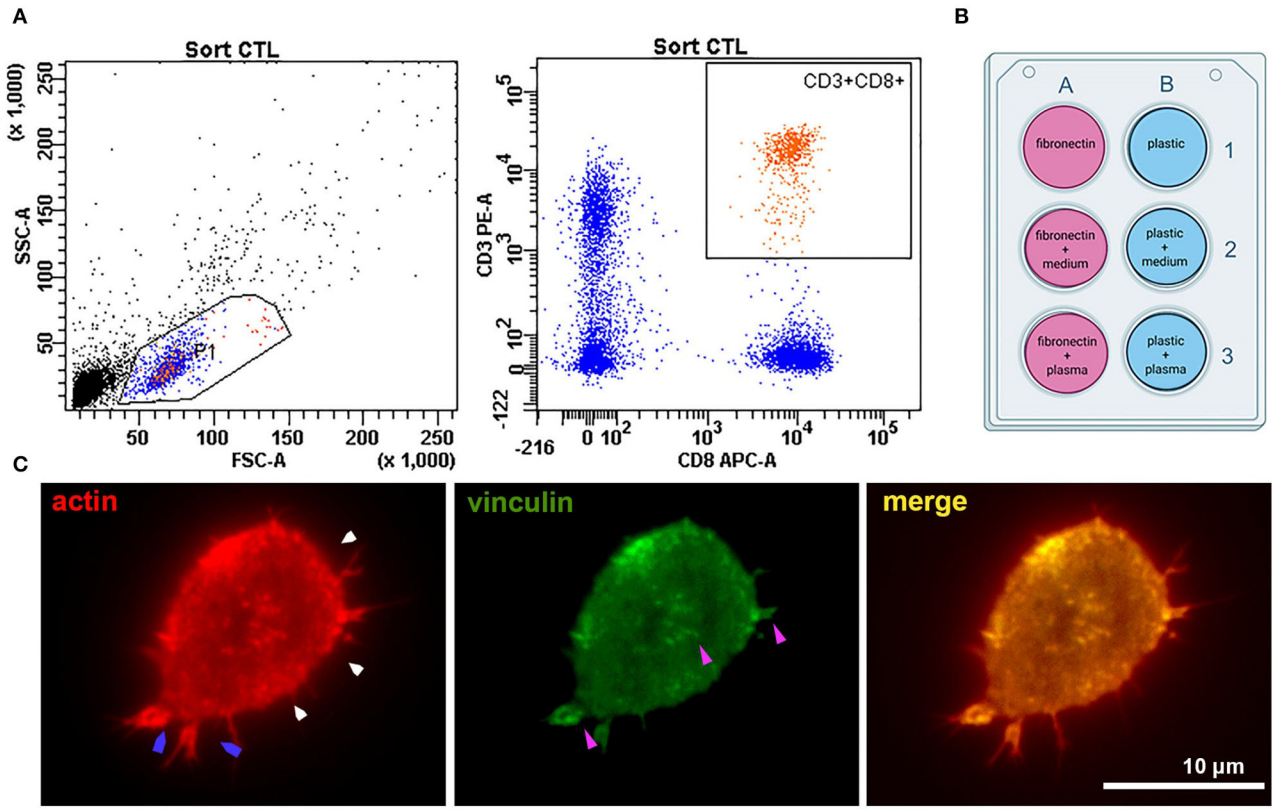

FIGURE 1 | Experiment setup and cell adhesion metrics were calculated for all types of coating. **(A)** Sorting CTLs from peripheral blood; the gates are set on the CD3+CD8+ T-cell population. **(B)** The six types of surface coating tested for each experiment. Fibronectin coating was applied for 45 min at room temperature – 100 µl of 50 µg/ml solution per 1 cm^2 surface. Fibronectin coating was air-dried before applying other ligands. Plasma and conditioned culture medium were stored after centrifugation at −80°C and thawed only once to coat the surfaces for T-cell seeding. Conditioned medium for coating in all experiments was derived from one batch (medium conditioned for 3 days by an atherosclerotic plaque explants from a male patient (age 61 years) with an ischemic stroke and atherosclerosis of carotid artery). Plasma was used from four different batches – one batch for each patient + donor pair (by number, as provided in **Supplementary Table 1**). All plasma was obtained from patients with confirmed atherosclerosis of carotid arteries and neurological symptoms (thrombosis and stroke) **(C)** Representative fluorescence image of a CD8+ T-lymphocyte seeded on a coverslip (patient 2, fibronectin coating) and stained against actin and vinculin after 24 h' incubation. The cell forms small lamellipodia (blue arrows), actin is organized into a thin cortical network (white arrows). Focal adhesions (purple arrows, visualized by anti-vinculin fluorescence staining) form spots mostly at the T-cell periphery.

Tubes were centrifuged at 2,000 g for 20 min. The ring of mononuclear cells was collected and washed twice in PBS (PanEco, Russia) at 1,000 g 15 min. Surface staining was performed in PBS with anti-CD3-APC (clone OKT3, BioLegend, USA) and anti-CD8a-PE (clone HIT8a, BioLegend, USA) antibodies for 20 min in the dark at RT. CD8+ T-lymphocytes were sorted using a FACSAria SORP cell sorter (BD Biosciences, USA) with a 70 um nozzle and corresponding pressure parameters. The sorting gate is presented in **Figure 1A**. Cells were collected into AIM V serum-free medium (Thermo Fisher Scientific, USA) and further cultured in it.

Plastic and Glass Coating

Plastic wells and glass coverslips placed at the bottom of the wells were coated with plasma or conditioned medium in the presence or absence of fibronectin. Fibronectin (Sigma-Aldrich, USA) coating was performed on 24-well-plates according to Sigma protocol (45 min at room temperature – 100 µl of 50 µg/ml solution per 1 cm^2 surface), the wells were air-dried. The additional coating was performed by placing 350 µl of thawed aliquots of patient plasma or conditioned AIM V medium from atherosclerotic plaques into the well. In 2 h, the medium was washed out with PBS (PanEco, Russia). The experimental setup with different types of coating is presented in **Figure 1B**.

T-Lymphocyte Viability

For viability experiments sorted CD8+ T-cells were seeded at 50 × 10^3 cells per well. Viability was assessed by flow cytometry using a FACSAria SORP cell sorter (BD Biosciences, USA) 24 h after seeding. Triple staining of cells was performed in 0.5 ml AIM V for 15 min in the dark using 100 nM TMRE (Thermo Fisher Scientific, USA), 1 µg/ml DAPI (Thermo Fisher Scientific, USA), and 240 µg/ml Annexin V-FITC (BioLegend, USA).

Random Walk Assay

Sorted CD8+ T-cells were seeded at 25–30 × 10^3 cells per well. After 24 h of incubation at 37°C/5% CO_2, the medium was changed and time-lapse videos of cells were made for each well. In the random walk assay, we evaluated the total distance, cell velocity, and migration efficiency. Total distance was the displacement that a cell made during observation. Medium cell velocity was calculated by dividing the track distance by track time, and migration efficiency was calculated by dividing the total distance by track distance. At least 20 cells were analyzed per experimental condition for each donor/patient.

Fluorescence Staining

Sorted CD8+ T-cells were seeded at 25–30 × 10^3 cells on glass coverslips. After 24 h of incubation at 37°C/5% CO_2, the medium was changed and cells were fixed on glass in 4% paraformaldehyde for 15 min at room temperature and washed in PBS 3 times. After permeabilization in 0.01% Triton-×100 in PBS, cells were stained with antibodies.

For vinculin/actin staining the primary antibodies against vinculin (clone VLN01, Thermo Fisher Scientific, USA) was used at 1:100, 37°C for 60 min. Cells were washed in PBS 3 times and stained with secondary antibodies anti-mouse-Alexa488, at 1:100, 37°C for 60 min. Cells were washed in PBS 3 times and co-stained with phalloidin-Alexa555 (Thermo Fisher Scientific, USA) at 37°C for 60 min.

For integrin beta1/integrin alpha4 staining the directly conjugated anti-beta1-APC antibody was used at 1:100 (clone MAR4, BD, USA). For anti-alpha4 cells were stained with primary (clone D2E1 Cell Signaling) antibody at 1:100 and secondary antibody anti-rabbit-Cy2 (Sigma, USA) as described for vinculin.

After washing in PBS 3 times all specimens were mounted in Mowiol (Thermo Fisher Scientific, USA).

RNA and cDNA

Sorted CD8+ T-cells were seeded at 50×10^3 cells per well. After 24 h of incubation at 37°C/5%, CO_2 (six types of experimental conditions) cells were taken for RNA isolation and RTqPCR. RNA was extracted from cell suspensions using RNeasy Mini Kit (Qiagen, USA) according to the manufacturer's instructions. RNA concentration was measured using a NanoPhotometer (Implen, Germany), and its purity was assessed according to the A260/A280 and A260/A230 ratios. cDNA was transcribed using the iScript Advanced cDNA synthesis kit (Bio-Rad Laboratories, USA) according to the manufacturer's instructions, and 50 ng of total RNA was taken into reaction.

Primers and Real-Time PCR

Real-time qPCR was performed using a CFX96 (Bio-Rad Laboratories Inc., USA) cycler.

The relative amounts of integrin-coding mRNAs were detected using iTaq Universal SYBR Green Supermix (Biorad Laboratories Inc., USA). The reaction protocol included denaturation (95°C, 10 min) and 39 amplification cycles [95°C, 15 s; Ta°C (annealing temperature is provided in **Supplementary Table 2**), 30 s; and 72°C, 60 s]. All samples were processed in duplicate. One sample of cDNA put into each PCR run served as an inter-run calibrator for combining data into one experiment. Primer sequences are provided in **Supplementary Table 2**. Primers were purchased from "DNA-Synthesis" (Moscow, Russia). Primer specificity was confirmed by melting curve analysis. The Ct values were determined for real-time PCR curves by setting the threshold at 5 SD for each run. qPCR data were normalized according to Vandesompele et al. (19) using *UBC* and *HPRT1* as reference genes.

The relative amounts of chemokine receptor-coding mRNAs were detected using primers with TaqMan probes. Primers and probes were purchased from "DNA-Synthesis" (Moscow, Russia), all sequences are provided in **Supplementary Table 3**. The reaction protocol included denaturation (95°C, 5 min), followed by 50 amplification cycles (95°C, 10 s; Ta°C (annealing temperature is provided in **Supplementary Table 3**), 30 s; and 72°C, 40 s). All samples were processed in duplicate. The qPCR data were normalized according to Vandesompele et al. (19) using *UBC* and *YWHAZ* as reference genes.

Imaging

Live imaging was performed on an inverted Zeiss AxioObserver fluorescence microscope operating under Zen 3.1 Blue Edition software with × 20/1.6 objective (phase contrast) at 36.5–37°C in AIM-V (Gibco, Thermo Fisher Scientific, Waltham, MA, USA) using Hamamatsu ORCA-Flash 4.0 V2 (Hamamatsu Photonics, Hamamatsu, Japan) with 30 s intervals between frames, each video took at least 2 h. Images were analyzed using ImageJ software (NIH). Cell tracks were measured using the integrated MTrackJ plugin. Based on cell track data in a random walk assay, we evaluated the final distance, cell velocity, and migration efficiency. On the raw time-lapse videos, we measured the number of attached cells during 100 frames as a percentage of attached cells to all cells per field of view and the average time of attachment for them.

To visualize the actin fibers and vinculin standard FITC/Cy-3 filter cubes were used. Fluorescence images of attached T-cells were processed using ImageJ and finalized using Adobe Photoshop (Adobe Systems, USA) software.

Confocal integrin beta1/integrin alpha4 visualization was performed using Zeiss LSM900 with Ex.640nm/650-700nm Airyscan for integrin beta1-APC and Ex.488nm/502–545 nm Airyscan for integrin alpha4-Cy2.

Data Analysis

The data were analyzed and plotted using GraphPad Prism 7 software (GraphPad Software, USA). Further statistical analysis was performed in R (20) with basic package "stats" ver. 4.1.1 and additional packages "margins" ver. 0.3.26 (21) and "ggplot2" ver. 3.3.5 (22): to evaluate the differences in gene expression levels between samples in different experimental conditions generalized linear models (GLM) were constructed. Normalized mRNA expression level was used as the dependent variable and "status–donor/patient," "surface–fibronectin/plastic," "addition–plasma/no plasma" and "addition–medium/no medium"- as predictors. Optimal model structure selection was

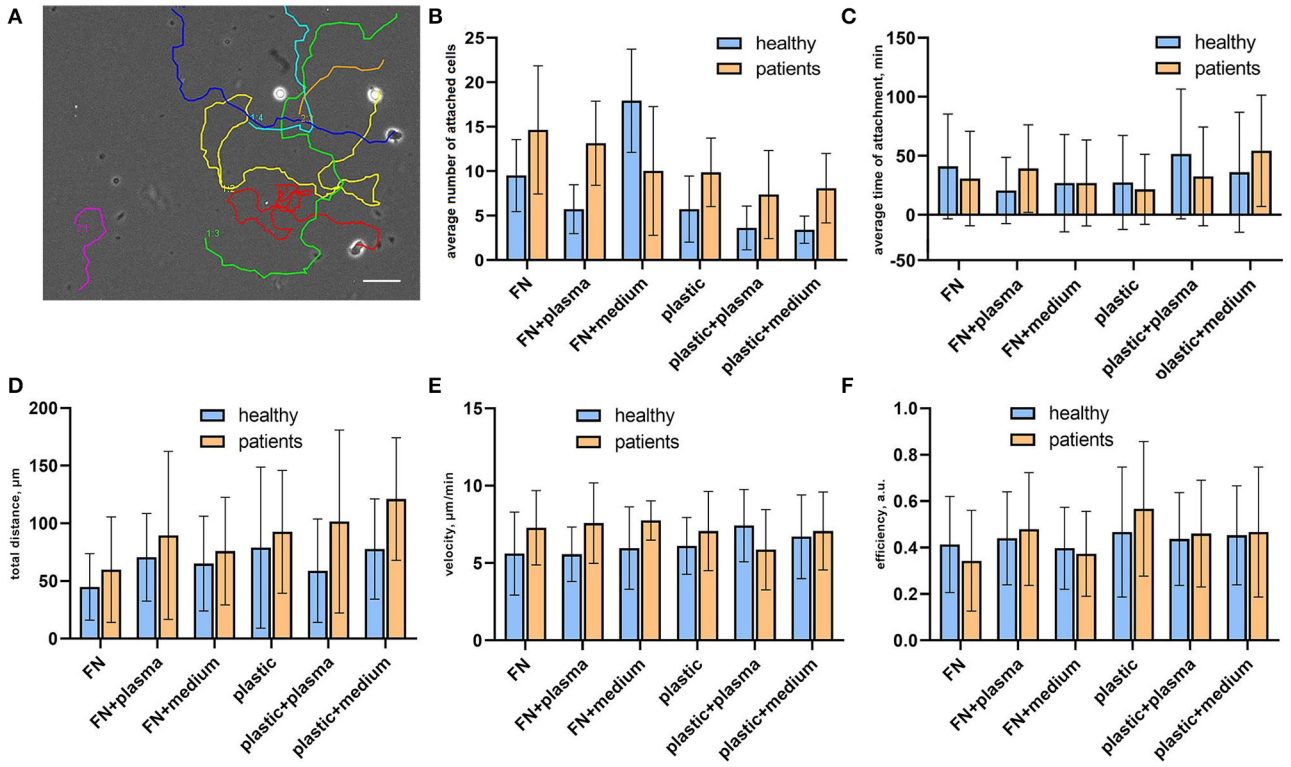

FIGURE 2 | Random migration assay for sorted CTLs. **(A)** Representative migration tracks from a phase contrast time-lapse video summarized and plotted on one frame. Each video lasted for no <2 h with inter-frame interval of 30 s. **(B)** Cell adhesiveness in the tested conditions expressed as average number of attached cells per observation period. The data was obtained from phase contrast time-lapse videos. The number of attached cells was elevated in all samples from patients compared to healthy donors, the difference was statistically significant ($p = 0.02$, mixed 2-way ANOVA model) irrespective of substrate type or source of soluble ligands. **(C)** Cell adhesiveness in the tested conditions is expressed as the average time of attachment for attached cells. The time of the attachment was assessed as the time interval between the first frame with the cell attached to the substrate and the frame where it is detached. The data was obtained from phase contrast time-lapse videos. **(D)** Total migration distance of attached CTLs calculated as a displacement that a cell made during the time-lapse video, at least 20 cells were analyzed per experimental condition for each donor/patient. Each video lasted for no <2 h with an inter-frame interval of 30 s. **(E)** Medium cell velocity of attached CTLs calculated by dividing the track distance by track time. The data was obtained from phase contrast time-lapse videos, each video lasted for no <2 h with inter-frame interval of 30 s. At least 20 cells were analyzed per experimental condition for each donor/patient. **(F)** Migration efficiency of attached CTLs calculated by dividing the total distance by track distance. The data was obtained from phase contrast time-lapse videos, each video lasted for no <2 h with an inter-frame interval of 30 s. At least 20 cells were analyzed per experimental condition for each donor/patient.

performed using a stepwise algorithm according to the Akaike criterion (AIC).

RESULTS

Sorted CTLs Demonstrate Similar Cell Viability and Cell Morphology on Different Types of Coating

In each experiment CD8+ T-lymphocytes were sorted (**Figure 1A**) and seeded on 6 types of coatings (**Figure 1B**): 1 – non-coated plastic; 2 – plastic coated with conditioned medium from atherosclerotic plaque; 3 – plastic coated with plasma from patients with atherosclerosis; 4 – fibronectin-coated plastic (FN); 5 – fibronectin-coated plastic with conditioned medium from atherosclerotic plaque (FN+medium); 6 – fibronectin-coated plastic with plasma from patients with atherosclerosis (FN+plasma). The viability of sorted CTLs was not affected by the coating and non-viable cells did not exceed 10.2% (**Supplementary Figure 1**).

In all experimental conditions, cells retained a generally similar morphology with short protrusions; actin was organized into a thin cortical network, and focal adhesion sites were visible at the T-cell edge and as small spots in the T-cell body (visualized with antibodies to vinculin) (**Figure 1C**).

CTLs From Patients With Atherosclerosis Demonstrate Higher Adhesiveness Compared to Healthy Donors

To verify how surface coating affects the CTLs' adhesiveness and 2D migration parameters we analyzed attached cells and cell tracks in a random walk assay (**Figure 2A**). Cell adhesiveness was measured as the average number of cells attached to the substrate during the observation period and the average time they spent in the attached state. We found increased numbers

of attached cells on fibronectin compared to non-coated plastic both for cells from patients and healthy donors (**Figure 2B**), except for cells attached on fibronectin with conditioned medium from atherosclerotic plaque. We found no differences in the percentage of attached cells in wells with added plasma and wells with added conditioned medium from atherosclerotic plaques, thus indicating that soluble ligands have no effect on T-cell adhesiveness in a 2D microenvironment. Most importantly, the percentage of attached cells was elevated in all samples from patients compared to healthy donors irrespective of substrate type or source of soluble ligands, the difference was statistically significant ($p = 0.02$, mixed 2-way ANOVA model). The average time of attachment was not affected by coating and was similar for CTLs from patients and healthy donors (**Figure 2C**).

Cell Motility Parameters of CTLs Show a Trend for Upregulation in Patients With Atherosclerosis Compared to Healthy Donors

CTL tracks were further analyzed for cell motility parameters. The representative movies of motile CTLs with tracks are provided in **Supplementary materials** (**Supplementary Videos 1–3**). To describe the parameters of randomly migrating cells we measured the total displacement that a cell made during the observation time ("total distance"), as well as cell velocity and migration efficiency. Migration efficiency was calculated by dividing the total distance by track distance. A representative migration track with plotted track distance and the total distance is shown in **Supplementary Figure 2**. Mean values and distributions of migration descriptors were almost similar on different substrates. We observed a trend for the elevation of mean values of total distance and velocity for CTLs from patients in all conditions, thus indicating that CTLs from patients moved slightly faster than CTLs from healthy donors and thus could migrate to longer distances (although due to large ranges these differences were not statistically significant) (**Figures 2D,E**). The migration efficiency coefficients were almost similar for all conditions, indicating that neither CTLs from patients, nor CTLs from healthy donors could move persistently in the absence of a ligand gradient (**Figure 2F**). Cell velocity weakly correlated with the migration efficiency (Spearman $R = 0.28$) and total distance ($R = 0.32$), whereas the total distance moderately correlated with the migration efficiency ($R = 0.49$). This shows that fast-moving cells don't necessarily move farther, but rather cells that can maintain directional movement.

mRNA Expression of ITGB1, ITGA1, and ITGA4 Is Upregulated in CTLs From Patients With Atherosclerosis Compared to Healthy Donors

As lymphocytes from healthy donors and patients demonstrated different adhesion capacities both on plastic and fibronectin, we evaluated the adhesion profile of CD8+ T-cells by measuring the expression of mRNAs coding α1, α4, α5, αE, β7, and β1 integrins (as the most common integrin subunits of CD8+ T-lymphocytes). The relative normalized expression levels are provided in **Supplementary Figure 3**. We assessed the role of fibronectin coating on integrin gene expression by comparing fibronectin-containing and non-containing experimental setups in a pairwise manner using a Wilcoxon test. Comparisons were made in groups of patients and healthy donors separately. The differences were statistically significant ($p < 0.05$) for *ITGB1, ITGA1, ITGAE* for healthy donors, and *ITGB1, ITGA1, ITGA4, and ITGAE* for patients. We have thus proved that substrate enhances the expression of specific integrin patterns in patient and donor CTLs. Most notably, we observed a substantial upregulation of integrin subunits in CTLs from patients with atherosclerosis compared to those from healthy donors. To estimate the precise contribution of each experimental condition (independent variables: patient/donor status, fibronectin in the coating, addition of plasma, the addition of conditioned medium) on integrin subunit mRNA expression (dependent variables) we built the generalized linear model of our assay. Using this model (**Figure 3A**, model coefficients and average marginal effect (AME) values are presented in **Supplementary Table 4**), we confirmed that fibronectin positively regulates the expression of all integrin subunits (AME from 0.20 to 0.37, $p < 0.05$). Moreover, mRNA expression of *ITGA1, ITGA4, and ITGB1* are upregulated (AME from 0.21 to 0.33, $p < 0.01$), and *ITGAE* is downregulated (AME −0.24, $p < 0.01$) in patients compared to healthy donors. We also showed the addition of plasma significantly upregulated *ITGA5, and ITGB1* (AME from 0.28 to 0.29, $p < 0.005$), while the addition of conditioned medium from plaque upregulated *ITGA5* (AME 0.23, $p < 0.01$) and downregulated *ITGA4* (AME −0.23, $p < 0.03$). Spearman correlation analysis (**Figure 3B**) revealed a group of co-expressed integrin mRNAs: *ITGA1, ITGA4, ITGB1,* and *ITGA5* in CTLs. We evaluated the mRNA levels of chemokine receptors typically present on blood CD8+ CTLs (**Supplementary Figure 4**). The mRNAs coding CCR4, CCR5, and CX3CR1 were all expressed at high levels, did not differ significantly between patients and healthy donors, and did not depend on the coating type as assessed in the generalized linear model (data not shown). However, we observed a strong positive correlation between the levels of these mRNAs in the whole sample set (Spearman coefficient >0.9, **Figure 3B**).

CTLs were immunostained with anti-β1 and anti-α4 in all experimental conditions followed by confocal imaging. No correlation of morphologic features or integrin distribution with experimental conditions was observed. However, in all cases, the β1 and α4 integrins were localized on the plasma membrane as shown by maximal intensity projection images and co-localized at the sites of focal adhesions (**Supplementary Figures 5A–L**).

DISCUSSION

T-lymphocytes are among the most motile cells in the human organism with a maximum *in vivo* velocity of 25 um/min (23) measured for migration within the lymph node and shown to be integrin-independent (24, 25). In this study, we sought to work out the model of integrin-dependent CTL migration that would allow assessment of their adhesion/migration metrics and

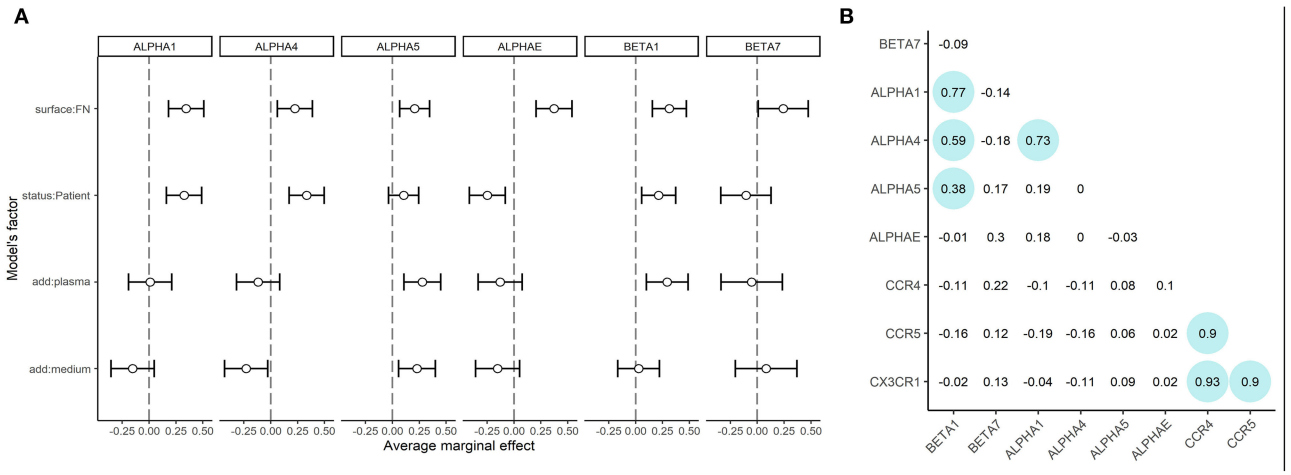

FIGURE 3 | mRNA expression of integrin subunits and in CTLs **(A)** Integrin mRNA expression. Average marginal effects (AME) for linear generalized model, where zero states are CTLs from healthy donors, seeded on plastic without soluble ligands from plasma or conditioned medium from atherosclerotic plaques. The changed (model) factors are: (1) the status of the individual: donor/patient with atherosclerosis, (2) use of fibronectin in coating; (3) use of conditioned medium from atherosclerotic plaque in coating; (4) use of plasma from patients with atherosclerosis in coating. The dependent variable is the expression of integrins beta1, beta7, alpha1, alpha4, alpha5 or alphaE mRNAs.*ITGB1, ITGB7, ITGA1, ITGA4, ITGA5, and ITGAE* are upregulated (dependent, $p < 0.05$) in the presence of fibronectin. *ITGB1, ITGA1, ITGA4* are upregulated (dependent, $p < 0.05$) in patients compared to healthy donors. *ITGAE* is downregulated (dependent, $p < 0.05$) in patients compared to healthy donors. *ITGB1 and ITGA5* are upregulated (dependent, $p < 0.05$) in the presence of plasma. *ITGA5* is upregulated (dependent, $p < 0.05$) and *ITGA4* are downregulated (dependent, $p < 0.05$) in the presence of a conditioned medium from atherosclerotic plaque. **(B)** Spearman coefficients of correlation for mRNA expression data. The significant correlations ($p < 0.05$) are outlined in circles. A strong positive correlation is observed between *CCR5, CCR4, and CX3CR1* mRNAs expression. The mRNAs expression of *ITGB1, ITGA1, and ITGA4* also show positive correlation, additionally, *ITGB1* shows a weaker correlation with *ITGA5*.

to evaluate the expression levels of integrins and chemokine receptors in it. The model of migration on rigid substrate fibers accounts for the integrin switch that takes place in transendothelial (26) and intra-tissue migration of some T-cell populations during inflammation (27) *in vivo*. It allows the assessment of the resulting alterations in cell motility descriptors and is thus relevant *in vitro* model of plaque infiltration.

We used fibronectin coating as a source of extracellular matrix fibers and patient plasma/conditioned medium as additional sources of ligands associated with atherosclerosis. There is a lot of evidence that the blood plasma of patients with atherosclerosis is enriched in activation molecules, including chemokines which can drive CTL migration, e.g., CCL5, CCL4, CCL3, CX3CL1 (28, 29). A similar pattern of chemokines has been detected in atherosclerotic plaque lysates and in conditioned media from plaque explants (18, 29), although due to some differences in chemokine content we decided to use plasma and conditioned medium as two independent sources of stimulatory molecules. To analyze the activation status of CTLs in our assay, we measured the mRNA expression levels of chemokine receptors that were justified in previous studies: We and other authors showed that CCR4, CCR5, and CX3CR1 chemokine receptors are differentially expressed on T-lymphocytes in atherosclerotic plaques compared to peripheral blood T-lymphocytes and that mRNAs of *CCL2*, *CCL3,* and *CX3CL1* that code chemokine ligands to these receptors are expressed in plaques (30, 31). We observed a strong positive correlation of these receptors' expression both in CTLs from patients and healthy donors and that did not depend on the experimental conditions in this study. T-cell adhesion and migration were shown to be independently regulated in other models involving cell cultures and mice (32). This may also be the case for human *ex vivo* CTLs as is seen from the lack of correlation between the chemokine receptors' and integrins' expression.

To analyze the expression patterns of adhesion molecules in our assay we measured the mRNA expression levels of *ITGA1, ITGA4, ITGA5, ITGAE, ITGB1, and ITGB7* that encode the α1, α4, α5, αE, β1, and β7 integrins. As expected, in our model we observed the substantial upregulation of α4, α5, and β1 in CTLs plated on fibronectin, as it is an activation ligand for these molecules, but other integrins were also upregulated on fibronectin coating compared to non-coated plastic, possibly due to non-specific activation. It is worth noting that integrins are capable of promoting taxis as well as adhesion: as co-stimulatory molecules, some integrins may also play a role in T-lymphocyte activation and migration by binding glycoproteins on endothelial cells: thus CTLs may be co-stimulated by β1 integrin-dependent interaction with fibronectin (33, 34). To further understand the cross-talk between the integrins and chemokine receptors a signaling gradient must be added to the model.

Using the generalized linear model we showed that the expression levels of *ITGA1, ITGA4, and ITGB1* were elevated in CTLs from patients compared to healthy donors, and also that *ITGA5, ITGB1* could be elevated by the addition of plasma and/or conditioned medium from atherosclerotic plaques thus indicating the integrin patterns for CTLs of patients with atherosclerosis. This is important as the current

works on gene expression report differential signaling, and pro-inflammatory and immune regulation-associated gene patterns for both bloods- and plaque-derived cells [30, 35]. No specific plaque-infiltrating phenotype [by analogy with skin-infiltrating and gut-infiltrating phenotypes (35)] that would include both integrins and chemokine receptors has been reported for these CTLs so far. The upregulated α4β1 and α1β1 integrins are known to provide the firm adhesion to endothelial cells before T-cell transmigration (36, 37), so their upregulation could be expected for CTLs of patients with atherosclerosis. To assess the integrin expression/localization at the protein level, we visualized β1 and α4 integrins in patient and donor CTLs. In all experimental conditions, the subunits were localized on the plasma membrane and co-localized at the sites of focal adhesions, although no significant differences in FA morphology were found using confocal imaging.

However, in our assay, the CTLs from patients with atherosclerosis showed significantly elevated adhesiveness. Also, CTLs from patients moved slightly faster and further than CTLs from healthy donors, but to prove the statistically significant differences high-throughput microscopy should be applied. In line with other experiments, we showed that CTLs could not maintain directional movement without the gradient of soluble ligands (38).

In conclusion, our study demonstrates the common effect of substrate on all integrins and justifies the use of extracellular fibers in CTL adhesion/migration experiments. On the other hand, it highlights a number of specific integrins that have elevated expression in CTLs of patients with atherosclerosis compared to healthy donors (*ITGA1, ITGA4, ITGB1*) and integrins that are upregulated in contact with the plasma of patients with atherosclerosis and/or conditioned media from atherosclerotic plaques (*ITGA5, ITGB1*). Such elevation may contribute to their enhanced adhesiveness and be of clinical importance in view of their plaque infiltration capacity *in vivo*.

DATA AVAILABILITY STATEMENT

The original contributions presented in the study are included in the article/**Supplementary Material**, further inquiries can be directed to the corresponding author.

ETHICS STATEMENT

The studies involving human participants were reviewed and approved by Interuniversity Committee of Ethics, Moscow (Prot #11 16.12.2021). The patients/participants provided their written informed consent to participate in this study.

AUTHOR CONTRIBUTIONS

DP, AS, and AT conceived and performed the experiments, analyzed the data, and wrote the manuscript. AA and AB provided clinical material and summarized the clinical data. LM and EV conceived the experiments, analyzed the data, and edited the manuscript. All authors contributed to the article and approved the submitted version.

FUNDING

The work was supported by the RSF grant #20-75-10085.

ACKNOWLEDGMENTS

We are grateful to the Moscow State University Development Program for providing access to the Confocal Microscope Zeiss LSM900.

SUPPLEMENTARY MATERIAL

The Supplementary Material for this article can be found online at: https://www.frontiersin.org/articles/10.3389/fmed.2022.891916/full#supplementary-material

REFERENCES

1. Krummel M, Bartumeus F, Gérard A. T cell migration, search strategies and mechanisms. *Nat Rev Immunol.* (2016) 16:193–201. doi: 10.1038/nri.2015.16
2. Schmidt ME, Varga SM. The CD8 T cell response to respiratory virus infections. *Front Immunol.* (2018) 9:678. doi: 10.3389/fimmu.2018.00678
3. Weigelin B, Krause M, Friedl P. Cytotoxic T lymphocyte migration and effector function in the tumor microenvironment. *Immunol Lett.* (2011) 138:19–21. doi: 10.1016/j.imlet.2011.02.016
4. Mellado M, Martínez-Muñoz L, Cascio G, Lucas P, Pablos JL, Rodríguez-Frade JM. T cell migration in rheumatoid arthritis. *Front Immunol.* (2015) 6:384. doi: 10.3389/fimmu.2015.00384
5. Saigusa R, Winkels H, Ley K. T cell subsets and functions in atherosclerosis. *Nat Rev Cardiol.* (2020) 17:387–401. doi: 10.1038/s41569-020-0352-5
6. Li J, Ley K. Lymphocyte migration into atherosclerotic plaque. *Arterioscler Thromb Vasc Biol.* (2015) 35:40–9. doi: 10.1161/ATVBAHA.114.303227
7. Soehnlein O, Libby P. Targeting inflammation in atherosclerosis — from experimental insights to the clinic. *Nat Rev Drug Discov.* (2021) 20:589–610. doi: 10.1038/s41573-021-00198-1
8. Roman MJ, Shanker BA, Davis A, Lockshin MD, Sammaritano L, Simantov R, et al. Prevalence and correlates of accelerated atherosclerosis in systemic lupus erythematosus. *N Engl J Med.* (2003) 349:2399–406. doi: 10.1056/NEJMoa035471
9. Avina-Zubieta JA, Choi HK, Sadatsafavi M, Etminan M, Esdaile JM, Lacaille D. Risk of cardiovascular mortality in patients with rheumatoid arthritis: a meta-analysis of observational studies. *Arthritis Rheum.* (2008) 59:1690–7. doi: 10.1002/art.24092
10. Kearns A, Gordon J, Burdo TH, Xuebin Q. HIV-1-associated atherosclerosis: unraveling the missing link. *J Am Coll Cardiol.* (2017) 69:3084–98. doi: 10.1016/j.jacc.2017.05.012
11. Grivel JC, Ivanova O, Pinegina N, Blank PS, Shpektor A, Margolis LB, et al. Activation of T-lymphocytes in atherosclerotic plaques. *Arterioscler Thromb Vasc Biol.* (2011) 31:2929–37. doi: 10.1161/ATVBAHA.111.237081
12. Tabas I, Lichtman AH. Monocyte-macrophages and T cells in atherosclerosis. *Immunity.* (2017) 47:621–34. doi: 10.1016/j.immuni.2017.09.008
13. Shaefer S, Zernecke A. CD8+ T cells in atherosclerosis. *Cells.* (2021) 10:37. doi: 10.3390/cells10010037
14. Kyaw T, Winship A, Tay C, Kanellakis P, Hosseini H, Cao A. Cytotoxic and proinflammatory CD8+ T lymphocytes promote development of vulnerable atherosclerotic plaques in apoE-deficient mice. *Circulation.* (2013) 127:1028–39. doi: 10.1161/CIRCULATIONAHA.112.001347

15. Berencsi K, Rani P, Zhang T, Gross L, Mastrangelo M, Meropol MJ. *In vitro* migration of cytotoxic T lymphocyte derived from a colon carcinoma patient is dependent on CCL2 and CCR2. *J Transl Med.* (2011) 9:33. doi: 10.1186/1479-5876-9-33
16. Sadjadi Z, Zhao R, Hoth M, Qu B, Rieger H. Migration of cytotoxic t lymphocytes in 3D collagen matrices. *Biophys J.* (2020) 119:2141–52. doi: 10.1016/j.bpj.2020.10.020
17. Cheung SMS, Ostergaard HL. Pyk2 controls integrin-dependent CTL migration through regulation of de-adhesion. *J Immunol*. (2016) 197:1945–56. doi: 10.4049/jimmunol.1501505
18. Lebedeva A, Vorobyeva D, Vagida M, Ivanova O, Felker E, Fitzgerald W. *Ex vivo* culture of human atherosclerotic plaques: a model to study immune cells in atherogenesis. *Atherosclerosis.* (2017) 267:90–8. doi: 10.1016/j.atherosclerosis.2017.10.003
19. Vandesompele J, De Preter K, Pattyn F, Poppe B, Van Roy N, De Paepe A. Accurate normalization of real-time quantitative RT-PCR data by geometric averaging of multiple internal control genes. *Genome Biol*. (2002). doi: 10.1186/gb-2002-3-7-research0034
20. R Core Team R. *A Language and Environment for Statistical Computing*. R Foundation for Statistical Computing, Vienna, Austria (2021). Available online at: https://www.R-project.org/
21. Leeper TJ. margins: Marginal Effects for Model Objects. R package version 0.3.26 (2021). Available online at: https://cran.r-project.org/web/packages/margins/citation.html
22. Wickham H. *ggplot2: Elegant Graphics for Data Analysis*. Springer-Verlag New York (2016). Available online at: https://cran.r-project.org/web/packages/ggplot2/citation.html
23. Miller MJ, Wei SH, Parker I, Cahalan MD. Two-photon imaging of lymphocyte motility and antigen response in intactlymph node. *Science.* (2002) 296:1869–73. doi: 10.1126/science.1070051
24. Woolf E, Grigorova I, Sagiv A, Grabovsky V, Feigelson SW, Shulman Z, et al. Lymph node chemokines promote sustained T lymphocyte motility without triggering stable integrin adhesiveness in the absence of shear forces. *Nat Immunol.* (2007) 8:1076–85. doi: 10.1038/ni1499
25. Lammermann T, Bader BL, Monkley SJ, Worbs T, Wedlich-Soldner R, Hirsch K, et al. Rapid leukocyte migration by integrin-independent flowing and squeezing. *Nature.* (2008) 453:51–5. doi: 10.1038/nature06887
26. Muller WA. The regulation of transendothelial migration: new knowledge and new questions. *Cardiovasc Res.* (2015) 107:310–20. doi: 10.1093/cvr/cvv145
27. Overstreet MG, Gaylo A, Angermann BR, Hughson A, Hyun YM, Lambert K, et al. Inflammation-induced interstitial migration of effector CD4 T cells is dependent on integrin alpha. *Nat Immunol.* (2013) 14:949–58. doi: 10.1038/ni.2682
28. Basiak M, Kosowski M, Hachula M, Okopien B. Plasma concentrations of cytokines in patients with combined hyperlipidemia and atherosclerotic plaque before treatment initiation—a pilot study. *Medicina.* (2022) 58:624. doi: 10.3390/medicina58050624
29. Edsfeldt A, Grufman H, Asciutto G, Nitulescu M, Persson A, Nilsson M, et al. Circulating cytokines reflect the expression of pro-inflammatory cytokines in atherosclerotic plaques. *Atherosclerosis.* (2015) 241:443–9. doi: 10.1016/j.atherosclerosis.2015.05.019
30. Fernandez DM, Rahman AH, Fernandez NF, Chudnovskiy A, Amir ED, Amadori L. Single-cell immune landscape of human atherosclerotic plaques. *Nat Med.* (2019) 25:1576–88. doi: 10.1038/s41591-019-0590-4
31. Komissarov A, Potashnikova D, Freeman ML, Gontarenko V, Maytesyan D, Lederman MM. Driving T cells to human atherosclerotic plaques: CCL3/CCR5 and CX3CL1/CX3CR1 migration axes. *Eur J Immunol.* (2021) 51:1857–9. doi: 10.1002/eji.202049004
32. Köchl R, Thelen F, Vanes L, Brazao TF, Fountain K, Xie J. WNK1 kinase balances T cell adhesion versus migration *in vivo*. *Nat Immunol.* (2016) 17:1075–83. doi: 10.1038/ni.3495
33. Matsuyama T, Yamada A, Kay J, Yamada KM, Akiyama SK, Schlossman SF. Activation of CD4 cells by fibronectin and anti-CD3 antibody. A synergistic effect mediated by the VLA-5 fibronectin receptor complex. *J Exp Med.* (1989) 170:1133–48. doi: 10.1084/jem.170.4.1133
34. Nojima Y, Humphries MJ, Mould AP, Komoriya A, Yamada KM, Schlossman SF. VLA-4 mediates CD3-dependent CD4+ T cell activation via the CS1 alternatively spliced domain of fibronectin. *J Exp Med.* (1990) 172:1185–92. doi: 10.1084/jem.172.4.1185
35. Nolz JC. Molecular mechanisms of CD8(+) T cell trafficking and localization. *Cell Mol Life Sci.* (2015) 72:2461–73. doi: 10.1007/s00018-015-1835-0
36. Osborn L, Vassallo C, Benjamin CD. Activated endothelium binds lymphocytes through a novel binding site in the alternately spliced domain of vascular cell adhesion molecule-1. *J Exp Med.* (1992) 176:99–107. doi: 10.1084/jem.176.1.99
37. Hermann GG, Geertsen PF, von der Maase H, Steven K, Andersen C, Hald T, et al. Recombinant interleukin-2 and lymphokine-activated killer cell treatment of advanced bladder cancer: clinical results and immunological effects. *Cancer Res*. (1992) 52:726–33.
38. Poznansky M, Olszak I, Foxall R, Evans RH, Luster AD, Scadden DT. Active movement of T cells away from a chemokine. *Nat Med.* (2000) 6:543–8. doi: 10.1038/75022

Conflict of Interest: The authors declare that the research was conducted in the absence of any commercial or financial relationships that could be construed as a potential conflict of interest.

Publisher's Note: All claims expressed in this article are solely those of the authors and do not necessarily represent those of their affiliated organizations, or those of the publisher, the editors and the reviewers. Any product that may be evaluated in this article, or claim that may be made by its manufacturer, is not guaranteed or endorsed by the publisher.

frontiers | Frontiers in Medicine

TYPE Mini Review
PUBLISHED 05 October 2022
DOI 10.3389/fmed.2022.1026521

OPEN ACCESS

EDITED BY
Vadim V. Sumbayev,
University of Kent, United Kingdom

REVIEWED BY
Helge Meyer,
University of Oldenburg, Germany
Jugal Das,
Texas A&M Health Science Center, United States

*CORRESPONDENCE
David A. Fox
dfox@med.umich.edu

SPECIALTY SECTION
This article was submitted to Pathology, a section of the journal Frontiers in Medicine

RECEIVED 24 August 2022
ACCEPTED 16 September 2022
PUBLISHED 05 October 2022

CITATION
Gurrea-Rubio M and Fox DA (2022) The dual role of CD6 as a therapeutic target in cancer and autoimmune disease. *Front. Med.* 9:1026521. doi: 10.3389/fmed.2022.1026521

The dual role of CD6 as a therapeutic target in cancer and autoimmune disease

Mikel Gurrea-Rubio and David A. Fox*

Division of Rheumatology, Department of Internal Medicine, University of Michigan, Ann Arbor, MI, United States

Autoimmune disease involves loss of tolerance to self-antigen, while progression of cancer reflects insufficient recognition and response of the immune system to malignant cells. Patients with immune compromised conditions tend to be more susceptible to cancer development. On the other hand, cancer treatments, especially checkpoint inhibitor therapies, can induce severe autoimmune syndromes. There is recent evidence that autoimmunity and cancer share molecular targets and pathways that may be dysregulated in both types of diseases. Therefore, there has been an increased focus on understanding these biological pathways that link cancer and its treatment with the appearance of autoimmunity. In this review, we hope to consolidate our understanding of current and emerging molecular targets used to treat both cancer and autoimmunity, with a special focus on Cluster of Differentiation (CD) 6.

KEYWORDS

CD6, CD318, ALCAM (CD166), NK cells, CD8 lymphocytes+, autoimmunity, cancer

Cancer and autoimmunity

Cancer cells can take advantage of physiologic immunoregulatory mechanisms to evade immune responses. Typically, a decrease in numbers and/or function of regulatory T and B cells, dendritic cells and M2 macrophages favors autoimmunity, while an increase in the same cell subsets or functions is associated with cancer progression. In most cancers, the immune infiltrate is composed of macrophages, T regulatory cells (Tregs), cytotoxic T cells and NK cells, whereas neutrophils and dendritic cells are typically found outside the tumor border (1). Autoimmune conditions are usually associated with increased T helper (Th) type 1 and 17 cells, and in some diseases infiltrates that also include B lymphocytes and plasma cells (2).

The tumor microenvironment (TME) is increasingly recognized as having a key role in tumor progression, largely due to the interactions between cancer, immune, vascular and stromal cells that take place in and around the tumor site. One distinct characteristic of the TME is its high levels of TGF-β (transforming growth factor beta), which is regarded as a key cytokine in promotion of immunosuppression (3). Tregs, which are typically characterized by an up-regulated expression of forkhead box P3 *(FoxP3)*, are found in high proportions within the TME of most cancers. These highly activated and immunosuppressive cells are known to infiltrate the lung, breast and pancreatic TME and

have the ability to suppress cytotoxic CD8+ T cells, NK cells, NKT cells, M1 macrophages and the maturation of dendritic cells (4). The mechanisms by which Tregs suppress anti-tumor immunity remain largely undefined, although recent studies point out that most Tegs can suppress NK cells by (i) deprivation of IL-2, (ii) induction of apoptosis and (iii) generation of Indoleamine 2,3-dioxygenase (IDO) and adenosine (ADO) *via* the expression of CD39 and CD73 (5, 6). Tumor specific CD8+ T cell cytotoxicity is suppressed both *in vitro* and *in vivo* through TGF-β signals (7).

Current therapeutic targets for autoimmunity and cancer

Autoimmunity is known to act as a substrate for the emergence of cancer and *vice versa*. Chronic inflammation causes DNA damage and creates an environment favorable for the development of cancer. Conversely, many patients with malignancies develop autoimmune and rheumatic manifestations, especially those who are treated with checkpoint inhibition therapies. Therefore, there has been a recent interest in developing new targets linked to molecular pathways and cell surface proteins that are known to be important in the development of both cancer and autoimmunity.

CD20 is expressed on the surface of mature B cells and is known to contribute to the activation and proliferation of B cells by intracellular tyrosine phosphorylation. Monoclonal antibodies against CD20 (rituximab and ofatumumab) have been successfully used for the treatment of B-cell lymphoma and some autoimmune diseases such as rheumatoid arthritis (8–11).

CXCR3 (GPR9/CD183) has also been studied as target for autoimmunity and cancer. This chemokine receptor is primarily expressed on CD4+ and CD8+ T cells, dendritic cells, NK cells and on non-immune cells such as fibroblastic, endothelial and epithelial cells (12). Among the CXCR3-binding chemokines, two groups can be distinguished based on their structural form. The first group is composed of CXCL9, CXCL10 and CXCL11, which are key immune chemoattractants during interferon-induced inflammatory responses. The second group is formed by the platelet-derived ligands CXCL4 and CXCL4L1, which are known to exhibit potent antiangiogenic activity and bind both CXCR3A and CXCR3B (12). The roles of CXCR3 ligands in autoimmunity have been extensively studied. In rheumatoid arthritis (RA), high CXCR3 expression on mast cells is associated with CXCL9 and CXCL10 expression in synovial fluid from RA patients but not in traumatic arthritis or osteoarthritis patients (13). Synovial CXCL10 expression is highly elevated in juvenile idiopathic arthritis (JIA) and, interestingly, raised levels of CXCL4 in plasma have also been observed in a subset of RA patients, specifically in those with vascular lesions.

The CXCR3 axis is also implicated in the pathogenesis of lupus nephritis and inflammatory bowel disease. For instance, in murine models of lupus nephritis, CXC3R directs pathogenic effector T cells into the kidney (14). In cancer, CXCR3 ligands, as well as several other chemokines, recruit innate and adaptive immune cells into the tumor microenvironment. For instance, CXCR3+ lymphocytes are attracted by CXCL9, which is secreted by stromal cells in gastric and ovarian cancer, thus facilitating the entrance of lymphocytes into the tumor sites. CXCL10 also potentiates the accumulation of CXCR3+ effector T cells, particularly CD8+ T cells, into the tumor microenvironment and directly suppresses tumor growth in various cancers (15, 16). Another important role of CXCR3 ligands in anti-tumor immunity relies on the effectiveness of CXCL4 and CXCL4L1 (factors produced by platelets) at inhibiting lymphangiogenesis and preventing metastatic escape of tumor cells *via* the lymphatic vasculature (17).

The pro-inflammatory cytokine interleukin-6 (IL-6) is another example of a therapeutic target that has been linked to both autoimmunity and cancer. The IL-6 signaling cascade is known to play a role in Th17 differentiation (18). Several IL-6 blocking antibodies have been approved for the treatment of rheumatoid arthritis. More recently, because the IL-6-STAT3 signaling pathway can be directly involved in progression and metastasis of prostate cancer, evaluation of IL-6 and its receptor as targets for cancer treatment is currently being explored (19).

Celecoxib and rofecoxib are two cyclooxygenase-2 (COX-2) inhibitors that have been used to relieve the inflammation and pain of patients with osteoarthritis (OA) and rheumatoid arthritis (RA). These inhibitors and are also found to extend the overall survival of stage III colon cancer patients and non-small cell lung cancer patients (20). There is, however, a concern regarding the use of COX-2 inhibitors and the risk of developing cardiovascular disease.

The recent success of immune checkpoint inhibitors for the treatment of cancer has encouraged researchers to assess the potential use of checkpoint agonists for the treatment of autoimmunity. Currently, there are multiple clinical trials investigating these therapies. Strategies to treat autoimmunity safely and successfully through manipulation of checkpoint interactions will need to consider the multiple ligands and receptors pertinent to these targets.

Novel therapeutic targets for autoimmunity and cancer: CD6

CD6 is a 105 to 130 kDa type I transmembrane glycoprotein belonging to the highly conserved scavenger receptor cysteine-rich superfamily (SRCR-SF). It is expressed by virtually all T cells, a subset of NK cells, B-lymphocyte B1a subsets, immature B cells and certain regions of the brain. Structurally, CD6 has an extracellular region composed of three SRCR domains and an intracellular portion with sites for the phosphorylation and recruitment of signal transduction

proteins (21). Functionally, CD6 is involved in lymphocyte activation and differentiation upon adhesive contacts with antigen-presenting cells (APCs). Thus, far, CD6 has two known ligands: CD166 (activated leukocyte cell adhesion molecule or ALCAM) and CD318 (CDCP1, TRASK, SIMA135, or gp140). ALCAM/CD166 is expressed on activated T cells, monocytes, endothelium, epithelial cells and synovial fibroblasts. CD318 is expressed on epithelial and tumor cells with which T cells interact, but not by immune cells (22).

CD6-ALCAM interaction

The first known ligand for CD6 was the Activated Cell Adhesion Molecule (ALCAM), also known as CD166. ALCAM is a cell surface glycoprotein related to the immunoglobulin superfamily molecules. It can be proteolytically cleaved by metalloproteases, causing its ectodomain to shed (23). The interaction between CD6 and its ALCAM (CD166) is important during immune development and in alloreactivity. It stabilizes the adhesive contacts established between T cells and APCs and optimizes subsequent proliferative and differentiation responses. In recent years, the CD6-ALCAM axis has been implicated in the pathogenesis of multiple autoimmune diseases and cancer (24).

CD6 was first identified and validated as risk gene for multiple sclerosis (MS) in 2009 and, soon after, the CD6-ALCAM axis was shown to play a crucial role in the pathogenesis of this disease. In a large genetic study of CD6, ALCAM and neuroinflammation, a polymorphism of ALCAM (rs579565G>A) and two SNPs of CD6 (rs17824933C>G and rs12360861G>A) were found to be strongly associated with risk, development and progression of MS. The risk of MS for AA individuals in rs12360861 was three-fold lower in comparison to GG individuals. Furthermore, significantly lower expression of CD6 mRNA was found in lymphocytes from MS patients compared to healthy individuals (25).

Knockout mice of CD6 and its ligands have been extensively studied in models of inflammation and autoimmunity. For instance, $CD6^{-/-}$ mice are protected from experimental autoimmune encephalomyelitis (EAE), an animal model of autoimmune inflammatory diseases of the central nervous system commonly used for the study of MS. In these mice, CD6 deficiency leads to reduced Th1 and Th17 polarization and provides protection from spinal cord demyelination *in vivo* (26). $ALCAM^{-/-}$ mice, however, develop a more severe autoimmune encephalomyelitis, due to an increased permeability of the brain blood barrier. This is believed to be caused by a dysregulation of junctional adhesion molecules with which ALCAM indirectly binds, suggesting an important function of ALCAM in maintaining the blood brain barrier integrity (27).

The CD6-ALCAM pathway is also implicated in the pathogenesis of lupus nephritis (LN). In mouse models of lupus, blockade of CD6 with an anti-mouse CD6 monoclonal antibody decreases T cell infiltration, cytokine levels and overall renal pathology (28). Furthermore, a recent study has shown that ALCAM and CD6 are elevated in patients with LN. High numbers of CD6+ cells were found exclusively in T cells from patients with LN, while ALCAM was expressed by renal cells, also at higher levels compared to normal individuals. Notably, itolizumab is currently being evaluated for safety, pharmacokinetics and pharmacodynamics for the treatment of LN. Itolizumab is an IgG1 monoclonal antibody that targets the extracellular SRCR distal domain 1 of CD6. Itolizumab has been shown to significantly reduce differentiation of T cells to Th17 cells and decrease production of IL-17 in patients with psoriasis in India (24, 29).

Similar to MS and LN, rheumatoid arthritis (RA) is another autoimmune disease in which CD6 is involved in its pathogenesis. CD6 and its ligands are strongly expressed in RA joints and are important for the initiation and maintenance of collagen induced arthritis (CIA), a T cell driven mouse model for RA. $CD6^{-/-}$ mice develop lower clinical arthritis scores than wildtype (WT) mice, proving that CD6 can tune the severity of joint inflammation in these mice. Collagen-specific Th9 and Th17 are also decreased in $CD6^{-/-}$ mice, as well as multiple pro-inflammatory joint cytokines. Unsurprisingly, treatment with UMCD6 (anti-CD6) in CD6 humanized mice, displays similarly effective responses in reducing joint inflammation in CIA (30).

Sjogren's syndrome and inflammatory bowel disease are two other autoimmune diseases in which CD6 and its ligand ALCAM (CD166) might play an important role in their pathogenesis. In Sjögren's syndrome, ALCAM is overexpressed in the salivary glands of these patients and the use of itolizumab as therapeutic option has been proposed for clinical trials (31). Similarly, the expression of both CD6 and ALCAM (CD166) is markedly increased in the inflamed mucosa of inflammatory bowel disease patients compared with normal controls (32–34).

In cancer, ALCAM has been linked to poorer prognosis and higher metastatic risk in some cancers such as breast, thyroid, head and neck and liver cancer (35). ALCAM-positive cells have superior sphere-forming ability and cancer-initiating potential in prostate cancer and promote evasion of apoptosis in breast cancer. Specifically in breast cancer, high expression of ALCAM occurs in approximately 50% of patients with triple-negative cancers and around 80% in patients with estrogen receptor positive, human epidermal growth factor receptor 2 (HER2) tumors (36). Praluzatamab ravtansine or CX-2009, an activated antibody-drug conjugate that targets ALCAM, is currently undergoing phase II clinical trials for the treatment of breast cancer (36). Notably, a single-chain antibody named scFv173, which recognizes ALCAM, has been shown to reduce ALCAM-mediated adhesion in breast cancer, both *in vitro* and *in vivo* (35). ALCAM is also up-regulated in liver tissue and serum from patients with hepatocellular carcinoma (HCC). In pancreatic

cancer, patients whose circulating cancer cells have high levels of ALCAM, tend to have significantly shorter survival. Moreover, high levels of ALCAM in colorectal tumors are strictly associated with poorer survival, nodal status, tumor grade and high risk of metastasis (29). Use of ALCAM targeted therapeutics for cancer might raise issues of off target consequences related to widespread expression of ALCAM on other cell types including many types of cells of the immune system.

However, ALCAM expression is not always linked to bad prognosis in cancer. In sarcomas, the vast majority of patients with high levels of ALCAM have more favorable outcomes and tend to remain metastasis free (37). Similarly, in a recent multivariate survival analysis in patients with non-small cell lung cancer, expression of ALCAM strongly correlated with a better prognosis/longer patient survival (38).

CD6-CD318 interaction

Cub domain-containing protein 1 (CDCP1), also known as CD318, is a transmembrane glycoprotein expressed by fibroblasts and the epithelium of normal and cancer cells. CD318 is phosphorylated by Src family kinases before recruiting and activating protein kinase C delta type (PKCδ) (39).

In rheumatoid arthritis (RA), both known CD6 ligands, ALCAM and CD318, are known to participate in adhesion of T cells to fibroblast-like synoviocytes (FLS) derived from RA synovial tissue. Moreover, soluble CD318 (sCD318) is found in RA synovial fluid at levels higher than in normal or RA serum, and sCD318 is chemotactic for T cells at concentrations similar to the levels found in RA synovial fluid (22). As in *CD6*$^{-/-}$ mice, *CD318*$^{-/-}$ mice are also protected from autoimmune encephalomyelitis and collagen induced arthritis. In both *CD6*$^{-/-}$ mice and CD6-humanized mice treated with UMCD6 (mouse anti-human CD6 mAb), striking reductions in clinical signs of disease, pathogenic Th1/Th17 responses, and inflammatory cell infiltration into the target organs are observed, making the CD6-CD318 axis a novel and exciting regulator of T-cell driven autoimmunity (22). Similar studies have been done to examine the role of CD6 and its ligand CD318/CDCP1 in autoimmune uveitis (EAU). In these studies, *CD6*$^{-/-}$ mice with EAU had significantly decreased retinal inflammation and reduced autoreactive T cell responses, indicating that CD6-targeted therapies are a promising new treatment for uveitis (33, 34).

The role of CD318 (CDCP1) in cancer has been extensively explored. Overexpression of CD318 (CDCP1) uniformly correlates with poor overall survival in lung, colon, ovarian, breast, renal, hepatocellular, acute myeloid leukemia and pancreatic cancers, partly due to its involvement in tumor metastasis formation *via* Src. The first hints suggesting a link between CD318 and Src family kinases in cancer metastasis, came from studies of pharmacological inhibition of Src with PP2 and dasatinib. In these studies, both Src inhibitors strongly suppressed the growth of CD318-overexpressing cells in 3D cultures of soft agar (40).

Not only does CD318 (CDCP1) play an important role in the initiation of metastasis, but it also mediates cancer progression by altering cancer cell growth. Multiple studies have now demonstrated that CD318 expression is involved in cancer cell growth through its interaction with receptor tyrosine kinases (RTKs) and HER2 signaling pathways and their subsequent downstream proteins Ras, Src and AKT. For instance, the interaction between CD318 and HER2 promotes *in vitro* colony formation and *in vivo* orthotopic tumor growth in several models of breast cancer (41). In non-small lung cancer, Ras induces the expression of CD318 and drives Src-mediated survival in *in vitro* models of lung cancer (42). In ovarian cancers, CD318 mediates spheroid growth and is involved in the activation of AKT (43). Interestingly, some studies in pancreatic cancer also support the role of CD318 in cell migration and matrix degradation *via* different molecular mechanisms involving Src, PKCδ and MMP9 (27, 44).

Soon after CD318 was recognized as a second ligand of CD6, efforts were made to understand its potential role in anti-tumor immunity. Recent studies on the potential involvement of CD318 in anti-tumor immunity indicate that disrupting CD6-CD318 interaction is highly effective in experimental systems as a novel cancer immunotherapy. In co-culture experiments with cell lines derived from human triple-negative breast cancer, non-small-cell lung cancer, and prostate cancer, substantial enhancement of cancer cell death and reduced survival of cancer cells was found in the presence of human lymphocytes and UMCD6 (anti-CD6) (38). Importantly, this effect was consistently more robust than the effect of either pembrolizumab or nivolumab, two monoclonal antibodies against the Programmed Cell Dead Protein 1 (PD-1). The augmentation of lymphocyte cytotoxicity by targeting the CD6-CD318 axis with UMCD6 is due to direct effects of anti-CD6 on NK cells and CD8+ T cells when CD6 is internalized. Both *in vitro* and *in vivo,* multiple gene expression changes are seen in CD8+ T cells and NK cells treated with UMCD6, along with changes in the levels of the corresponding proteins, all of which are consistent with enhanced cytotoxic capabilities such as over-production of granzyme-b, perforin and activating receptors (e.g., NKG2D) and down-regulation of inhibitory receptors (e.g., NKG2A). Moreover, UMCD6 exerted similar effects *in vivo* in a human breast cancer xenograft system in immunodeficient mice. In those experiments, mice that received UMCD6 showed marked shrinkage of tumors by 1 week, accompanied by an aggressive infiltration of lymphocytes, dominated by NK cells (38). Using a different approach, high doses of recombinant CD6 that masked CD6 ligands *in vivo* generated a modest anti-cancer effect (45).

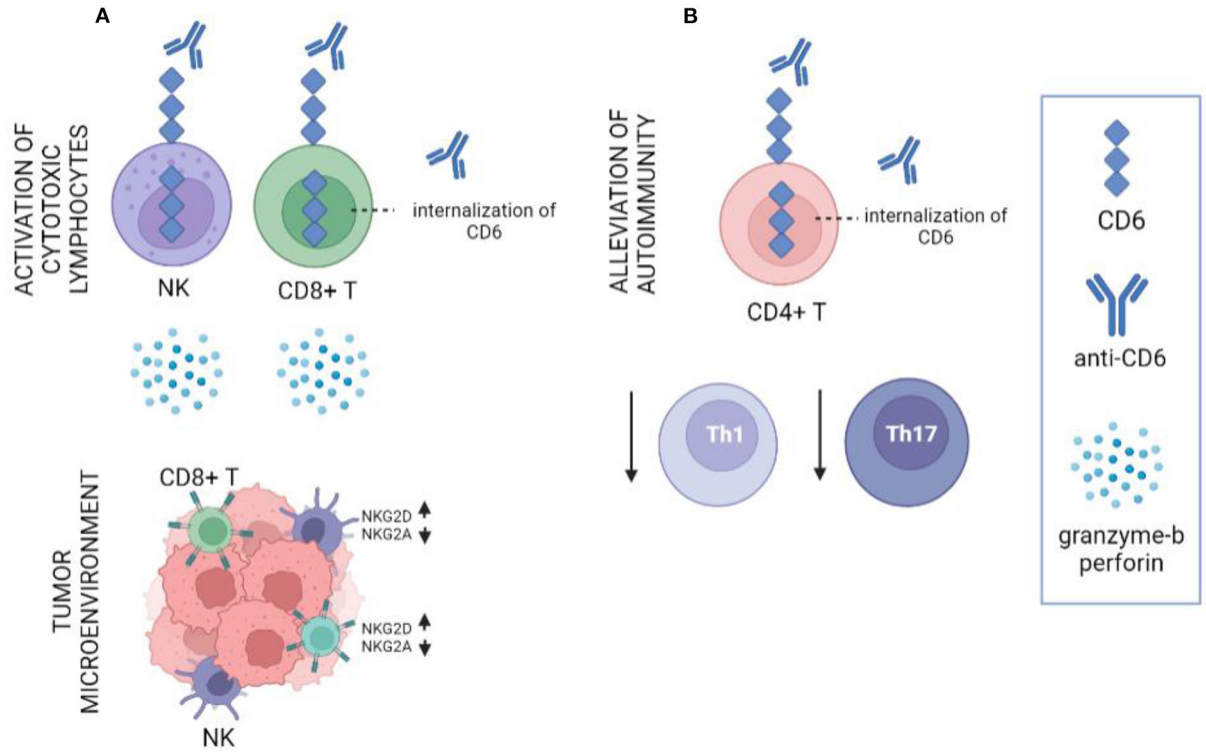

FIGURE 1
Schematic representation of the role of anti-CD6 (UMCD6) in cancer and autoimmunity. **(A)** Internalization of CD6 on CD8+ T cells and NK cells with UMCD6 induces the activation of these cells by up-regulation of granzyme-b, perforin and the activating receptors NKG2D, and down-regulation of the inhibitory receptor NKG2A. **(B)** UMCD6 provides a protective effect in autoimmune diseases by suppression of differentiation of effect Th1 and Th17 cells.

Despite CD318 being expressed in normal tissues, several findings suggest that toxicities associated with inhibition of its interactions with CD6 in patients with cancer, will be clinically manageable. CD318 knockout mice develop and reproduce normally and are protected from T cell driven autoimmunity, indicating that its functions are not essential for normal physiology. In contrast, humans or mice that lack PD-1 or cytotoxic T lymphocyte-associated antigen 4 (CTLA-4) exhibit a global autoimmune diathesis that corresponds to the toxicities observed when these structures are targeted in immunotherapy of cancer. A monoclonal antibody against CD318 has also been studied in the context of anti-tumor autoimmunity. Anti-CD318 produces a more modest effect on cancer cell death and survival compared to UMCD6 (anti-CD6). The more modest effect of anti-CD318 could be attributable to a dual effect of UMCD6: rapid internalization of CD6 prevents or reverses engagement of CD6 by its ligands on cancer cells, and UMCD6 also directly activates the cytotoxic properties of CD8+ and NK cells, whereas anti-CD318 does not have any effect on lymphocyte cytotoxicity (36, 52).

These findings point out that targeting CD6 and its ligand CD318 could both suppress autoimmune diseases through its effects on differentiation of effector CD4 cell subsets, while also activating the anti-cancer cytotoxic properties of CD8+ and NK cells, creating the potential for an approach to cancer immunotherapy that would suppress rather than instigate serious autoimmune diseases (Figure 1).

Conclusion

The association between autoimmunity and cancer is an area of particular interest for oncologists and rheumatologists, especially after the introduction of checkpoint inhibitors for the treatment of cancer. Many autoimmune disorders and immunosuppressive therapies have been linked to an increased risk for cancer. And many cancer patients develop autoimmune disorders as a result of cancer treatments. Currently, there are only a few approved therapeutics capable of treating both autoimmunity and cancer. These therapies presented above may have additional applications in both autoimmunity and cancer. With other molecular targets, such as CTLA-4, the approaches to treatment of cancer vs. autoimmunity are opposite, agonistic vs. antagonistic.

Pre-clinical studies, involving the CD6-CD318 axis, and an anti-CD6 monoclonal antibody, suggest new strategies that could treat autoimmunity and cancer simultaneously, through distinct effects on subsets of lymphocytes CD6 blockade concurrently reduces Th1 and Th17 differentiation and increases T cell and NK cell cytotoxicity. Better understanding of new mechanisms connecting autoimmunity and cancer provide hope that these two conditions can be successfully treated simultaneously.

Author contributions

All authors listed have made a substantial, direct, and intellectual contribution to the work and approved it for publication.

Acknowledgments

The authors would like to thank the following funding sources for their generous support: NIH Autoimmunity Center of Excellence and NIH Training Grant T32AR007080, the University of Michigan Rogel Cancer Center, the Michigan Translational Research & Commercialization program, and the Frederick G.L. Huetwell and William D. Robinson Professorship in Rheumatology at the University of Michigan.

Conflict of interest

The authors declare that the research was conducted in the absence of any commercial or financial relationships that could be construed as a potential conflict of interest.

Publisher's note

All claims expressed in this article are solely those of the authors and do not necessarily represent those of their affiliated organizations, or those of the publisher, the editors and the reviewers. Any product that may be evaluated in this article, or claim that may be made by its manufacturer, is not guaranteed or endorsed by the publisher.

References

1. Baghban R, Roshangar L, Jahanban-Esfahlan R, Seidi K, Ebrahimi-Kalan A, Jaymand M, et al. Tumor microenvironment complexity and therapeutic implications at a glance. *Cell Commun Signal.* (2020) 18:59. doi: 10.1186/s12964-020-0530-4

2. Bolon B. Cellular and molecular mechanisms of autoimmune disease. *Toxicol Pathol.* (2012) 40:216–29. doi: 10.1177/0192623311428481

3. Laine A, Labiad O, Hernandez-Vargas H, This S, Sanlaville A, Leon S, et al. Regulatory T cells promote cancer immune-escape through integrin alphavbeta8-mediated TGF-beta activation. *Nat Commun.* (2021) 12:6228. doi: 10.1038/s41467-021-26352-2

4. Shang B, Liu Y, Jiang SJ, Liu Y. Prognostic value of tumor-infiltrating FoxP3+ regulatory T cells in cancers: a systematic review and meta-analysis. *Sci Rep.* (2015) 5:15179. doi: 10.1038/srep15179

5. Li T, Yang Y, Hua X, Wang G, Liu W, Jia C, et al. Hepatocellular carcinoma-associated fibroblasts trigger NK cell dysfunction via PGE2 and IDO. *Cancer Lett.* (2012) 318:154–61. doi: 10.1016/j.canlet.2011.12.020

6. Hoskin DW, Mader JS, Furlong SJ, Conrad DM, Blay J. Inhibition of T cell and natural killer cell function by adenosine and its contribution to immune evasion by tumor cells (Review). *Int J Oncol.* (2008) 32:527–35. doi: 10.3892/ijo.32.3.527

7. Chen ML, Pittet MJ, Gorelik L, Flavell RA, Weissleder R, von Boehmer H, et al. Regulatory T cells suppress tumor-specific CD8 T cell cytotoxicity through TGF-beta signals *in vivo*. *Proc Natl Acad Sci U S A.* (2005) 102:419–24. doi: 10.1073/pnas.0408197102

8. Dabritz JH Yu Y, Milanovic M, Schonlein M, Rosenfeldt MT, Dorr JR, et al. CD20-targeting immunotherapy promotes cellular senescence in B cell lymphoma. *Mol Cancer Ther.* (2016) 15:1074–81. doi: 10.1158/1535-7163.MCT-15-0627

9. Pavlasova G, Mraz M. The regulation and function of CD20: an "enigma" of B-cell biology and targeted therapy. *Haematologica.* (2020) 105:1494–506. doi: 10.3324/haematol.2019.243543

10. Mok CC. Rituximab for the treatment of rheumatoid arthritis: an update. *Drug Des Devel Ther.* (2013) 8:87–100. doi: 10.2147/DDDT.S41645

11. Taylor PC, Quattrocchi E, Mallett S, Kurrasch R, Petersen J, Chang DJ. Ofatumumab, a fully human anti-CD20 monoclonal antibody, in biological-naive, rheumatoid arthritis patients with an inadequate response to methotrexate: a randomized, double-blind, placebo-controlled clinical trial. *Ann Rheum Dis.* (2011) 70:2119–25. doi: 10.1136/ard.2011.151522

12. Kuo PT, Zeng Z, Salim N, Mattarollo S, Wells JW, Leggatt GR. The role of CXCR3 and its chemokine ligands in skin disease and cancer. *Front Med.* (2018) 5:271. doi: 10.3389/fmed.2018.00271

13. Ruschpler P, Lorenz P, Eichler W, Koczan D, Hanel C, Scholz R, et al. High CXCR3 expression in synovial mast cells associated with CXCL9 and CXCL10 expression in inflammatory synovial tissues of patients with rheumatoid arthritis. *Arthritis Res Ther.* (2003) 5:R241–52. doi: 10.1186/ar783

14. Steinmetz OM, Turner JE, Paust HJ, Lindner M, Peters A, Heiss K, et al. CXCR3 mediates renal Th1 and Th17 immune response in murine lupus nephritis. *J Immunol.* (2009) 183:4693–704. doi: 10.4049/jimmunol.0802626

15. Nagpal ML, Davis J, Lin T. Overexpression of CXCL10 in human prostate LNCaP cells activates its receptor (CXCR3) expression and inhibits cell proliferation. *Biochim Biophys Acta.* (2006) 1762:811–8. doi: 10.1016/j.bbadis.2006.06.017

16. Barash U, Zohar Y, Wildbaum G, Beider K, Nagler A, Karin N, et al. Heparanase enhances myeloma progression *via* CXCL10 downregulation. *Leukemia.* (2014) 28:2178–87. doi: 10.1038/leu.2014.121

17. Van Raemdonck K, Van den Steen PE, Liekens S, Van Damme J, Struyf S. CXCR3 ligands in disease and therapy. *Cytokine Growth Factor Rev.* (2015) 26:311–27. doi: 10.1016/j.cytogfr.2014.11.009

18. Zheng Y, Sun L, Jiang T, Zhang D, He D, Nie H. TNFalpha promotes Th17 cell differentiation through IL-6 and IL-1beta produced by monocytes in rheumatoid arthritis. *J Immunol Res.* (2014) 2014:385352. doi: 10.1155/2014/385352

19. Chen T, Wang LH, Farrar WL. Interleukin 6 activates androgen receptor-mediated gene expression through a signal transducer and activator of transcription 3-dependent pathway in LNCaP prostate cancer cells. *Cancer Res.* (2000) 60:2132–5.

20. Liu B, Qu L, Yan S. Cyclooxygenase-2 promotes tumor growth and suppresses tumor immunity. *Cancer Cell Int.* (2015) 15:106. doi: 10.1186/s12935-015-0260-7

21. Bodian DL, Skonier JE, Bowen MA, Neubauer M, Siadak AW, Aruffo A, et al. Identification of residues in CD6 which are critical for ligand binding. *Biochemistry.* (1997) 36:2637–41. doi: 10.1021/bi962560+

22. Enyindah-Asonye G, Li Y, Ruth JH, Spassov DS, Hebron KE, Zijlstra A, et al. CD318 is a ligand for CD6. *Proc Natl Acad Sci U S A.* (2017) 114:E6912–E21. doi: 10.1073/pnas.1704008114

23. van Kempen LC, Nelissen JM, Degen WG, Torensma R, Weidle UH, Bloemers HP, et al. Molecular basis for the homophilic activated leukocyte cell adhesion molecule (ALCAM)-ALCAM interaction. *J Biol Chem.* (2001) 276:25783–90. doi: 10.1074/jbc.M011272200

24. Bughani U, Saha A, Kuriakose A, Nair R, Sadashivarao RB, Venkataraman R, et al. Correction: T cell activation and differentiation is modulated by a CD6 domain 1 antibody Itolizumab. *PLoS ONE.* (2018) 13:e0192335. doi: 10.1371/journal.pone.0192335

25. Wagner M, Bilinska M, Pokryszko-Dragan A, Sobczynski M, Cyrul M, Kusnierczyk P, et al. ALCAM and CD6–multiple sclerosis risk factors. *J Neuroimmunol.* (2014) 276:98–103. doi: 10.1016/j.jneuroim.2014.08.621

26. Li Y, Singer NG, Whitbred J, Bowen MA, Fox DA, Lin F. CD6 as a potential target for treating multiple sclerosis. *Proc Natl Acad Sci U S A.* (2017) 114:2687–92. doi: 10.1073/pnas.1615253114

27. Lecuyer MA, Saint-Laurent O, Bourbonniere L, Larouche S, Larochelle C, Michel L, et al. Dual role of ALCAM in neuroinflammation and blood-brain barrier homeostasis. *Proc Natl Acad Sci U S A.* (2017) 114:E524–E33. doi: 10.1073/pnas.1614336114

28. Chalmers SA, Ramachandran RA, Garcia SJ, Der E, Herlitz L, Ampudia J, et al. The CD6/ALCAM pathway promotes lupus nephritis via T cell-mediated responses. *J Clin Invest.* (2022) 132:e147334. doi: 10.1172/JCI147334

29. Tachezy M, Zander H, Marx AH, Stahl PR, Gebauer F, Izbicki JR, et al. ALCAM (CD166) expression and serum levels in pancreatic cancer. *PLoS ONE.* (2012) 7:e39018. doi: 10.1371/journal.pone.0039018

30. Li Y, Ruth JH, Rasmussen SM, Athukorala KS, Weber DP, Amin MA, et al. Attenuation of murine collagen-induced arthritis by targeting CD6. *Arthritis Rheumatol.* (2020) 72:1505–13. doi: 10.1002/art.41288

31. Alonso R, Buors C, Le Dantec C, Hillion S, Pers JO, Saraux A, et al. Aberrant expression of CD6 on B cell subsets from patients with Sjogren's syndrome. *J Autoimmun.* (2010) 35:336–41. doi: 10.1016/j.jaut.2010.07.005

32. Ma C, Wu W, Lin R, Ge Y, Zhang C, Sun S, et al. Critical role of CD6 high CD4+ T cells in driving Th1/Th17 cell immune responses and mucosal inflammation in IBD. *J Crohns Colitis.* (2019) 13:510–24. doi: 10.1093/ecco-jcc/jjy179

33. Zhang L, Li Y, Qiu W, Bell BA, Dvorina N, Baldwin WM. 3rd, et al. Targeting CD6 for the treatment of experimental autoimmune uveitis. *J Autoimmun.* (2018) 90:84–93. doi: 10.1016/j.jaut.2018.02.004

34. Zhang L, Borjini N, Lun Y, Parab S, Enyindah-Asonye G, Singh R, et al. CDCP1 regulates retinal pigmented epithelial barrier integrity for the development of experimental autoimmune uveitis. *JCI Insight.* (2022). doi: 10.1172/jci.insight.157038

35. Yang Y, Sanders AJ, Dou QP, Jiang DG, Li AX, Jiang WG. The clinical and theranostic values of Activated Leukocyte Cell Adhesion Molecule (ALCAM)/CD166 in human solid cancers. *Cancers.* (2021) 13:5187. doi: 10.3390/cancers13205187

36. Jeong YJ, Oh HK, Park SH, Bong JG. Prognostic significance of Activated Leukocyte Cell Adhesion Molecule (ALCAM) in association with promoter methylation of the ALCAM gene in breast cancer. *Molecules.* (2018) 23:131. doi: 10.3390/molecules23010131

37. Yang Y, Ma Y, Gao H, Peng T, Shi H, Tang Y, et al. A novel HDGF-ALCAM axis promotes the metastasis of Ewing sarcoma *via* regulating the GTPases signaling pathway. *Oncogene.* (2021) 40:731–45. doi: 10.1038/s41388-020-01485-8

38. Ruth JH, Gurrea-Rubio M, Athukorala KS, Rasmussen SM, Weber DP, Randon PM, et al. CD6 is a target for cancer immunotherapy. *JCI Insight.* (2021) 6:e145662. doi: 10.1172/jci.insight.145662

39. Liu H, Ong SE, Badu-Nkansah K, Schindler J, White FM, Hynes RO. CUB-domain-containing protein 1 (CDCP1) activates Src to promote melanoma metastasis. *Proc Natl Acad Sci U S A.* (2011) 108:1379–84. doi: 10.1073/pnas.1017228108

40. Congleton J, MacDonald R, Yen A. Src inhibitors, PP2 and dasatinib, increase retinoic acid-induced association of Lyn and c-Raf (S259) and enhance MAPK-dependent differentiation of myeloid leukemia cells. *Leukemia.* (2012) 26:1180–8. doi: 10.1038/leu.2011.390

41. Alajati A, Guccini I, Pinton S, Garcia-Escudero R, Bernasocchi T, Sarti M, et al. Interaction of CDCP1 with HER2 enhances HER2-driven tumorigenesis and promotes trastuzumab resistance in breast cancer. *Cell Rep.* (2015) 11:564–76. doi: 10.1016/j.celrep.2015.03.044

42. Hsu JL, Hung MC. The role of HER2, EGFR, and other receptor tyrosine kinases in breast cancer. *Cancer Metastasis Rev.* (2016) 35:575–88. doi: 10.1007/s10555-016-9649-6

43. Harrington BS, He Y, Khan T, Puttick S, Conroy PJ, Kryza T, et al. Anti-CDCP1 immuno-conjugates for detection and inhibition of ovarian cancer. *Theranostics.* (2020) 10:2095–114. doi: 10.7150/thno.30736

44. Schafer D, Tomiuk S, Kuster LN, Rawashdeh WA, Henze J, Tischler-Hohle G, et al. Identification of CD318, TSPAN8 and CD66c as target candidates for CAR T cell based immunotherapy of pancreatic adenocarcinoma. *Nat Commun.* (2021) 12:1453. doi: 10.1038/s41467-021-21774-4

45. Velasco-de Andres M, Casado-Llombart S, Catala C, Leyton-Pereira A, Lozano F, Aranda F. Soluble CD5 and CD6: lymphocytic class I scavenger receptors as immunotherapeutic agents. *Cells.* (2020) 9:2589. doi: 10.3390/cells9122589

frontiers | Frontiers in Medicine

TYPE Mini Review
PUBLISHED 13 October 2022
DOI 10.3389/fmed.2022.1034764

OPEN ACCESS

EDITED BY
Bernhard F. Gibbs,
University of Oldenburg, Germany

REVIEWED BY
Vadim V. Sumbayev,
University of Kent, United Kingdom

*CORRESPONDENCE
Katrina K. Hoyer
khoyer2@ucmerced.edu

†These authors have contributed equally to this work and share first authorship

SPECIALTY SECTION
This article was submitted to Pathology, a section of the journal Frontiers in Medicine

RECEIVED 02 September 2022
ACCEPTED 23 September 2022
PUBLISHED 13 October 2022

CITATION
Turner CN, Mullins GN and Hoyer KK (2022) CXCR5$^+$CD8 T cells: Potential immunotherapy targets or drivers of immune-mediated adverse events? *Front. Med.* 9:1034764. doi: 10.3389/fmed.2022.1034764

CXCR5$^+$CD8 T cells: Potential immunotherapy targets or drivers of immune-mediated adverse events?

Christi N. Turner [1†], Genevieve N. Mullins [1†] and Katrina K. Hoyer [1,2,3*]

[1]Quantitative and Systems Biology Graduate Program, University of California, Merced, Merced, CA, United States, [2]Department of Molecular and Cell Biology, School of Natural Sciences, University of California, Merced, Merced, CA, United States, [3]Health Sciences Research Institute, University of California, Merced, Merced, CA, United States

CXCR5$^+$CD8 T cells have attracted significant interest within multiple areas of immunology, cancer, and infection. This is in part due to their apparent dual functionality. These cells perform as cytotoxic cells in a variety of infection states including LCMV, HBV, HIV and SIV. However, CXCR5$^+$CD8 T cells also associate with B cells in peripheral organs and function to stimulate B cell proliferation, antibody/B cell receptor class-switch, and antibody production. CXCR5$^+$CD8 T cells are similar to CXCR5$^+$CD4 T follicular helpers in their genetic make-up, B cell interactions, and functionality despite possessing elevated programmed cell death 1 and cytotoxic proteins. Within cancer CXCR5$^+$CD8 T cells have risen as potential prognostic markers for overall survival and are functionally cytotoxic within tumor microenvironments. In inflammatory disease and autoimmunity, CXCR5$^+$CD8 T cells are implicated in disease progression. During viral infection and cancer, CXCR5 expression on CD8 T cells generally is indicative of progenitor memory stem-like exhausted cells, which are more responsive to immune checkpoint blockade therapy. The use of immune checkpoint inhibitors to overcome immune exhaustion in cancer, and subsequent consequence of immune adverse events, highlights the dual nature of the cellular immune response. This review will detail the functionality of CXCR5$^+$CD8 T cells in cancer and autoimmunity with potential repercussions during immune checkpoint blockade therapy discussed.

KEYWORDS

immunotherapy (ICB), immune-related adverse events (IRAE), immune-mediated adverse events (IMAE), CD4 T follicular helper (CD4 Tfh), T follicular helper (Tfh), CD8 Tfc, CXCR5$^+$ CD8 T cell, autoimmune disease

Introduction

In the past decade research has focused on elucidating the regulation and functionality of CXCR5$^+$ T follicular cells (Tfh) during infection, cancer, and autoimmune disease. CXCR5$^+$ T cells interact with germinal center B cells and initiate differentiation into antibody-producing (plasma) cells or memory formation

through proliferation, somatic hypermutation, and class-switch recombination (1–6). CXCR5$^+$CD4 T follicular helpers (CD4 Tfh) have received most of the limelight for their contribution to germinal center migration, functionality, and B cell help within infection, cancer, and autoimmunity (6–9). CXCR5$^+$CD8 T cells have slowly come into focus with their unique ability to provide B cell help within germinal centers similar to CD4 Tfh and also maintain a cytolytic capacity in infection, autoimmunity and tumor microenvironments resembling CD8 T effector cells (Figure 1) (1–5, 10, 11). This mini-review focuses on CXCR5$^+$CD8 T cells in cancer, and implications for immune-mediated adverse event (IMAEs) development in patient immunotherapy treatments.

CXCR5$^+$CD8 T cell cytotoxicity and cancer

Tumor microenvironments contain an abundance of innate and adaptive immune cells ranging from tissue-resident cells, such as macrophages, to migratory cells, such as T and B lymphocytes, each with a specific purpose (12). CD8 T cells traditionally activate and differentiate into cytolytic effectors responsible for killing virally infected and cancerous cells. Cytotoxic CD8 T cells are defined by the ability to induce antigen-specific apoptosis of target cells (13). Cytotoxicity is mediated by granzymes, perforin, CD107a, IFNγ, TNFα, TNFβ, and FasL and regulated and defined by key transcription factors, including Blimp-1, eomesodermin (eomes), T-bet, Id1, Id2, and Id3 (14). CXCR5$^+$CD8 T cells localize within blood circulation and tumor microenvironments of cancer patients (15–18). T follicular cells produce varying levels of IL-21 and effector molecules within blood circulation compared to lymph nodes and organs, but their ability to assist B cells remains unaltered indicating that T follicular cell functionality may not be site specific (9, 10).

CXCR5$^+$CD8 T cells have cytotoxic and proliferative capacity within cancer ranging from liquid to solid tumors. CXCL13 upregulation by tumors induces migration, signaling and functional changes by CXCR5-expressing immune cells, but the specific functional capacity of CXCR5$^+$CD8 T cells versus other CXCR5-expressing cells, including B cells and tumors, is poorly characterized in cancer. CXCR5$^+$CD8 T cells from human peripheral blood mononuclear cells, tumor tissues and tumor associated lymph nodes upregulate effector molecules such as IFNγ, TNFα, granzyme B, and perforin compared to CXCR5$^-$CD8 T cells (10, 17–28). CXCR5$^+$CD8 T cells upregulate CD107a, proliferate, and induce specific cell lysis of *in vitro* co-cultured tumor cells (17, 19, 21, 22, 24, 25). CXCR5$^+$CD8 T cell infiltration of hepatocellular carcinomas generate a robust anti-tumor response in association with B cell antibody production, through IL-21 production, that correlates with a reduction in early tumor recurrence, and is not associated with peritumoral liver or blood tissues (29). This demonstrates the importance of CXCR5$^+$CD8 T cells within the tumor microenvironment and surrounding tissues to patient

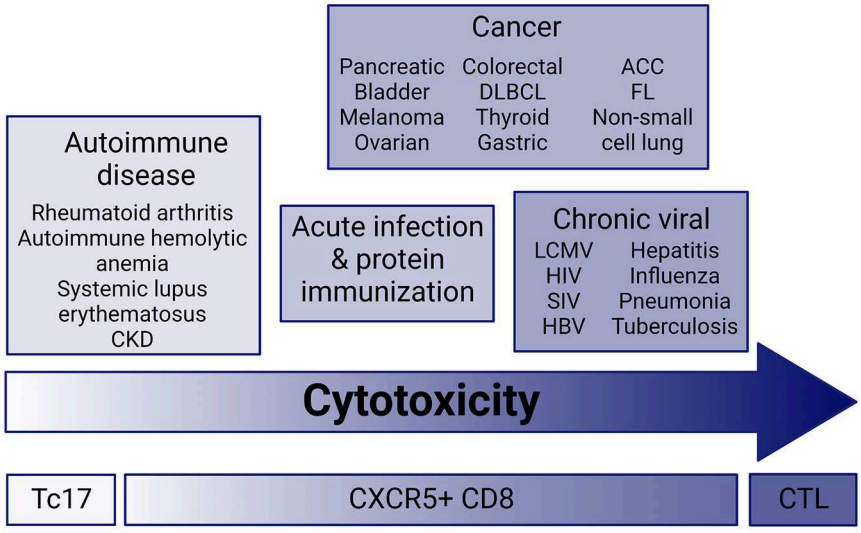

FIGURE 1
Cytotoxic potential across disease. CXCR5$^+$CD8 T cells have a range of cytolytic potential in infection, cancer, and autoimmune disease. Current research suggests that cytolytic and effector molecule expression ranges from very low in autoimmune disease similar to Tc17 effector cells, and high in chronic infection and cancer. CXCR5$^+$CD8 T cells from acute infection and immunization with protein maintain an intermediate cytolytic potential. CKD, chronic kidney disease; ACC, Adenoid cystic carcinoma; FL, follicular lymphoma; DLBCL, diffuse large B cell lymphoma; CTL, cytotoxic T lymphocyte; Tc17, IL-17-secreting CD8 T cells.

outcomes and identifies possible tumor eradication mechanisms utilized by CD8 T cells. Furthermore, $CXCR5^+$CD8 T cells appear resistant to immune checkpoint blockade therapy (ICB) induced apoptosis compared to susceptible $CXCR5^-$CD8 T cells and, instead, demonstrate an effector-like phenotype in infection and chronic lymphocytic leukemia (11, 27). $CXCR5^+$CD8 T cells maintain resistance to immune modulation in spite of high program cell death-1 (PD-1) expression, an inhibitory receptor, that is a marker of Tfh. PD-1 on CD4 Tfh retains these cells within germinal centers, with their localization regulated by PD-L1 ligand expression on B cells (6, 30). Since $CXCR5^+$CD8 T cells are similar in gene regulation, action, and surface protein expression to CD4 Tfh this mechanism may also regulate $CXCR5^+$CD8 T cell homing to germinal centers of lymphoid organs and tertiary lymphoid structures in tumors.

$CXCR5^+$CD8 T cells and markers of exhaustion in infection, cancer, and autoimmunity

T cell exhaustion is defined by successive upregulation of inhibitory receptors on CD8 and CD4 T cells in the presence of chronic antigen stimulation in cancer, infection, and autoimmune disease. T cell exhaustion status is sequential and reversible with a phenotypic range from dysfunctional T effector cells to memory progenitors with cytolytic ability to terminal exhaustion with unknown capacity for functional reactivation (31, 32). Under high antigen and inflammation, a step-wise process of inhibitory receptor activation, effector cytokine reduction, and cytolytic effector downregulation on $CD8^+$ T effectors leads to two exhaustion stages, pre-exhausted (Tpex) and terminally exhausted (Tex) (33). Tpex cells are defined by PD-1^{int}TCF1^{hi} and Tex cells by PD-1^{hi}TIM3^{hi} expression (34). Subsequently, nine Tex subtypes were identified through high-dimensional mass cytometry suggesting that transition between Tpex and Tex involves multiple stages or that multiple inhibitory receptors have overlapping function in driving terminal exhaustion (35). Initiation of exhaustion to Tex begins with loss of IL-2 signaling leading to decreases in TNFα and perforin (32, 36). Cytolytic activity of CD107a degranulation is initially maintained along with regulatory cytokines, such as IL-10, which may upregulate and prompt the exhaustive state. Finally, it is thought that some Tex cells, such as CD8 tumor-infiltrating lymphocytes, undergo activation-induced cell death (AICD) following the loss of proliferative capacity (33). This cell death is FAS ligand activated by FAS upregulation on tumor infiltrating lymphocytes and FAS ligand on adjacent tumor cells (37). AICD associates with Tfh and regulates peripheral tolerance, and AICD loss leads to autoimmune progression possibly due to release of self-reactive lymphocytes from cell death mechanisms (6, 38). In tumor microenvironments, ICB T cell reactivation reduces AICD influence potentially enabling self-reactive Tfh activation and driving IMAEs (39, 40).

PD-1 is the canonical marker of T cell exhaustion and a marker of germinal center immune cells. In infection, PD-1 upregulation induces functional $CD8^+$ T cell exhaustion resembling a Tpex cell type (6, 11). $CD8^+$PD-1^+ T cells are heterogeneous across infection, cancer, and autoimmunity based on identification of multiple T cell subsets within each disease (10, 41–43). $CXCR5^+$CD8 T cells appear functional with effector/cytolytic capacity in cancer despite high PD-1 expression. $CXCR5^+$CD8 T cells are also described as memory precursor effector cells (MPECs) in various settings (Figure 2; Supplementary Table S1) (11, 27, 44–46). MPECs express CD127, TCF1 (TCF7), and T-bet, lack KLRG1, and produce low effector cytokines (33, 47). These cells persist when transferred generating memory and terminally exhausted cells (33, 47). $CXCR5^+$CD8 T cell subset identified as TCF1^+PD-1^+TIM3^{low} maintain low cytotoxic capability (27, 45), resembling a Tpex subset with limited proliferation but cytokine production (27, 34, 45). Due to their self-renewal capacity and responsiveness to anti-PD-1 therapy these cells have potential as therapeutic targets (11, 46). A tissue resident exhausted progenitor population expressing TCF1 and cytolytic effector molecules is a self-renewing precursor to circulatory and terminally exhausted populations in LCMV and cancer (44). Upregulation of multiple inhibitory receptors regulate the pathway to Tex, including PD-1, TIM3, CTLA4, Lag3, 2B4 in various combinations. Within LCMV infection, $CXCR5^+$TCF1^+TIM3^- Tex expand after PD-1 blockade into $CXCR5^-$Tcf1^-Tim3^+ Tex cells, and in other murine and human settings less exhaustive states exist such as PD-1^{lo}KLRG1^{hi}TIM3^{lo} and $CXCR5^+$PD-1^+Tim3^- that maintain cytolytic capacity (11, 48, 49). $CXCR5^+$TCF1^+TIM3^- Tex is possibly a memory population that upon functional reactivation becomes terminally exhausted by upregulating the inhibitory receptor, TIM3, as a secondary means of inhibition in high antigen environments, whereas less exhaustive states with downregulated TIM3 expression demonstrate highly functional $CXCR5^+$CD8 T cells.

$CXCR5^+$CD8 T cell heterogeneity also exists within cancer and complicates our use of therapies directed at CD8 T effectors (44). $CXCR5^+$ T cell subset variation is found across solid and liquid tumors, from non-small cell lung cancer to follicular B cell non-Hodgkin's lymphoma, where PD-1 and TIM3 expression creates diverging populations (10, 50, 51). In hepatocellular carcinoma, follicular lymphoma, thyroid and high-grade serous ovarian cancer, PD-1 is upregulated on $CXCR5^+$CD8 T cells while TIM3 and CTLA4 are downregulated compared to $CXCR5^-$CD8 T cells possibly indicating a Tpex versus Tex phenotype (15, 21, 24, 25). $CXCR5^+$CD8 T cells in pancreatic cancer express both PD-1 and TIM3 suggesting a Tex phenotype that varies from other cancers (17). Inhibitory marker expression also fluctuates by tissue region, for example in hepatocellular carcinoma upregulated PD-1 is expressed in

10.3389/fmed.2022.1034764

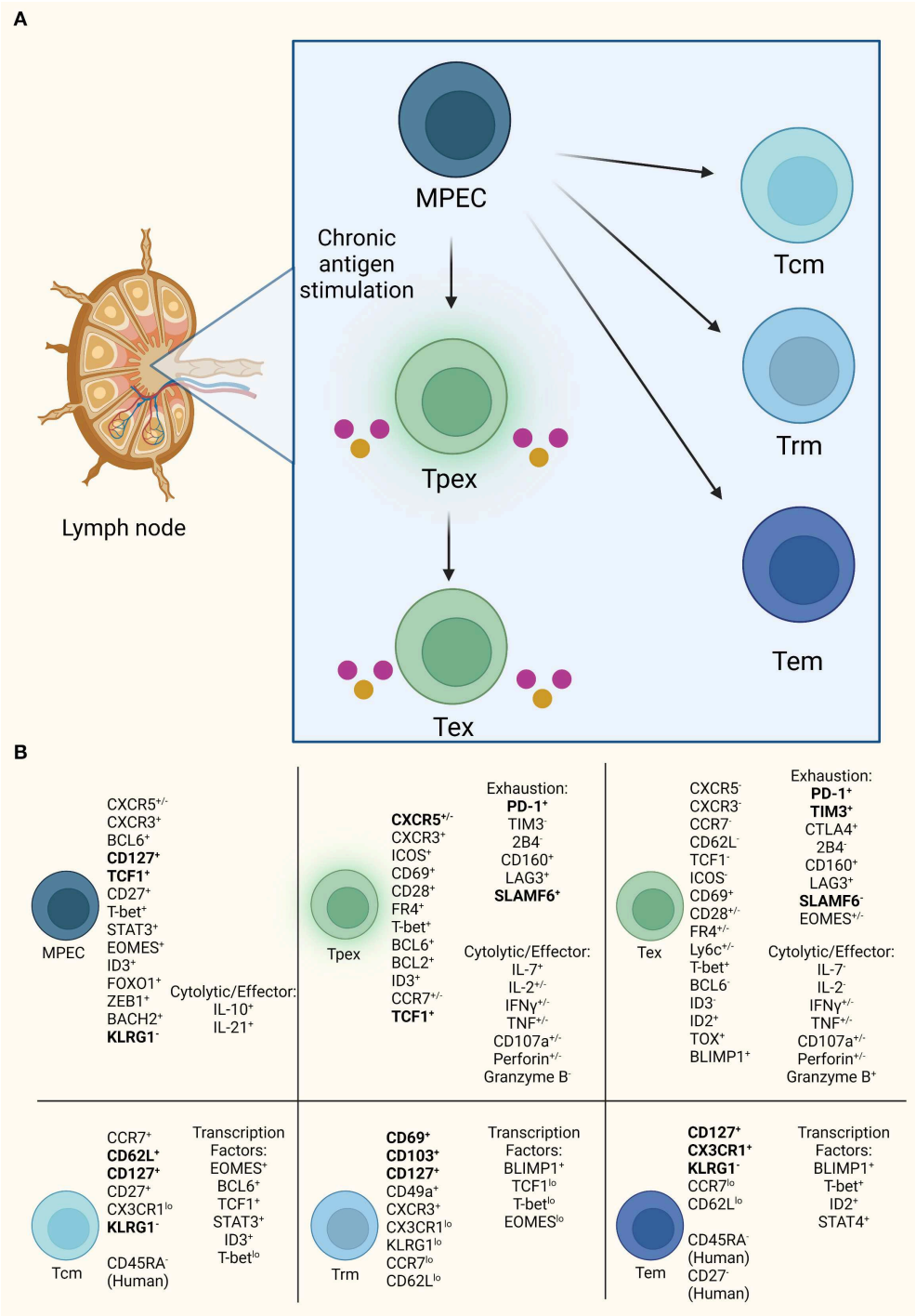

FIGURE 2
CXCR5$^+$CD8 T cell progenitor lineages. **(A)** CXCR5$^+$CD8 T cells resemble progenitor cells with self-renewal, such as MPECs, that are capable of diverging into two lineages of either exhausted T cells under high antigen exposure or memory cells with effector functionality. **(B)** Established markers defining CD8 T cells for each subset diverging from MPEC. Bold indicates consistently used markers for population identification. Also, listed are the currently demonstrated cytolytic and effector molecules in exhausted subsets.

human liver and tumor tissue compared to blood circulation (29). PD-1, TIM3, 2B4, and Lag3 are downregulated in CXCR5$^+$CD8 T cells in colon cancer, but within gastric cancer PD-1, Lag3, CTLA4, and Tigit are upregulated (23, 26).

Furthermore, differences are associated with human versus murine models of disease, such as in metastatic melanoma where CXCR5$^+$PD-1$^+$CD8 T cells were identified by single-cell sequencing in humans, but not identified in a B16 melanoma mouse model (10, 52). Additional research in CXCR5$^+$CD8 T cell effector status and ability to maintain functionality or diverge into exhaustive states within high antigen environments is needed. Characterization of CXCR5$^+$CD8 T cell exhaustion in chronic or high antigen environments is limited for infection, cancer and autoimmunity.

Investigating exhaustion dynamics of CXCR5$^+$ T cells within autoimmunity is challenging due to the association of PD-1 as an activating and inhibitory receptor. There is potential for functional differences between CXCR5$^+$CD8 and CD4 Tfh cells within germinal centers that may resemble antibody-suppressor CXCR5$^+$IFNg$^+$CD8 T cells (53, 54). Antibody-suppressor cells, namely CXCR5$^+$PD-1$^-$CD8 T cells, may activate effector functions on self-reactive B cells and CD4 Tfh cells leading to tolerance and inhibition of plasma cell formation thus halting autoantibody production associated with many autoimmune diseases. Lag3 loss on intra-islet non-obese diabetic CD8 T cells accelerates autoimmune diabetes and highlights Lag3 T cell inhibition differences between autoimmunity, cancer and infection (55, 56). Rao et al. identified a CXCR5$^+$PD-1^{hi}CD4 population within peripheral blood from rheumatoid arthritis patients, but not within synovial fluid, that expressed Tigit and SLAMF6 suggesting Tfh interaction with B cells, and regulation of inhibitory receptor functionality (57). Within human chronic kidney disease, CCR6$^-$CXCR3$^-$CXCR5$^+$PD-1$^+$CD4 and exhausted CD8 T cells are upregulated compared to end-stage kidney disease showcasing exhausted populations in CD4 and CD8 T cells during autoimmunity (58). These studies suggest that non-exhausted and exhausted CXCR5$^+$ T cell subsets exist and influence autoimmunity, and their functions may be different than in infection and cancer. ICB induced reactivation of exhausted CXCR5$^+$ T cells during autoimmunity may enable new autoimmune disease therapies. Alternatively, since exhaustion downregulates T cell effector function, exhaustion itself may provide an additional inhibitory tool in regulating self-reactive T cells.

Could CXCR5$^+$CD8 T cells initiate the development of immune mediated adverse events?

ICB created a paradigm shift in how we understand cancer, the immune system and treatment modalities for cancer patients. A deeper immune-driven exploration of tumor microenvironments is needed to understand how these treatments enable or disrupt immune cell functions promoting patient survival or tumor progression. ICB reactivates exhausted T cells through downregulating inhibitory receptors and ligands on tumors and immune populations by blocking specific protein receptors such as PD-1, PD-L1, and CTLA4 with monoclonal antibodies (59). By blocking T cell exhaustion, effector T cells regain cytolytic function, including CXCR5$^+$CD8 T cells. CXCR5$^+$CD8 T cells initiate a proliferative burst of effector T cells following PD-1 immunotherapy administration in LCMV (11). This reinvigoration increases tumor destruction plus prolongs overall survival, approximately 21 months, in many cancer types: melanoma, non-small cell lung, renal cell, head and neck squamous cell, bladder, Merkel cell, hepatocellular, Hodgkin's lymphoma and more (60, 61). Of the patients approved for treatment with ICBs only 15-20% experience cancer remission and majority develop IMAEs or immune-related adverse events following treatment (62).

IMAEs are adverse events resembling organ specific to systemic autoimmunity and cause patients to end treatment early (63). IMAE biomarker development has focused on autoantibodies associated with known autoimmune conditions, such as Anti-Smith, Anti-dsDNA, ACPAs, Rh factor and more, however, these autoimmune biomarkers are poorly defined in cancer and vary in their baseline associations of IMAE outcomes (64). To account for the large autoantibody repertoire for identifying IMAE progression, blood serum from ICB treated patients could be collected pre- and post-treatment to establish a baseline and standardized by high-throughput proteome techniques (65–67). Current studies have utilized microarray, SEREX cDNA library, immunofluorescence, and immunoassay technologies for screening of IMAE associated autoantibodies, such as thyroiditis, hypophysitis, rash, colitis, arthritis, myocarditis, myalgia, and endocrine disorders in response to singular/combination treatments of CTLA4, PD-1 and PD-L1 in melanoma, advanced/metastatic solid tumors, renal cell carcinoma, non-small cell lung, prostate, and bladder cancers (68–73).

CXCR5$^+$CD8 T cells correlate with disease-free or overall survival in pancreatic, colon, follicular lymphoma, gastric, high-grade serous ovarian, hepatocellular, and bladder cancers and thus is considered a potential biomarker (15, 17, 20, 23, 25, 26). On the contrary, decreases in disease-free survival in non-small cell lung and salivary adenoid cystic carcinomas are associated with infiltrating CXCR5$^+$CD8 T cells (74, 75). Functional studies beyond correlative data and mRNA expression remains lacking as to how these cells benefit or negate a tumor microenvironment. Chemokine, CXCR5, knockdown has proven to have negative prognostic value in certain cancers and cell lines (76). Tumors express CXCR5 and produce its ligand, CXCL13, to recruit B cells and T cells into tumor microenvironments where tertiary lymphoid structures, resembling germinal centers, are developed and antibody production occurs (77–79). CXCR5 promotes proliferation of clear cell renal carcinoma through activating PI3K/AKT/mTOR pathway in the presence of its ligand, CXCL13, and this signaling

pathway has also been reported in colon cancer proliferation (76, 80). CXCL13-CXCR5 axis in tumors leads to increased migration, invasion of tumor cells and unfavorable tumor prognostic values in patients, but not in the case of ICB treatment (77, 79, 81). In patients treated with ICB, high CXCL13 expression leads to more favorable tumor outcomes perhaps due to $CXCR5^+$CD8 T cells expanding the effector T cell pool or as a consequence of these cells increasing proliferation while resisting apoptosis (11, 82). $CXCR5^+$CD8 T cell persistence following ICB may generate a greater antibody repertoire based on their known B cell interactions that could be beneficial for tumor eradication or generate organ specific detriments and IMAEs (1, 79, 83).

$CXCR5^+$CD8 T cell ability to initiate IMAEs during ICB remains unknown. These cells are capable of upregulating effector molecules in cancer and lysing tumor cells in co-culture. In autoimmune disease, $CXCR5^+$CD8 T cells enable B cell differentiation and exacerbate disease (1, 2). Correlations exist based on immune cell infiltration and IMAE development in patients without a complete understanding of tolerance mechanisms. For example, granzyme B producing CD4 T cells infiltrate thyroids in response to anti-PD1 therapy at a greater frequency than CD8 T cells and are associated with development of mouse and human thyroiditis (84). Production of IL-21, CXCL13, and infiltration by cytolytic CD4 and CD8 T cell infiltrates associate with IMAE development in tumor models and human plasma (85). Whether or not these cells express CXCR5 remains unknown but their ability to produce granzyme B, IL-21, and migrate to CXCL13 warrants further $CXCR5^+$ T cell research in IMAE development. A direct link between IMAEs and autoimmune mechanisms is currently unknown. PD-1 elimination and ICB accelerates autoimmunity in murine models of systemic lupus erythematosus and autoimmune diabetes (86, 87). Reversal of inhibitory tolerance mechanisms is capable of reactivating T cell receptors to recognize self-antigen (86). Autoreactive CD8 T cell activation after PD-1 ICB induces autoimmune diabetes in Rip-mOVA mice indicating that loss of CD8 T cell self-tolerance following immune modulation therapies increases autoimmunity (88). Additional studies are needed to determine if self-reactive cells lose tolerance and transform into active effector T cells capable of cytolytic activity on tumor and self-tissues. Also, research is needed to determine if initiation of IMAEs and autoimmunity occur *via* similar or distinct pathways.

Discussion

$CXCR5^+$CD8 T cell research is expanding in multiple areas as they are identified in advanced technologies, such as single-cell sequencing. As with most areas of cancer research heterogeneity between cancer types, biomarkers, and tumor microenvironments creates cumbersome and often contrasting phenotypic conclusions regarding $CXCR5^+$CD8 T cell functions. $CXCR5^+$CD8 T cells are a newly developing area of study that allow for a unique perspective and growth in the fields of cancer research and immune checkpoint blockade. ICB research is now focused on combining treatment modulations to identify ways to overcome immune-mediated adverse events. Awareness and focus on IMAEs is in its initial stages. How $CXCR5^+$CD8 T cells affect the tumor microenvironment, B cell infiltration, autoantibody response, T cell tissue residency, and peripheral organ involvement after ICB remains unknown. Defining functionality in these different areas, particularly identifying how these cells respond in cancer initiation and progression, would provide a major step forward. We speculate that $CXCR5^+$CD8 T cells may slowly migrate into circulation after ICB treatment but become primed and activated by dendritic cells in peripheral organs generating an effector phenotype that then infiltrates tissues and establishes IMAEs (45, 86, 89). Because of cancer heterogeneity, identifying $CXCR5^+$CD8 T cells requires a robust screen across multiple cancer types to enable a sound and clear prognostic value for using $CXCR5^+$CD8 T cells as a biomarker or immune cell therapy target.

Questions about $CXCR5^+$CD8 T cell effects on IMAEs remain. $CXCR5^+$CD8 T cell ability to interact with B cells and promote antibodies suggests that some $CXCR5^+$CD8 T cells, after ICB, could reverse tolerance and initiate autoantibody production. Data from multiple studies now suggests that PD-1 blockade releases self-tolerance constraints increasing autoimmunity. As ICB induces IMAEs, it raises the question of whether IMAEs are caused by autoimmune mechanisms or some other immune dysfunction. With sequencing techniques advancing, teasing out the implications of protein antigens from tumor proteins or self-proteins would delineate if $CXCR5^+$CD8 T cells pose a threat to the development of IMAEs (10). Studying $CXCR5^+$CD8 T cells using animal models that perpetuate autoimmunity would explain how these cells respond to ICB and if they initiate disease development. An autoimmune disease model, B6/*lpr*, treated with combination ICB in the presence of colon adenocarcinoma develops T cell immune-infiltration of multiple organs with increased tumor growth following steroid treatment (90). Corticosteroids are a drug of choice when patients develop IMAEs but based on this study could result in decreased ICB effectiveness. Promoting tolerance mechanisms in T cells while patients receive ICB may enhance therapy effectiveness. VISTA regulates tolerance mechanisms and its loss induces autoimmune disease in mice, by incorporating a VISTA agonist along with ICB may enhance cancer therapy while eliminating IMAEs (91, 92). In humanized mice, $CXCR5^+$CD8 T cells develop after human cord blood hematopoietic stem cell engraftment and HIV infection while maintaining PD-1, cytotoxicity, cytokine production, and homing to peripheral organs (93). These studies

provide novel models for elucidating CXCR5$^+$CD8 T cells in the context of mouse and human responses, in addition to, existing human tumor resections and peripheral blood mononuclear cells for translational research.

Author contributions

CT and GM conceptualization, literature evaluation, original draft writing, and generated and visualized figures. KH conceptualization, writing and review, visualization, funding acquisition, and supervision. All authors contributed to the article and approved the submitted version.

Funding

This work was supported by the National Institutes of Health Grant R15HL146779 to KH.

Acknowledgments

The authors thank Maria Pimentel for her assistance with reference management. All figures were created with BioRender.com.

Conflict of interest

The authors declare that the research was conducted in the absence of any commercial or financial relationships that could be construed as a potential conflict of interest.

Publisher's note

Supplementary material

The Supplementary Material for this article can be found online at: https://www.frontiersin.org/articles/10.3389/fmed.2022.1034764/full#supplementary-material

References

1. Valentine KM, Davini D, Lawrence TJ, Mullins GN, Manansala M, Al-Kuhlani M, et al. CD8 follicular T cells promote B cell antibody class switch in autoimmune disease. *J Immunol.* (2018) 201:31–40. doi: 10.4049/jimmunol.1701079

2. Valentine KM, Mullins GN, Davalos OA, Seow LW, Hoyer KK. CD8 follicular T cells localize throughout the follicle during germinal center reactions and maintain cytolytic and helper properties. *J Autoimmun.* (2021) 123:102690. doi: 10.1016/j.jaut.2021.102690

3. Li Y, Tang L, Guo L, Chen C, Gu S, Zhou Y, et al. CXCL13-mediated recruitment of intrahepatic CXCR5$^+$CD8$^+$ T cells favors viral control in chronic HBV infection. *J Hepatol.* (2020) 72:420–30. doi: 10.1016/j.jhep.2019.09.031

4. Tyllis TS, Fenix KA, Norton TS, Kara EE, McKenzie DR, David SC, et al. CXCR5$^+$CD8$^+$ T cells shape antibody responses in vivo following protein immunisation and peripheral viral infection. *Front Immunol.* (2021) 12:1–14. doi: 10.3389/fimmu.2021.626199

5. Chen Y, Yu M, Zheng Y, Fu G, Xin G, Zhu W, et al. CXCR5$^+$PD-1$^+$ follicular helper CD8 T cells control B cell tolerance. *Nat Commun.* (2019) 10:4415. doi: 10.1038/s41467-019-12446-5

6. Shi J, Hou S, Fang Q, Liu X, Liu X, Qi H. PD-1 Controls follicular T helper cell positioning and function. *Immunity.* (2018) 49:264–74. doi: 10.1016/j.immuni.2018.06.012

7. Cao G, Chi S, Wang X, Sun J, Zhang Y. CD4$^+$CXCR5$^+$PD-1$^+$ T follicular helper cells play a pivotal role in the development of rheumatoid arthritis. *Med Sci Monit Int Med J Exp Clin Res.* (2019) 25:3032–40. doi: 10.12659/MSM.914868

8. Crotty S. Follicular helper CD4 T cells (TFH). *Annu Rev Immunol.* (2011) 29:621–63. doi: 10.1146/annurev-immunol-031210-101400

9. Spaan M, Kreefft K, Graav GN de, Brouwer WP, Knegt RJ de, Kate FJW, et al. CD4$^+$CXCR5$^+$ T cells in chronic HCV infection produce less IL-21, yet are efficient at supporting B cell responses. *J Hepatol.* (2015) 62:303–10. doi: 10.1016/j.jhep.2014.09.024

10. Brummelman J, Mazza EMC, Alvisi G, Colombo FS, Grilli A, Mikulak J, et al. High-dimensional single cell analysis identifies stem-like cytotoxic CD8$^+$ T cells infiltrating human tumors. *J Exp Med.* (2018) 215:2520–35. doi: 10.1084/jem.20180684

11. Im SJ, Hashimoto M, Gerner MY, Lee J, Kissick HT, Burger MC, et al. Defining CD8$^+$ T cells that provide the proliferative burst after PD-1 therapy. *Nature.* (2016) 537:417–21. doi: 10.1038/nature19330

12. Lei X, Lei Y, Li J-K, Du W-X, Li R-G, Yang J, et al. Immune cells within the tumor microenvironment: biological functions and roles in cancer immunotherapy. *Cancer Lett.* (2020) 470:126–33. doi: 10.1016/j.canlet.2019.11.009

13. Gravano DM, Hoyer KK. Promotion and prevention of autoimmune disease by CD8$^+$ T cells. *J Autoimmun.* (2013) 45:68–79. doi: 10.1016/j.jaut.2013.06.004

14. Zhang N, Bevan MJ. CD8$^+$ T Cells: foot soldiers of the immune system. *Immunity.* (2011) 35:161–8. doi: 10.1016/j.immuni.2011.07.010

15. Yang M, Lu J, Zhang G, Wang Y, He M, Xu Q, et al. CXCL13 shapes immunoactive tumor microenvironment and enhances the efficacy of PD-1 checkpoint blockade in high-grade serous ovarian cancer. *J Immunother Cancer.* (2021) 9:e001136. doi: 10.1136/jitc-2020-001136

16. Simon S, Voillet V, Vignard V, Wu Z, Dabrowski C, Jouand N, et al. PD-1 and TIGIT coexpression identifies a circulating CD8 T cell subset predictive of response to anti-PD-1 therapy. *J Immunother Cancer.* (2020) 8:e001631. doi: 10.1136/jitc-2020-001631

17. Bai M, Zheng Y, Liu H, Su B, Zhan Y, He H. CXCR5$^+$ CD8$^+$ T cells potently infiltrate pancreatic tumors and present high functionality. *Exp Cell Res.* (2017) 361:39–45. doi: 10.1016/j.yexcr.2017.09.039

18. Xing J, Li X. E J, Wang C, Wang H. Inverse relationship between CD40L expression and cytolytic molecule expression by CD8$^+$CXCR5$^+$ T follicular cytotoxic cells in colorectal cancer. *Exp Cell Res.* (2020) 389:111892. doi: 10.1016/j.yexcr.2020.111892

19. Tang J, Zha J, Guo X, Shi P, Xu B. CXCR5$^+$CD8$^+$ T cells present elevated capacity in mediating cytotoxicity toward autologous tumor cells through interleukin 10 in diffuse large B-cell lymphoma. *Int Immunopharmacol.* (2017) 50:146–51. doi: 10.1016/j.intimp.2017.06.020

20. Huang Q, Zhou Q, Zhang H, Liu Z, Zeng H, Chen Y, et al. Identification and validation of an excellent prognosis subtype of muscle-invasive bladder cancer patients with intratumoral CXCR5$^+$ CD8$^+$ T cell abundance. *Oncoimmunology.* (n.d.) 9:1810489. doi: 10.1080/2162402X.2020.1810489

21. Jin Y, Lang C, Tang J, Geng J, Song HK, Sun Z, et al. CXCR5$^+$CD8$^+$ T cells could induce the death of tumor cells in HBV-related hepatocellular carcinoma. *Int Immunopharmacol.* (2017) 53:42–8. doi: 10.1016/j.intimp.2017.10.009

22. Xing J, Zhang C, Yang X, Wang S, Wang Z, Li X, et al. CXCR5$^+$CD8$^+$ T cells infiltrate the colorectal tumors and nearby lymph nodes, and are associated with enhanced IgG response in B cells. *Exp Cell Res.* (2017) 356:57–63. doi: 10.1016/j.yexcr.2017.04.014

23. E J, Yan F, Kang Z, Zhu L, Xing J, Yu E. CD8$^+$CXCR5$^+$ T cells in tumor-draining lymph nodes are highly activated and predict better prognosis in colorectal cancer. *Hum Immunol.* (2018) 79:446–452. doi: 10.1016/j.humimm.2018.03.003

24. Zhou Y, Guo L, Sun H, Xu J, Ba T. CXCR5$^+$ CD8 T cells displayed higher activation potential despite high PD-1 expression, in tumor-involved lymph nodes from patients with thyroid cancer. *Int Immunopharmacol.* (2018) 62:114–9. doi: 10.1016/j.intimp.2018.07.002

25. Chu F, Li HS, Liu X, Cao J, Ma W, Ma Y, et al. CXCR5$^+$CD8$^+$ T cells are a distinct functional subset with antitumor activity. *Leukemia.* (2019) 33:2640–53. doi: 10.1038/s41375-019-0464-2

26. Wang J, Li R, Cao Y, Gu Y, Fang H, Fei Y, et al. Intratumoral CXCR5$^+$CD8$^+$T associates with favorable clinical outcomes and immunogenic contexture in gastric cancer. *Nat Commun.* (2021) 12:3080. doi: 10.1038/s41467-021-23356-w

27. Hofland T, Martens AWJ, van Bruggen JAC, de Boer R, Schetters S, Remmerswaal EBM, et al. Human CXCR5$^+$PD-1$^+$ CD8 T cells in healthy individuals and patients with hematologic malignancies. *Eur J Immunol.* (2021) 51:703–13. doi: 10.1002/eji.202048761

28. Valentine KM, Hoyer KK. CXCR5$^+$ CD8 T cells: protective or pathogenic? *Front Immunol.* (2019) 10:1–10. doi: 10.3389/fimmu.2019.01322

29. Ye L, Li Y, Tang H, Liu W, Chen Y, Dai T, et al. CD8$^+$CXCR5$^+$T cells infiltrating hepatocellular carcinomas are activated and predictive of a better prognosis. *Aging.* (2019) 11:8879–91. doi: 10.18632/aging.102308

30. Good-Jacobson KL, Szumilas CG, Chen L, Sharpe AH, Tomayko MM, Shlomchik MJ. PD-1 regulates germinal center B cell survival and the formation and affinity of long-lived plasma cells. *Nat Immunol.* (2010) 11:535–42. doi: 10.1038/ni.1877

31. Kao C, Oestreich KJ, Paley MA, Crawford A, Angelosanto JM, Ali MA, et al. T-bet represses expression of PD-1 and sustains virus-specific CD8 T cell responses during chronic infection. *Nat Immunol.* (2011) 12:663–71. doi: 10.1038/ni.2046

32. Wherry EJ, Kurachi M. Molecular and cellular insights into T cell exhaustion. *Nat Rev Immunol.* (2015) 15:486–99. doi: 10.1038/nri3862

33. Verdon DJ, Mulazzani M, Jenkins MR. Cellular and molecular mechanisms of CD8$^+$ T cell differentiation, dysfunction, and exhaustion. *Int J Mol Sci.* (2020) 21:7357. doi: 10.3390/ijms21197357

34. Kallies A, Zehn D, Utzschneider DT. Precursor exhausted T cells: key to successful immunotherapy? *Nat Rev Immunol.* (2020) 20:128–36. doi: 10.1038/s41577-019-0223-7

35. Bengsch B, Ohtani T, Herati RS, Bovenschen N, Chang KM, Wherry EJ. Deep immune profiling by mass cytometry links human T and NK cell differentiation and cytotoxic molecule expression patterns. *J Immunol Methods.* (2018) 453:3–10. doi: 10.1016/j.jim.2017.03.009

36. Wherry EJ, Blattman JN, Murali-Krishna K, van der Most R, Ahmed R. Viral persistence alters CD8 T-cell immunodominance and tissue distribution and results in distinct stages of functional impairment. *J Virol.* (2003) 77:4911–27. doi: 10.1128/JVI.77.8.4911-4927.2003

37. Radoja S, Saio M, Frey AB. CD8$^+$ Tumor-infiltrating lymphocytes are primed for fas-mediated activation-induced cell death but are not apoptotic *in situ*. *J Immunol.* (2001) 166:6074–83. doi: 10.4049/jimmunol.166.10.6074

38. Zhang J, Bárdos T, Mikecz K, Finnegan A, Glant TT. Impaired Fas signaling pathway is involved in defective T cell apoptosis in autoimmune murine arthritis. *J Immunol.* (2001) 166:4981–6. doi: 10.4049/jimmunol.166.8.4981

39. Gargett T, Yu W, Dotti G, Yvon ES, Christo SN, Hayball JD, et al. GD2-specific CAR T cells undergo potent activation and deletion following antigen encounter but can be protected from activation-induced cell death by PD-1 blockade. *Mol Ther.* (2016) 24:1135–49. doi: 10.1038/mt.2016.63

40. Perez-Ruiz E, Minute L, Otano I, Alvarez M, Ochoa MC, Belsue V, et al. Prophylactic TNF blockade uncouples efficacy and toxicity in dual CTLA-4 and PD-1 immunotherapy. *Nature.* (2019) 569:428–32. doi: 10.1038/s41586-019-1162-y

41. Yao C, Sun H-W, Lacey NE Ji Y, Moseman EA, Shih H-Y, et al. Single-Cell RNA-Seq reveals TOX as a key regulator of CD8$^+$ T cell persistence in chronic infection. *Nat Immunol.* (2019) 20:890–901. doi: 10.1038/s41590-019-0403-4

42. Mitchell AM, Michels AW. T cell receptor sequencing in autoimmunity. *J Life Sci Westlake Village Calif.* (2020) 2:38–58. doi: 10.36069/JoLS/20201203

43. Shen Y, Qu Q, Jin M, Chen C. Investigating the role of circulating CXCR5-expressing CD8$^+$ T-cells as a biomarker for bacterial infection in subjects with pneumonia. *Respir Res.* (2019) 20:54. doi: 10.1186/s12931-019-1011-4

44. Beltra J-C, Manne S, Abdel-Hakeem MS, Kurachi M, Giles JR, Chen Z, et al. Developmental relationships of four exhausted CD8$^+$ T cell subsets reveals underlying transcriptional and epigenetic landscape control mechanisms. *Immunity.* (2020) 52:825–41. doi: 10.1016/j.immuni.2020.04.014

45. Herve M-G de G de, Abdoh M, Jaafoura S, Durali D, Taoufik Y. Follicular CD4 t cells tutor CD8 early memory precursors: an initiatory journey to the frontier of B cell territory. *iScience.* (2019) 20:100–9. doi: 10.1016/j.isci.2019.09.012

46. Im SJ, Konieczny BT, Hudson WH, Masopust D, Ahmed R. PD-1$^+$ stemlike CD8 T cells are resident in lymphoid tissues during persistent LCMV infection. *Proc Natl Acad Sci.* (2020) 117:4292–9. doi: 10.1073/pnas.1917298117

47. Herndler-Brandstetter D, Ishigame H, Shinnakasu R, Plajer V, Stecher C, Zhao J, et al. KLRG1$^+$ Effector CD8$^+$ T cells lose KLRG1, differentiate into all memory T cell lineages, and convey enhanced protective immunity. *Immunity.* (2018) 48:716–29. doi: 10.1016/j.immuni.2018.03.015

48. Hudson WH, Gensheimer J, Hashimoto M, Wieland A, Valanparambil RM, Li P, et al. Proliferating transitory T cells with an effector-like transcriptional signature emerge from PD-1$^+$ stem-like CD8$^+$ T cells during chronic infection. *Immunity.* (2019) 51:1043–58. doi: 10.1016/j.immuni.2019.11.002

49. He R, Hou S, Liu C, Zhang A, Bai Q, Han M, et al. Follicular CXCR5-expressing CD8$^+$ T cells curtail chronic viral infection. *Nature.* (2016) 537:412–6. doi: 10.1038/nature19317

50. Shi W, Yang B, Sun Q, Meng J, Zhao X, Du S, et al. PD-1 regulates CXCR5$^+$ CD4 T cell-mediated proinflammatory functions in non-small cell lung cancer patients. *Int Immunopharmacol.* (2020) 82:106295. doi: 10.1016/j.intimp.2020.106295

51. Yang Z-Z, Grote DM, Ziesmer SC, Xiu B, Novak AJ, Ansell SM. PD-1 expression defines two distinct T-cell sub-populations in follicular lymphoma that differentially impact patient survival. *Blood Cancer J.* (2015) 5:e281. doi: 10.1038/bcj.2015.1

52. Martinez-Usatorre A, Carmona SJ, Godfroid C, Yacoub Maroun C, Labiano S, Romero P. Enhanced phenotype definition for precision isolation of precursor exhausted tumor-infiltrating CD8 T cells. *Front Immunol.* (2020) 11:340. doi: 10.3389/fimmu.2020.00340

53. Zimmerer JM, Ringwald BA, Elzein SM, Avila CL, Warren RT, Abdel-Rasoul M, et al. Antibody-suppressor CD8$^+$ T cells require CXCR5. *Transplantation.* (2019) 103:1809–20. doi: 10.1097/TP.0000000000002683

54. Zimmerer JM, Basinger MW. Ringwald BA, Abdel-Rasoul M, Pelletier RP, Rajab A, et al. Inverse association between the quantity of human peripheral blood CXCR5$^+$IFN-γ+CD8$^+$T cells with De Novo DSA production in the first year after kidney transplant. *Transplantation.* (2020) 104:2424–34. doi: 10.1097/TP.0000000000003151

55. Grebinoski S, Zhang Q, Cillo AR, Manne S, Xiao H, Brunazzi EA, et al. Autoreactive CD8$^+$ T cells are restrained by an exhaustion-like program that is maintained by LAG3. *Nat Immunol.* (2022) 23:868–77. doi: 10.1038/s41590-022-01210-5

56. Crowl JT, Heeg M, Ferry A, Milner JJ, Omilusik KD, Toma C, et al. Tissue-resident memory CD8$^+$ T cells possess unique transcriptional, epigenetic and functional adaptations to different tissue environments. *Nat Immunol.* (2022) 23:1121–31. doi: 10.1038/s41590-022-01229-8

57. Rao DA, Gurish MF, Marshall JL, Slowikowski K, Fonseka CY, Liu Y, et al. Pathologically expanded peripheral T helper cell subset drives B cells in rheumatoid arthritis. *Nature.* (2017) 542:110–4. doi: 10.1038/nature20810

58. Hartzell S, Bin S, Cantarelli C, Haverly M, Manrique J, Angeletti A, et al. Kidney failure associates with T cell exhaustion and imbalanced follicular helper T cells. *Front Immunol.* (2020) 11.

59. Waldman AD, Fritz JM, Lenardo MJ. A guide to cancer immunotherapy: from T cell basic science to clinical practice. *Nat Rev Immunol.* (2020) 20:651–68. doi: 10.1038/s41577-020-0306-5

60. Esfahani K, Roudaia L, Buhlaiga N, Del Rincon SV, Papneja N, Miller WH, et al. Review of cancer immunotherapy: from the past, to the present, to the future. *Curr Oncol.* (2020) 27:S87–97. doi: 10.3747/co.27.5223

61. Sharma P, Hu-Lieskovan S, Wargo JA, Ribas A. Primary, adaptive, and acquired resistance to cancer immunotherapy. *Cell.* (2017) 168:707–23. doi: 10.1016/j.cell.2017.01.017

62. Haslam A, Prasad V. Estimation of the percentage of US patients with cancer who are eligible for and respond to checkpoint inhibitor immunotherapy drugs. *JAMA Netw Open.* (2019) 2:e192535. doi: 10.1001/jamanetworkopen.2019.2535

63. Postow MA, Sidlow R, Hellmann MD. Immune-related adverse events associated with immune checkpoint blockade. *N Engl J Med.* (2018) 378:158–68. doi: 10.1056/NEJMra1703481

64. Ghosh N, Chan KK, Jivanelli B, Bass AR. Autoantibodies in patients with immune-related adverse events from checkpoint inhibitors: a systematic literature review. *JCR J Clin Rheumatol.* (2022) 28:e498. doi: 10.1097/RHU.0000000000001777

65. Yu R, Yang S, Liu Y, Zhu Z. Identification and validation of serum autoantibodies in children with B-cell acute lymphoblastic leukemia by serological proteome analysis. *Proteome Sci.* (2022) 20:3. doi: 10.1186/s12953-021-00184-w

66. Wang Z, Liu X, Muther J, James JA, Smith K, Wi S. Top-down mass spectrometry analysis of human serum autoantibody antigen-binding fragments. *Sci Rep.* (2019) 9:2345. doi: 10.1038/s41598-018-38380-y

67. Ignjatovic V, Geyer PE, Palaniappan KK, Chaaban JE, Omenn GS, Baker MS, et al. Mass spectrometry-based plasma proteomics: considerations from sample collection to achieving translational data. *J Proteome Res.* (2019) 18:4085–97. doi: 10.1021/acs.jproteome.9b00503

68. Tahir SA, Gao J, Miura Y, Blando J, Tidwell RSS, Zhao H, et al. Autoimmune antibodies correlate with immune checkpoint therapy-induced toxicities. *Proc Natl Acad Sci.* (2019) 116:22246–51. doi: 10.1073/pnas.1908079116

69. Purde M-T, Niederer R, Wagner NB, Diem S, Berner F, Hasan Ali O, et al. Presence of autoantibodies in serum does not impact the occurrence of immune checkpoint inhibitor-induced hepatitis in a prospective cohort of cancer patients. *J Cancer Res Clin Oncol.* (2022) 148:647–56. doi: 10.1007/s00432-021-03870-6

70. Labadzhyan A, Wentzel K, Hamid O, Chow K, Kim S, Piro L, et al. Endocrine Autoantibodies determine immune checkpoint inhibitor-induced endocrinopathy: a prospective study. *J Clin Endocrinol Metab.* (2022) 107:1976–82. doi: 10.1210/clinem/dgac161

71. Gowen MF, Giles KM, Simpson D, Tchack J, Zhou H, Moran U, et al. Baseline antibody profiles predict toxicity in melanoma patients treated with immune checkpoint inhibitors. *J Transl Med.* (2018) 16:82. doi: 10.1186/s12967-018-1452-4

72. Ghosh N, Postow M, Zhu C, Jannat-Khah D, Li Q-Z, Vitone G, et al. Lower baseline autoantibody levels are associated with immune-related adverse events from immune checkpoint inhibition. *J Immunother Cancer.* (2022) 10:e004008. doi: 10.1136/jitc-2021-004008

73. de Moel EC, Rozeman EA, Kapiteijn EH, Verdegaal EME, Grummels A, Bakker JA, et al. Autoantibody development under treatment with immune-checkpoint inhibitors. *Cancer Immunol Res.* (2019) 7:6–11. doi: 10.1158/2326-6066.CIR-18-0245

74. Yue Z, Ningning D, Lin Y, Jianming Y, Hongtu Z, Ligong Y, et al. Correlation between CXCR4, CXCR5 and CCR7 expression and survival outcomes in patients with clinical T1N0M0 non-small cell lung cancer. *Thorac Cancer.* (2020) 11:2955–65. doi: 10.1111/1759-7714.13645

75. Zhang M, Wu J-S, Xian H-C, Chen B-J, Wang H-F, Yu X-H, et al. CXCR5 induces perineural invasion of salivary adenoid cystic carcinoma by inhibiting microRNA-187. *Aging.* (2021) 13:15384–99. doi: 10.18632/aging.203097

76. Zheng Z, Cai Y, Chen H, Chen Z, Zhu D, Zhong Q, et al. CXCL13/CXCR5 Axis predicts poor prognosis and promotes progression through PI3K/AKT/MTOR pathway in clear cell renal cell carcinoma. *Front Oncol.* (2019) 8:1–10. doi: 10.3389/fonc.2018.00682

77. Tan P, Shi M, Lai L, Tang Z, Xie N, Xu H, et al. Regulative role of the CXCL13-CXCR5 axis in the tumor microenvironment. *Precis Clin Med.* (2018) 1:49–56.

78. Hsieh C-H, Jian C-Z, Lin L-I, Low G-S, Ou P-Y, Hsu C, et al. Potential role of CXCL13/CXCR5 signaling in immune checkpoint inhibitor treatment in cancer. *Cancers.* (2022) 14:294. doi: 10.3390/cancers14020294

79. Meylan M, Petitprez F, Becht E, Bougoüin A, Pupier G, Calvez A, et al. Tertiary lymphoid structures generate and propagate anti-tumor antibody-producing plasma cells in renal cell cancer. *Immunity.* (2022) 55:527–41. doi: 10.1016/j.immuni.2022.02.001

80. Zhu Z, Zhang X, Guo H, Fu L, Pan G, Sun Y. CXCL13-CXCR5 axis promotes the growth and invasion of colon cancer cells via PI3K/AKT pathway. *Mol Cell Biochem.* (2015) 400:287–95. doi: 10.1007/s11010-014-2285-y

81. Chen L, Huang Z, Yao G, Lyu X, Li J, Hu X, et al. The expression of CXCL13 and its relation to unfavorable clinical characteristics in young breast cancer. *J Transl Med.* (2015) 13:168. doi: 10.1186/s12967-015-0521-1

82. Siddiqui I, Schaeuble K, Chennupati V, Fuertes Marraco SA, Calderon-Copete S, Pais Ferreira D, et al. Intratumoral Tcf1^{+}PD-1^{+}CD8^{+} T cells with stem-like properties promote tumor control in response to vaccination and checkpoint blockade immunotherapy. *Immunity.* (2019) 50:195–211.e10. doi: 10.1016/j.immuni.2018.12.021

83. Liudahl SM, Coussens LM. B cells as biomarkers: predicting immune checkpoint therapy adverse events. *J Clin Invest.* (2018) 128:577–9. doi: 10.1172/JCI99036

84. Yasuda Y, Iwama S, Sugiyama D, Okuji T, Kobayashi T, Ito M, et al. CD4^{+} T cells are essential for the development of destructive thyroiditis induced by anti–PD-1 antibody in thyroglobulin-immunized mice. *Sci Transl Med.* (2021) 13:eabb7495. doi: 10.1126/scitranslmed.abb7495

85. Tsukamoto H, Komohara Y, Tomita Y, Miura Y, Motoshima T, Imamura K, et al. Aging-associated and CD4 T-cell–dependent ectopic CXCL13 activation predisposes to anti–PD-1 therapy-induced adverse events. *Proc Natl Acad Sci.* (2022) 119:e2205378119. doi: 10.1073/pnas.2205378119

86. Fife BT, Pauken KE, Eagar TN, Obu T, Wu J, Tan Q, et al. Interactions between PD-1 and PD-L1 promote tolerance by blocking the TCR–induced stop signal. *Nat Immunol.* (2009) 10:1185–92. doi: 10.1038/ni.1790

87. Nishimura H, Nose M, Hiai H, Minato N, Honjo T. Development of lupus-like autoimmune diseases by disruption of the PD-1 gene encoding an ITIM motif-carrying immunoreceptor. *Immunity.* (1999) 11:141–51. doi: 10.1016/S1074-7613(00)80089-8

88. Martin-Orozco N, Wang Y-H, Yagita H, Dong C. Cutting edge: programed death (PD) ligand-1/PD-1 interaction is required for CD8^{+} T cell tolerance to tissue antigens. *J Immunol.* (2006) 177:8291–5. doi: 10.4049/jimmunol.177.12.8291

89. Tilstra JS, Avery L, Menk AV, Gordon RA, Smita S, Kane LP, et al. Kidney-infiltrating T cells in murine lupus nephritis are metabolically and functionally exhausted. *J Clin Invest.* (2018) 128:4884–97. doi: 10.1172/JCI120859

90. Adam K, Iuga A, Tocheva AS, Mor A. A novel mouse model for checkpoint inhibitor-induced adverse events. *PLoS ONE.* (2021) 16:e0246168. doi: 10.1371/journal.pone.0246168

91. Han X, Vesely MD, Yang W, Sanmamed MF, Badri T, Alawa J, et al. PD-1H (VISTA)–mediated suppression of autoimmunity in systemic and cutaneous lupus erythematosus. *Sci Transl Med.* (2019) 11:eaax1159. doi: 10.1126/scitranslmed.aax1159

92. Pourakbari R, Hajizadeh F, Parhizkar F, Aghebati-Maleki A, Mansouri S, Aghebati-Maleki L. Co-stimulatory agonists: an insight into the immunotherapy of cancer. *Excli J.* (2021) 20:1055–85.

93. Perdomo-Celis F, Medina-Moreno S, Davis H, Bryant J, Taborda NA, Rugeles MT, et al. Characterization of CXCR5^{+} CD8^{+} T-cells in humanized NSG mice. *Immunobiology.* (2020) 225:151885. doi: 10.1016/j.imbio.2019.11.020

frontiers | Frontiers in Medicine

TYPE Clinical Trial
PUBLISHED 17 October 2022
DOI 10.3389/fmed.2022.1023224

OPEN ACCESS

EDITED BY
Vadim V. Sumbayev,
University of Kent, United Kingdom

REVIEWED BY
Luca Cimino,
IRCCS Local Health Authority of Reggio Emilia, Italy
Barbara H. Zimmermann,
University of Los Andes, Colombia, Colombia

*CORRESPONDENCE
Gerhild Wildner
gerhild.wildner@med.uni-muenchen.de

SPECIALTY SECTION
This article was submitted to Pathology, a section of the journal Frontiers in Medicine

RECEIVED 19 August 2022
ACCEPTED 26 September 2022
PUBLISHED 17 October 2022

CITATION
Thurau S, Deuter CME, Heiligenhaus A, Pleyer U, Van Calster J, Barisani-Asenbauer T, Obermayr F, Sperl S, Seda-Zehetner R and Wildner G (2022) A new small molecule DHODH-inhibitor [KIO-100 (PP-001)] targeting activated T cells for intraocular treatment of uveitis — A phase I clinical trial. *Front. Med.* 9:1023224. doi: 10.3389/fmed.2022.1023224

A new small molecule DHODH-inhibitor [KIO-100 (PP-001)] targeting activated T cells for intraocular treatment of uveitis — A phase I clinical trial

Stephan Thurau[1], Christoph M. E. Deuter[2], Arnd Heiligenhaus[3], Uwe Pleyer[4], Joachim Van Calster[5], Talin Barisani-Asenbauer[6], Franz Obermayr[7,8], Stefan Sperl[7], Romana Seda-Zehetner[7] and Gerhild Wildner[1]*

[1]Department of Ophthalmology, University Hospital, LMU München, München, Germany, [2]University Eye Hospital, Eberhard-Karls-University, Tübingen, Germany, [3]Department of Ophthalmology, St.-Franziskus-Hospital, Münster, Germany, [4]Department of Ophthalmology, Charité — Universitätsmedizin Berlin, Corporate Member of Freie Universität Berlin and Humboldt-Universität zu Berlin, Berlin, Germany, [5]Department of Ophthalmology, University Hospitals Leuven, Leuven, Belgium, [6]Medical University of Vienna, Vienna, Austria, [7]Panoptes Pharma GmbH, Vienna, now Kiora Pharmaceuticals Inc., Vienna, Austria, [8]Epics Therapeutics, Gosselies, Belgium

Uveitis is a T cell-mediated, intraocular inflammatory disease and one of the main causes of blindness in industrialized countries. There is a high unmet need for new immunomodulatory, steroid-sparing therapies, since only ciclosporin A and a single TNF-α-blocker are approved for non-infectious uveitis. A new small molecule inhibitor of dihydroorotate dehydrogenase (DHODH), an enzyme pivotal for *de novo* synthesis of pyrimidines, has a high potency for suppressing T and B cells and has already proven highly effective for treating uveitis in experimental rat models. Systemic and intraocular application of KIO-100 (PP-001) (previously called PP-001, now KIO-100) could efficiently suppress rat uveitis in a preventive as well as therapeutic mode. Here we describe the outcome of the first clinical phase 1 trial comparing three different doses of a single intraocular injection of KIO-100 (PP-001) in patients with non-infectious posterior segment uveitis. No toxic side effects on intraocular tissues or other adverse events were observed, while intraocular inflammation decreased, and visual acuity significantly improved. Macular edema, a sight-threatening complication in uveitis, showed regression 2 weeks after intraocular KIO-100 (PP-001) injection in some patients, indicating that this novel small molecule has a high potential as a new intraocular therapy for uveitis.

Clinical trial registration: [https://www.clinicaltrials.gov/ct2/show/NCT03634475], identifier [NCT03634475].

KEYWORDS

uveitis, humans, experimental autoimmune uveitis, rat, intravitreal therapy, clinical phase 1 trial, macular edema, visual acuity

Introduction

Within the group of intraocular inflammatory diseases, non-infectious uveitis is supposed to be of autoimmune origin. It often runs a chronic or relapsing course and has a high risk of visual deterioration and burden of illness, especially if the posterior segment of the eye is involved. Systemic treatment modalities include corticosteroids, disease-modifying anti-rheumatic drugs, ciclosporin A and adalimumab, a TNF-alpha inhibitor (1, 2). Intravitreal treatments consist of corticosteroids only, which are associated with significant local side effects like cataract and glaucoma (3). Therefore, novel intraocular anti-inflammatory strategies are still an unmet need.

The disease is mediated by T helper cells of the Th1 and Th17 type, which must be activated to be able to pass the blood eye-barriers that protect the immune privileged eye from assaults of the immune system (4–6). Activated leukocytes may enter the inner eye and screen for potential pathogens, but only those T cells that recognize their antigen presented within the eye can get reactivated to secrete chemokines and cytokines for recruiting inflammatory cells like macrophages and granulocytes to the eye, which cause the typical signs of inflammation and tissue destruction (7, 8).

Upon activation, T cells but also B cells have an increased need of nucleotides for mRNA and DNA synthesis. Activated T cells have an 8-fold increased need of pyrimidines, which cannot be provided from the salvage pool, therefore *de novo* synthesis of nucleobases must be initiated (9–11). A pivotal enzyme for the synthesis of pyrimidines is dihydroorotate dehydrogenase (DHODH), which can be blocked by the small molecule KIO-100 (PP-001) 150-times more potently than by leflunomide (12–14).

To prove the efficiency of KIO-100 (PP-001) on uveitis we have used two rat models of experimental autoimmune uveitis (EAU), a chronic, clinically monophasic disease with chorioretinal neovascularization as later sequel, and a spontaneous relapsing-remitting disease. In both models we first applied the small molecule orally to obtain a systemic immunosuppression for preventing uveitis by treatment starting with immunization, but we were also successful with late treatment in ongoing disease, reducing relapses and neovascularization. *In vitro*, rat T cell proliferation and cytokine secretion was significantly suppressed in a dose-dependent manner (13).

To avoid a general systemic immunosuppression, we also applied the small molecule locally by intraocular injection into rat eyes (15). The rationale of this experiment was to inhibit the intraocular reactivation of the autoreactive T cells and their ability to recruit inflammatory cells. We could show that a single intraocular injection of KIO-100 (PP-001) after the resolution of the primary course of relapsing EAU significantly inhibited the frequency and intensity of relapses in the small molecule-treated eyes compared with vehicle treatment. According to the pharmacokinetics (PK) performed in rabbits the concentration of the injected KIO-100 (PP-001) in the eye had dropped to 10% after 12 h and was not detectable any more after 96 h, while the immunosuppressive effect in the rat model was lasting for at least 6 days. We hypothesized that the intravitreally injected small molecule targeted the T cells, which were present in the eye at that time and prevented their reactivation and thus the induction of recurrent inflammation. No adverse effects on intraocular tissues were observed, and *in vitro* investigations with a human retinal pigment epithelial cell line revealed no toxic effect on this cell type with respect of viability, proliferation, and cytokine/chemokine production (15).

Here we show the results of a prospective, first in man phase 1 clinical trial in patients with posterior uveitis, the type of autoimmune disease, which has the greatest risk for retinal destruction and permanent vision loss. Twelve patients with chronic, non-infectious, bilateral uveitis from six centers received a single intravitreal injection of 0.3, 0.6, or 1.2 μg KIO-100 (PP-001), respectively. In addition to the assessment of general and uveitis-specific ocular symptoms and visual acuity, pharmacokinetic evaluation of plasma levels of the study drug was performed. Except for some minor side effects related to the injection procedure but not to the study drug we found no major systemic or ocular side effects, especially no increase of intraocular pressure. Plasma levels of the small molecule were below the detection limit in our patients. Within the first week visual acuity increased in a dose-dependent fashion in all eyes until the end of the study on day 28, despite a very short intraocular half-life of the study drug. In addition to a regression of intraocular inflammation a decrease of retinal thickness was found in 3 of 4 eyes 2 weeks after receiving the 1.2 μg dose and a reduction of cystoid macular edema (CME) in two eyes with doses of 0.6 or 1.2 μg. Thus, in this phase 1 trial the new DHODH inhibitor KIO-100 (PP-001) presented as a potential and promising new drug for the intraocular treatment of uveitis.

Materials and methods

Study drug

The study drug KIO-100 (PP-001) is a new small molecule inhibitor of DHODH, a mitochondrial enzyme that is required for the *de novo* synthesis of pyrimidine nucleotides, and thus impeding DNA and RNA synthesis.

KIO-100 (PP-001) is a biphenyl-4-ylcarbomyl thiophene carboxylic acid derivative (**Figure 1**) with a molecular mass of 479,3 D and has a 50% inhibitory concentration for DHODH of less than 4 nM and therefore a 150-fold higher potency than leflunomide (IC50 of 650 nM), an established drug with a similar mode of action (16). In addition, KIO-100 (PP-001) is highly specific for DHODH and does not inhibit tyrosine kinase or cause hepatotoxicity like leflunomide since, like other small

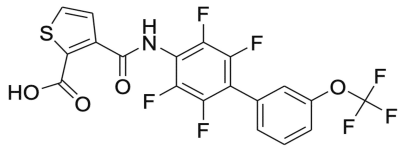

FIGURE 1
Structure of KIO-100 (PP-001). See also compound 13 in Leban et al. (16).

molecule DHODH inhibitors, it does not need to be converted from a prodrug to its active form in the liver (16–18).

Neither the preclinical uveitis rat models nor toxicology studies in rabbits have shown any toxic effects of the small molecule on intraocular cells/tissue at relevant exposure (15). Pharmacological investigations revealed that the amount of the study drug in the plasma of rabbits after intravitreal injection of high doses of KIO-100 (PP-001) was negligibly low. The half-life of KIO-100 (PP-001) in rabbit eyes after intravitreal injection was between 12 and 21 h, and all toxicity studies proved safety of this drug. The study drug was applied once intravitreally in a sterile, buffered, isotonic aqueous solution.

Patient selection

The study protocol and the informed consent form were reviewed and approved by the relevant Independent Ethics Committees (IEC) at each center prior to the start of the study (see **Supplementary Table 1**). Patients had to give their written informed consent. The study was registered with the Paul-Ehrlich-Institute in Langen, Germany and listed at ClinicalTrials.gov Identifier: NCT03634475.

For this first-in-man, open-label, phase-1 clinical trial 12 patients with bilateral chronic, non-infectious intermediate, posterior or pan-uveitis as defined by the Standardization of Uveitis Nomenclature (SUN) Working Group (19) were selected to receive a single intravitreal injection of KIO-100 (PP-001) in one eye. All patients had structural and vision threatening complications. For each patient only the worse eye was injected. Male or female patients at the age of at least 18 years were eligible and had to use two combined methods of contraception if females or female partners of male participants were in an age of childbearing potential. All females had to undergo a negative pregnancy test. Systemic or ocular infection had to be ruled out. Best corrected ETDRS (Early Treatment Diabetic Retinopathy Study) visual acuity had to be better than 10 (20/630), and worse than 50 letters (20/100) in the study eye, and 70 letters (20/40) or better in the fellow eye.

Any disease activity was acceptable, so there was no minimum requirement for disease activity according to the SUN criteria (19), since treatment effects as frequently referred to in phase 2 or 3 clinical trials were not a primary target in this phase 1 trial.

Most importantly, exclusion criteria included significant media opacities, any ongoing systemic treatment with biologicals or cytostatic agents, fluocinolone implants within the past 3 years, dexamethasone-implants within 6 months or any other intravitreal injection within 90 days before injection with KIO-100 (PP-001) (day 0). Patients with uncontrolled glaucoma, hypotony, aphacic eyes or eyes with anterior but not posterior chamber lens were also excluded; see **Supplementary Table 2** for the complete list of inclusion and exclusion criteria.

The primary study objective was to assess the safety and tolerability of ascending doses of KIO-100 (PP-001) in patients with chronic, non-infectious uveitis when administered as a single intravitreal injection of 100 µl containing 0.3, 0.6, or 1.2 µg KIO-100 (PP-001) (n = 4/group). Secondary objectives included the assessment of improvement of inflammation, and the pharmacokinetics (PK) of KIO-100 (PP-001) in plasma at screening, 4 ± 1 h after intravitreal injection and on day 2.

Patients were examined at screening, baseline, pre and post injection days 2, 7, 14, and 21 and at the final exit visit on day 28 after injection. A safety telephone call was scheduled on day 1.

Assessments and procedures are listed in **Table 1**.

For safety reasons the minimum time interval between injection of patients was 7 days to ensure sufficient time for development of adverse events before injecting the next patient. After each group of four patients and before proceeding to the next higher dose of KIO-100 (PP-001) a Data Safety Monitoring Board evaluated the safety of the previous dosing group after the final visit (day 28) of the last patient and had to consent on proceeding to the next higher dosing group.

Surgical procedure

Injection of the study drug was performed in an operating room or surgical suite using sterile technique. The final diluted KIO-100 (PP-001) solution had to be clear and colorless and was injected at the required dose in a volume of 100 µl. For safety reasons it was mandatory for patients to remain in the hospital for at least 4 h after the injection procedure.

Results

Demographic of patients

Twelve patients (eight females and four males) with an average age of 52 years (range 27–69) were included. All patients completed the study until the final visit. Average duration of uveitis was 10 years (range 13 months to 23 years). At baseline average visual acuity was log[MAR] (logarithm of minimum angle of resolution) 0.87 (range

TABLE 1 List of assessments and procedures.

Best corrected visual acuity (ETDRS)
Slit lamp examination
Intraocular pressure
Dilated fundoscopy
Corneal endothelial microscopy
Optical coherence tomography
Fluorescein angiogram
Amsler grid
Fundus photography
Visual field (computerized 30°)
Electroretinography
Visually evoked cortical potential
Study drug injection
Blood sampling for PK analysis
Urine pregnancy test
Medical and ophthalmic histories
Vital signs
Twelve-lead electrocardiogram
Laboratory assessments
Patient-reported outcomes
Concomitant medication
Serious medical events
Adverse events

1.3–0.4), which is equivalent to 20/150 (range 20/400–20/50). For assignment of diagnosis to dosing groups see Table 2.

Safety measurements

Systemic and ocular safety as well as PK analysis from peripheral blood were investigated.

Systemic safety

Vital signs were recorded at each visit in the study center. No substantial changes from screening to Day 28 in mean values of all blood chemistry parameters (blood urea nitrogen, creatinine, glucose, sodium, potassium, chloride, calcium, magnesium, phosphorus, aspartate aminotransferase (AST), alanine transaminase (ALT), gamma-glutamyltransferase (gamma-GT), alkaline phosphatase, creatine phosphokinase, total and direct bilirubin, uric acid, albumin, and total protein) were observed in all treatment dose cohorts. Minor changes were seen in the 0.3 μg group for creatinine, potassium, phosphorus, creatine phosphokinase (CPK), gamma-GT and albumin, in the 0.6 μg group for CPK and in the 1.2 μg group for CPK, gamma-GT and alkaline phosphatase. None of these changes were categorized as clinically significant. Twelve-lead electrocardiogram at base line and final visit on day 28 did not show any pathologic changes in any patient. Patients also did not report about any health issue potentially associated with the study, and no serious medical events nor systemic adverse events were observed.

Blood sampling for pharmacokinetics analysis

For PK analysis blood was drawn at screening, 4 h after intravitreal injection, and on day 2. KIO-100 (PP-001) was not reported in any of the samples. The quantification limit of the assay was 10 ng/ml.

Ocular findings

Procedure related events

Injection-related events occurring with the procedure included a transient increase in intraocular pressure in one eye, and mild conjunctival hemorrhages or conjunctival hyperemia at the injection site in all eyes. No intravitreal complications were observed. None of these complications were considered to be substance related.

Visual acuity

Visual acuity was tested using ETDRS charts and results were converted to log[MAR]. On the log[MAR] scale smaller numbers represent better visual acuity. In the PP-001/0.3 μg group visual acuity increased slightly throughout the study. Patients receiving 0.6 μg had an improved VA at day 14 by one line, and in the 1.2 μg-group VA improved by 0.3 log[MAR], which represents an increase by three lines or a doubling in resolution, at days 14 and 28. In the high-dose group VA improved already on day 2, continued to increase until day 14 and remained stable until day 28. This increase was statistically significant ($p \leq 0.05$) in this group at day 14, 21, and 28. None of the eyes had a loss of VA of more than two lines compared to baseline at any time point (Figure 2).

TABLE 2 List of diagnosis and group assignment.

Group	List of diagnosis
0.3 mg	Panuveitis ($n = 1$), intermediate uveitis ($n = 1$), and idiopathic posterior uveitis ($n = 2$)
0.6 μg	Serpiginous choroiditis ($n = 1$), choroiditis ($n = 1$), and intermediate uveitis ($n = 2$)
1.2 μg	Serpiginous choroiditis ($n = 1$), panuveitis ($n = 1$), intermediate uveitis ($n = 1$), and idiopathic posterior uveitis ($n = 1$)

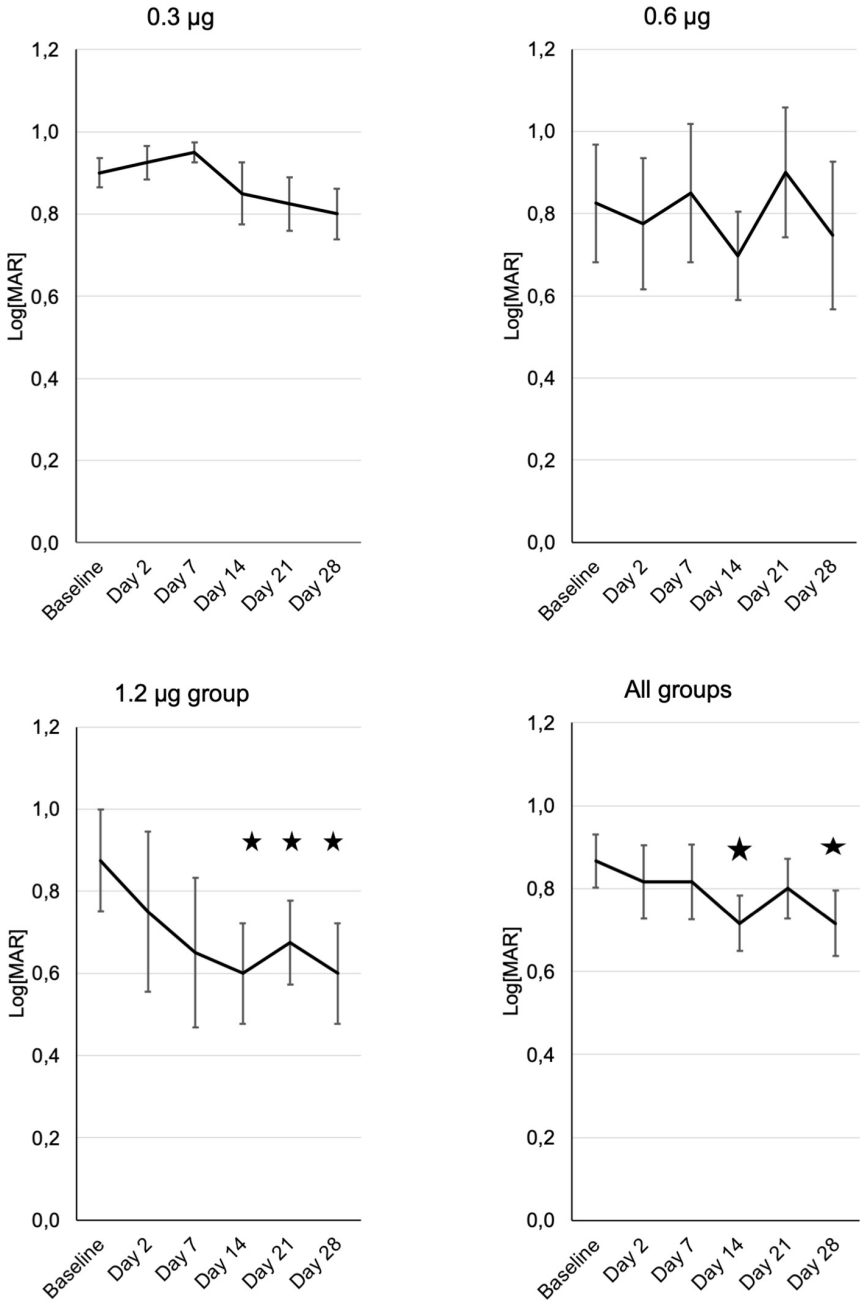

FIGURE 2
Development of visual acuity in the three treatment groups (n = 4) from baseline until the end of the study at day 28, assessed at the respective visits. "All patients" shows the means of visual acuity ± SE from all patients of the different treatment groups. Note that decreasing Log[MAR] values represent increasing visual acuity. Asterisks represent significant ($p \leq 0.05$) differences to baseline.

Intraocular pressure

In a single case a transient increase of intraocular pressure (IOP) to 32 mmHg was observed directly after the injection. In all other cases and time points the IOP remained within the normal limits between 7 and 19 mmHg. There was also no trend toward an increase or reduction within the follow up in any group (**Figure 3** and **Supplementary Figure 1**).

Inflammatory cells in the anterior chamber and vitreal haze

Signs of active inflammation according to the SUN were very subtle or negative in most patients at inclusion. According to SUN grading scheme, six ordinal grading steps are defined (0+, 0.5+, 1+, 2+, 3+, and 4+) for anterior chamber (AC) cells as well as the vitreal haze (19, 20).

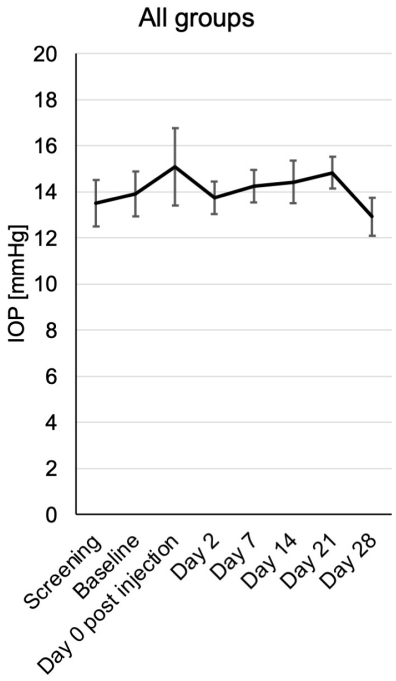

FIGURE 3
Intraocular pressure (IOP) from baseline until the end of the study at day 28, assessed at the respective visits. Mean mmHg ± SE is shown for all patients from the different treatment groups.

There were only two patients with 1+ anterior chamber cells in this study, who were randomly assigned to the 0.6 μg KIO-100 (PP-001) group. In both patients AC cells as well as vitreal haze improved within 7 days after injection. All other patients had 0.5+ or less cells and therefore a therapeutic effect on inflammation could not be detected (**Figure 4A** and **Supplementary Figure 2**).

Vitreal haze in the 0.3 μg group had increased on day 2 and showed a trend toward improvement in the follow up, also in the 0.6 μg group with an improvement by one step on the SUN scale. In the group receiving 1.2 μg KIO-100 (PP-001) only one patient had trace (0.5+) haze at baseline, which had disappeared after 2 weeks (**Figure 4B** and **Supplementary Figure 3**).

Since this phase 1 trial was aiming at safety of the drug, disease activity was not an inclusion criterion and therefore only a trend of a positive treatment effect could be determined. However, no worsening but rather an improvement has been observed.

Central retinal thickness

Central retinal thickness (CRT) was measured by optical coherence tomography (OCT). During the follow-up there was no significant change in CRT. Nevertheless, there was a trend toward reduced CRT in the 0.6 and 1.2 μg groups at day 2 and days 2, 7, and 14, respectively (**Figure 5** and **Supplementary Figure 4**).

Cystoid macular edema (CME) is an important feature of inflammatory macular disease and has been recorded separately from central macular thickness in this study. In the groups receiving 0.6 and 1.2 μg a total of five eyes had CME at the baseline examination which significantly improved clinically in two eyes, one in the 0.6 and one in the 1.2 μg-group (**Figure 6**). In these cases, the improvement of CME correlated with reduced CRT.

Electrophysiology

Electrophysiological testing included visually evoked cortical potentials (VECP) and electroretinography (ERG) and was performed according to the International Society for Clinical Electrophysiology of Vision (ISCEV)-standards (21) at screening or baseline and final visit at day 28. ERG was repeated at day 14 (visit 7) but was not available at all centers. Due to the destructive nature of the disease and the advanced stages of uveitis in this study most participants had pathological VECP and ERG findings at beginning, but during follow up there was no trend toward further elongation of latency or reduction of amplitude in VECP nor reduction of amplitudes in scotopic or photopic ERG.

Visual field

Computerized 30° visual fields at baseline, days 14 and 28 revealed a small but not significant trend toward improvement

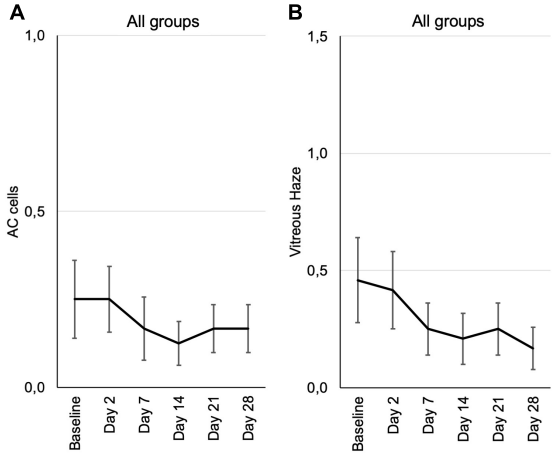

FIGURE 4
Inflammation parameters according to the SUN grading from baseline until the end of the study at day 28, assessed at the respective visits. **(A)** Cells in the anterior chamber (AC cells). **(B)** Vitreous haze. Mean grading score of AC cells ± SE **(A)** and mean vitreous haze scores ± SE **(B)** are shown for all patients from the three different dosing groups at each visit. According to the SUN grading scheme for AC cells and vitreous haze six grading steps are defined (0+, 0.5+, 1+, 2+, 3+, and 4+) (19, 20).

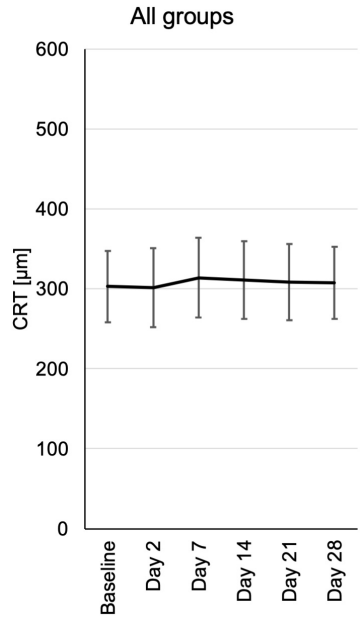

FIGURE 5
Central retinal thickness (CRT) from baseline until the end of the study at day 28, assessed at the respective visits. CRT measurements were extracted from automated standard OCT (optical coherence tomography) of the central fovea of the macula. CRT is depicted for each visit of all patients pooled from the three different dosing groups.

by a reduction of mean defects in all treatment groups. There were no losses of 2 dB (decibel) or more compared to baseline or any previous test in the follow up (**Figure 7** and **Supplementary Figure 5**).

Fluorescein angiography

Standard fluorescein angiography (FA) was performed at screening and final visit (day 28). At screening FA showed the typical signs of uveitis with vascular leakage, retinal and papillary staining and hyperfluorescence, only one eye had a normal FA. In four eyes there was a reduction in retinal staining intensity (leakage) seen in all three dosing groups, while in the other eight eyes there was no change in fluorescein pathology.

Corneal endothelial microscopy

Corneal endothelial cells were counted at baseline, days 7 and 28 and remained stable throughout the study in all three dosing groups (**Supplementary Figure 6**).

Discussion

Prior to the initiation of this phase 1 trial the effect of the small molecule DHODH-inhibitor KIO-100 (PP-001) had been demonstrated on rat EAU by preventive systemic (oral) application and revealed a dose-dependent, almost complete suppression of EAU. Using a spontaneous relapsing model of rat EAU a significant suppression of relapses was still obtained when the oral KIO-100 (PP-001)-treatment was initiated in a therapeutic mode after the resolution of the first course of uveitis (13). In a chronic model of EAU, where the autoreactive T cells secrete VEGF and thus induce chorioretinal neovascularization (CNV), also CNV-induction was significantly reduced by inhibiting T cells and their VEGF secretion when the oral KIO-100 (PP-001)-treatment was commenced during ongoing disease. Both, proliferation of rat and human T cells and their cytokine and chemokine secretion was suppressed by KIO-100 (PP-001) *in vitro* (13, 15). Cytokine production of RPE cells, shown with primary human RPE cells and the human ARPE-19 cell line, was not affected by treatment with KIO-100 (PP-001) (15).

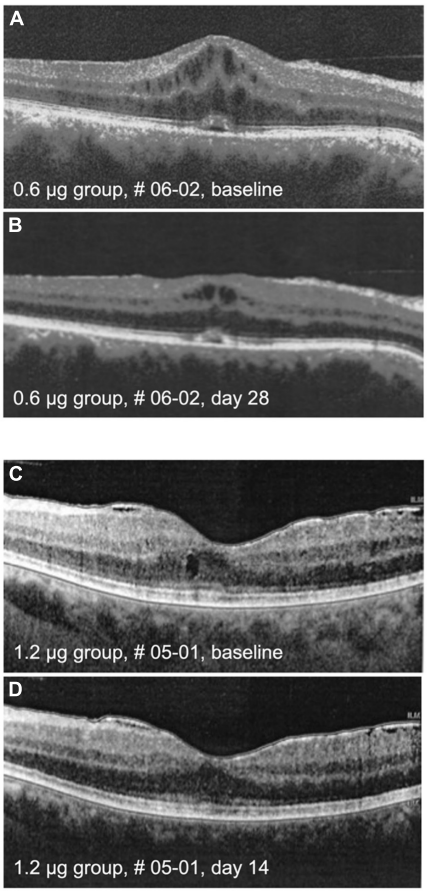

FIGURE 6
Optical coherence tomography (OCT) images. The upper panel shows macula of patient # 06-02 at baseline **(A)** and on day 28 **(B)** after intraocular injection of 0.6 µg KIO-100 (PP-001). Note a clinically meaningful reduction of cystoid macular edema (CME) in the region of the macula. In the lower panel the macula of patient # 05-01 is shown at baseline **(C)** and at day 14 **(D)** after injection of 1.2 µg of KIO-100 (PP-001). In this case the initial size of CME spaces was much smaller, but after injection the CME has disappeared completely.

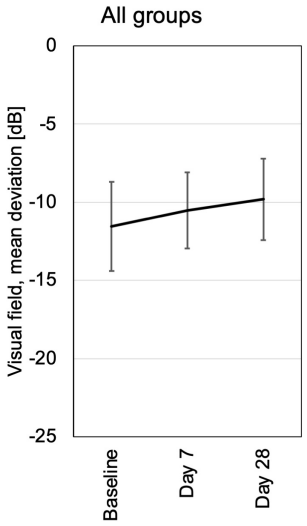

FIGURE 7
Visual field testing was performed at baseline, days 7 and 28. Mean deviation from normal is shown for each visit of all patients pooled from the three different dosing groups. All patients had loss of visual field sensitivity at baseline due to pre-existing destruction of previous chronic uveitis. In the follow up were no additional losses of more the 2 dB in a single patient. At day 28 the average visual field sensitivity had increased slightly, probably in part by training effects.

The therapeutic potency of intraocular KIO-100 (PP-001) on uveitis was previously investigated in a spontaneously relapsing rat model of EAU (15). Therapeutic injection of KIO-100 (PP-001) was performed in diseased rat eyes after the first course of intraocular inflammation to prevent further relapses. Although the retinal concentration of KIO-100 (PP-001) rapidly and massively decreased within the first 8 h to about 30% of the injected dose, further dropped to about 5% after 12 h and was below the detection limit after 4 days, we observed a significant suppression of the frequency of relapses and their intensity within the first 6 days after injection (15). We hypothesized that the activation of intraocular T cells present in the eye at the time of the intravitreal injection was hampered by KIO-100 (PP-001) and T cells were therefore unable to recruit inflammatory cells to induce a relapse.

In this prospective, open labeled, controlled clinical trial the substance KIO-100 (PP-001) was administered to humans for the first time. The route of administration was once intravitreal with 3 different doses of 0.3, 0.6, and 1.2 μg. Side effects, deemed by investigators as not clinically meaningful, occurred with the surgical procedure including a single incidence of transiently increased intraocular pressure and conjunctival bleedings or conjunctival hyperemia.

The primary goal of this study was to demonstrate safety and tolerability of intravitreal injections of KIO-100 (PP-001). Basically, all measurements and clinical observations served this aspect. In none of the cases we observed any drug-related ocular side effect. Since the amount of the injected study drug was very low the systemic exposure in the peripheral blood was below the quantification level of the assay. We could neither detect any systemic nor ocular toxicity. In summary, all safety measures demonstrated KIO-100 (PP-001) to be safe at the tested doses within the observation period of 4 weeks.

Although the study design and patient selection were targeted at detecting ocular or systemic side effects and not at anti-inflammatory, therapeutic effects, we could observe a clinical improvement in the two groups receiving the higher doses, in which visual acuity increased 14 days after injection. This improvement was significant and still observed after 28 days in the highest dose group. Also, classical signs of inflammatory activity like anterior chamber cells and vitreal haze were reduced in the two higher dose groups demonstrating a potential positive effect on uveitis. However, since this study aimed at assessing safety of the study drug the patients assigned to the different dose groups differed with respect of diagnoses and disease intensities, which might have influenced the outcome of the three treatment groups.

The frequency of the relapses in rat EAU is much higher than in human uveitis, which might explain that the latency for recurrences of 6 days observed in rats was extended to at least 4 weeks without recurrent inflammation in patients. The observation period of this study ended 28 days after injection, therefore no data are available beyond this point. All rat eyes were investigated histologically after the termination of these experiments, and no alterations except for the usual signs of inflammation-induced retinal destruction from uveitis had been observed in both, the KIO-100 (PP-001) and the vehicle-treated groups.

Intraocular application of therapeutic drugs can avoid potential systemic side effects and will only affect the autoreactive cells in the target organ of the disease. The only presently available intraocular therapeutics for uveitis are corticosteroids, which can be introduced with sustained-release carriers and therapeutic effects between 4 months and some years. However, corticosteroids can have side effects in the eye, including cataract development and glaucoma (22). Due to the single application and the short half-life of KIO-100 (PP-001) we could not observe such adverse events within the 4 weeks observation time, especially no elevated intraocular pressure pointing to glaucoma development.

The effect of intraocular KIO-100 (PP-001) on signs of inflammation like cells and haze in the vitreous was visible only after 7–14 days, which points to suppressed T cell activation rather than to an immediate anti-inflammatory effect. This is in coincidence with previous *in vitro* data of peripheral blood lymphocytes from human donors showing that KIO-100 (PP-001) suppresses proliferation of lymphocytes and their cytokine secretion, but has no effect on the secretion of monokines, which suggests that monocytes/macrophages are not affected by DHODH inhibition (15).

Also, in the groups receiving higher doses, in 2 of 5 patients their pre-existing CME resolved transiently, associated with a decrease in central retinal thickness. Although in one patient the CME had previously been therapy-refractive and had not responded to systemic or intravitreal steroids including dexamethasone slow releasing devices, we could observe a regression of the edema after injection of KIO-100 (PP-001). Macular edema as a complication of uveitis accounts for about 40% of cases with visual impairment (23). Mast cells have been found in the uveal tract and are described to play a role in macular edema fostering leakage of blood vessels (24–30). DHODH-inhibition was shown to induce apoptosis in mast cells (31), which might explain the positive effect of KIO-100 (PP-001) on increased retinal thickness and macular edema, respectively, in addition to the suppression of T cells that fuel the inflammation by the activation of innate immune cells.

The T cell type responsible for the induction and maintenance of uveitis is not yet completely clear. In experimental mouse models an important role of Th1 and Th17 type cells for the pathogenicity was postulated (6, 32), which has led to the initiation of clinical trials targeting IL-17. Those trials had not been successful so far (33), explained by the fact that T helper cells and especially Th17 cells are not restricted to the production of one cytokine, but are producing a cocktail of different cytokines which are tuning their function (5, 34).

In our rat models of experimental autoimmune uveitis (EAU) we have shown that both, Th1 and Th17 cells, are differently expresses in diseased eyes depending on the type of uveitis. In a spontaneous relapsing-remitting rat model induced by immunization with R14, a peptide from interphotoreceptor retinoid-binding protein IRBP and adjuvant Th17 cells are obviously necessary to guide autoreactive T cells to the eye, since they are mainly found in the eyes at onset of the first attack of uveitis, which is suggesting a function in facilitating invasion of inflammatory cells. In the later course of EAU and especially during relapses Th1 cells are dominating (5, 35). The role of Th1 cells and their lead cytokine IFN-γ was further demonstrated by the induction of synchronized relapses after intraocular injection of IFN-γ. The other model, induced with retinal S-antigen peptide PDSAg, displays only one clinically visible inflammatory attack, which is then followed by chorioretinal neovascularization as a late sequel. This is caused by the VEGF secretion of the autoreactive, PDSAg-specific T cells, a rarely described feature of T lymphocytes (13, 36). This type of uveitis is initiated by an early intraocular invasion of predominantly Th1 cells, while Th17 cells are increasing at the resolution of inflammation, probably playing an important role as regulatory cells, since they are co-expressing IL-10. In our rat models we could demonstrate that the T cell populations within the eyes during uveitis are highly dynamic, they change their phenotype by co-expressing IFN-γ and IL-17, even together with IL10, indicating that they might convert to Tregs, since the IFN-γ/IL-17/IL-10 co-expressing cells increase at the resolution of the monophasic disease and decrease during the course of the relapsing uveitis. In late remission of the monophasic EAU the Foxp3+ Treg population is higher than in the eyes of rats with relapsing-remitting disease. This shift of T cell populations is only observed in the eyes, but not in the lymph nodes of the same animals (5). In human non-infectious uveitis, where only peripheral blood is available for investigation, Th17 cells were rather found to facilitate ocular invasion of inflammatory cells and later converting to T regs than driving the autoimmune response (37–39).

These points to the fact that within the tissue affected by the autoimmune disease T cell populations undergo changes of phenotype and potentially of their function that is not reflected by peripheral lymphocyte populations. That is, why local targeting of autoreactive T cells, here by injecting therapeutic drugs into the eyes, might have a different effect on the T cells and thus on the disease than just systemic treatment, suppressing the activity of the tissue-invading lymphocytes (5). When rats are concomitantly immunized with both antigens, the monophasic disease phenotype dominates, and the intraocular IL-10+ and Foxp3+ T cell populations correspond to the populations detected in the monophasic, PDSAg-induced disease, irrespective of whether the animals were immunized with a mixture or both antigens separately in contralateral legs (40). Interestingly, in both rat models, irrespective of a relapsing or monophasic course, green fluorescent protein (GFP) + autoreactive T cells can still be detected within the retinal tissue even weeks after resolution of intraocular inflammation (40). Those cells form clusters during spontaneous relapses, suggesting intraretinal expansion of the remaining autoreactive T cells. They might be a reservoir for recurrences or fuel subclinical inflammation, and moreover, they seem to attract newly invading T cells (40). Those cells would be targeted by intraocular, T cell suppressing treatment as proposed and tested here in this clinical phase 1 trial.

The role of B cells that also can be targeted by KIO-100 (PP-001) in uveitis is not yet clear, it varies from promoting T cell activity and its function as antigen-presenting cells to regulation by their production of IL-10 and IL-35 (41–44). In rare cases of therapy-refractive juvenile uveitis or uveitis accompanying multiple sclerosis targeting B cells has shown some effect (45–48). Nevertheless, since inhibition of DHODH also impedes B cell activation, the therapeutic effect of KIO-100 (PP-001) exceeds an exclusive T cell suppression as gained by the presently approved therapies for uveitis, ciclosporin A and TNF-blocker Adalimumab (2).

The effect of intraocular KIO-100 (PP-001) is primarily the suppression of T cell activation, which is in coincidence with previous *in vitro* data of peripheral blood lymphocytes from human donors showing that KIO-100 (PP-001) suppresses proliferation of lymphocytes and their cytokine secretion, but has no effect on the secretion of monokines, suggesting

that monocytes/macrophages are not affected by DHODH inhibition (15).

The number of patients in this first clinical trial of KIO-100 (PP-001) in humans was limited by design, and therefore too small to attribute certain positive effects to a clinical diagnosis or disease activity. To answer those questions further studies aiming at clinical efficacy are required to fully explore the potential of the small molecule DHODH inhibitor in the treatment of inflammatory eye disease and cystoid macular edema.

Data availability statement

The original contributions presented in this study are included in the article/**Supplementary material**, further inquiries can be directed to the corresponding author.

Ethics statement

The studies involving human participants were reviewed and approved by the Ethical Committee of the LMU Münich, Pettenkoferstr. 8a, 80336 München, Germany (CEC). The patients/participants provided their written informed consent to participate in this study.

Author contributions

ST, FO, RS-Z, SS, and GW had drafted the study protocol. ST, CD, AH, UP, JV, and TB-A had acquired and documented the patient's data. ST, FO, SS, RS-Z, and GW had conducted the preclinical studies. ST and GW had resumed the clinical study data and written the manuscript. ST had designed the figures. All authors have read and revised the manuscript and approved the submitted version.

Funding

This study received funding from Panoptes Pharma GmbH, Wien, Austria (now Kiora Pharmaceuticals Inc.). The funder had the following involvement with the study: contribution to the development of study design, supply of study drug, PK-analysis (data collection), consent to decision to publish and to submission of manuscript. Trial and authors are compliant with the Consolidated Standards of Reporting Trials (CONSORT). Participants were not randomized due to the fact that this is an open label phase-1 trial.

Conflict of interest

Authors FO, SS, and RS-Z were employed by Kiora Pharmaceuticals Inc. (previously Panoptes Pharma GmbH).

The remaining authors declare that the research was conducted in the absence of any commercial or financial relationships that could be construed as a potential conflict of interest.

Publisher's note

Supplementary material

The Supplementary Material for this article can be found online at: https://www.frontiersin.org/articles/10.3389/fmed.2022.1023224/full#supplementary-material

References

1. Rosenbaum JT, Bodaghi B, Couto C, Zierhut M, Acharya N, Pavesio C, et al. New observations and emerging ideas in diagnosis and management of non-infectious uveitis: a review. *Semin Arthritis Rheum.* (2019) 49:438–45. doi: 10.1016/j.semarthrit.2019.06.004

2. Nguyen QD, Merrill PT, Jaffe GJ, Dick AD, Kurup SK, Sheppard J, et al. Adalimumab for prevention of uveitic flare in patients with inactive non-infectious uveitis controlled by corticosteroids (VISUAL II): a multicentre, double-masked, randomised, placebo-controlled phase 3 trial. *Lancet.* (2016) 388:1183–92. doi: 10.1016/s0140-6736(16)31339-3

3. Thomas AS, Lin P. Local treatment of infectious and noninfectious intermediate, posterior, and panuveitis: current concepts and emerging therapeutics. *Curr Opin Ophthalmol.* (2020) 31:174–84. doi: 10.1097/ICU.0000000000000651

4. Shechter R, London A, Schwartz M. Orchestrated leukocyte recruitment to immune-privileged sites: absolute barriers versus educational gates. *Nat Rev Immunol.* (2013) 13:206–18. doi: 10.1038/nri3391

5. Kaufmann U, Diedrichs-Mohring M, Wildner G. Dynamics of intraocular IFN-gamma, IL-17 and IL-10-producing cell populations during relapsing and monophasic rat experimental autoimmune uveitis. *PLoS One.* (2012) 7:e49008. doi: 10.1371/journal.pone.0049008

6. Luger D, Silver PB, Tang J, Cua D, Chen Z, Iwakura Y, et al. Either a Th17 or a Th1 effector response can drive autoimmunity: conditions of disease induction affect dominant effector category. *J Exp Med.* (2008) 205:799–810. doi: 10.1084/jem.20071258

7. Thurau SR, Mempel TR, Flugel A, Diedrichs Mohring M, Krombach F, Kawakami N, et al. The fate of autoreactive, GFP+ T cells in rat models of uveitis analyzed by intravital fluorescence microscopy and FACS. *Int Immunol.* (2004) 16:1573–82. doi: 10.1093/intimm/dxh158

8. Prendergast RA, Iliff CE, Coskuncan NM, Caspi RR, Sartani G, Tarrant TK, et al. T cell traffic and the inflammatory response in experimental autoimmune uveoretinitis. *Invest Ophthalmol Vis Sci.* (1998) 39:754–62.

9. Fairbanks LD, Bofill M, Ruckemann K, Simmonds HA. Importance of ribonucleotide availability to proliferating T-lymphocytes from healthy humans: disproportionate expansion of pyrimidine pools and contrasting effects of de novo synthesis inhibitors. *J Biol Chem.* (1995) 270:29682–9.

10. Marijnen YM, de Korte D, Haverkort WA, den Breejen EJ, van Gennip AH, Roos D. Studies on the incorporation of precursors into purine and pyrimidine nucleotides via 'de novo' and 'salvage' pathways in normal lymphocytes and lymphoblastic cell-line cells. *Biochim Biophys Acta.* (1989) 1012:148–55. doi: 10.1016/0167-4889(89)90088-8

11. Zaharevitz DW, Anderson LW, Malinowski NM, Hyman R, Strong JM, Cysyk RL. Contribution of de-novo and salvage synthesis to the uracil nucleotide pool in mouse tissues and tumors in vivo. *Eur J Biochem.* (1992) 210:293–6. doi: 10.1111/j.1432-1033.1992.tb17420.x

12. Loffler M, Jockel J, Schuster G, Becker C. Dihydroorotat-ubiquinone oxidoreductase links mitochondria in the biosynthesis of pyrimidine nucleotides. *Mol Cell Biochem.* (1997) 174:125–9.

13. Diedrichs-Möhring M, Leban J, Strobl S, Obermayr F, Wildner G. A new small molecule for treating inflammation and chorioretinal neovascularization in relapsing-remitting and chronic experimental autoimmune uveitis a new small molecule to treat monophasic and chronic EAU. *Invest Ophthalmol Vis Sci.* (2015) 56:1147–57. doi: 10.1167/iovs.14-15518

14. Fitzpatrick LR, Deml L, Hofmann C, Small JS, Groeppel M, Hamm S, et al. 4SC-101, a novel immunosuppressive drug, inhibits IL-17 and attenuates colitis in two murine models of inflammatory bowel disease. *Inflamm Bowel Dis.* (2010) 16:1763–77. doi: 10.1002/ibd.21264

15. Diedrichs-Möhring M, Niesik S, Priglinger CS, Thurau SR, Obermayr F, Sperl S, et al. Intraocular DHODH-inhibitor PP-001 suppresses relapsing experimental uveitis and cytokine production of human lymphocytes, but not of RPE cells. *J Neuroinflamm.* (2018) 15:54. doi: 10.1186/s12974-018-1088-6

16. Leban J, Kralik M, Mies J, Gassen M, Tentschert K, Baumgartner R. SAR, species specificity, and cellular activity of cyclopentene dicarboxylic acid amides as DHODH inhibitors. *Bioorg Med Chem Lett.* (2005) 15:4854–7. doi: 10.1016/j.bmcl.2005.07.053

17. Pytel D, Sliwinski T, Poplawski T, Ferriola D, Majsterek I. Tyrosine kinase blockers: new hope for successful cancer therapy. *Anticancer Agents Med Chem.* (2009) 9:66–76. doi: 10.2174/187152009787847752

18. Biolato M, Bianco A, Lucchini M, Gasbarrini A, Mirabella M, Grieco A. The disease-modifying therapies of relapsing-remitting multiple sclerosis and liver injury: a narrative review. *CNS Drugs.* (2021) 35:861–80. doi: 10.1007/s40263-021-00842-9

19. Jabs DA, Nussenblatt RB, Rosenbaum JT. Standardization of uveitis nomenclature for reporting clinical data. Results of the first international workshop. *Am J Ophthalmol.* (2005) 140:509–16.

20. Nussenblatt RB, Palestine AG, Chan CC, Roberge F. Standardization of vitreal inflammatory activity in intermediate and posterior uveitis. *Ophthalmology.* (1985) 92:467–71. doi: 10.1016/s0161-6420(85)34001-0

21. Odom JV, Bach M, Brigell M, Holder GE, McCulloch DL, Tormene AP, et al. ISCEV standard for clinical visual evoked potentials (2009 update). *Doc Ophthalmol.* (2010) 120:111–9. doi: 10.1007/s10633-009-9195-4

22. Gaballa SA, Kompella UB, Elgarhy O, Alqahtani AM, Pierscionek B, Alany RG, et al. Corticosteroids in ophthalmology: drug delivery innovations, pharmacology, clinical applications, and future perspectives. *Drug Deliv Transl Res.* (2021) 11:866–93. doi: 10.1007/s13346-020-00843-z

23. Rothova A, Suttorp-van Schulten MS, Frits Treffers W, Kijlstra A. Causes and frequency of blindness in patients with intraocular inflammatory disease. *Br J Ophthalmol.* (1996) 80:332. doi: 10.1136/bjo.80.4.332

24. Krystel-Whittemore M, Dileepan KN, Wood JG. Mast cell: a multi-functional master cell. *Front Immunol.* (2016) 6:620. doi: 10.3389/fimmu.2015.00620

25. Bousquet E, Zhao M, Thillaye-Goldenberg B, Lorena V, Castaneda B, Naud MC, et al. Choroidal mast cells in retinal pathology: a potential target for intervention. *Am J Pathol.* (2015) 185:2083–95. doi: 10.1016/j.ajpath.2015.04.002

26. Sato T, Morishita S, Horie T, Fukumoto M, Kida T, Oku H, et al. Involvement of premacular mast cells in the pathogenesis of macular diseases. *PLoS One.* (2019) 14:e0211438. doi: 10.1371/journal.pone.0211438

27. de Kozak Y, Sainte-Laudy J, Benveniste J, Faure JP. Evidence for immediate hypersensitivity phenomena in experimental autoimmune uveoretinitis. *Eur J Immunol.* (1981) 11:612–7. doi: 10.1002/eji.1830110805

28. McMenamin PG, Polla E. Mast cells are present in the choroid of the normal eye in most vertebrate classes. *Vet Ophthalmol.* (2013) 16(Suppl. 1):73–8. doi: 10.1111/vop.12035

29. Steptoe RJ, McMenamin C, McMenamin PG. Choroidal mast cell dynamics during experimental autoimmune uveoretinitis in rat strains of differing susceptibility. *Ocul Immunol Inflamm.* (1994) 2:7–22. doi: 10.3109/09273949409057797

30. Daruich A, Matet A, Moulin A, Kowalczuk L, Nicolas M, Sellam A, et al. Mechanisms of macular edema: beyond the surface. *Prog Retin Eye Res.* (2018) 63:20–68. doi: 10.1016/j.preteyeres.2017.10.006

31. Sawamukai N, Saito K, Yamaoka K, Nakayamada S, Ra C, Tanaka Y. Leflunomide inhibits PDK1/Akt pathway and induces apoptosis of human mast cells. *J Immunol.* (2007) 179:6479–84. doi: 10.4049/jimmunol.179.10.6479

32. Amadi-Obi A, Yu CR, Liu X, Mahdi RM, Clarke GL, Nussenblatt RB, et al. TH17 cells contribute to uveitis and scleritis and are expanded by IL-2 and inhibited by IL-27/STAT1. *Nat Med.* (2007) 13:711–8. doi: 10.1038/nm1585

33. Dick AD, Tugal-Tutkun I, Foster S, Zierhut M, Melissa Liew SH, Bezlyak V, et al. Secukinumab in the treatment of noninfectious uveitis: results of three randomized, controlled clinical trials. *Ophthalmology.* (2013) 120:777–87. doi: 10.1016/j.ophtha.2012.09.040

34. Chong WP, Mattapallil M, Raychaudhuri K, Silver PB, Jittayasothorn Y, Chan C-C, et al. A novel self-regulatory mechanism of Th17 cells controls autoimmune uveitis through interleukin-24. *J Immunol.* (2020) 204(1 Suppl.):142.5.

35. Jia X, Hu M, Wang C, Wang C, Zhang F, Han Q, et al. Coordinated gene expression of Th17- and Treg-associated molecules correlated with resolution of the monophasic experimental autoimmune uveitis. *Mol Vis.* (2011) 17:1493–507.

36. Mor F, Quintana FJ, Cohen IR. Angiogenesis-inflammation cross-talk: vascular endothelial growth factor is secreted by activated T cells and induces Th1 polarization. *J Immunol.* (2004) 172:4618–23. doi: 10.4049/jimmunol.172.7.4618

37. Kim Y, Kim TW, Park YS, Jeong EM, Lee D-S, Kim I-G, et al. The role of interleukin-22 and its receptor in the development and pathogenesis of experimental autoimmune uveitis. *PLoS One.* (2016) 11:e0154904. doi: 10.1371/journal.pone.0154904

38. Gilbert RM, Zhang X, Sampson RD, Ehrenstein MR, Nguyen DX, Chaudhry M, et al. Clinical remission of sight-threatening non-infectious uveitis is characterized by an upregulation of peripheral t-regulatory cell polarized towards T-bet and TIGIT. *Front Immunol.* (2018) 9:907. doi: 10.3389/fimmu.2018.00907

39. Wildner G, Diedrichs-Möhring M. Resolution of uveitis. *Semin Immunopathol.* (2019) 41:727–36. doi: 10.1007/s00281-019-00758-z

40. Diedrichs-Möhring M, Kaufmann U, Wildner G. The immunopathogenesis of chronic and relapsing autoimmune uveitis – Lessons from experimental rat models. *Prog Retinal Eye Res.* (2018) 65:107–26. doi: 10.1016/j.preteyeres.2018.02.003

41. Smith JR, Stempel AJ, Bharadwaj A, Appukuttan B. Involvement of B cells in non-infectious uveitis. *Clin Transl Immunol.* (2016) 5:e63. doi: 10.1038/cti.2016.2

42. Wang R-X, Yu C-R, Dambuza IM, Mahdi RM, Dolinska MB, Sergeev YV, et al. Interleukin-35 induces regulatory B cells that suppress autoimmune disease. *Nat Med.* (2014) 20:633–41.

43. Dambuza IM, He C, Choi JK, Yu C-R, Wang R, Mattapallil MJ, et al. IL-12p35 induces expansion of IL-10 and IL-35-expressing regulatory B cells and ameliorates autoimmune disease. *Nat Commun.* (2017) 8:719. doi: 10.1038/s41467-017-00838-4

44. Egwuagu CE, Yu C-R. Interleukin 35-producing B cells (i35-Breg): a new mediator of regulatory B-cell functions in CNS autoimmune diseases. *Crit Rev Immunol.* (2015) 35:49–57. doi: 10.1615/critrevimmunol.2015012558

45. Heiligenhaus A, Miserocchi E, Heinz C, Gerloni V, Kotaniemi K. Treatment of severe uveitis associated with juvenile idiopathic arthritis with anti-CD20 monoclonal antibody (rituximab). *Rheumatology.* (2011) 50:1390–4. doi: 10.1093/rheumatology/ker107

46. Bar-Or A, Pachner A, Menguy-Vacheron F, Kaplan J, Wiendl H. Teriflunomide and its mechanism of action in multiple sclerosis. *Drugs.* (2014) 74:659–74. doi: 10.1007/s40265-014-0212-x

47. Li L, Liu J, Delohery T, Zhang D, Arendt C, Jones C. The effects of teriflunomide on lymphocyte subpopulations in human peripheral blood mononuclear cells in vitro. *J Neuroimmunol.* (2013) 265:82–90. doi: 10.1016/j.jneuroim.2013.10.003

48. Stascheit F, Rübsam A, Otto C, Meisel A, Ruprecht K, Pleyer U. Anti-CD20 therapy for multiple sclerosis-associated uveitis: a case series. *Eur J Neurol.* (2022) 29:3028–38. doi: 10.1111/ene.15453

frontiers | Frontiers in Medicine

TYPE Original Research
PUBLISHED 24 October 2022
DOI 10.3389/fmed.2022.1034594

OPEN ACCESS

EDITED BY
Bernhard F. Gibbs,
University of Oldenburg, Germany

REVIEWED BY
Cheng-Rong Yu,
National Eye Institute (NIH), United States
Lucia Bongiovanni,
San Raffaele Hospital (IRCCS), Italy

*CORRESPONDENCE
Todd Bradley
tcbradley@cmh.edu

SPECIALTY SECTION
This article was submitted to Pathology, a section of the journal Frontiers in Medicine

RECEIVED 01 September 2022
ACCEPTED 05 October 2022
PUBLISHED 24 October 2022

CITATION
Geanes ES, Krepel SA, McLennan R, Pierce S, Khanal S and Bradley T (2022) Development of combinatorial antibody therapies for diffuse large B cell lymphoma. *Front. Med.* 9:1034594. doi: 10.3389/fmed.2022.1034594

Development of combinatorial antibody therapies for diffuse large B cell lymphoma

Eric S. Geanes[1], Stacey A. Krepel[1], Rebecca McLennan[1], Stephen Pierce[1,2], Santosh Khanal[1] and Todd Bradley[1,2,3,4]*

[1]Genomic Medicine Center, Children's Mercy Research Institute, Kansas City, MO, United States, [2]Department of Pathology and Laboratory Medicine, University of Kansas Medical Center, Kansas City, KS, United States, [3]Department of Pediatrics, University of Kansas Medical Center, Kansas City, KS, United States, [4]Department of Pediatrics, University of Missouri-Kansas City, Kansas City, MO, United States

Diffuse large B-cell lymphoma (DLBCL), the most common form of lymphoma, is typically treated with chemotherapy combined with the immunotherapy rituximab, an antibody targeting the B cell receptor, CD20. Despite the success of this treatment regimen, approximately a third of DLBCL patients experience either relapse or have refractory disease that is resistant to rituximab, indicating the need for alternative therapeutic strategies. Here, we identified that CD74 and IL4R are expressed on the cell surface of both CD20 positive and CD20 negative B cell populations. Moreover, genes encoding *CD74* and *IL4R* are expressed in lymphoma biopsies isolated from all stages of disease. We engineered bispecific antibodies targeting CD74 or IL4R in combination with rituximab anti-CD20 (anti-CD74/anti-CD20 and anti-IL4R/anti-CD20). Bispecific antibody function was evaluated by measuring direct induction of apoptosis, antibody-dependent cellular phagocytosis (ADCP), and antibody-dependent cellular cytotoxicity in both rituximab-sensitive and rituximab-resistant DLBCL cell lines. Both anti-CD74/anti-CD20 and anti-IL4R/anti-CD20 were able to mediate ADCC and ADCP, but CD74-targeting therapeutic antibodies could also mediate direct cytotoxicity. Overall, this study strongly indicates that development of bispecific antibodies that target multiple B cell receptors expressed by lymphoma could provide improved defense against relapse and rituximab resistance.

KEYWORDS

bispecific antibody, lymphoma, diffuse large B cell lymphoma, rituximab, cancer therapy, CD20, CD74, IL4R

Introduction

About 4% of all cancer diagnoses in the United States each year are classified as Non-Hodgkin's lymphomas (NHL) (1). The most common type of NHL is diffuse large B cell lymphoma (DLBCL), which represents 40% of all newly diagnosed lymphomas annually (2). There are many subtypes of DLBCL, which are based on gene expression profiling

and location of initiation (3–5). Despite being genetically and phenotypically diverse, most patients with DLBCL are treated with common therapy regardless of the subtypes involved. However, with the advances in immunotherapy, more targeted therapeutic approaches are being implemented.

One such therapeutic is the monoclonal antibody rituximab, which targets the B cell marker CD20 (6). Rituximab was the first monoclonal antibody approved by the United States Food and Drug Administration (FDA) for use in cancer treatment in the late 1990's, and in the early 2000's, it was added to the standard DLBCL chemotherapeutic regimen, CHOP, which includes cyclophosphamide, vincristine, doxorubicin, and prednisone (7–13). With the addition of rituximab, R-CHOP demonstrated a 10-year disease-free survival of approximately 64%, an improvement compared to the 42.5% disease-free survival with CHOP treatment alone (8). Despite this success, 30–40% of DLCBL patients experience either relapse or refractory disease with R-CHOP treatment (14–18). There have been various mechanisms proposed for the development of rituximab resistance, including a decrease in complement-dependent cytotoxicity, resistance to killing *via* antibody-dependent cell-mediated cytotoxicity, and resistance to apoptosis (19). One of the most strongly supported hypotheses attributes resistance to the loss of CD20 expression on B cells following initial rituximab treatment (19–21). Importantly, rituximab targets only select subpopulations of B cells and is not a pan-B cell therapeutic (22). For example, plasma B cells do not express CD20 and are not targeted by rituximab. This has led to the development of immunotherapies targeting other B cells markers to have broader clinical application. Due to the phenotypically diverse nature of DLCBL subtypes, it has been suggested that targeting multiple B cell specific pathways or receptors would be a more effective treatment (3). Additionally, development of resistance may prove to be more difficult if there are multiple therapeutic targets, as these targets would need to be simultaneously mutated or expression level reduced to effectively escape treatment (3).

Bispecific antibodies are a new immunotherapy that allows for expression of an antibody that targets two cell surface receptors, simultaneously. There are multiple mechanisms associated with bispecific antibody efficacy, including complement activation; recruitment of macrophages for antibody-dependent cellular phagocytosis (ADCP); recruitment of natural killer (NK) cells or T-cells for antibody-dependent cell-mediated cytotoxicity (ADCC); apoptosis activation; and priming for cross-presentation by antigen-presenting cells (19, 23, 24). One advantage of bispecific antibodies over more conventional treatments is the decreased risk of resistance against two different targets.

In this study, using a bispecific antibody approach, we sought to broaden the therapeutic benefit of rituximab by developing novel lymphoma-targeted bispecific antibodies. We identified CD74 and IL4R as surface receptors that are expressed on B cell populations that have CD20 or do not have CD20 expression, respectively. Moreover, we found that these markers are expressed in lymphomas and could serve as potential therapeutic targets on B cells. We engineered bispecific antibodies against these targets in combination with anti-CD20. We then evaluated these antibodies for functional targeting of lymphoma cell lines.

Materials and methods

Single cell RNA sequencing analysis

Single cell RNA sequencing (scRNA-seq) data was acquired from a previously published dataset of scRNA-seq performed on peripheral blood mononuclear cells (PBMCs) from 12 healthy and HIV-infected subjects that were deidentified from Duke University (25). Original sample collection was reviewed and approved by the Duke Medicine Institutional Review Board. The data is publicly available at SRA BioProject ID: PRJNA681021. PBMCs were thawed, washed and placed in single-cell suspensions with PBS + 0.04% bovine serum albumin (BSA). Cellular suspensions were loaded on a GemCode Single-Cell instrument (10X Genomics, Pleasanton, CA, USA) to generate single-cell beads in emulsion. Single-cell RNA-seq libraries were then prepared using a GemCode Single Cell 3′ Gel bead and library kit version 2 (10X Genomics). Single-cell barcoded cDNA libraries were quantified by quantitative PCR (Kappa Biosystems, Potters Bar, UK) and sequenced on an Illumina (San Diego, CA, USA) NextSeq 500 (26–29). Read lengths were 26 bp for read 1, 8 bp i7 index, and 98 bp read 2. Cells were sequenced to greater than 50,000 reads per cell.

After sequencing, the Cell Ranger Single Cell Software Suite (version 2.1.1) was used to generate sequencing FASTQ files and to perform sample de-multiplexing, barcode processing, reference alignment and single-cell 3′ gene counting (30). Reads were aligned to the human genome (GRCH38). Samples were aggregated using the CellRanger Aggr function to create a single matrix of cell barcodes and gene counts for the groups. During the process each library was normalized for mapped sequencing depth. In order to control for variation in the number of reads per sample (sequencing depth), reads were subsampled from higher-depth libraries until they all had an equal number of reads per cell that were confidently mapped to the transcriptome. Finally, in order to control for technical variation and correct for any batch effects we used the Seurat analysis pipeline Multi CCA method to regress out cell-cell variation in gene expression. The union of variable genes across all individual samples were utilized to renormalize the data.

Matrices of cell barcodes and gene counts generated by Cell Ranger were loaded into Seurat R package (v3.2.3) for graph-based cell clustering, dimensionality reduction and data visualization (31–33). We filtered low quality cells that

had lower than 200 expressed transcripts and percentage of mitochondrial genes expressed greater than 20% and for the primary cell model we reduced this threshold to greater than 10% mitochondrial genes. We included up to 45 PCA dimensions for the PBMCs and 48 PCA for the primary cell model for downstream graph-based clustering and UMAP visualization. All other parameters we followed the default Seurat recommendations. We then selected cells that were B cells using *CD79A* transcript expression and utilized this subset of cells for further analysis. Genes that correlated with *MS4A1* or *CXCR4* transcript expression were calculated by Pearson correlation and corrected for multiple comparisons using Bonferroni. Graphs and plots were generated using the Seurat and ggplot2 (v3.3.3) R packages and Graphpad Prism version 8 (Graphpad Software, San Diego, CA, USA). The single-cell RNA seq unprocessed reads have been deposited in the NCBI SRA database under the BioProject ID: PRJNA681021. Code and other processed file formats are available from corresponding author/s upon reasonable request.

Lymphoma panel gene expression assay

Lymphoma cDNA Array I and Array II were purchased from OriGene Technologies, Inc. (Rockville, MD, USA). The 2 panels consisted of cDNA from the following tumor samples: 12 normal, 15 stage IE, 41 stage I, 1 stage IIB, 12 stage IIE, 6 stage II, 1 stage III, 7 stage IV, and 1 N/R. Plates with lyophilized cDNA were warmed to room temperature, centrifuged for 30 s at 1,000 revolutions per minute, and pellets from each well suspended in 30 μl of qPCR master mix. For a single 30 μl reaction, the qPCR master mix consisted of 15 μl of 2x Taqman Fast Advanced Master Mix (Applied Biosystems, Waltham, MA, USA), 1.5 μl of 20x Taqman probe (Thermo Fisher Scientific, Waltham, MA, USA), and 13.5 μl of PCR-grade water (Invitrogen, Waltham, MA, USA). Probes utilized in the assay targeted *IGSF9* (Hs00325279_m1), *CD209* (Hs01588349_m1), *MS4A1* (Hs00544819_m1), *IL4R* (Hs00965056_m1), and *CD74* (Hs00269961_m1). An *18S* probe (Hs03003631_g1) was used as a housekeeping control. Only 1 probe was used per master mix. Following resuspension, plates were vortexed, centrifuged and placed on ice. Plates were loaded into the QuantStudio 12 Flex (Applied Biosystems). After loading, the reactions underwent an initial 50°C for 2 min activation followed by a 95°C for 10 min pre-soak for 1 cycle. The remaining 42 cycles were performed in two steps: denaturing at 95°C for 15 s followed by annealing at 60°C for 1 min. Data was analyzed by subtracting the Ct values of *18S* from the Ct value of the target gene. This difference (x) was transformed *via* the function 2^(-x) and plotted on a logarithmic scale to illustrate target gene expression relative to *18S* for each sample.

Cell culture

SU-DHL-4 (CRL-2957), NU-DUL-1 (CRL-2969), and SU-DHL-8 (CRL-2961) cell lines were purchased from the Non-Hodgkin's Lymphoma Cell Line Panel at ATCC (Manassas, VA, USA) and maintained in RPMI-1640 medium (Gibco, Grand Island, NY, USA) supplemented with 10% fetal bovine serum (Thermo Fisher Scientific). All cell lines were cultured at 37°C under 5% CO_2. Media was refreshed every 48 h.

RT-PCR

RNA extraction was performed according to manufacturer protocol using RNeasy Plus Mini Kit with the additional use of Qiashredder from Qiagen (Hilden, Germany). cDNA synthesis was performed using SuperScript™ VILO™ cDNA Synthesis kit and High-Capacity cDNA Reverse Transcription Kit (Thermo Fisher Scientific). RT-PCR was performed using TaqMan Fast Advanced Master Mix (Thermo Fisher Scientific) and the following Advanced Biosystems Taqman Probes: *18S* TaqMan Probe (FAM-MGB) Assay ID: Hs99999901_s1, *MS4A1* TaqMan Probe (FAM-MGB) Assay ID: Hs00544819_m1, *CD74* TaqMan Probe (FAM-MGB) Assay ID: Hs00269961_m1, *IL4R* TaqMan Probe (FAM-MGB) Assay ID: Hs00965056_m1.

Antibodies

Rituximab was purchased from Creative Biolabs (Shirley, NY, USA) and Invivogen (San Diego, CA, USA). Milatuzumab (TAB-763), Dupilumab (TAB-021ML) were purchased from Creative Biolabs. Bispecific antibodies were produced in collaboration with Creative Biolabs. Expression vectors encoding the antibody heavy and light chain gene sequences were transiently transfected and expressed in HEK293F cells. Secreted antibody was purified by Protein A affinity chromatography, ultrafiltration and then subjected to 0.2-micron sterile filtration. Purified antibodies were stored at PBS, pH 7.4. For sequences used for each heavy and light chain in each of the anti-CD20/anti-CD74 bispecific antibody and anti-CD20/anti-IL4R bispecific antibodies (see **Supplementary Data 1**). Quality of bispecific antibodies was measured by Creative Biolabs by reducing SDS-PAGE and size exclusion chromatography-HPLC (**Supplementary Figure 1**). AffiniPure Goat Anti-Human IgG, Fcγ fragment specific (109-005-098) cross-linking antibody was purchased from Jackson ImmunoResearch Laboratories, Inc. (West Grove, PA, USA).

Enzyme-linked immunosorbent assays

Enzyme-linked immunosorbent assays (ELISAs) were performed using the following antigens and antibodies:

recombinant CD20 full length protein (Acro Biosystems, Newark, DE, USA), recombinant CD74 protein (R&D Systems, Minneapolis, MN, USA), recombinant IL4R protein (R&D Systems), human Anti-CD20 antibody (Invivogen), Milatuzumab/Anti-CD74 Antibody (Creative Biolabs), Dupilumab/IL4R monoclonal antibody (Creative Biolabs), bispecific anti-CD20/anti-CD74 antibody (Creative Biolabs), bispecific anti-CD20/anti-IL4R antibody (Creative Biolabs). Antigens were all diluted to 2 μg/mL in 0.1 M sodium bicarbonate and incubated on high-binding plates (Corning Inc., Corning, NY, USA) overnight at 4 degrees. Antibodies were diluted to 33.3 μg/mL in superblock buffer with sodium azide followed by subsequent 1:3 dilutions until a final dilution of 0.565 ng/mL. Secondary Goat anti-human IgG antibody (Jackson ImmunoResearch Laboratories, Inc.) dilutions were done in superblock buffer without sodium azide within range of manufacturer's recommendations at 1:50,000 dilution. SureBlue Reserve Microwell Substrate (VWR, Radnor, PA, USA) was added and incubated in the dark for 15 min. Immediately after, 0.33 N HCl Acid Stop solution was added to the plate and absorbance was measured at 450 nm.

Crosslinking apoptosis assay

Cells were seeded at 50,000 cells per well in 24 well dishes. 10 μg/mL of respective antibody and AffiniPure Goat Anti-Human IgG, Fcγ fragment specific cross-linking antibody (Jackson ImmunoResearch Laboratories, Inc.) was added to wells and incubated for 8 h. Cells were collected and incubated in the Muse Annexin V reagent according to the manufacture's protocol. Total cell death was measured and recorded on the Muse Cell Analyzer (Luminex Corporation, Austin, TX, USA) in reference to crosslinking antibody control wells with the addition of only crosslinking antibody.

Antibody-dependent cellular cytotoxicity assay

ADCC Bioassay Core Kit (Promega, Madison, WI, USA) was performed using the manufacturer protocol with the addition of SU-DHL-4 (CRL-2957), NU-DUL-1 (CRL-2969), and SU-DHL-8 (CRL-2961) cell lines as target cells purchased from ATCC. ADCC Bioassay Complete Kit (Promega) was performed using the manufacturer protocol with the provided Raji target cells. Antibodies were treated at 1 μg/mL and subsequently diluted at a 1:3 ratio until a final concentration of 0.152 ng/mL. Respective target cells were incubated with antibody and modified Jurkat NFAT-luc FcγRIIIa effector cells for 6 h. Bio-Glo luciferase assay reagent was added to each well and luminescence was measured.

Antibody-dependent cellular phagocytosis assay

ADCP Bioassay Complete Kit (Promega) was performed using the manufacturer protocol with the provided Raji target cells and modified Jurkat NFAT-luc FcγRIIa-H effector cells. Antibodies were treated at 1 μg/mL and subsequently diluted at a 1:3 ratio until a final concentration of 0.152 ng/mL. Raji target cells were incubated with antibody and modified Jurkat NFAT-luc FcγRIIa-H effector cells for 6 h. Bio-Glo luciferase assay reagent was added to each well and luminescence was measured.

Results

Identification of candidate therapeutic targets on CD20 positive and negative B cells

To identify putative B cell specific targets for the engineering of bispecific antibodies against DLBCL, we performed expression analysis of B cells isolated from healthy individuals using single cell RNA sequencing from a prior published study (SRA BioProject ID: PRJNA681021). CD20, the target of rituximab, is encoded by the *MS4A1* gene. Initial evaluation of the *MS4A1* levels showed heterogeneous expression within the B cell subpopulations (**Figure 1A**). CD20 and the chemokine receptor CXCR4 are critical for B cell trafficking and are molecular targets for cancer immunotherapies (34–37). Moreover, a prior study demonstrated that cells with high *CXCR4* expression were less responsive to rituximab treatment suggesting an inverse expression pattern (38, 39). Therefore, we examined the expression *CXCR4* and confirmed an inverse relationship between *CXCR4* and *CD20,* with a low Pearson correlation score of 0.008 (**Figure 1A** and **Supplementary Table 1**). CXCR4 is known to be expressed by many other immune cell types such as neutrophils and T cells, making it less specific therapeutic targeting of B cells (40–44). Thus, we focused on putative targets that correlated highly with *CXCR4* expression, were expressed on the B cell surface, and had FDA-approved monoclonal antibodies available. *CD74* and *IL4R* were identified as candidates for further investigation, with expression that overlapped with *CXCR4* and Pearson correlation scores of 0.325 and 0.307, respectively (**Figures 1B,C** and **Supplementary Table 1**). Additionally, *CD74* was broadly expressed and correlated highly with *MS4A1* expression while *IL4R* did not, with correlation scores of 0.523 and −0.064, respectively (**Supplementary Table 1**). Thus, both CD74 and IL4R could target B cells, even when CD20 is low or not present.

Next, we determined *MS4A1* (CD20), *CD74* and *IL4R* gene expression levels in 84 lymphoma samples across different

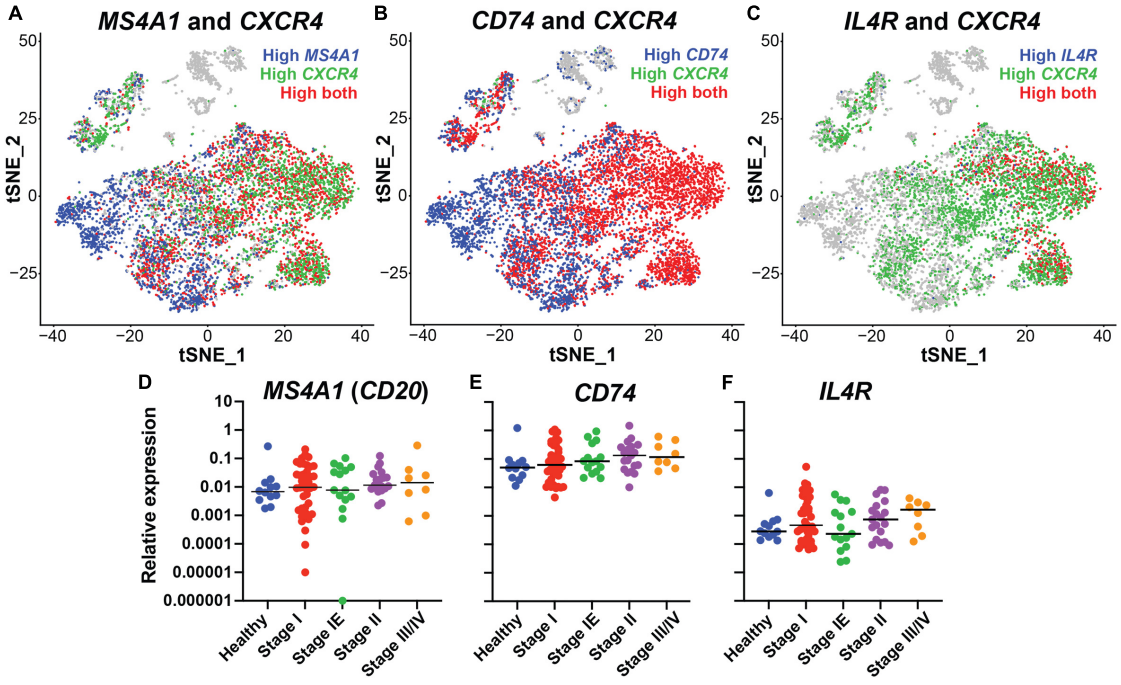

FIGURE 1
CD74 and IL4R identified as good candidates for bispecific antibody development, in conjunction with CD20, by single cell RNA sequencing. **(A)** tSNE plot of *MS4A1* (Blue) and *CXCR4* (Green). **(B)** tSNE plot of *CD74* (Blue) and *CXCR4* (Green). **(C)** tSNE plot of *IL4R* (Blue) and *CXCR4* (Green). **(D)** Relative expression of *MS4A1* in samples collected from healthy donors and donors with lymphoma at different stages of disease. Each dot represents one individual. **(E)** Relative expression of *CD74* in samples collected from healthy donors and donors with lymphoma at different stages of disease. **(F)** Relative expression of *IL4R* in samples collected from healthy donors and donors with lymphoma at different stages of disease. *n* = 12 healthy, 41 stage I, 15 stage IE, 19 stage II, 8 stage III/IV.

tumor stages (stage I-III/IV) and compared to expression in 12 healthy tissue controls using quantitative PCR of tissue biopsies. We found that all three genes were expressed in lymphoma samples of all stages, with no significant difference compared to healthy control samples. *CD74* had the highest relative expression level followed by *MS4A1* and *IL4R*. There were no significant correlations with gene expression and tumor stage, although *CD74* expression did trend higher in later tumor stages (Figures 1D–F). These results demonstrated that with CD20, genes encoding CD74 and IL4R are highly expressed in lymphoma tissues, in addition to being broad B cell markers, and could represent candidate therapeutic targets for lymphoma.

Engineering bispecific antibodies targeting CD74 or IL4R with anti-CD20

There are therapeutic antibodies that target CD74 (milatuzumab), IL4R (dupilumab), and CD20 (rituximab) that are approved for clinical use. We utilized these antibody combinations to engineer bispecific antibodies to combine anti-CD74 with anti-CD20 and anti-IL4R with anti-CD20 (Figure 2A). After bispecific antibody expression and purification, we determined antibody binding specificity against CD20, CD74, and IL4R recombinant protein antigens using ELISA. Using area under the curve (AUC) to compare binding response, anti-CD20 (rituximab) (AUC 78.1), bispecific anti-CD20/anti-CD74 (AUC 70.1) and bispecific anti-CD20/anti-IL4R (AUC 79.8) all bound to the recombinant CD20 with no appreciable non-specific binding from either anti-CD74 (milatuzumab) (AUC 1.6) or anti-IL4R (dupilumab) (AUC 1.5) antibodies (Figure 2B). Anti-CD74 (AUC 131.9) and bispecific anti-CD20/anti-CD74 (AUC 132.5) bound exclusively to CD74 with comparable levels of binding (Figure 2C). Likewise, anti-IL4R (AUC 132.6) and bispecific anti-CD20/anti-IL4R (AUC 133) bound exclusively and comparably to IL4R (Figure 2D). These data confirmed antibody specificity and similar binding levels between the monoclonal, single target antibodies and the bispecific antibodies.

Anti-CD20 and anti-CD74-targeting antibodies mediate direct antibody-mediated cytotoxicity

We determined the ability of the antibodies to mediate direct cytotoxicity of three lymphoma cell lines by measuring apoptosis using annexin V in the presence of a cross-linking

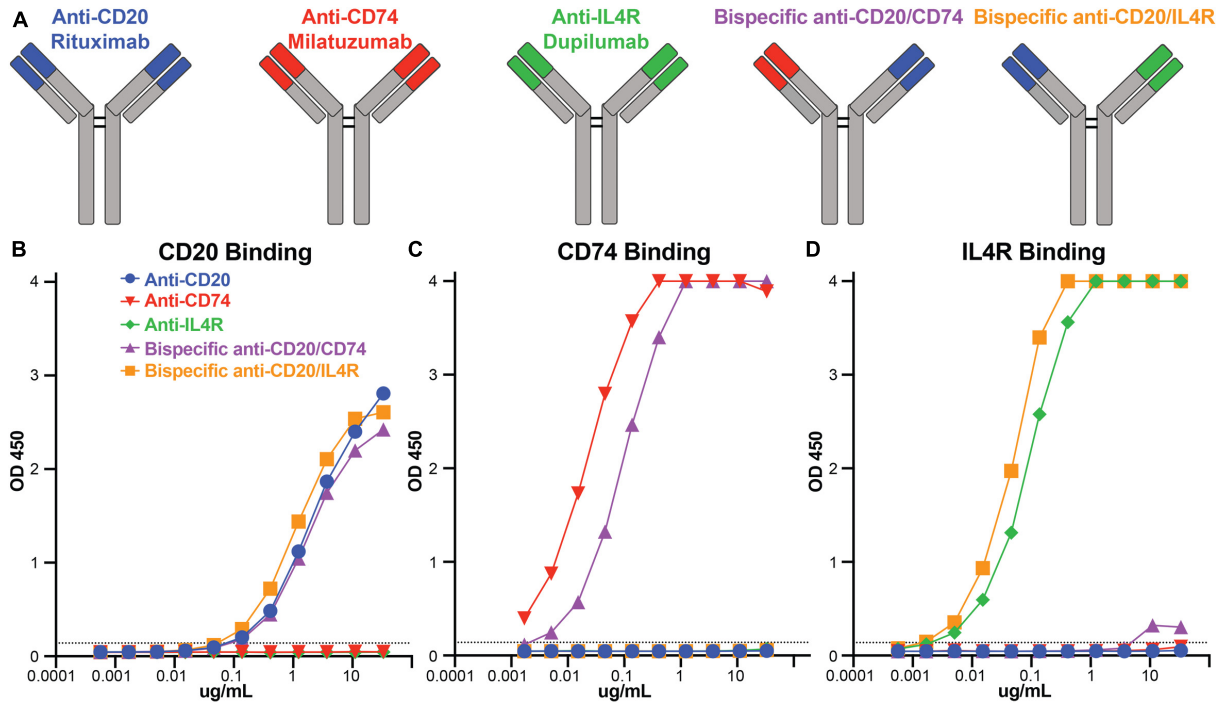

FIGURE 2
Bispecific antibody construction and antibody binding responses. **(A)** Schematic representation of rituximab, milatuzumab, dupilumab, and the bispecific antibodies constructed with anti-CD20/anti-CD74 heavy chains and anti-CD20/anti-IL4R heavy chains. **(B)** Line graph of OD450 absorbance obtained by ELISA measuring antibody binding to CD20 at serial dilutions. **(C)** Line graph of OD450 absorbance obtained by ELISA measuring antibody binding to CD74 at serial dilutions. **(D)** Line graph of OD450 absorbance obtained by ELISA measuring antibody binding to IL4R at serial dilutions. Background absorbance, represented by the dashed line, was considered 3X blank well OD450 measurement.

antibody. We utilized a rituximab-sensitive (SU-DHL-4), rituximab-intermediate (NH-DUL-1) and rituximab-resistant (SU-DHL-8) cell lines (38). First, we determined the expression of *MS4A*1, *CD74*, and *IL4R* in each cell line using qPCR (**Supplementary Figure 2**). *MS4A1* (CD20) gene expression was detected in all three cell lines but was reduced in the rituximab-intermediate and resistant cell lines (**Supplementary Figure 2**). *CD74* expression was detectable in all three cell lines, with no significant difference in expression level between the different cell lines. Similarly, *IL4R* was detectable in all three cell lines, and like *MS4A1*, was reduced in the rituximab-intermediate and resistant cell lines (**Supplementary Figure 2**). This data suggested that reduced gene expression of CD20 and IL4R in the NH-DUL-1 and SU-DHL-8 cell lines could contribute to the observed resistance to antibody therapy. Next, we measured antibody-mediated direct cytotoxicity of the cell lines. We found that the anti-CD20 antibody induced 25.5% apoptosis of the rituximab-sensitive SU-DHL-4 cell line (**Figure 3A**), 18.3 and 2.3% apoptosis of the intermediate (NH-DUL-1) and resistant (SU-DHL-8) cell lines, respectively (**Figures 3B,C**). Anti-CD74 antibody also induced direct cytotoxicity of SU-DHL-4 cell line at 8.6% and had higher percent cytotoxicity compared to rituximab (**Figure 3A**), of the NU-DUL-1 and SU-DHL-8 cell lines with 22.1 and 16.2% induced apoptosis, respectively (**Figures 3B,C**). Anti-IL4R antibody did not directly induce apoptosis in any of the tested cell lines with 2.7, 0.4, and 0.4% for the SU-DHL-4, NU-DUL-1 and SU-DHL-8 cell lines, respectively (**Figures 3A–C**). This data indicated that antibodies that are cross-linked to CD20 or CD74 could induce direct cellular cytotoxicity of lymphoma cells, whereas antibodies targeting IL4R could not. Moreover, reduced expression of CD20 on lymphoma cells reduced this cytotoxicity by anti-CD20 antibody.

The bispecific antibodies anti-CD20/anti-CD74 or anti-CD20/anti-IL4R could also mediate direct toxicity of the SU-DHL-4 cell line with 23.6 and 21.9% apoptosis, respectively, albeit not higher than anti-CD20 alone (25.5% apoptosis) (**Figure 3A**). However, the two bispecific antibodies had higher percent apoptosis of the rituximab-resistant cell lines NU-DUL-1 and SU-DHL-8 compared to anti-CD20 alone (**Figures 3B,C**). These results demonstrated that bispecific antibodies targeting CD20 and either CD74 or IL4R could mediate direct cytotoxicity of lymphoma cells, but when using a rituximab resistant lymphoma cell line (SU-DHL-8), bispecific anti-CD20/anti-CD74 or anti-CD74 alone induced the highest levels of apoptosis.

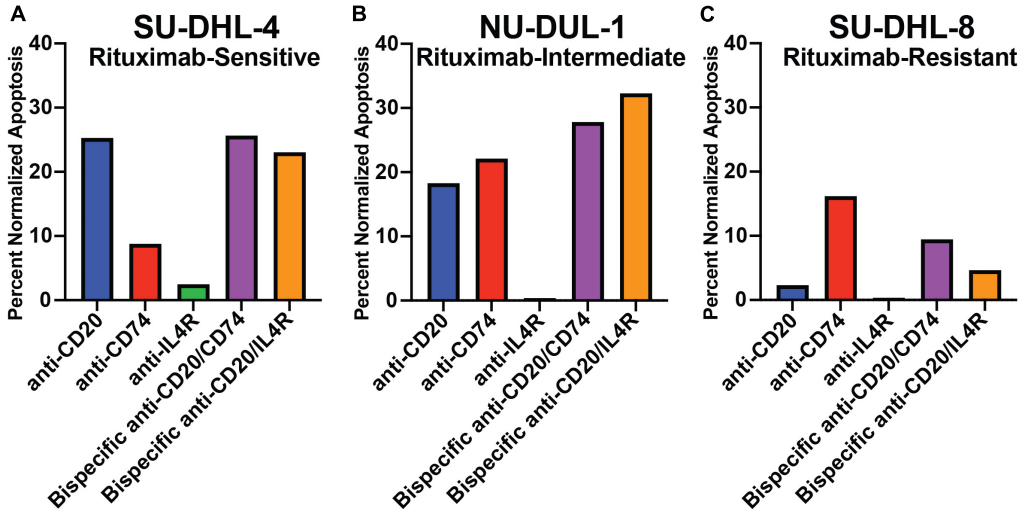

FIGURE 3
Apoptotic response to crosslinking antibodies within varying rituximab-resistant lymphoma cell lines, measured by annexin V staining. **(A)** Bar graph of the percent of total apoptosis within rituximab-sensitive, high CD20 expressing, SU-DHL-4 cells after 8 h of exposure to antibodies and crosslinking antibodies. **(B)** Bar graph of the percent of total apoptosis within rituximab-intermediate, intermediate CD20 expressing, NU-DUL-1 cells after 8 h of exposure to antibodies and crosslinking antibodies. **(C)** Bar graph of the percent of total apoptosis within rituximab-resistant, low CD20 expressing, SU-DHL-8 cells after 8 h of exposure to antibodies and crosslinking antibodies. All bar graphs normalized to respective cell line crosslinking antibody control.

Bispecific antibodies could mediate antibody-mediated cytotoxicity and phagocytosis of lymphoma antibody-dependent cellular cytotoxicity and antibody-dependent cellular phagocytosis

In addition to direct cytotoxicity of lymphoma cells by engaging cellular receptors, therapeutic antibodies can engage and recruit effector cells through Fc-Fc receptor interactions to mediate antibody-dependent cellular cytotoxicity (ADCC) or ADCP. We utilized a cell-based assay employing a reporter gene that generates luciferase downstream of the Fc receptor pathway (Promega). For ADCC, FcγRIIIa is engaged and for ADCP, FcγRIIa-H is primarily engaged (**Figure 4A**). We utilized these cell lines as proxies for ADCC and ADCP activities. We found that anti-CD20 alone could mediate ADCC with increasing concentrations of antibody using Raji (AUC 50,712), SU-DHL-4 (11,125), NU-DUL-1 (AUC 6,535), and SU-DHL-8 (AUC 22,929) lymphoma targets (**Figure 4B**). The two bispecific antibodies (anti-CD20/anti-CD74 and anti-CD20/anti-IL4R) could also induce ADCC, but at lower levels than anti-CD20 alone. Anti-CD20/anti-CD74 bispecific ADCC AUC for Raji, SU-DHL-4, NU-DUL-1 and SU-DHL-8 cell targets were: 10,512, 1,351, 1,798, and 9,815, respectively (**Figure 4B**). Anti-CD20/anti-IL4R bispecific ADCC AUC for Raji, SU-DHL-4, NU-DUL-1 and SU-DHL-8 cell targets were: 10,001, 2,123, 1,623, and 11,610, respectively (**Figure 4B**). Similarly, anti-CD20 and the bispecific antibodies could induce ADCP of Raji cell targets using our cell reporter system, with anti-CD20 having a higher magnitude of response (**Figure 4C**). The AUC for anti-CD20, bispecific anti-CD20/anti-CD74, and bispecific anti-CD20/anti-IL4R being 1,679, 482, and 510, respectively. These data showed that the anti-CD20 monoclonal antibody and both bispecific antibodies containing anti-CD20 could induce ADCC and ADCP immune responses, although the bispecific antibodies had lower magnitude of ADCC and ADCP at the same antibody concentrations.

Discussion

Although therapeutic applications of bispecific antibodies are relatively new, the dual nature of the antibodies could be predicted to decrease the ability of lymphomas to escape treatment or develop resistance as two cellular targets would need to be escaped. Besides tagging cells for destruction, bispecific antibodies may also be designed to deliver nanoparticles or drugs to target cells (45). Additionally, some treatments such as CAR-T cells require significant modifications specific to each patient, a costly and time-consuming series of steps that may be avoided with the use of bispecific antibodies (46, 47). Here, we investigated the ability of anti-CD20/anti-CD74 and anti-CD20/anti-IL4R bispecific

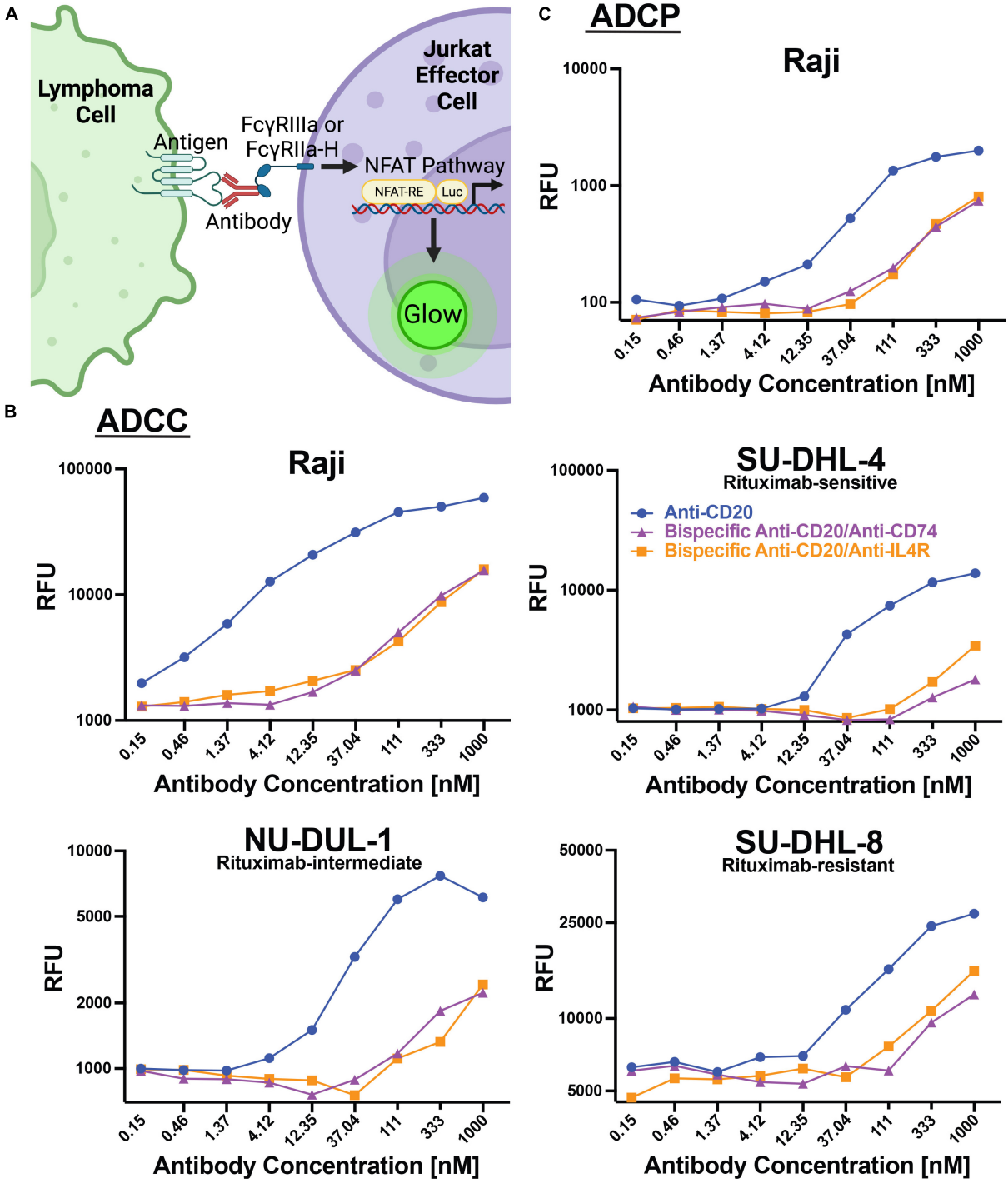

FIGURE 4
Antibodies induce ADCC and ADCP responses within lymphoma cell lines. **(A)** Schematic representation of the assays used to measure ADCC and ADCP response within modified Jurkat effector cells. Created with BioRender.com. **(B)** Line graphs of the relative fluorescent units (RFU) of luciferase produced by ADCC activation of FcγRIIIa modified Jurkat cells when incubated with Raji, SU-DHL-4, NU-DUL-1, or SU-DHL-8 DLBCL cell lines and serial diluted anti-CD20 (Blue), bispecific anti-CD20/anti-CD74 (Purple), or bispecific anti-CD20/anti-IL4R (Orange) antibodies. **(C)** Line graph of the relative fluorescent units (RFU) of luciferase produced by ADCC activation of FcγRIIa-H modified Jurkat cells when incubated with Burkitt's lymphoma Raji cells and serial diluted anti-CD20 (Blue), bispecific anti-CD20/anti-CD74 (Purple), or bispecific anti-CD20/anti-IL4R (Orange) antibodies.

antibodies to bind their designated targets on lymphoma cells and to kill their targeted cells *via* different mechanisms.

Using B cells isolated from healthy patients, we explored other potential B cell markers that previously have FDA-approved antibody therapies available and focused on CD74 and IL4R. CD74, a transmembrane glycoprotein that functions as a survival receptor, is highly expressed in malignant B cells (48, 49). Stein et al. demonstrated survival of immune-deficient mice with lymphoma was significantly improved when treated with anti-CD74 antibody, especially when administered in conjunction with rituximab (50). Milatuzumab, the first anti-CD74 monoclonal antibody approved by the FDA for clinical practice, is effective at treating aggressive B cell malignancies such as multiple myeloma, especially in combination with rituximab (49–51). When PBMC samples from patients were treated with milatuzumab, naïve and memory B cells were bound by milatuzumab 98.3 and 97% of the time, respectively (52). Although IL4R expression was limited to a smaller population of total B cells, it provided an opportunity to target cells otherwise capable of escaping rituximab treatment due to their low CD20 expression. Cells treated with the IL4 antagonist, APG201, were more susceptible to chemotherapeutics, suggesting a role for IL4 pathway signaling in chemotherapy resistance (53). Furthermore, anti-IL4R treatments reduced inflammatory cell recruitment, improved measurable lung function and decreased overall asthma symptoms in both humans and monkeys (54, 55). Consequently, both targets would help expand the range of targeted cells compared to current rituximab treatment.

The bispecific antibodies, anti-CD74/anti-CD20 and anti-IL4R/anti-CD20, caused significantly more apoptosis than anti-CD20 alone in both the rituximab intermediate (NU-DUL-1) and rituximab resistant (SU-DHL-8) cell, while the rituximab-sensitive (SU-DHL-4) cell line showed comparable levels of apoptosis between the bispecific antibodies and anti-CD20. These data demonstrate the potential benefit of using bispecific antibodies in conditions of rituximab resistance without losing significant apoptosis induction in conditions of continued rituximab sensitivity. It is interesting to note that the relative patterns of apoptosis induction by anti-CD74 across the cell lines appear to be negatively correlated with CD20 expression: the rituximab-resistant cell line exhibited higher killing by anti-CD74 compared to anti-CD20, while the rituximab-sensitive cell line exhibited lower apoptosis by anti-CD74. Milatuzumab, which has previously been shown to reduce cell growth and proliferation of B cells (52), mediated direct apoptosis of the lymphoma cells in this study. The anti-IL4R drug, dupilumab, an antagonist for the IL4 signaling pathway (56, 57), did not robustly elicit cytotoxicity here. This highlights both CD20 and CD74 as targets to facilitate direct killing of lymphoma cells without the need for effector cells. The significant utility of bispecific antibodies is demonstrated here as anti-IL4R treatment only was quite ineffective, while using an anti-CD20/anti-IL4R bispecific antibody caused apoptosis significantly higher than—or at least comparable to—the anti-CD20 treatment in all cell lines. Gupta et al. presented similar results in other bispecific antibodies, with very little apoptosis after treatment with monoclonal antibodies for CD20 or CD74, but anti-CD20/anti-CD74 bispecific antibodies displayed 3–4 times higher apoptosis than either monoclonal antibody alone (58).

ADCC experiments revealed high activity with anti-CD20 treatment, though the bispecific antibodies showed decreased activity in all cell lines. The decrease in ADCC of the bispecific antibodies could be due to the having only a single Fab arm of the antibody for each target resulting in reduced antibody affinity or other binding kinetic attributes. The decreased effectiveness of the bispecific antibody containing anti-CD74 may also be due to the rapid internalization causing difficulty for the effector cells to detect cell surface antibodies, therefore making cell recruitment unlikely (59–61). Stein et al. explicitly demonstrated that anti-CD74 antibody treatment did not produce significant ADCC in Raji cells when cocultured with purified human leukocyte populations from peripheral blood samples (50). Here, ADCC experiments utilized only T-lymphocytes, however, it is possible that ADCC *via* NK cells would occur with anti-CD74 treatment (62, 63). ADCP activity was high in Raji cells when treated with anti-CD20, with both anti-CD20/anti-CD74 and anti-CD20/anti-IL4R bispecific antibodies having lower than anti-CD20 but still elevated ADCP response. These bispecific antibodies have shown to be effective in all methods of cell killing evaluated, similar to those results of anti-CD20 alone.

Bispecific antibodies are already being tested in clinical trials and are demonstrating their utility in a broad range of diseases (64–68). The bispecific anti-CD20/anti-CD74 antibody has been tested in mantle cell lymphoma, an NHL sub-type and has significantly improved survival of mice with lymphoma (58). Furthermore, an anti-IL4Rα/anti-IL5 bispecific antibody decreased the number of recruited lymphocytes and eosinophils during asthmatic reactions in mice more effectively than when either antibody was administered alone or concurrently, demonstrating the ability of IL4R bispecific antibodies to be effective in alleviating symptoms of asthma (54). Finally, an anti-CD20/anti-CD3 bispecific antibody targeted lymphoma and cytotoxic T-cells, showed high killing capacity both *in vivo* and *in vitro*, even with very low cell surface expression of CD20; anti-CD20 alone was unable to cause significant cell death (46). Phase I clinical trials of this anti-CD20/anti-CD3 antibody, Glofitamab, showed that at high doses, nearly 50% of previously treated patients with aggressive NHL had complete recovery after treatment, and 81% of those remained disease free past 2 years following treatment (47). Previous reports in mantle cell lymphoma cell lines show distinct cytoskeletal dynamics, ROS generation, and disruptions of NF-κB pathways after treatment with rituximab and milatuzumab (51). Future studies

would benefit from the use of single-cell RNA sequencing to identify unique downstream pathways of cell death induced by these bispecific anti-CD20/anti-CD74 and anti-CD20/anti-IL4R antibodies.

There were several key limitations of our study that should be addressed in future work. One major limitation is that we evaluated the function of the antibodies in *in vitro* model systems. While these models could identify promising therapeutic targets and antibodies, *in vivo* evaluation of the antibodies in animal models will confirm the therapeutic efficacy of these bispecific antibodies. Moreover, *in vivo* studies will be needed to determine any off-target, and other toxicities, that could be caused by these antibodies. Studies *in vivo* will also be required to determine the pharmacokinetics of these antibodies in order to determine the clinical feasibility of using them for treatment. Lastly, we evaluated cytotoxicity of several lymphoma cell lines that may not represent primary tumors of broad types. Further study with primary tumors or other types of B-cell derived tumors will be required.

In summary, bispecific antibodies targeting CD74 or IL4R could mediate ADCC and ADCP, while anti-CD74 targeting antibodies could mediate direct cellular cytotoxicity similar to anti-CD20. This observation, coupled with higher expression of CD74 on lymphoma cells, leads to anti-CD74 and anti-CD20 immunotherapies as better therapeutic targets. To further develop these bispecific antibodies as a potential future therapeutic, it would be beneficial to evaluate the level of acquired resistance that develops with the use of prolonged bispecific antibodies both *in vitro* and *in vivo*. These data demonstrate that the dual specificity of engineered bispecific antibodies is an effective future prospect of cancer immunotherapy.

Data availability statement

The original contributions presented in this study are included in the article/**Supplementary material**, further inquiries can be directed to the corresponding author. The single-cell RNA Sequencing Data SRA BioProject ID: PRJNA681021.

Author contributions

TB and EG: conceptualization. EG, SAK, and SP: laboratory experimentation. EG and SK: data analysis. TB, RM, SAK, and EG: writing. All authors contributed to the article and approved the submitted version.

Funding

This work was supported through internal institutional funds from the Children's Mercy Research Institute and Children's Mercy Kansas City.

Conflict of interest

The authors declare that the research was conducted in the absence of any commercial or financial relationships that could be construed as a potential conflict of interest.

Publisher's note

All claims expressed in this article are solely those of the authors and do not necessarily represent those of their affiliated organizations, or those of the publisher, the editors and the reviewers. Any product that may be evaluated in this article, or claim that may be made by its manufacturer, is not guaranteed or endorsed by the publisher.

Supplementary material

The Supplementary Material for this article can be found online at: https://www.frontiersin.org/articles/10.3389/fmed.2022.1034594/full#supplementary-material

References

1. Siegel RL, Miller KD, Fuchs HE, Jemal A. Cancer statistics, 2022. *CA Cancer J Clin.* (2022) 72:7–33.

2. Siegel RL, Miller KD, Jemal A. Cancer statistics, 2019. *CA Cancer J Clin.* (2019) 69:7–34.

3. Alizadeh AA, Eisen MB, Davis RE, Ma C, Lossos IS, Rosenwald A, et al. Distinct types of diffuse large B-cell lymphoma identified by gene expression profiling. *Nature.* (2000) 403:503–11.

4. Khanal S, Bradley T. A prognostic gene signature for predicting survival outcome in diffuse large B-cell lymphoma. *Cancer Genet.* (2021) 252-253:87–95. doi: 10.1016/j.cancergen.2021.01.001

5. Li S, Young KH, Medeiros LJ. Diffuse large B-cell lymphoma. *Pathology.* (2018) 50:74–87.

6. Sacchi S, Federico M, Dastoli G, Fiorani C, Vinci G, Clo V, et al. Treatment of B-cell non-hodgkin's lymphoma with anti CD 20 monoclonal antibody rituximab. *Crit Rev Oncol Hematol.* (2001) 37:13–25. doi: 10.1016/s1040-8428(00)00069-x

7. Coleman M, Lammers PE, Ciceri F, Jacobs IA. Role of rituximab and rituximab biosimilars in diffuse large B-cell lymphoma. *Clin Lymphoma Myeloma Leuk.* (2016) 16:175–81. doi: 10.1016/j.clml.2016.01.004

8. Coiffier B, Thieblemont C, Van Den Neste E, Lepeu G, Plantier I, Castaigne S, et al. Long-term outcome of patients in the LNH-98.5 trial, the first randomized study comparing rituximab-CHOP to standard CHOP chemotherapy in DLBCL

patients: a study by the groupe d'etudes des lymphomes de l'adulte. *Blood.* (2010) 116:2040–5. doi: 10.1182/blood-2010-03-276246

9. Griffin MM, Morley N. Rituximab in the treatment of non-hodgkin's lymphoma–a critical evaluation of randomized controlled trials. *Expert Opin Biol Ther.* (2013) 13:803–11. doi: 10.1517/14712598.2013.786698

10. Lee L, Crump M, Khor S, Hoch JS, Luo J, Bremner K, et al. Impact of rituximab on treatment outcomes of patients with diffuse large b-cell lymphoma: a population-based analysis. *Br J Haematol.* (2012) 158:481–8. doi: 10.1111/j.1365-2141.2012.09177.x

11. Lindenmeyer LP, Hegele V, Caregnato JP, Wust D, Grazziotin L, Stoll P. Follow-up of patients receiving rituximab for diffuse large B cell lymphoma: an overview of systematic reviews. *Ann Hematol.* (2013) 92:1451–9. doi: 10.1007/s00277-013-1811-4

12. Press OW, Leonard JP, Coiffier B, Levy R, Timmerman J. Immunotherapy of non-hodgkin's lymphomas. *Hematology Am Soc Hematol Educ Program.* (2001) 2001:221–40.

13. Sehn LH, Donaldson J, Chhanabhai M, Fitzgerald C, Gill K, Klasa R, et al. Introduction of combined CHOP plus rituximab therapy dramatically improved outcome of diffuse large B-cell lymphoma in British Columbia. *J Clin Oncol.* (2005) 23:5027–33. doi: 10.1200/JCO.2005.09.137

14. Cai Q, Westin J, Fu K, Desai M, Zhang L, Huang H, et al. Accelerated therapeutic progress in diffuse large B cell lymphoma. *Ann Hematol.* (2014) 93:541–56.

15. Cultrera JL, Dalia SM. Diffuse large B-cell lymphoma: current strategies and future directions. *Cancer Control.* (2012) 19:204–13.

16. Davis TA, Grillo-Lopez AJ, White CA, McLaughlin P, Czuczman MS, Link BK, et al. Rituximab anti-CD20 monoclonal antibody therapy in non-hodgkin's lymphoma: safety and efficacy of re-treatment. *J Clin Oncol.* (2000) 18:3135–43. doi: 10.1200/JCO.2000.18.17.3135

17. Falgas A, Pallares V, Unzueta U, Cespedes MV, Arroyo-Solera I, Moreno MJ, et al. A CXCR4-targeted nanocarrier achieves highly selective tumor uptake in diffuse large B-cell lymphoma mouse models. *Haematologica.* (2020) 105:741–53. doi: 10.3324/haematol.2018.211490

18. Feugier P, Van Hoof A, Sebban C, Solal-Celigny P, Bouabdallah R, Ferme C, et al. Long-term results of the R-CHOP study in the treatment of elderly patients with diffuse large B-cell lymphoma: a study by the groupe d'etude des lymphomes de l'adulte. *J Clin Oncol.* (2005) 23:4117–26. doi: 10.1200/JCO.2005.09.131

19. Rezvani AR, Maloney DG. Rituximab resistance. *Best Pract Res Clin Haematol.* (2011) 24:203–16.

20. Beers SA, French RR, Chan HT, Lim SH, Jarrett TC, Vidal RM, et al. Antigenic modulation limits the efficacy of anti-CD20 antibodies: implications for antibody selection. *Blood.* (2010) 115:5191–201. doi: 10.1182/blood-2010-01-263533

21. Davis TA, Czerwinski DK, Levy R. Therapy of B-cell lymphoma with anti-CD20 antibodies can result in the loss of CD20 antigen expression. *Clin Cancer Res.* (1999) 5:611–5.

22. Leandro MJ. B-cell subpopulations in humans and their differential susceptibility to depletion with anti-CD20 monoclonal antibodies. *Arthritis Res Ther.* (2013) 15 Suppl 1:S3. doi: 10.1186/ar3908

23. Cruz JW, Damko E, Modi B, Tu N, Meagher K, Voronina V, et al. A novel bispecific antibody platform to direct complement activity for efficient lysis of target cells. *Sci Rep.* (2019) 9:12031. doi: 10.1038/s41598-019-48461-1

24. Del Bano J, Chames P, Baty D, Kerfelec B. Taking up cancer immunotherapy challenges: bispecific antibodies, the path forward? *Antibodies (Basel).* (2015) 5:1. doi: 10.3390/antib5010001

25. Pollara J, Khanal S, Edwards RW, Hora B, Ferrari G, Haynes BF, et al. Single-cell analysis of immune cell transcriptome during HIV-1 infection and therapy. *BMC Immunol* (2022) 23:48. doi: 10.1186/s12865-022-00523-2

26. Bradley T, Ferrari G, Haynes BF, Margolis DM, Browne EP. Single-cell analysis of quiescent hiv infection reveals host transcriptional profiles that regulate proviral latency. *Cell Rep.* (2018) 25:107–17.e3. doi: 10.1016/j.celrep.2018.09.020

27. Bradley T, Kuraoka M, Yeh CH, Tian M, Chen H, Cain DW, et al. Immune checkpoint modulation enhances HIV-1 antibody induction. *Nat Commun.* (2020) 11:948.

28. Bradley T, Peppa D, Pedroza-Pacheco I, Li D, Cain DW, Henao R, et al. RAB11FIP5 expression and altered natural killer cell function are associated with induction of HIV broadly neutralizing antibody responses. *Cell.* (2018) 175:387–99.e17. doi: 10.1016/j.cell.2018.08.064

29. Han Q, Bradley T, Williams WB, Cain DW, Montefiori DC, Saunders KO, et al. Neonatal Rhesus macaques have distinct immune cell transcriptional profiles following HIV envelope immunization. *Cell Rep.* (2020) 30:1553–69.e6. doi: 10.1016/j.celrep.2019.12.091

30. Zheng GX, Terry JM, Belgrader P, Ryvkin P, Bent ZW, Wilson R, et al. Massively parallel digital transcriptional profiling of single cells. *Nat Commun.* (2017) 8:14049.

31. Macosko EZ, Basu A, Satija R, Nemesh J, Shekhar K, Goldman M, et al. Highly parallel genome-wide expression profiling of individual cells using nanoliter droplets. *Cell.* (2015) 161:1202–14. doi: 10.1016/j.cell.2015.05.002

32. Satija R, Farrell JA, Gennert D, Schier AF, Regev A. Spatial reconstruction of single-cell gene expression data. *Nat Biotechnol.* (2015) 33:495–502.

33. Stuart T, Butler A, Hoffman P, Hafemeister C, Papalexi E, Mauck WM III, et al. Comprehensive integration of single-cell data. *Cell.* (2019) 177:1888–1902.e21.

34. Beider K, Ribakovsky E, Abraham M, Wald H, Weiss L, Rosenberg E, et al. Targeting the CD20 and CXCR4 pathways in non-hodgkin lymphoma with rituximab and high-affinity CXCR4 antagonist BKT140. *Clin Cancer Res.* (2013) 19:3495–507. doi: 10.1158/1078-0432.CCR-12-3015

35. Nie Y, Waite J, Brewer F, Sunshine MJ, Littman DR, Zou YR. The role of CXCR4 in maintaining peripheral B cell compartments and humoral immunity. *J Exp Med.* (2004) 200:1145–56. doi: 10.1084/jem.20041185

36. Reinholdt L, Laursen MB, Schmitz A, Bodker JS, Jakobsen LH, Bogsted M, et al. The CXCR4 antagonist plerixafor enhances the effect of rituximab in diffuse large B-cell lymphoma cell lines. *Biomark Res.* (2016) 4:12. doi: 10.1186/s40364-016-0067-2

37. Tedder TF, Streuli M, Schlossman SF, Saito H. Isolation and structure of a cDNA encoding the B1 (CD20) cell-surface antigen of human B lymphocytes. *Proc Natl Acad Sci USA.* (1988) 85:208–12. doi: 10.1073/pnas.85.1.208

38. Laursen MB, Reinholdt L, Schonherz AA, Due H, Jespersen DS, Grubach L, et al. High CXCR4 expression impairs rituximab response and the prognosis of R-CHOP-treated diffuse large B-cell lymphoma patients. *Oncotarget.* (2019) 10:717–31. doi: 10.18632/oncotarget.26588

39. Pavlasova G, Borsky M, Seda V, Cerna K, Osickova J, Doubek M, et al. Ibrutinib inhibits CD20 upregulation on CLL B cells mediated by the CXCR4/SDF-1 axis. *Blood.* (2016) 128:1609–13. doi: 10.1182/blood-2016-04-709519

40. Eash KJ, Means JM, White DW, Link DC. CXCR4 is a key regulator of neutrophil release from the bone marrow under basal and stress granulopoiesis conditions. *Blood.* (2009) 113:4711–9. doi: 10.1182/blood-2008-09-177287

41. Arieta Kuksin C, Gonzalez-Perez G, Minter LM. CXCR4 expression on pathogenic T cells facilitates their bone marrow infiltration in a mouse model of aplastic anemia. *Blood.* (2015) 125:2087–94. doi: 10.1182/blood-2014-08-594796

42. Monaco G, Lee B, Xu W, Mustafah S, Hwang YY, Carre C, et al. RNA-Seq signatures normalized by MRNA abundance allow absolute deconvolution of human immune cell types. *Cell Rep.* (2019) 26:1627–40.e7. doi: 10.1016/j.celrep.2019.01.041

43. Schmiedel BJ, Singh D, Madrigal A, Valdovino-Gonzalez AG, White BM, Zapardiel-Gonzalo J, et al. Impact of genetic polymorphisms on human immune cell gene expression. *Cell.* (2018) 175:1701–15.e16.

44. Susek KH, Karvouni M, Alici E, Lundqvist A. The role of CXC chemokine receptors 1-4 on immune cells in the tumor microenvironment. *Front Immunol.* (2018) 9:2159. doi: 10.3389/fimmu.2018.02159

45. Tekewe A, Saleh M, Kassaye M. Proteins and peptides as targeting carriers in anticancer drug delivery: a review. *Int J Pharm Sci Res.* (2013) 4:1–18.

46. Sun LL, Ellerman D, Mathieu M, Hristopoulos M, Chen X, Li Y, et al. Anti-CD20/CD3 T cell-dependent bispecific antibody for the treatment of B cell malignancies. *Sci Transl Med.* (2015) 7:287ra70. doi: 10.1126/scitranslmed.aaa4802

47. Hutchings M, Morschhauser F, Iacoboni G, Carlo-Stella C, Offner FC, Sureda A, et al. Glofitamab, a novel, bivalent CD20-targeting T-cell-engaging bispecific antibody, induces durable complete remissions in relapsed or refractory B-cell lymphoma: a phase I trial. *J Clin Oncol.* (2021) 39:1959–70. doi: 10.1200/JCO.20.03175

48. Starlets D, Gore Y, Binsky I, Haran M, Harpaz N, Shvidel L, et al. Cell-surface CD74 initiates a signaling cascade leading to cell proliferation and survival. *Blood.* (2006) 107:4807–16. doi: 10.1182/blood-2005-11-4334

49. Stein R, Mattes MJ, Cardillo TM, Hansen HJ, Chang CH, Burton J, et al. CD74: a new candidate target for the immunotherapy of B-cell neoplasms. *Clin Cancer Res.* (2007) 13:5556s–63s. doi: 10.1158/1078-0432.CCR-07-1167

50. Stein R, Qu Z, Cardillo TM, Chen S, Rosario A, Horak ID, et al. Antiproliferative activity of a humanized anti-CD74 monoclonal antibody, hLL1, on B-cell malignancies. *Blood.* (2004) 104:3705–11. doi: 10.1182/blood-2004-03-0890

51. Alinari L, Yu B, Christian BA, Yan F, Shin J, Lapalombella R, et al. Combination anti-CD74 (milatuzumab) and anti-CD20 (rituximab) monoclonal antibody therapy has *in vitro* and *in vivo* activity in mantle cell lymphoma. *Blood.* (2011) 117:4530–41. doi: 10.1182/blood-2010-08-303354

52. Frolich D, Blassfeld D, Reiter K, Giesecke C, Daridon C, Mei HE, et al. The anti-CD74 humanized monoclonal antibody, milatuzumab, which targets the invariant Chain of MHC II complexes, alters B-cell proliferation, migration, and adhesion molecule expression. *Arthritis Res Ther.* (2012) 14:R54. doi: 10.1186/ar3767

53. Natoli A, Lupertz R, Merz C, Muller WW, Kohler R, Krammer PH, et al. Targeting the IL-4/IL-13 signaling pathway sensitizes Hodgkin lymphoma cells to chemotherapeutic drugs. *Int J Cancer.* (2013) 133:1945–54. doi: 10.1002/ijc.28189

54. Godar M, Deswarte K, Vergote K, Saunders M, de Haard H, Hammad H, et al. A bispecific antibody strategy to target multiple type 2 cytokines in asthma. *J Allergy Clin Immunol.* (2018) 142:1185–193.e4. doi: 10.1016/j.jaci.2018.06.002

55. Wenzel SE, Wang L, Pirozzi G. Dupilumab in persistent asthma. *N Engl J Med.* (2013) 369:1276.

56. Le Floc'h A, Allinne J, Nagashima K, Scott G, Birchard D, Asrat S, et al. Dual blockade of IL-4 and IL-13 with dupilumab, an IL-4Ralpha antibody, is required to broadly inhibit type 2 inflammation. *Allergy.* (2020) 75:1188–204. doi: 10.1111/all.14151

57. Kim JE, Jung K, Kim JA, Kim SH, Park HS, Kim YS. Engineering of anti-human interleukin-4 receptor alpha antibodies with potent antagonistic activity. *Sci Rep.* (2019) 9:7772. doi: 10.1038/s41598-019-44253-9

58. Gupta P, Goldenberg DM, Rossi EA, Cardillo TM, Byrd JC, Muthusamy N, et al. Dual-targeting immunotherapy of lymphoma: potent cytotoxicity of anti-CD20/CD74 bispecific antibodies in mantle cell and other lymphomas. *Blood.* (2012) 119:3767–78. doi: 10.1182/blood-2011-09-381988

59. Roche PA, Teletski CL, Stang E, Bakke O, Long EO. Cell surface HLA-DR-invariant chain complexes are targeted to endosomes by rapid internalization. *Proc Natl Acad Sci USA.* (1993) 90:8581–5. doi: 10.1073/pnas.90.18.8581

60. Ong GL, Goldenberg DM, Hansen HJ, Mattes MJ. Cell surface expression and metabolism of major histocompatibility complex class II invariant chain (CD74) by diverse cell lines. *Immunology.* (1999) 98:296–302.

61. Binsky I, Haran M, Starlets D, Gore Y, Lantner F, Harpaz N, et al. IL-8 secreted in a macrophage migration-inhibitory factor- and CD74-dependent manner regulates B cell chronic lymphocytic leukemia survival. *Proc Natl Acad Sci USA.* (2007) 104:13408–13. doi: 10.1073/pnas.0701553104

62. Karakikes I, Morrison IE, O'Toole P, Metodieva G, Navarrete CV, Gomez J, et al. Interaction of HLA-DR and CD74 at the cell surface of antigen-presenting cells by single particle image analysis. *FASEB J.* (2012) 26:4886–96. doi: 10.1096/fj.12-211466

63. Jiang YZ, Couriel D, Mavroudis DA, Lewalle P, Malkovska V, Hensel NF, et al. Interaction of natural killer cells with MHC class II: reversal of HLA-DR1-mediated protection of K562 transfectant from natural killer cell-mediated cytolysis by brefeldin-A. *Immunology.* (1996) 87:481–6. doi: 10.1046/j.1365-2567.1996.483556.x

64. Heiss MM, Strohlein MA, Jager M, Kimmig R, Burges A, Schoberth A, et al. Immunotherapy of malignant ascites with trifunctional antibodies. *Int J Cancer.* (2005) 117:435–43.

65. Kontermann RE, Brinkmann U. Bispecific antibodies. *Drug Discov Today.* (2015) 20:838–47.

66. Heiss MM, Murawa P, Koralewski P, Kutarska E, Kolesnik OO, Ivanchenko VV, et al. The trifunctional antibody catumaxomab for the treatment of malignant ascites due to epithelial cancer: results of a prospective randomized phase II/III trial. *Int J Cancer.* (2010) 127:2209–21. doi: 10.1002/ijc.25423

67. Acheampong DO. Bispecific antibody (bsAb) construct formats and their application in cancer therapy. *Protein Pept Lett.* (2019) 26:479–93.

68. Fan G, Wang Z, Hao M, Li J. Bispecific antibodies and their applications. *J Hematol Oncol.* (2015) 8:130.

frontiers | Frontiers in Medicine

TYPE Original Research
PUBLISHED 26 October 2022
DOI 10.3389/fmed.2022.1036787

OPEN ACCESS

EDITED BY
Vadim V. Sumbayev,
University of Kent, United Kingdom

REVIEWED BY
Jill M. Kramer,
University at Buffalo, United States
Myriam Chimen,
University of Birmingham,
United Kingdom

*CORRESPONDENCE
Naozumi Ishimaru
ishimaru.n@tokushima-u.ac.jp

SPECIALTY SECTION
This article was submitted to Pathology,
a section of the journal
Frontiers in Medicine

RECEIVED 05 September 2022
ACCEPTED 12 October 2022
PUBLISHED 26 October 2022

CITATION
Sato M, Arakaki R, Tawara H, Nagao R, Tanaka H, Tamura K, Kawahito Y, Otsuka K, Ushio A, Tsunematsu T and Ishimaru N (2022) Disturbed natural killer cell homeostasis in the salivary gland enhances autoimmune pathology *via* IFN-γ in a mouse model of primary Sjögren's syndrome. *Front. Med.* 9:1036787. doi: 10.3389/fmed.2022.1036787

Disturbed natural killer cell homeostasis in the salivary gland enhances autoimmune pathology *via* IFN-γ in a mouse model of primary Sjögren's syndrome

Mami Sato, Rieko Arakaki, Hiroaki Tawara, Ruka Nagao, Hidetaka Tanaka, Kai Tamura, Yuhki Kawahito, Kunihiro Otsuka, Aya Ushio, Takaaki Tsunematsu and Naozumi Ishimaru*

Department of Oral Molecular Pathology, Tokushima University Graduate School of Biomedical Sciences, Tokushima, Japan

Objective: Innate lymphoid cells (ILCs), including natural killer (NK) cells, ILC1, ILC2, lymphoid tissue-inducer (LTi) cells, and ILC3 cell, play a key role in various immune responses. Primary Sjögren's syndrome (pSS) is an autoimmune disease characterized by chronic inflammation of exocrine glands, such as the lacrimal and salivary glands (SGs). The role of NK cells among ILCs in the pathogenesis of pSS is still unclear. In this study, the characteristics and subsets of NK cells in the salivary gland (SG) tissue were analyzed using a murine model of pSS.

Methods: Multiple phenotypes and cytotoxic signature of the SG NK cells in control and pSS model mice were evaluated by flow cytometric analysis. Intracellular expression of interferon-γ (IFN-γ) among T cells and NK cells from the SG tissues was compared by *in vitro* experiments. In addition, pathological analysis was performed using anti-asialo-GM1 (ASGM1) antibody (Ab)-injected pSS model mice.

Results: The number of conventional NK (cNK) cells in the SG of pSS model mice significantly increased compared with that in control mice at 6 weeks of age. The production level of IFN-γ was significantly higher in SG NK cells than in SG T cells. The depletion of NK cells by ASGM1 Ab altered the ratio of tissue resident NK (rNK) cells to cNK cells, which inhibited the injury to SG cells with the recovery of saliva secretion in pSS model mice.

Conclusion: The results indicate that SG cNK cells may enhance the autoreactive response in the target organ by upregulating of IFN-γ, whereas

SG rNK cells protect target cells against T cell cytotoxicity. Therefore, the activation process and multiple functions of NK cells in the target organ could be helpful to develop potential markers for determining autoimmune disease activity and target molecules for incurable immune disorders.

KEYWORDS

NK cell, IFN-γ, T cell, autoimmunity, Sjögren's syndrome

Introduction

Innate lymphoid cells (ILCs), including natural killer (NK) cell, ILC1, ILC2, lymphoid tissue-inducer (LTi) cell, and LIC3, significantly contribute to various immune responses (1–3). ILCs lack adoptive antigen receptors generated by the recombination of genetic elements, unlike T cells, which bear T cell antigen receptors. NK cells and ILC1s react to intracellular pathogens and to tumors in type 1 immunity through interferon-γ (IFN-γ) or cytotoxicity (2, 4, 5). ILC2s respond to large extracellular parasites and allergens in type 2 immunity through interleukin-4 (IL-4), IL-13, or IL-27 (2, 6–8). ILC3s combat extracellular microbes in type 3 immunity *via* IL-22 or IL-17 (2, 9, 10). Additionally, LTi cells are associated with the formation of secondary lymphoid structures (2, 11, 12). Although ILCs contribute to the pathogenesis of infectious or allergic disorders, the differentiation of various immune cells, and the development of lymphoid tissue structures, the precise molecular or cellular mechanisms for the onset or development of autoimmune diseases through ILCs remain unclear.

NK cells, among ILCs, have been focused on when studying the pathogenesis of several systemic or organ-specific autoimmune disorders, such as type 1 diabetes mellitus, primary biliary cholangitis, systemic lupus erythematosus, multiple sclerosis, rheumatoid arthritis, and Sjögren's syndrome (SS) (13–18). The multiple functions of cytotoxicity and cytokine production with perforin/granzyme and IFN-γ in NK cells are controlled by the expression T-box expressed in T cells (T-bet) *via* the Janus kinase-signal transduction and activation of transcription (JAK-STAT) or phosphatidylinositol-3-kinase-AKT-mammalian target of rapamycine1 (PI3K-AKT-mTORC1) signaling pathway (19, 20). The phenotypes or functions of tissue resident NK cells are considerably different in the target organs of autoimmune diseases (21). Moreover, NK cells are involved in the perpetuation of diseases through the activation of autoreactive T cells in the presence of antigen-presenting cells within the target organ in autoimmunity, such as pSS (18, 22–28). However, the precise relationship between NK cells and autoimmune responses remains unclear.

Primary SS (pSS) is an systemic autoimmune disease characterized by chronic inflammation of exocrine glands, such as SGs, with many different organ-specific manifestations (29–31). Among target organs, the lacrimal glands and SGs are the main target organs in pSS, characterized by progressive lymphocytic infiltration (32). Th1/Th2 cytokine balance or Th17 cells in exocrine glands are involved in the initiation of the autoimmune response in pSS (33–36). IFN-γ-producing Th1 cells play a central role in the pathogenesis of the disease, from the onset to its chronic stage, in addition to various immune cells, such as B cells, macrophages, dendritic cells, and NK cells, in the SGs and lacrimal glands of mouse models of pSS and patients with pSS (18, 37–39). The number of NK cells in the SGs of healthy mice is significantly higher than that of ILC subpopulations (27). In contrast, the detailed cellular or molecular mechanisms related to tissue resident NK cells for the pathogenesis of pSS are unclear.

In this study, the phenotypes and pathogenic role of tissue resident NK cells within the SGs were analyzed using a mouse model of pSS to better understand the autoimmune response between various immune cells, including NK cells in the target organ. Additionally, a new therapy based on the pathogenic role of NK cells was elucidated using the mouse model. The activation process and multiple functions of tissue resident NK cells in the target organ could help develop potential markers for autoimmune disease activity and target molecules for incurable immune disorders.

Materials and methods

Mice

Female NFS/N mice carrying the mutant *sld* were bred and maintained in a specific pathogen-free mouse colony in the animal facility at Tokushima University (Tokushima, Japan). Neonatal thymectomy was performed on day 3 after birth to develop pSS model mice. The control mice used in this study were sham (non)-thymectomized NFS/*sld* mice that did not exhibit inflammatory lesions in the SGs and lacrimal glands. This study was conducted according to the Fundamental Guidelines for Proper Conduct of Animal Experiment and Related Activities in Academic Research Institutions under the jurisdiction of the Ministry

of Education, Culture, Sports, Science, and Technology of Japan. The study protocol was approved by the Committee on Animal Experiments of Tokushima University, Japan (Permit Number: T-2021-48). All experiments were performed after the administration of anesthesia, and all efforts were made to minimize suffering. Female NFS/*sld* mice (6–12 weeks) were used in this study.

Administration of anti-asialo GM1 antibody to deplete natural killer cells

Mice were intraperitoneally injected with 100 μg of rabbit anti-asialo GM1 antibody (Fujifilm) or control rabbit IgG twice a week from 9 weeks of age. The mice were euthanized at 12 weeks.

Cell isolations

Mouse SG suspension cells were prepared for the detection of NK cells using flow cytometry. SG tissues were minced into 1–3 mm^2 pieces and were digested with 1 mg/mlL collagenase (Fujifilm), 1 mg/mL hyaluronidase (Tokyo Chemical Industry Co., Ltd.) and 10 ng/mL DNase (Roche) in Dulbecco's Modified Eagle's Medium (DMEM) containing 10% fetal calf serum at 37°C for 35 min with gentleMACS Dissociators (Miltenyi Biotec). The digested suspension cells were washed and passed through pre-separation filters (20 μm) (Miltenyi Biotec). For the detection of cytokine produced cells, the single cells in the SG were purified using CD45 MicroBeads (Miltenyi Biotec).

Flow cytometric analysis

Splenocytes and the prepared SG suspension cells were stained using the indicated Abs and 7-amino-actinomycin D (7-AAD) (Biolegend) after pre-incubation with anti-CD16/32 Ab. Abs against mouse fluorescein isothiocyanate (FITC)-conjugated NKp46, phycoerythrin (PE)-conjugated CD49a, CD11b, TRAIL, IFN-γ, DR5, PE-Cyanine7 (Cy7)-conjugated CD19, CD4, allophycocyanin (APC)-conjugated CD49b, CD27, KLRG1, TNF-α, EOMES, APC-Cy7-conjugated CD3, CD8, peridinin chlorophyll protein-cyanine5.5-conjugated CD19, Alexa Fluor® 700 conjugated-CD45.2Abs were purchased from Biolegend. Isotype control Abs for rat IgG1, rat IgG2a, rat IgG2b, rat IgM, and hamster IgG were purchased from Biolegend. A CytoFLEX flow cytometer (Beckman Coulter) was used to identify the cell populations according to expression profile. To determine intracellular cytokine expression, purified $CD45.2^+$ cells were stimulated with phorbol myristate acetate (PMA) (50 ng/mL) and ionomycin (1 μg/mL) in the presence of brefeldin A (eBioscience) in a 96-well round bottom plate for 24 h. Cells producing IFN-γ and TNF-α were stained with the indicated Abs using IC Fixation Buffer and Permeabilization Buffer (eBioscience), and were detected using flow cytometry. Viable cells were checked by gating on side scatter (SSC)/forward scatter (FSC), FSC-H/FSC-A, 7AAD. Data were analyzed using the FlowJo FACS Analysis software (Tree Star Inc.).

Histological analysis

Salivary gland tissues were fixed with 10% phosphate-buffered formaldehyde (pH 7.2) and were prepared for histological examination. Sections were stained with hematoxylin and eosin (HE). Histological changes were histologically graded on a 0–4 scale as described previously (40). The number of lymphocytes that infiltrated into SG tissues per mm^2 was measured using HE-stained sections (41). The focus number was assessed as a focus with ≥50 mononuclear cells per 2×2 mm^2 in inflammatoy lesions of SG tissues.

Immunohistochemistry

Tissue sections (5 μm) were deparaffinized in xylenes and were rehydrated by passing through serial dilutions of ethanol in distilled water. Heat-induced antigen retrieval was performed in ImmunoActive antigen retrieval solution (Matsunami Glass Ind. Ltd.) with microwave thrice for 5 min. Goat anti-mouse NKp46 antibody (R&D systems) was applied to the sections; then, the sections were incubated overnight at 4°C. After washing with phosphate-buffered saline (PBS), the sections were incubated with goat IgG horseradish peroxidase (HRP) polymer antibody (R&D systems). HRP reacted with the 3, 3'-diaminobenzidine (DAB) substrate using the SignalStain® DAB Substrate kit (Cell Signaling Technology). The sections were counterstained with hematoxylin.

Measurement of saliva secretion

All mice were anesthetized with isoflurane (Pfizer) using a small animal inhalation anesthesia machine (Laboratory & Medical Supplies) 5 min before testing and then orally administered with 500 μg/kg body weight of pilocarpine (Fujifilm). The mice were held in a slightly downward tilt, and then, a weighed filter paper was placed into the oral cavity, following which the filter paper was changed every 5 min during the 15 min observation period. The absorbed saliva weight was calculated by subtracting the weight of the filter paper before measurement from that after measurement. The amount of saliva secretion was expressed as the amount of saliva secreted per 10 g of body weight every 5 min.

Statistical analysis

Differences between individual groups were determined using two-tailed Student's *t*-test, one-way analysis of variance (ANOVA), or two-way ANOVA. *P*-values of less than 0.05 were used to denote statistical significance. Power calculations were performed before the initiation of the experiments to determine the sample size for experiments using animals. Data are presented as means ± standard errors of the mean.

Results

Salivary gland natural killer cells in primary Sjögren's syndrome model mice

In this mouse model of pSS, autoimmune lesions in the SGs are observed from 6 weeks of age in females dominantly (42, 43). Lymphocytic infiltration around the salivary duct with the destruction of acinar cells was observed in pSS model mice at 8 weeks of age (**Figure 1A**). A report demonstrated that the number of NK cells, among ILCs, was largely increased within SG tissue (24). Immunohistochemical analysis of the SG tissues of pSS model mice revealed that SG NKp46$^+$ NK cells were observed in the inflammatory lesions, whereas a few NK cells were observed in the SG tissue of control mice (**Figure 1B**). Flow cytometric analysis revealed that the number of SG NK cells was significantly higher in pSS model mice than in control mice at 6 weeks of age (**Figure 1C**). Moreover, in pSS model mice, the number of SG NK cells was significantly higher at 6 weeks of age than that at 12 weeks of age (**Figure 1C**). In contrast, no difference in the number of splenic NK cells were observed between pSS model and control mice at both 6 and 12 weeks of age (**Figure 1D**). These findings imply that an increase number of SG NK cells may be associated with the development of autoimmune lesions in pSS model mice.

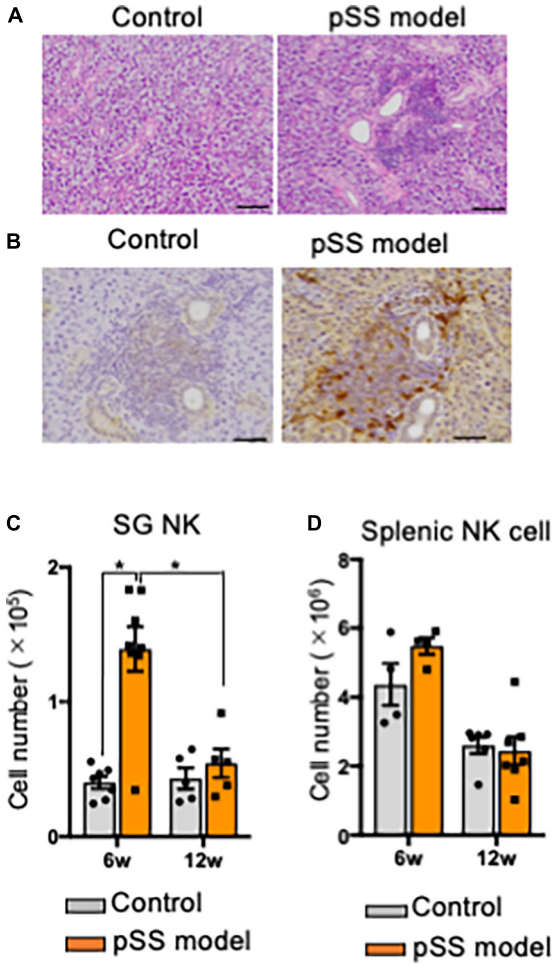

FIGURE 1
NK cells in salivary glands of pSS model mice. **(A)** Pathological analysis of salivary gland (SG) tissues in control and pSS model mice. Sections stained with hematoxylin and eosin (HE) were used. Photos are representative of each group. Scale bar: 100 μm. **(B)** Immunohistochemical analysis of SG NK cells in pSS model mice. Isotype control antibody (Ab) was used in place of anti-NKp46 Ab. Scale bar: 50 μm. **(C)** Alexa 568 (red)-conjugated anti-NKp46 Ab, and Alexa 488 (green)-conjugated anti-CD3, CD19, and CD11c Abs were used for the detection of NKp46$^+$ NK cells in SG tissues of SS model mice. A photo is representative of five samples. Scale bar: 20 μm. **(C)** The number of NKp46$^+$ SG NK cells at 6 and 12 weeks of age was measured using automatic cell counter and flow cytometric analysis. Data are presented as the means ± standard deviation (SD) with five or seven mice from each group. *$P < 0.05$ (two-way ANOVA). **(D)** The number of NKp46$^+$ splenic NK cells at 6 and 12 weeks of age was measured, and data are presented as the means ± SD with five or seven mice from each group.

Differentiation of salivary gland natural killer cells in primary Sjögren's syndrome model mice

Immature and mature NK cells express Eomesodermin (EOMES), a key transcription molecule (7, 44). When the expression of EOMES in SG NK cells of pSS model mice was detected by intracellular flow cytometric analysis, a significant increase in the proportion of EOMES$^+$ cells of SG NK cells in pSS model mice was observed compared with that of control mice (**Figures 2A,B**). To further understand the differentiation and maturation of SG NK cells in pSS model mice, the differential expression of CD27 and CD11b was examined to discriminate four consecutive stages of NK cell maturation: CD27$^+$CD11b$^-$ (mature stage 1: M1), CD27$^+$CD11b$^+$ (M2), CD27$^-$CD11b$^+$ (M3), and CD27$^-$CD11b$^-$ (immature stage: M0) NK cells (45–47). While the proportion of M0–M3 subpopulations of SG NK cells in pSS model mice was similar

to that in control mice at 6 and 12 weeks of age (**Figures 2C,D**), the number of all the subsets in SG NK cells in pSS model mice increased, but not significantly, compared with that in control mice (**Figures 2C,D**). Additionally, the number of M0 and M3 SG NK cells was significantly higher in pSS model mice than in control mice at 12 weeks of age (**Figure 2D**). No differences were found in the proportion and number of each NK cell subset in spleen between control and pSS model mice (**Figures 2E,F**). The results suggest that the unique maturation of SG NK cells is promoted in pSS model mice.

Unique phenotypes of salivary gland natural killer cells in primary Sjögren's syndrome model mice

SG ILCs express several unique phenotypes, such as CD49a and CD49b, which promote lymphocyte homing to non-lymphoid tissues (24, 48): $CD49a^{+}CD49b^{-}$ (resident NK cell: rNK), $CD49a^{+}CD49b^{+}$ (DP), $CD49a^{-}CD49b^{+}$ (conventional NK cell: cNK), and $CD49a^{-}CD49b^{-}$ (DN) (24). $CD49a^{+}$NK cells are considered tissue-resident NK cells (24.47). No changes in the proportions of rNK, DP, cNK, and DN cells among SG NK cells were found in control and pSS model mice at 6 and 12 weeks of age (**Figures 3A,B**). Regarding cell number, the number of cNK cells in pSS model mice was significantly increased compared with that in control mice at 6 weeks of age whereas the number of cNK cells was drastically reduced at 12 weeks of age (**Figure 3B**). No difference in the number of the other NK cell subsets was observed between control and pSS model mice (**Figure 3B**). Almost all splenic NK cells had the cNK cell phenotype, and no differences in the proportion of splenic cNK cells were observed between control and pSS model mice at 6 and 12 weeks of age (**Figures 3C,D**). The phenotypic changes in SG NK cells may be occurred during development of inflammatory lesions in pSS model mice.

Cytotoxic features of salivary gland natural killer cells in primary Sjögren's syndrome model mice

Killer cell lectin-like receptor subfamily G member 1 (KLRG1) is a lymphocyte co-inhibitory or immune checkpoint receptor, expressed predominantly on late-differentiated effector and effector memory $CD8^{+}$ T and NK cells (49, 50). The expression of KLRG1 is associated with the cytotoxic effector function of NK cells (51, 52). No difference in the expression of KLRG1 in SG NK cells was observed between control and pSS model mice in the terms of proportion, cell number, and geometric mean fluorescence intensity (gMFI) (**Figure 4A**). Moreover, tumor necrosis factor (TNF)-related apoptosis-inducing ligand (TRAIL)-expressing SG NK cells control $CD4^{+}$ T cell response during chronic viral infection to limit autoimmunity (53). Although no changes in the proportion and number of $TRAIL^{+}$ SG NK cells were found in control and pSS model mice at 12 weeks of age, the gMFI of TRAIL expression in SG NK cells of pSS model mice was significantly downregulated compared with that of control mice (**Figure 4B**). Furthermore, one of the receptors for TRAIL, death receptor 5 (DR5), on $CD4^{+}$T cells plays an important role in T cell regulation through NK cells in the SGs during chronic viral infection (53). The number of activated $DR5^{+}$ $CD44^{high}$ $CD4^{+}$T cells in the SGs from pSS model mice was significantly higher than that in the SGs from control mice, whereas no changes in the proportion and gMFI of activated $DR5^{+}$ $CD44^{high}$ $CD4^{+}$T cells were observed between control and SS model mice (**Figure 4C**).

Interferon-γ production from T cells and natural killer cells in the target organ of primary Sjögren's syndrome model mice

Th1 cells that produce inflammatory cytokines, such as IFN-γ, play a key role in the pathogenesis of pSS (35, 38). Particularly, IFN-γ from SG tissues in patients with pSS and pSS model mice is associated with the activation of T cells, antigen-presenting cells, and epithelial cells (39). When $CD45.2^{+}$ lymphoid cells within SG tissues, including T cells and NK cells, in pSS model mice were stimulated with phorbol 12-myristate 13-acetate (PMA) for 24 h, IFN-γ production could be detected by flow cytometric analysis with intracellular staining. Surprisingly, the production level of IFN-γ in SG NK cells was significantly higher than that in $CD4^{+}$ and $CD8^{+}$ T cells within SG tissues (**Figure 5A**). In contrast, no difference in the intracellular TNF-α production was found among $CD4^{+}$, $CD8^{+}$ T cells, and NK cells in SG tissues in pSS model mice (**Figure 5B**). These results indicate that SG NK cells can produce abundant IFN-γ in the target organ of pSS.

Therapeutic effects of natural killer cell depletion on autoimmune lesions in primary Sjögren's syndrome model mice

To confirm the effects of NK cell depletion on inflammatory lesions in the SGs in pSS model mice, anti-asialo-GM1 antibody (ASGM1 Ab) was intraperitoneally injected into mice twice a week from 9 to 12 weeks of age. To examine the functions of the SG, saliva weight was measured after intraoral administration of pilocarpine, which is an inducer of saliva secretion as a muscarine receptor antagonist. Five minutes after pilocarpine

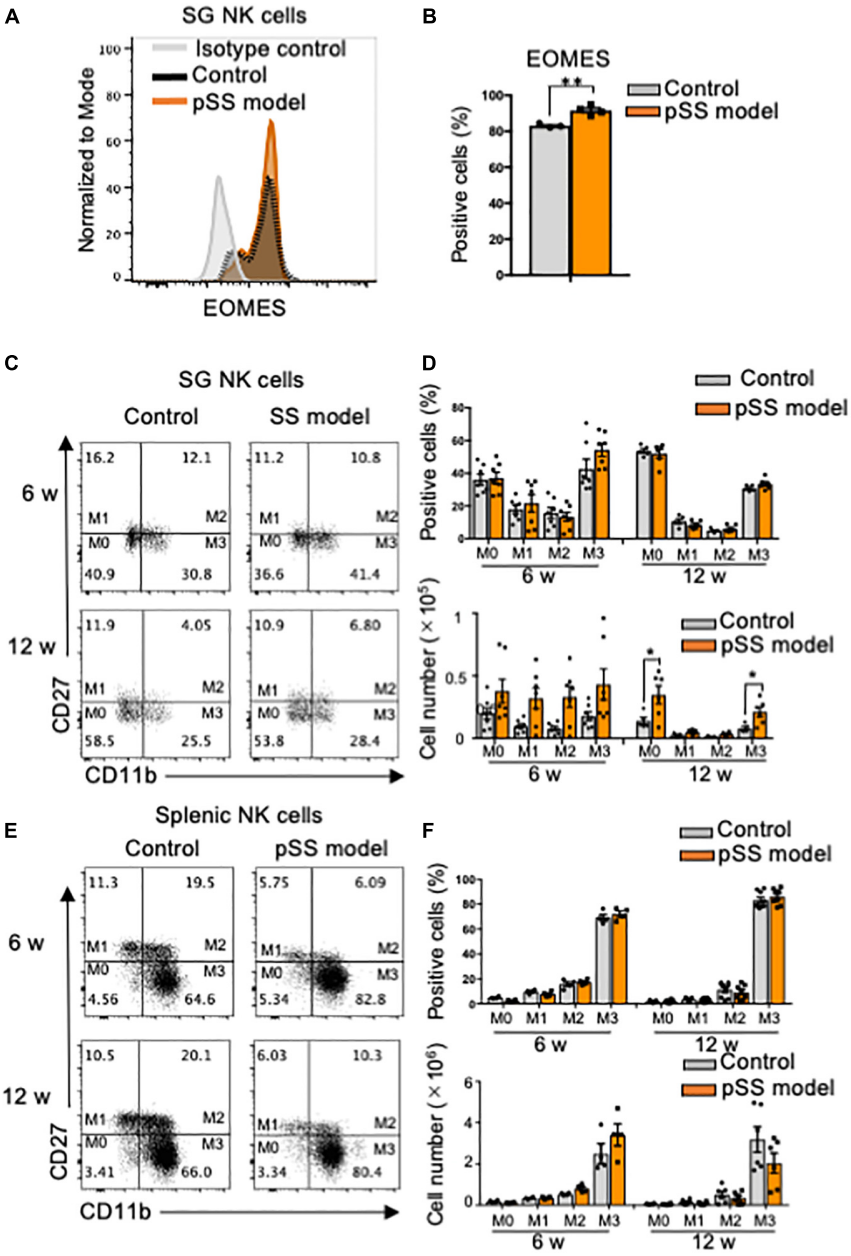

FIGURE 2
Phenotype and maturation of SG NK cells in pSS model mice. **(A)** The intracellular expression of EOMES in NKp46$^+$ SG NK cells was analyzed using flow cytometry. An overlayed histogram shows EOMES expression. The results are representative of each group. **(B)** The proportion of EOMES$^+$ cells among NKp46$^+$ SG NK cells at 8 weeks of age was evaluated using flow cytometric analysis. Data are presented as the mean ± SD with four mice from each group. $^{**}P < 0.005$ (two-tailed Student's *t*-test), vs. control. The experiments were repeated twice and the results are representative of them. **(C)** NK cell maturation was evaluated using CD11b and CD27 expression by flow cytometric analysis. Flow cytometric panels are representative of each group at 6 and 12 weeks of age. Maturation stage is showed as M0 to M3. M0: CD11b$^-$CD27$^-$, M1: CD11b$^-$CD27$^+$, M2: CD11b$^+$CD27$^+$, M3: CD11b$^+$CD27$^-$. **(D)** The proportion (upper figure) and cell number (lower figure) of each stage in SG NK cells at 6 and 12 weeks of age were measured by flow cytometric analysis. Data are presented as the means ± SD with seven mice from each group. $^*P < 0.005$ (two-way ANOVA), vs. control. **(E)** NK cell maturation in the spleen was evaluated using CD11b and CD27 expression by flow cytometric analysis. **(F)** The proportion (upper) and cell number of each stage in splenic NK cells at 6 and 12 weeks of age were measured by flow cytometric analysis. Data are presented as the means ± SD with seven mice from each group.

injection, the saliva weight of ASGM1 Ab-treated pSS model mice significantly increased compared with that of control mice (Figure 6A). After 5 min, the saliva weight in ASGM1 Ab-treated mice increased in contrast to that in control mice; however, the difference was not statistically significant (Figure 6A). We have repeated the experiments three times,

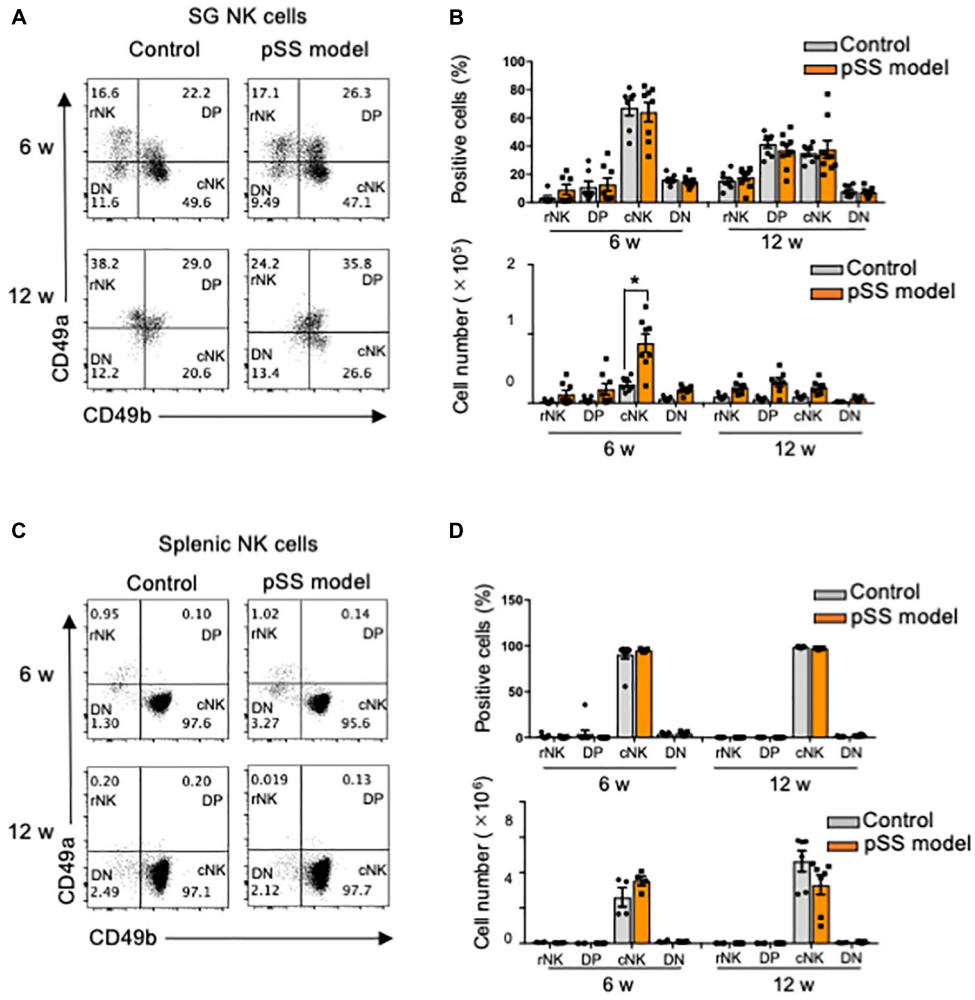

FIGURE 3
Differentiation of SG NK cells in pSS model mice. **(A)** NK cell differentiation was evaluated using CD49a and CD49b expression by flow cytometric analysis. Flow cytometric panels are representative of each group at 6 and 12 weeks of age. Each subset is showed as DN: $CD49a^{-}CD49b^{-}$, rNK: $CD49a^{+}CD49b^{-}$, DP: $CD49a^{+}CD49b^{+}$, and cNK: $CD49a^{-}CD49b^{+}$. **(B)** The proportion (upper figure) and cell number (lower figure) of each subset in SG $NKp46^{+}$NK cells at 6 and 12 weeks of age were measured by flow cytometric analysis. Data are presented as the means ± SDs with seven mice from each group. *$P < 0.005$ (two-way ANOVA), vs. control. **(C)** NK cell subsets in the spleen were evaluated using CD49a and CD49b expression by flow cytometric analysis. **(D)** The proportion (upper) and cell number of each subset in splenic $NKp46^{+}$ NK cells at 6 and 12 weeks of age were measured by flow cytometric analysis. Data are presented as the means ± SD with four to seven mice from each group.

and obtained the similar results that saliva secretion of ASGM1 Ab-treated mice was significantly higher than control mice only at the early stage after stimulation. A significant difference in terms of the depletion of $NKp46^{+}$NK cells in $CD45.2^{+}$ cells in the spleen was observed between control and ASGM1 Ab-treated mice (Figure 6B). However, the proportion of $NKp46^{+}$ SG NK cells among $CD45.2^{+}$ cells in ASGM1 Ab-treated mice did not significantly decrease (Figure 6C). The proportion of $CD49a^{+}CD49b^{-}$ rNK cells among SG NK cells was significantly higher in ASGM1 Ab-treated mice than in control mice, whereas the proportion of $CD49a^{-}CD49b^{+}$ cNK cells was significantly decreased following ASGM1 Ab administration (Figure 6D). The ratio of rNK/cNK cells in the SG was significantly higher following ASGM1 Ab administration (Figure 6E). To understand the pathological mechanism of the effectiveness of NK cell depletion, SG tissues from pSS model mice were histopathologicaliy analyzed. Inflammatory lesions, including lymphocyte infiltration around ductal cells, were found in both isotype control and ASGM1 Ab treated mice (Figure 6F). Three evaluations for inflammatory severity were analyzed by histological grading, lymphocyte number/mm^2, and fucus number/2 × 2 mm^2. No differences in inflammatory severity were observed between isotype control and ASGM1 Ab-treated mice (Figures 6G,H,I). In this experiment, ASGM1 Ab treatment could recover the salivation, but not inflammatory lesions in pSS model mice.

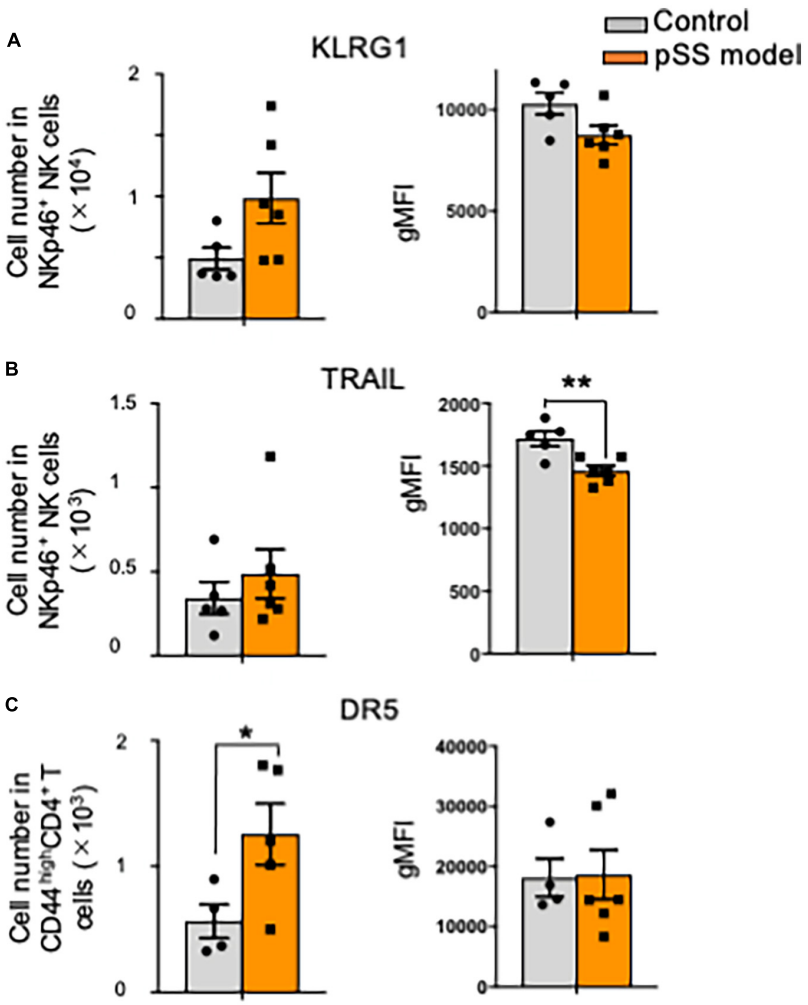

FIGURE 4
Cytotoxic signature of SG NK cells against T cells in pSS model mice. **(A)** The number (left) and geometric mean fluorescence intensity (gMFI) (right) of KLRG1$^+$ SG NK cells were evaluated by flow cytometric analysis. Data are presented as the means ± SD with five or six mice from each group. **(B)** The number (left) and gMFI (right) of TRAIL$^+$ SG NK cells were evaluated by flow cytometric analysis. Data are presented as the means ± SD with five or six mice from each group. $^{**}P < 0.0005$ (two-tailed Student's *t*-test), vs. control. **(C)** The number (left) and gMFI (right) of DR5 SG T cells were evaluated by flow cytometric analysis. Data are presented as the means ± SD with five or six mice from each group. $^{*}P < 0.005$ (two-tailed Student's *t*-test), vs. control.

Discussion

Natural killer cells contribute to various immune responses. In this study, NK cells in the target organ of pSS were focused on, and the association between NK cells and the formation of autoimmune lesions was analyzed using pSS model mice. The maturation of SG NK cells in pSS model mice was promoted in response to the formation of autoimmune lesions in SG tissues. Additionally, mature rNK cells may control the recruitment of cNK cells to maintain homeostasis of the immune environment in SG tissues. Although the depletion of NK cells caused by the administration of ASGM1 Ab failed to protect lymphocytic infiltration in the SGs of pSS model mice, saliva secretion increased in the Ab-treated mice. These results suggest that SG NK cells may contribute to the cytotoxic activity of T cells during the development of pSS.

NKp46$^+$ SG NK cells were detectable in the marginal region of the foci of autoimmune lesions in pSS model mice. This finding was similar to that of lip biopsy materials in patients with SS (54). The main populations in the inflammatory lesion of SGs from the pSS model mice as well as the patients with SS are T and B cells (42). SG NK cells may support the autoimmune response by T or B cells. In this model, inflammatory lesions are observed from 6 week of age (42, 43). A significantly increased number of SG NK cells, including several cNK cells, were observed at 6 weeks of age in pSS model mice, whereas no difference was observed at 12 weeks of age, suggesting that increased SG NK cells may play a pathogenic role in the development of pSS. In

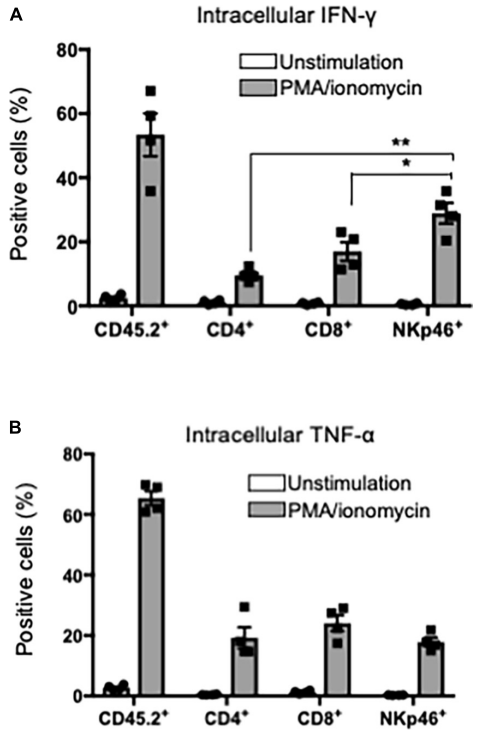

FIGURE 5
IFN-γ production in T and NK cells in SG. CD45.2$^+$ cells were purified from the SG tissues of pSS model mice and the purified cells were stimulated with PMA/ionomycin for 24 h. Intracellular IFN-γ or TNF-α expression was evaluated by flow cytometric analysis. **(A)** Intracellular IFN-γ expression in CD45.2$^+$, CD4$^+$, CD8$^+$ T cells, and NKp46$^+$NK cells was analyzed. The proportions of IFN-γ$^+$ cells were evaluated, and data are presented as the means ± SD with four mice from each group. *$P < 0.005$, **$P < 0.0005$ (two-tailed Student's *t*-test). **(B)** Intracellular TNF-α expression in CD45.2$^+$, CD4$^+$, CD8$^+$ T cells, and NKp46$^+$NK cells was analyzed, and the proportion of TNF-α$^+$ cells were evaluated, and data are presented as the means ± SD with four mice from each group. The experiments were repeated three times and the results are representative of them.

addition, our results suggest that the phenotypic changes in SG NK cells may contribute to the development of autoimmune lesions in pSS model mice. A recent report as for the other SS model mice demonstrates that the proportion of NK1.1$^+$ SG NK cells was significantly higher in C57BL/6 mice injected with an antagonist of the stimulator of IFN gene (STING) protein than in control mice (55), resembling the increase of SG NK cells during the onset in our model mice. Moreover, it is reported that the number of SG NK cells of normal mice is increased with aging (24). In our study, SG NK cells between 6 and 12 weeks of age were compared focusing on the development of inflammatory lesions in pSS model mice. More aged mice should be analyzed to understand the relationship between aging and NK cells in autoimmune lesions.

The maturation of SG NK cells was promoted at 6 weeks of age in pSS model mice. This result suggests that SG NK cells are accompanied by T cell response in the development of autoimmune lesions in pSS. The intracellular expression of EOMES in SG NK cells was higher in pSS model mice than in SG NK cells in control mice. EOMES is a key transcription regulator of mature NK cell homeostasis and cytotoxicity (56). As for cytotoxicity against activated T cells by SG NK cells in pSS model mice, KLRG1 or TRAIL expression was not upregulated, suggesting that the cytotoxic activity of SG NK cells is inadequate against autoreactive and activated T cells in the target organ of pSS. A report demonstrated that TRAIL$^+$ NK cells control CD4$^+$ T cell responses in the SGs during chronic viral infection to limit autoimmunity (53). In our model, TRAIL$^+$ NK cells failed to control CD4$^+$ T cell response attacking to target cells, unlike the condition during chronic viral infection. Our results suggest that SG NK cells fail to regulate activated or autoreactive CD4$^+$ T cells *via* TRAIL/DR5 in the target organ of pSS model mice.

Interferon-γ plays potent roles in the onset or development of pSS (33, 38, 39). The source of IFN-γ in SG tissue contains various cells, such as CD4$^+$ T cells, CD8$^+$ T cells, macrophages, NK cells, and ductal epithelial cells (38–40). In this study using *in vitro* stimulation with PMA/ionomycin, SG NK cells produced higher levels of IFN-γ than CD4$^+$ and CD8$^+$ T cells among CD45.2$^+$ hematopoietic cells in the SGs of pSS model mice. During the development process of SS, IFN-γ contributes to the activation of Th1 cells, the upregulation of MHC Class II of antigen-presenting or epithelial cells, the production of IFN-γ-inducible proteins, and the activation of various immune cells expressing IFN-γ receptor (37). A significantly increased number of cNK cells in the SGs of pSS model mice were observed at 6 weeks of age. Autoimmune lesions were found from 6 weeks pf age in this model. Plenty of IFN-γ produced from SG NK cells together with T cells can promote the autoimmune response within the target organ to form inflammatory and destructive lesions in pSS model mice.

The therapeutic effect of ASGM1 Ab injection was found on saliva secretion in pSS model mice. In contrast, the infiltration of lymphocytes into the SGs was not altered by the administration of ASGM1 Ab. The autoimmune response to the destruction of SG cells in pSS is considered to be dependent on T cell cytotoxicity (57). The findings in this study indicate that cNK cells in the SGs may promote T cell cytotoxicity. NK cells control virus-infected T cells to inhibit viral inflammation (25, 58, 59). Moreover, no changes in the proportion of SG NK cells were observed in ASGM1 Ab-treated pSS model mice, whereas the ratio of rNK to cNK cells in the SG was greatly increased. These findings suggest that the homeostasis of total SG NK cells is maintained by rNK cells.

We determined the dose of *in vivo* ASGM1 Ab injection by which systemic NK cells were completely deleted. In this study, the almost depletion of NK cells was confirmed in the spleen of ASGM1 Ab-treated pSS model mice. However, although cNK cells were depleted in the SG of ASGM1 Ab-treated pSS model

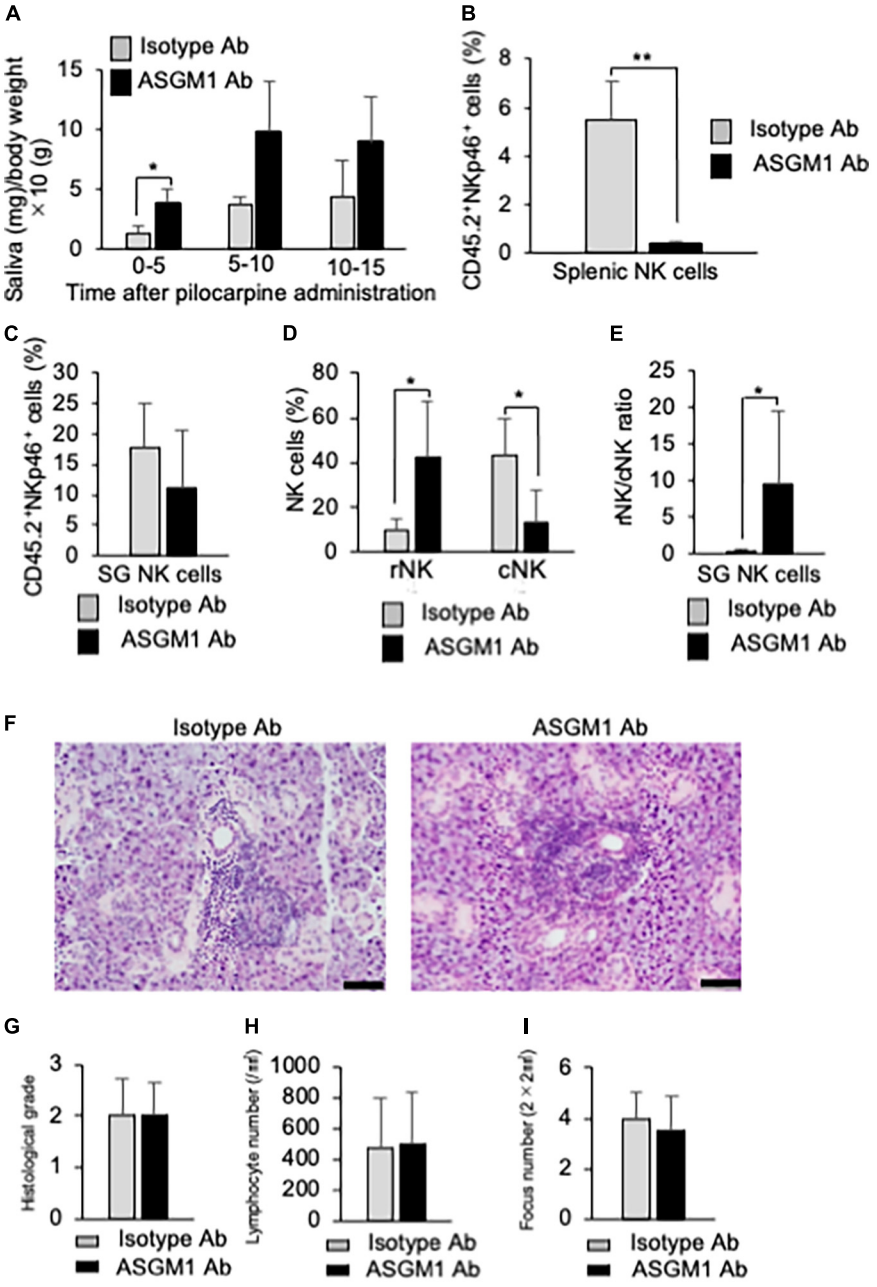

FIGURE 6
Effects of NK cell depletion on the SGs in pSS model mice. **(A)** The saliva weight of isotype antibody (Ab) and anti-asialo-GM1 (ASGM1) Ab-treated pSS model mice were measured from 5 min until 15 min after the oral administration of pilocarpine. Data are presented as the means ± SD of saliva weight (mg)/body weight × 10 (g) with four mice from each group. *$P < 0.05$ (two-way ANOVA). **(B)** The depletion of NK cells in the spleen was confirmed by flow cytometric analysis. Data are presented as the means ± SD of $CD45.2^+NKp46^+$ NK cells (%) with four mice from each group. **$P < 0.005$ (two-tailed Student's *t*-test). **(C)** The proportion of SG NK cells was evaluated by flow cytometric analysis. Data are presented as the means ± SD of $CD45.2^+NKp46^+$ NK cells (%) with four mice from each group. **(D)** Mature rNK ($CD49a^+CD49b^-$) and cNK ($CD49a^-CD49b^+$) cells among $CD45.2^+NKp46^+$ NK cells were measured by flow cytometric analysis. Data are presented as the means ± SD with four mice from each group. *$P < 0.05$ (two-tailed Student's *t*-test). **(E)** The ratio of rNK to cNK cells was presented as the means ± SD with four mice from each group. *$P < 0.05$ (two-tailed Student's *t*-test). **(F)** Pathological analysis of SG tissues in isotype Ab or ASGM1 Ab-treated pSS model mice. Sections stained with HE were used. Photos of are representative of each group. Scale bar: 50 μm. **(G)** Histological grade of SG tissues was evaluated using HE-stained sections. Data are presented as the means ± SD with four mice from each group. **(H)** The lymphocyte number of the SG/mm^2 was measured using histological sections. Data are presented as the means ± SD with four mice from each group. **(I)** Focus number/2 × 2 mm^2 was measured using histological sections. Data are presented as the means ± SD with four mice from each group. The experiments were repeated three times and the results are representative of them.

mice, the proportion of rNK cells was conversely increased. ASGM1 Ab may stimulate rNK cells rather than deplete them. As the recovery of saliva secretion was confirmed by ASGM1 Ab administration, the therapeutic administration of ASGM1 Ab was effective in recovering SG function.

The differentiation, phenotype, and function of NK cells are so complex that various cell markers are used to distinguish differential subsets of NK cells (47). In this study, various NK cell markers were examined to detect SG NK cells in control and pSS model mice. As for NK1.1, one of the most common markers of NK cell, the expression of NK1.1 in SG NK cells was dull, and therefore, NKp46 was used throughout all the experiments. The population that expressed NKp46 was used to discriminate various subsets of NK cells in the SG. Additionally, the distribution of NKp46$^+$ NK cells in the inflammatory lesions of patients with pSS is similar to that observed in pSS model mice (54).

Conclusion

In summary, SG NK cells play a pathogenic role in the development of autoimmune lesions in pSS model mice by prominently upregulating of IFN-γ within the target organ. In addition, controlling the proportion of rNK and cNK cells in SG tissues influences T cell cytotoxicity or autoreactivity in pSS model mice, indicating that rNK cells may play a potent role in regulating autoreactive T cells in the target organ of pSS. These results can be used develop new therapeutic strategies targeting NK cells for autoimmune diseases, including pSS.

Data availability statement

The raw data supporting the conclusions of this article will be made available by the authors, without undue reservation.

Ethics statement

This animal study was reviewed and approved by Committee on Animal Experiments of Tokushima University and Biological Safety Research Center, Japan (Permit No: T-2021-48).

Author contributions

NI supervised the study, acquired the funding, and wrote the original draft. MS and RA conceptualized, analyzed data, investigated, and wrote the original draft. HTaw, RN, HTan, KT, YK, KO, AU, and TT contributed to the analyzed data and investigated. All authors contributed to the article and approved the submitted version.

Funding

This study was supported by the Japan Society for the Promotion of Science KAKENHI (Grant Nos. 19H01070 and 21K19605).

Acknowledgments

We thank Michiko Kino and Hitomi Fukui for technical assistance with the maintenance of the mouse colony. This study was supported by the Research Cluster Program of Tokushima University.

Conflict of interest

The authors declare that the research was conducted in the absence of any commercial or financial relationships that could be construed as a potential conflict of interest.

Publisher's note

References

1. Klose CS, Artis D. Innate lymphoid cells as regulators of immunity, inflammation and tissue homeostasis. *Nat Immunol.* (2016) 17:765–74. doi: 10.1038/ni.3489

2. Vivier E, Artis D, Colonna M, Diefenbach A, Di Santo JP, Eberl G, et al. Innate lymphoid cells: 10 years on. *Cell.* (2018) 174:1054–66. doi: 10.1016/j.cell.2018.07.017

3. Bal SM, Golebski K, Spits H. Plasticity of innate lymphoid cell subsets. *Nat Rev Immunol.* (2020) 20:552–65. doi: 10.1038/s41577-020-0282-9

4. Reynders A, Yessaad N, Vu Manh TP, Dalod M, Fenis A, Aubry C, et al. Identity, regulation and in vivo function of gut NKp46+RORgammat+ and NKp46+RORgammat- lymphoid cells. *EMBO J.* (2011) 30:2934–47. doi: 10.1038/emboj.2011.201

5. Vosshenrich CA, Garcia-Ojeda ME, Samson-Villeger SI, Pasqualetto V, Enault L, Richard-Le Goff O, et al. A thymic pathway of mouse natural killer cell development characterized by expression of GATA-3 and CD127. *Nat Immunol.* (2006) 7:1217–24. doi: 10.1038/ni1395

6. Moro K, Yamada T, Tanabe M, Takeuchi T, Ikawa T, Kawamoto H, et al. Innate production of T(H)2 cytokines by adipose tissue-associated c-Kit(+)Sca-1(+) lymphoid cells. *Nature.* (2010) 463:540–4. doi: 10.1038/nature08636

7. Gasteiger G, Fan X, Dikiy S, Lee SY, Rudensky AY. Tissue residency of innate lymphoid cells in lymphoid and nonlymphoid organs. *Science.* (2015) 350:981–5. doi: 10.1126/science.aac9593

8. Moro K, Kabata H, Tanabe M, Koga S, Takeno N, Mochizuki M, et al. Interferon and IL-27 antagonize the function of group 2 innate lymphoid cells and type 2 innate immune responses. *Nat Immunol.* (2016) 17:76–86. doi: 10.1038/ni.3309

9. Cella M, Fuchs A, Vermi W, Facchetti F, Otero K, Lennerz JK, et al. A human natural killer cell subset provides an innate source of IL-22 for mucosal immunity. *Nature.* (2009) 457:722–5. doi: 10.1038/nature07537

10. Sonnenberg GF, Artis D. Innate lymphoid cell interactions with microbiota: implications for intestinal health and disease. *Immunity.* (2012) 37:601–10. doi: 10.1016/j.immuni.2012.10.003

11. Song C, Lee JS, Gilfillan S, Robinette ML, Newberry RD, Stappenbeck TS, et al. Unique and redundant functions of NKp46+ ILC3s in models of intestinal inflammation. *J Exp Med.* (2015) 212:1869–82. doi: 10.1084/jem.20151403

12. Shikhagaie MM, Bjorklund AK, Mjosberg J, Erjefalt JS, Cornelissen AS, Ros XR, et al. Neuropilin-1 is expressed on lymphoid tissue residing LTi-like group 3 innate lymphoid cells and associated with ectopic lymphoid aggregates. *Cell Rep.* (2017) 18:1761–73. doi: 10.1016/j.celrep.2017.01.063

13. Struyf NJ, Snoeck HW, Bridts CH, De Clerck LS, Stevens WJ. Natural killer cell activity in Sjogren's syndrome and systemic lupus erythematosus: stimulation with interferons and interleukin-2 and correlation with immune complexes. *Ann Rheum Dis.* (1990) 49:690–3. doi: 10.1136/ard.49.9.690

14. Gudbjornsson B, Hallgren R, Nettelbladt O, Gustafsson R, Mattsson A, Geijerstam E, et al. Phenotypic and functional activation of alveolar macrophages, T lymphocytes and NK cells in patients with systemic sclerosis and primary Sjogren's syndrome. *Ann Rheum Dis.* (1994) 53:574–9. doi: 10.1136/ard.53.9.574

15. Segerberg F, Lundtoft C, Reid S, Hjorton K, Leonard D, Nordmark G, et al. Autoantibodies to killer cell immunoglobulin-like receptors in patients with systemic lupus erythematosus induce natural killer cell hyporesponsiveness. *Front Immunol.* (2019) 10:2164. doi: 10.3389/fimmu.2019.02164

16. Hydes TJ, Blunt MD, Naftel J, Vallejo AF, Seumois G, Wang A, et al. Constitutive activation of natural killer cells in primary biliary cholangitis. *Front Immunol.* (2019) 10:2633. doi: 10.3389/fimmu.2019.02633

17. Ming B, Wu T, Cai S, Hu P, Tang J, Zheng F, et al. The increased ratio of blood CD56(bright) NK to CD56(dim) NK is a distinguishing feature of primary Sjogren's syndrome. *J Immunol Res.* (2020) 2020:7523914. doi: 10.1155/2020/7523914

18. Gianchecchi E, Delfino DV, Fierabracci A. Natural killer cells: potential biomarkers and therapeutic target in autoimmune diseases? *Front Immunol.* (2021) 12:616853. doi: 10.3389/fimmu.2021.616853

19. Ronnblom L, Eloranta ML. The interferon signature in autoimmune diseases. *Curr Opin Rheumatol.* (2013) 25:248–53. doi: 10.1097/BOR.0b013e32835c7e32

20. Huang C, Bi J. Expression regulation and function of T-Bet in NK cells. *Front Immunol.* (2021) 12:761920. doi: 10.3389/fimmu.2021.761920

21. Peng H, Tian Z. Diversity of tissue-resident NK cells. *Semin Immunol.* (2017) 31:3–10. doi: 10.1016/j.smim.2017.07.006

22. Takeda A, Minato N, Kano S. Selective impairment of alpha-interferon-mediated natural killer augmentation in Sjogren's syndrome: differential effects of alpha-interferon, gamma-interferon, and interleukin 2 on cytolytic activity. *Clin Exp Immunol.* (1987) 70:354–63.

23. Ciccia F, Guggino G, Giardina A, Ferrante A, Carrubbi F, Giacomelli R, et al. The role of innate and lymphoid IL-22-producing cells in the immunopathology of primary Sjogren's syndrome. *Expert Rev Clin Immunol.* (2014) 10:533–41. doi: 10.1586/1744666X.2014.884461

24. Cortez VS, Cervantes-Barragan L, Robinette ML, Bando JK, Wang Y, Geiger TL, et al. Transforming growth factor-beta signaling guides the differentiation of innate lymphoid cells in salivary glands. *Immunity.* (2016) 44:1127–39. doi: 10.1016/j.immuni.2016.03.007

25. Woyciechowski S, Weissert K, Ammann S, Aichele P, Pircher H. NK1.1(+) innate lymphoid cells in salivary glands inhibit establishment of tissue-resident memory CD8(+) T cells in mice. *Eur J Immunol.* (2020) 50:1952–8. doi: 10.1002/eji.202048741

26. Cortez VS, Fuchs A, Cella M, Gilfillan S, Colonna M. Cutting edge: salivary gland NK cells develop independently of Nfil3 in steady-state. *J Immunol.* (2014) 192:4487–91. doi: 10.4049/jimmunol.1303469

27. Erick TK, Anderson CK, Reilly EC, Wands JR, Brossay L. NFIL3 expression distinguishes tissue-resident NK cells and conventional NK-like cells in the mouse submandibular glands. *J Immunol.* (2016) 197:2485–91. doi: 10.4049/jimmunol.1601099

28. Christodoulou MI, Kapsogeorgou EK, Moutsopoulos HM. Characteristics of the minor salivary gland infiltrates in Sjogren's syndrome. *J Autoimmun.* (2010) 34:400–7. doi: 10.1016/j.jaut.2009.10.004

29. Brito-Zeron P, Baldini C, Bootsma H, Bowman SJ, Jonsson R, Mariette X, et al. Sjogren syndrome. *Nat Rev Dis Primers.* (2016) 2:16047. doi: 10.1038/nrdp.2016.47

30. Seror R, Nocturne G, Mariette X. Current and future therapies for primary Sjogren syndrome. *Nat Rev Rheumatol.* (2021) 17:475–86. doi: 10.1038/s41584-021-00634-x

31. Mariette X, Criswell LA. Primary Sjögren's syndrome. *N Engl J Med.* (2018) 378:931–8. doi: 10.1056/NEJMcp1702514

32. Fox RI. Sjogren's syndrome. *Lancet.* (2005) 366:321–31. doi: 10.1016/S0140-6736(05)66990-5

33. Fox RI, Kang HI, Ando D, Abrams J, Pisa E. Cytokine mRNA expression in salivary gland biopsies of Sjogren's syndrome. *J Immunol.* (1994) 152:5532–9.

34. Mustafa W, Zhu J, Deng G, Diab A, Link H, Frithiof L, et al. Augmented levels of macrophage and Th1 cell-related cytokine mRNA in submandibular glands of MRL/lpr mice with autoimmune sialoadenitis. *Clin Exp Immunol.* (1998) 112:389–96. doi: 10.1046/j.1365-2249.1998.00609.x

35. Kolkowski EC, Reth P, Pelusa F, Bosch J, Pujol-Borrell R, Coll J, et al. Th1 predominance and perforin expression in minor salivary glands from patients with primary Sjogren's syndrome. *J Autoimmun.* (1999) 13:155–62. doi: 10.1006/jaut.1999.0289

36. Verstappen GM, Corneth OBJ, Bootsma H, Kroese FGM. Th17 cells in primary Sjogren's syndrome: pathogenicity and plasticity. *J Autoimmun.* (2018) 87:16–25. doi: 10.1016/j.jaut.2017.11.003

37. Yin H, Vosters JL, Roescher N, D'Souza A, Kurien BT, Tak PP, et al. Location of immunization and interferon-gamma are central to induction of salivary gland dysfunction in Ro60 peptide immunized model of Sjogren's syndrome. *PLoS One.* (2011) 6:e18003. doi: 10.1371/journal.pone.0018003

38. Nocturne G, Mariette X. Advances in understanding the pathogenesis of primary Sjogren's syndrome. *Nat Rev Rheumatol.* (2013) 9:544–56. doi: 10.1038/nrrheum.2013.110

39. Ambrosi A, Wahren-Herlenius M. Update on the immunobiology of Sjogren's syndrome. *Curr Opin Rheumatol.* (2015) 27:468–75. doi: 10.1097/BOR.0000000000000195

40. Ishimaru N, Arakaki R, Yoshida S, Yamada A, Noji S, Hayashi Y. Expression of the retinoblastoma protein RbAp48 in exocrine glands leads to Sjogren's syndrome-like autoimmune exocrinopathy. *J Exp Med.* (2008) 205:2915–27. doi: 10.1084/jem.20080174

41. Otsuka K, Yamada A, Saito M, Ushio A, Sato M, Kisoda S, et al. Achaete-scute homologue 2-regulated follicular helper T cells promote autoimmunity in a murine model for Sjögren syndrome. *Am J Pathol.* (2019) 189:2414–27. doi: 10.1016/j.ajpath.2019.08.008

42. Haneji N, Hamano H, Yanagi K, Hayashi Y. A new animal model for primary Sjogren's syndrome in NFS/sld mutant mice. *J Immunol.* (1994) 153:2769–77.

43. Haneji N, Nakamura T, Takio K, Yanagi K, Higashiyama H, Saito I, et al. Identification of alpha-fodrin as a candidate autoantigen in primary Sjogren's syndrome. *Science.* (1997) 276:604–7. doi: 10.1126/science.276.5312.604

44. Zhang J, Marotel M, Fauteux-Daniel S, Mathieu AL, Viel S, Marcais A, et al. T-bet and Eomes govern differentiation and function of mouse and human NK cells and ILC1. *Eur J Immunol.* (2018) 48:738–50. doi: 10.1002/eji.201747299

45. Hayakawa Y, Smyth MJ. CD27 dissects mature NK cells into two subsets with distinct responsiveness and migratory capacity. *J Immunol.* (2006) 176:1517–24. doi: 10.4049/jimmunol.176.3.1517

46. Chiossone L, Chaix J, Fuseri N, Roth C, Vivier E, Walzer T. Maturation of mouse NK cells is a 4-stage developmental program. *Blood.* (2009) 113:5488–96. doi: 10.1182/blood-2008-10-187179

47. Held W, Jeevan-Raj B, Charmoy M. Transcriptional regulation of murine natural killer cell development, differentiation and maturation. *Cell Mol Life Sci.* (2018) 75:3371–9. doi: 10.1007/s00018-018-2865-1

48. Meharra EJ, Schon M, Hassett D, Parker C, Havran W, Gardner H. Reduced gut intraepithelial lymphocytes in VLA1 null mice. *Cell Immunol.* (2000) 201:1–5. doi: 10.1006/cimm.2000.1630

49. Henson SM, Akbar AN. KLRG1–more than a marker for T cell senescence. *Age (Dordr).* (2009) 31:285–91. doi: 10.1007/s11357-009-9100-9

50. Jonjic S. Functional plasticity and robustness are essential characteristics of biological systems: lessons learned from KLRG1-deficient mice. *Eur J Immunol.* (2010) 40:1241–3. doi: 10.1002/eji.201040506

51. Li Y, Li B, You Z, Zhang J, Wei Y, Li Y, et al. Cytotoxic KLRG1 expressing lymphocytes invade portal tracts in primary biliary cholangitis. *J Autoimmun.* (2019) 103:102293. doi: 10.1016/j.jaut.2019.06.004

52. Gamache A, Cronk JM, Nash WT, Puchalski P, Gillespie A, Wei H, et al. Ly49R activation receptor drives self-MHC-educated NK cell immunity against cytomegalovirus infection. *Proc Natl Acad Sci U.S.A.* (2019) 116:26768–78. doi: 10.1073/pnas.1913064117

53. Schuster IS, Wikstrom ME, Brizard G, Coudert JD, Estcourt MJ, Manzur M, et al. TRAIL+ NK cells control CD4+ T cell responses during chronic viral infection to limit autoimmunity. *Immunity.* (2014) 41:646–56. doi: 10.1016/j.immuni.2014.09.013

54. Rusakiewicz S, Nocturne G, Lazure T, Semeraro M, Flament C, Caillat-Zucman S, et al. NCR3/NKp30 contributes to pathogenesis in primary Sjogren's syndrome. *Sci Transl Med.* (2013) 5:195ra96. doi: 10.1126/scitranslmed.3005727

55. Papinska J, Bagavant H, Gmyrek GB, Sroka M, Tummala S, Fitzgerald KA, et al. Activation of stinmulator of interferon gene (STING) and Sjögren's syndrome. *J Dent Res.* (2018) 97:893–900. doi: 10.1177/0022034518760855

56. Wagner JA, Wong P, Schappe T, Berrien-Elliott MM, Cubitt C, Jaeger N, et al. Stage-specific requirement for Eomes in mature NK cell homeostasis and cytotoxicity. *Cell Rep.* (2020) 31:107720. doi: 10.1016/j.celrep.2020.107720

57. Hong X, Meng S, Tang D, Wang T, Ding L, Yu H, et al. Single-cell RNA sequencing reveals the expansion of cytotoxic CD4(+) T lymphocytes and a landscape of immune cells in primary Sjogren's syndrome. *Front Immunol.* (2020) 11:594658. doi: 10.3389/fimmu.2020.594658

58. Andrews DM, Estcourt MJ, Andoniou CE, Wikstrom ME, Khong A, Voigt V, et al. Innate immunity defines the capacity of antiviral T cells to limit persistent infection. *J Exp Med.* (2010) 207:1333–43. doi: 10.1084/jem.20091193

59. Cook KD, Whitmire JK. The depletion of NK cells prevents T cell exhaustion to efficiently control disseminating virus infection. *J Immunol.* (2013) 190:641–9. doi: 10.4049/jimmunol.1202448

frontiers | Frontiers in Medicine

TYPE Original Research
PUBLISHED 13 January 2023
DOI 10.3389/fmed.2022.1057252

OPEN ACCESS

EDITED BY
Vadim V. Sumbayev,
University of Kent, United Kingdom

REVIEWED BY
Hossein Khorramdelazad,
Rafsanjan University of Medical Sciences, Iran
Bernhard F. Gibbs,
University of Oldenburg, Germany

*CORRESPONDENCE
Jean-Paul Coutelier
✉ jean-paul.coutelier@uclouvain.be

SPECIALTY SECTION
This article was submitted to Pathology, a section of the journal Frontiers in Medicine

RECEIVED 29 September 2022
ACCEPTED 21 December 2022
PUBLISHED 13 January 2023

CITATION
Mandour MF, Soe PP, Castonguay A-S, Van Snick J and Coutelier J-P (2023) Inhibition of IL-12 heterodimers impairs TLR9-mediated prevention of early mouse plasmacytoma cell growth.
Front. Med. 9:1057252.
doi: 10.3389/fmed.2022.1057252

Inhibition of IL-12 heterodimers impairs TLR9-mediated prevention of early mouse plasmacytoma cell growth

Mohamed F. Mandour[1,2], Pyone Pyone Soe[1,3], Anne-Sophie Castonguay[1,4], Jacques Van Snick[1,5] and Jean-Paul Coutelier[1,6]*

[1]Unit of Experimental Medicine, Université catholique de Louvain, Brussels, Belgium, [2]Department of Clinical Pathology, Faculty of Medicine, Suez Canal University, Ismailia, Egypt, [3]Department of Pathology, University of Medicine (1) Yangon, Yangon, Myanmar, [4]Département de Pharmacologie et de Physiologie, Faculté de Médecine, Université de Montréal, Montréal, QC, Canada, [5]Ludwig Institute, de Duve Institute, Université catholique de Louvain, Brussels, Belgium, [6]de Duve Institute, Université catholique de Louvain, Woluwe-Saint-Lambert, Belgium

Introduction: Natural prevention of cancer development depends on an efficient immunosurveillance that may be modulated by environmental factors, including infections. Innate lymphoid cytotoxic cells have been shown to play a major role in this immunosurveillance. Interleukin-12 (IL-12) has been suggested to be a key factor in the activation of innate cytotoxic cells after infection, leading to the enhancement of cancer immunosurveillance.

Methods: The aim of this work was to analyze in mouse experimental models by which mechanisms the interaction between infectious agent molecules and the early innate responses could enhance early inhibition of cancer growth and especially to assess the role of IL-12 by using novel antibodies specific for IL-12 heterodimers.

Results: Ligation of toll-like receptor (TLR)9 by CpG-protected mice against plasmacytoma TEPC.1033.C2 cell early growth. This protection mediated by innate cytolytic cells was strictly dependent on IL-12 and partly on gamma-interferon. Moreover, the protective effect of CpG stimulation, and to a lesser extent of TLR3 and TLR7/8, and the role of IL-12 in this protection were confirmed in a model of early mesothelioma AB1 cell growth.

Discussion: These results suggest that modulation of the mouse immune microenvironment by ligation of innate receptors deeply modifies the efficiency of cancer immunosurveillance through the secretion of IL-12, which may at least partly explain the inhibitory effect of previous infections on the prevalence of some cancers.

KEYWORDS

cancer immunosurveillance, IL-12, plasmacytoma, NK/NKT cells, IFN-γ, TLR9, mesothelioma

1. Introduction

Although a causal relationship between infectious agents and about two million cancers each year has been recognized (1), a few observations suggest also that some infections may decrease further cancer development through enhanced cancer immunosurveillance (2). Clinical surveys have reported an inverse relationship between history of infections and/or vaccinations and subsequent development of cancer (3, 4), including melanoma (5–7). Such an effect of infections may explain a lower incidence of some cancers, including multiple myeloma (8) in developing countries when compared to industrialized countries. Cancer development has been shown to be prevented by previous infection with lactate dehydrogenase-elevating virus (LDV), a virus inducing lifelong viremia, (9) and *Trypanosoma brucei* (10) in experimental mouse models of myeloma and mesothelioma (11). This led to the proposal that a particular form of "hygiene hypothesis" might apply to cancer development. Such a preventive effect of infections may, at least partly, explain the lower incidence of some cancers in developing countries where infection incidences are high, when compared to industrialized countries.

The efficiency of cancer immunosurveillance has been shown to depend on the activation of the immune system, and especially on the secretion of gamma-interferon (IFN-γ) by innate lymphoid cytotoxic cells such as natural killer (NK) cells and NK/T cells (12, 13). CD8+ cells have also been shown to provide innate IFN-γ production when stimulated by the appropriate cytokines (14) and could therefore also be involved in cancer immunosurveillance. IFN-γ has indeed been shown to be at least partly responsible for the preventive effect of LDV and *T. brucei* on further mouse plasmacytoma development (9, 10). It may therefore be postulated that the effect of infections on cancer immunosurveillance correlates with their ability to modulate the immune microenvironment of their host, and especially the capacity of NK cells to destroy tumor cells.

Since infections have complex effects on their host immune system, it is difficult to assign to a single mechanism their modulation of cancer development. However, the first interactions between invading infectious agents and the immune system involve recognition of pathogen-associated molecular patterns (PAMPs) by pattern recognition receptors (PRRs). Among these PRRs, toll-like receptors (TLRs) have been reported to recognize PAMPs from bacteria, viruses, parasites, and fungi and to initiate potent early immune signals (15). These early signals induced by the interactions between PAMPs and TLRs include the secretion of cytokines, and especially of interleukin-12 (IL-12) that, in turn, will trigger the activation of innate lymphoid cells. Since activation of NK/Natural-killer T cells (NKT) cells through ligation of TLRs, and especially TLR7, 8 and 9 that recognize infectious agent genetic material in endosomes, has been shown to enhance anti-tumor responses (16), we investigated the potential of these TLRs in enhanced cancer immunosurveillance. Our results indicate that activation of TLRs, and especially CpG stimulation increase early prevention of plasmacytoma and mesothelioma growth. This effect was strongly dependent on the secretion of IL-12.

2. Materials and methods

2.1. Animals

Specific pathogen-free BALB/c female mice were bred at the Ludwig Institute for Cancer Research or were obtained from Janvier Labs and used when 7–10 weeks old. The total number of 715 mice was used for this project. This mouse strain was chosen since TEPC.1033.C2 and AB1 cells were derived from BALB/c animals. All experimental protocols and animal handling were approved by the local commission for animalcare: Comité d'Ethique facultaire pour l'Expérimentation Animale–Secteur des Sciences de la Santé–Université catholique de Louvain (ref. 2014/UCL/MD/008 and 2018/UCL/MD/007).

2.2. Tumor cells

Plasmacytoma TEPC.1033.C2 cells, originally obtained from Dr M. Potter (17) were cultured in Iscove's Modified Dulbecco's Medium (IMDM) (Gibco, Life technologies, Grand Isle, NY, USA) with 10% fetal bovine serum (FBS, Gibco, Life technologies, Grand Isle, NY, USA), 50 U/ml penicillin G and 50 μg/ml streptomycin (Gibco, Life technologies). Cells were collected by brief trypsinization, washed twice with phosphate buffered saline (PBS) and injected i.p. at a dose of 3–4 $\times$ 10^4 living cells (counted using trypan blue staining) in 500 μ l PBS.

AB1, a mouse mesothelioma cell line derived from mouse lung (18) was obtained from Sigma-Aldrich (Public Health England, general cell collection, Ref. 10092305) and maintained in RPMI 1,640 medium containing 25 mM HEPES, 5% FBS, 50 U/ml penicillin G, 50 μg/ml streptomycin, and 2 mM L-Glutamine (Gibco, Life technologies). Exponentially growing cells were collected by brief trypsinization, washed twice with PBS and injected i.p. at a dose of 0.5 $\times$ 10^6 living cells, counted using trypan blue staining, in 500 μ l PBS.

2.3. TLR ligands

Mice were injected i.p. with TLR2, 3, 4, 7/8 and 9 ligands for two successive days before inoculation of tumor cells. Peptidoglycan from *Methanobacterium* sp. (Sigma-Aldrich, ref. 78721) was injected at a dose of 10 μg/mouse. Polyinosinic–polycytidylic acid sodium salt [Poly (I:C) (Sigma-Aldrich, ref. P1530)] was injected at a dose of 50 μg/mouse. Lipopolysaccharide (LPS) from *Escherichia coli* 0111:B4 purified

by phenol extraction (Sigma-Aldrich, ref L2630) was injected at a dose of 10 μg/mouse. R848 (resiquimod) (Enzo, ref. ALX-420-038-M005) was injected at a dose of 50 μg/mouse. CpG-C DNA (ODN 2395) (Hycult biotech, ref HC4041) was injected at a dose of 10 μg/mouse.

2.4. Antibodies, NK cell depletion, and cytokine neutralization

Anti-asialoganglioside-GM1 (anti-ASGM1) polyclonal antibody from immunized rabbit was prepared and used following a protocol shown previously to successfully deplete NK cells and to suppress their function (19). *In vivo* NK cell depletion was achieved by i.p. injection of 2 mg anti-ASGM1 in 500 μl saline 2 days before tumor cell administration, followed by injection of 1 mg anti-ASGM1 in 300 μl saline the day of tumor inoculation.

F3 rat anti-mouse IFN-γ monoclonal antibody (mAb) (20, 21), purified with protein G-sepharose beads, was injected i.p. into mice at a dose of 500 μg 1 day before and 6 days after TLR9 ligation. MM12A1.6 mouse IgG2a anti-IL-12 mAb (22, 23) was injected i.p. into mice at a dose of 500 μg 1 day before and 6 days after TLR9 ligation. C1407C3 mouse IgG2a control mAb was injected at the same times and doses.

2.5. Isolation of spleen and peritoneal cells

After mice euthanasia, spleen was transferred to be processed into a sterile 35 mm petri dish containing 5 ml of sterile dissection medium (PBS + 1 mM EDTA). Then, spleen was mechanically crushed using the flat end of a sterile 3 cc syringe plunger by gentle circular motions. The released splenocytes were strained and filtered through a 70 μm cell strainer on a sterile 15 ml conical tube. After being centrifuged for 10 min at 8°C, (1,200 rpm), red blood cells were completely lysed using 2.5 ml Ammonium-Chloride-Potassium (ACK) lysis buffer [0.15 M NH_4Cl (Merck, #1.01149), 10 mM $KHCO_3$ (Merck, #1.00119), 0.1 mM Na_2EDTA (Sigma, #E5134), (pH 7.3)] for 5 min on ice. The tube was toped up with 5 ml PBS, centrifuged at 1,200 rpm for 10 min. After discarding the supernatant, the cell pellet was washed 1–2 times and resuspended in 1 ml PBS. Cells were counted and assessed for viability using trypan blue stain.

Peritoneal cells were harvested by washing the peritoneal cavity with 2 × 5 ml ice-cold PBS supplemented with 5% fetal bovine serum (FBS, Gibco, Life Technologies, Grand Isle, NY, USA), 50 U/ml penicillin G, 50 μg/ml streptomycin (Gibco, Life Technologies), and 2 mM EDTA (Sigma-Aldrich, St. Louis, MO, USA). The cells were washed, resuspended in Iscove's Modified Dulbecco's Medium (IMDM, Gibco Life Technologies) supplemented with 10% FBS, non-essential amino acids, 50 U/ml penicillin G, and 50 μg/ml streptomycin. Cells were counted and assessed for viability using trypan blue dye before further processing and staining.

2.6. Flow cytometry

Flow cytometry analysis of NK cells and IFN-γ -producing cells was carried out using BD-FACSVerse machine (Becton Dickinson, Franklin Lakes, NJ, USA). Peritoneal cells were first incubated for 4 h at 37°C with 10 μg/ml monensin (Biolegend, San Diego, CA, USA; Cat# 420701). γ-block was done using purified anti-mouse CD16/32 antibody (2.4G2; Biolegend, Cat# 101301). NK cells were labeled by surface staining with 1.0 μg APC-labeled anti-mouse CD49b mAb (DX5; Biolegend, Cat# 108909) per 10^6 cells. Anti-CD49b mAb was used, since it recognizes NK and NKT BALB/c cells. For intracellular labeling of IFN-γ, cells were fixed and permeabilized using Cyto-Fast™ Fix/Perm Buffer Set 111 (Biolegend, Cat# 426803) followed by staining with PE-labeled anti-IFN-γ mAb (XMG1.2; Biolegend, Cat# 505807). Data were analyzed by using FlowJo Software 9.8.1 (Tree Star, Ashland, OR, USA).

2.7. Statistical analysis

Results are expressed as means ± standard error of mean (SEM). When appropriate, one-way or two-way ANOVA tests with Bonferroni correction were performed using Prism 6 software (GraphPad Prism, La Jolla, CA, USA). Survival curves were analyzed using Log-rank (Mantel–Cox) test.

3. Results

3.1. Prevention of plasmacytoma early development after TLR ligation

Previous observations indicated that infections, including with a virus such as LDV occurring prior to tumor cell administration prevented early development of plasmacytoma, a mouse model of multiple myeloma (9). Similarly, decrease of cancer incidence has been reported in humans after various infectious stimuli (3–8). To extend in an animal model these observations to conditions mimicking the effect of diverse infections on the immune system, we treated mice with TLR ligands before administration of cancer cells. After administration of TEPC.1033.C2 plasmacytoma cells, all control mice died within 20 days (**Figure 1**). In contrast, mice treated with TLR9 ligand CpG-ODN were protected against plasmacytoma development and half of them were still alive after 1 month without clinical signs of cancer development

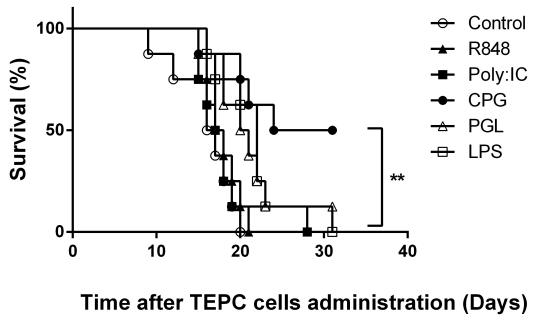

FIGURE 1
Effect of toll-like receptor (TLR) ligand administration on early plasmacytoma growth. Survival of groups of BALB/c mice (n = 8) either mock-treated (open circles) or treated with Poly (I:C) (closed squares), R848 (closed triangles), CpG-ODN (closed circles), lipopolysaccharide (LPS) (open squares), and peptidoglycan (open triangles) for two successive days before tumor administration. Groups were monitored daily after i.p. administration of plasmacytoma TEPC.1033.C2 cells. Experiment representative of three independent experiments. $^{**}P$ = 0.0013 by Log-rank (Mantel–Cox) test.

(Figure 1, p = 0.0013). A similar preventive effect of CpG-ODN was obtained in three independent experiments. Despite a statistically significant difference between survival of control mice and those treated with bacterial peptidoglycan and LPS, TLR2 and TLR4 ligands, (Figure 1, p = 0.01 and 0.004, respectively), the preventive effect of these molecules was much lower than after CpG-ODN treatment. In addition, TLR3 ligand Poly (I:C) and TLR7/8 ligand R848 had no preventive effect against plasmacytoma growth (Figure 1, p = 0.56 and 0.28, respectively). Since CpG-ODN stimulation induced the most efficient prevention of plasmacytoma early growth, we focused our analysis on this treatment.

3.2. Involvement of innate lymphoid cytotoxic cells in TLR9-mediated prevention of early plasmacytoma growth

Innate cytotoxic cells have been reported to play a major role in cancer immunosurveillance (13) and prevention of early cancer growth after LDV infection relies on these cells (9, 19). To determine whether these cells were also involved in TLR9-mediated plasmacytoma growth prevention, we treated mice with a polyclonal anti-ASGM1 antibody. As shown in Figure 2A, this treatment effectively suppressed spleen CD49b+ cells (4% CD49b+ cells without anti-ASGM1 treatment versus 0.43% CD49b+ cells after treatment). Anti-ASGM1 antibody administration resulted in almost complete abolition of CpG-ODN-mediated protective effect on plasmacytoma development after TEPC.1033.C2 cell administration (shown in Figure 2B for one representative experiment among three; difference with and without treatment: p = 0.0015). Therefore, innate cytotoxic lymphoid cells were required for protection against early plasmacytoma growth induced by CpG stimulation.

3.3. Role of IFN-γ and IL-12 in TLR9-mediated prevention of early plasmacytoma growth

It has been reported that CpG stimulation in mice induces both IL-12 and IFN-γ production (24). Moreover, those cytokines were involved in LDV-induced prevention of plasmacytoma growth (9). We therefore analyzed the role of these cytokines in TLR9-mediated prevention of early plasmacytoma development by treating mice with the neutralizing F3 anti-IFN-γ mAb and a specific anti-IL-12 mAb recognizing the heterodimeric cytokine (MM12A1.6) (23). After CpG-ODN administration, IL-12 neutralization resulted in a significant decrease in the survival after plasmacytoma inoculation (Figure 3, $p < 0.023$). The suppression of CpG-ODN induced plasmacytoma growth prevention after IFN-γ neutralization was less important and did not reach significance (Figure 3, p = 0.61). These results are representative of two independent experiments.

3.4. Effect of CpG-ODN stimulation on prevention of early mesothelioma growth

Lactate dehydrogenase-elevating virus infection has been shown to protect against mesothelioma early growth through mechanisms similar to those involved in protection against plasmacytoma (11). To determine whether our observation of protection against early plasmacytoma growth after CpG-ODN stimulation could be extended to other tumors, we repeated therefore our experiments after administration of AB1 mesothelioma cells. A similar preventive effect against tumor development was observed in mice treated with CpG-ODN (Figure 4A, p = 0.0096). Administration of Poly (I:C) and of R848 prevented also mesothelioma development (Figure 4A). This preventive effect of TLR3, 7/8 and 9 ligands was observed in three independent experiments. In contrast, neither TLR4 nor TLR2 stimulation with LPS and bacterial peptidoglycan, respectively, could prevent mesothelioma development (Figure 4A, p = 0.62 and 0.91, respectively).

The role of IL-12 and IFN-γ in this TLR9-induced protection against mesothelioma early growth was also analyzed with the same neutralizing antibodies. As shown in Figure 4B, IL-12 neutralization resulted in a significant decrease in the protective effect of CpG-ODN stimulation (p = 0.0008). In contrast, IFN-γ neutralization did not modify TLR9-mediated prevention of mesothelioma growth (p = 0.93). Interestingly,

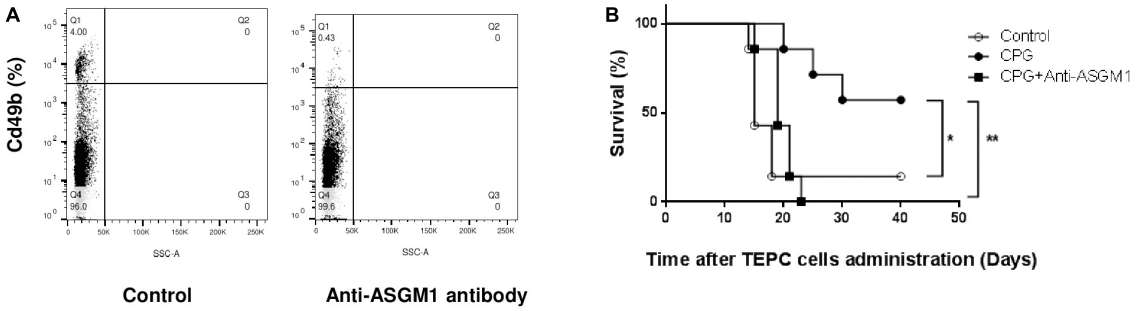

FIGURE 2
Role of innate lymphoid cytotoxic cells in toll-like receptor (TLR)9-mediated protection against plasmacytoma growth. **(A)** Flow cytometry analysis of CD49b+ cells in pooled spleen cells from 2 BALB/c mice with and without treatment with 2 mg anti-ASGM1 antibody. Experiment representative of two independent experiments. **(B)** Survival of groups of BALB/c mice (n = 7) either mocked-treated (open circles) or treated only with CpG-ODN (closed circles), or with CpG-ODN and anti-ASGM1 treatment (closed squares), was monitored daily after i.p. administration of TEPC.1033.C2 cells. Experiment representative of three independent experiments. *P = 0.0153 and **P = 0.0015 by Log-rank (Mantel–Cox) test.

neutralization of both IFN-γ and IL-12 suppressed completely prevention of mesothelioma growth after R848 treatment and largely after Poly (I:C) treatment (data not shown).

4. Discussion

In addition to their causative role in tumor development, infections have been reported to prevent further development of some cancers (3–7), a phenomenon that has been compared to the "hygiene hypothesis" or "old friends hypothesis" (2, 25), which could explain the increasing incidence of allergies and autoimmune diseases in industrialized countries with reduced prevalence of many infections. Such a cancer-related "hygiene hypothesis" could partly explain the low incidence of some cancers, including multiple myeloma (8) in developing countries where infection incidences with a large array of microorganisms, including viruses, bacteria and parasites are higher. This hypothesis has also been supported by experimental mouse models, showing a preventive or protective effect of virus and parasites on cancer early development (9–11). However, the mechanisms responsible for such a prevention of cancer development might be quite different from those triggered by infections and leading to a prevention of allergic and autoimmune diseases, that have been proposed to be linked with regulatory immune responses (26).

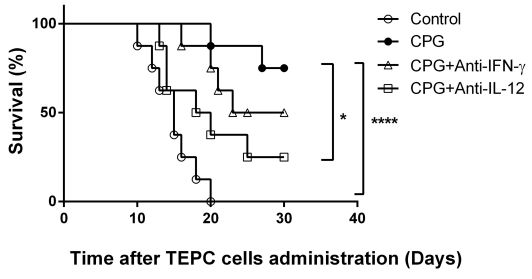

FIGURE 3
Role of IFN-γ and interleukin-12 (IL-12) in toll-like receptor (TLR)9-mediated protection against early plasmacytoma growth. Survival of groups of BALB/c mice (n = 8) either mocked treated (open circles) or CpG-ODN treated, without (closed circles) or with anti-IFN-γ (open triangles) and anti-IL-12 (open squares) treatment, was monitored daily after i.p. administration of TEPC.1033.C2 cells. Experiment representative of two independent experiments. *P = 0.023 (CpG vs. CpG+ anti-IL-12) and P = 0.24 (CpG vs. CpG+ anti-IFN-γ) by Log-rank (Mantel–Cox) test. ****$P \leq 0.0001$.

To analyze mechanisms induced by various infectious agents, it is easier to focus on common early interactions with the immune system rather than to develop many individual models of infections. One of the best studied early interactions of microorganisms with the immune system is their recognition by innate receptors and especially by TLRs. Indeed, those receptors trigger immune responses after recognition of a very large range of bacteria, viruses, yeast and parasites. TLR ligation has been shown to induce divergent effects on the development of various tumors [reviewed in Korneev (27)]. A therapeutic effect of CpG stimulation on mesothelioma growth has been reported previously in a model of mesothelioma using orthotopic xenografts in immunodeficient mice (28). CpG stimulation has also therapeutic effect on pancreas adenocarcinoma and colorectal cancer models (29). TLR9 agonists have been tested in early human clinical trials, including in combined therapies (30). However, TLR9 may also be involved in early promotion of some cancers such as gastric cancer, through enhancement of inflammation and of cell proliferation (31). B cell activity depends on the activation of TLR9 and TLR9 ligands may promote the growth and survival of multiple myeloma cells (32). So far, TLR ligand effects were reported after initiation of cancers. However, to the best of our knowledge, the modulation of the immune microenvironment after TLR ligation, leading to

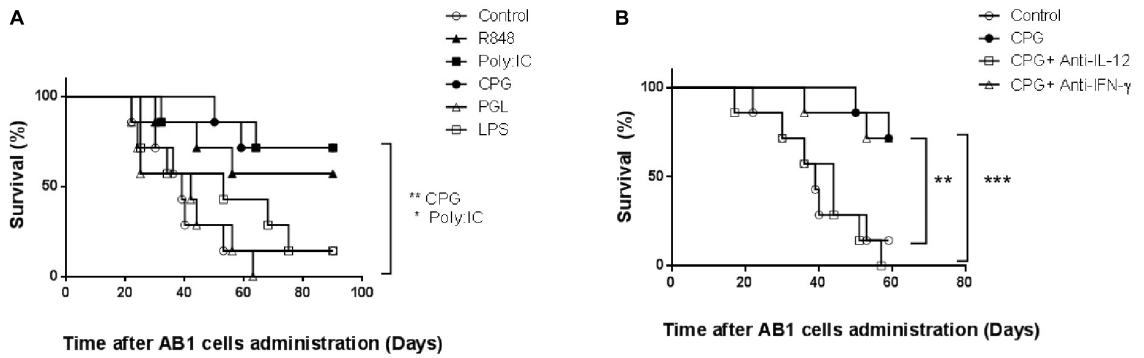

FIGURE 4
Effect of toll-like receptor (TLR)9 ligation and interleukin-12 (IL-12) secretion on protection against early mesothelioma growth. **(A)** Survival of groups of BALB/c mice (n = 8) either mock-treated (open circles) or treated with Poly (I:C) (closed squares), R848 (closed triangles), CpG-ODN (closed circles), lipopolysaccharide (LPS) (open squares) and peptidoglycan (open triangles) for two successive days before tumor administration. Groups were monitored daily after i.p. administration of mesothelioma AB1 cells. Experiment representative of three independent experiments. $^{**}P$ = 0.0096 (CpG vs. control), $^{*}P$ = 0.02 [Poly (I:C) vs. control], respectively, by Log-rank (Mantel–Cox) test. **(B)** Survival of groups of BALB/c mice (n = 7) either mocked treated (open circles) or treated for two successive days with CpG-ODN without (closed circles) or with anti-IFN-γ (open triangles) or anti-IL-12 (open squares) treatment, was monitored daily after i.p. administration of AB1 cells. Experiment representative of two independent experiments. $^{***}P$ = 0.0008 (CpG vs. CpG+anti-IL-12), $^{**}P$ = 0.0096 (CpG vs. control), and P = 0.023 (CpG+anti-IFN-γ vs. control), respectively by Log-rank (Mantel–Cox) test.

enhanced cancer immunosurveillance prior to the occurrence of any cancer cells, has not been deeply explored. We showed here that ligation of some TLRs, and especially of TLR9, may prevent the development of subsequently inoculated tumor cells in normal immunocompetent animals. CpG stimulation was shown to display preventive effect against plasmacytoma and mesothelioma development, which had not yet been reported. This observation suggests that TLR ligation may be one of the mechanisms by which infections enhance cancer immunosurveillance even before any occurrence of tumor cells. Interestingly, TLR9, in addition to viral DNA, recognizes hemozoin that is produced during infection by *Plasmodium* parasites (33) and these parasites trigger enhanced prevention of early plasmacytoma growth in mice (manuscript in preparation).

Cytotoxic lymphoid cells include NK cells, innate lymphocytes such as NKT cells and cytolytic T-cells (CTLs). While NK and NKT cells are fully innate, in the sense that they can recognize various targets without finely specific stimulation by a unique antigen, interestingly CTLs can also be stimulated non-specifically by cytokines (14) and therefore be part of a more general innate response. NK and NKT cells have been reported to play a major role in cancer immunosurveillance (12, 13) and have therapeutic activity in patients with multiple myeloma (34). They may also infiltrate mesothelioma and kill mesothelioma cells (35). Both NK cells, NKT cells and a subpopulation of CD8+ T-cells that share the capacity of early non-cognate response, including IFN-γ production express ASGM1 (36). Therefore, mice treatment with depleting anti-ASGM1 antibody provides information on the role of these cell populations. Their preventive role against early cancer development has been reported in mouse models of myeloma and mesothelioma after infection (9, 11) and was confirmed here after TLR9 ligation. It would be interesting to discriminate the respective role of these cell populations in future studies.

The mechanisms by which TLR ligation leads to innate cytotoxic cell activation remain to be determined. Expression of TLR mRNA in NK cells depends on their subset, state of activation and localization, both in mice and humans (37, 38). Although most TLRs have been found to be expressed on NK cells, expression of TLR1 seems at the highest levels, followed by TLR2, 3, 5, 6, while expression of TLR4 and 7 is very low (38). It has been reported that vaccinia virus infection directly activates NK cells through TLR2 signaling in the presence of accessory cytokines (39). However, NK cell activation after TLR ligation does not necessarily require TLR expression on NK cells, since it may be triggered indirectly by other cell populations that express these innate receptors (37). This might be the case for dendritic cells, able to secrete IL-12 after CpG stimulation (40). Similarly, anti-tumoral activity of NKT cells is enhanced after activation of TLR9, probably through a mechanism that involves dendritic cells (41). Moreover, activated NKT cells express TLR3, 5, 7, and 9 and can be directly stimulated by their ligands (42). TLR3, 7 and 9 are also expressed on CD8+ T-cells where their expression can be modulated by infection (43). An indirect effect on B-1 B cells that can promote tumor cell killing (44) cannot be excluded.

Although IL-12 alone had little effect on a multiple myeloma mouse model, it could enhance the efficiency of additional therapy (45). By using an antibody recognizing the complete heterodimeric cytokine, rather than a mere IL-12 p40 subunit, which is shared with IL-23 (23), our results strongly suggest the crucial role of this molecule in the enhancement of cancer immunosurveillance induced by ligation of TLR, and

especially of TLR9 prior to the occurrence of cancer cells. It is quite plausible that IL-12 is produced by dendritic cells or macrophages in response to CpG stimulation. However, so far, our attempts to determine the cellular origin of IL-12 after *in vivo* CpG-ODN stimulation have not been successful. As reported by many studies, IL-12 activates functions of innate cytotoxic cells, and especially their IFN-γ production. However, the latter cytokine may be dispensable in the involvement of these cells in cancer immunosurveillance.

In conclusion, our study indicates that TLR, and especially TLR9 ligation might be a mechanism by which infections can enhance a more efficient state of cancer immunosurveillance, even in the absence of tumor cells. This enhanced state of cancer immunosurveillance involves cytotoxic lymphoid cells that can include NK cells, NKT cells, and subpopulations of CD8+ T-cells, activated through innate mechanisms. It requires the production of IL-12, while IFN-γ, also necessary after some TLR stimulations, is dispensable in others. This capacity of some infections to enhance cancer immunosurveillance is balanced by the inverse effect of other infectious agents such as *Schistosoma* parasites that can inhibit cytokine production by NK cells and suppress the prevention of plasmacytoma early growth induced by CpG-ODN treatment (manuscript in preparation). Therefore, the final effect of infections on cancer immunosurveillance will depend on the susceptibility of cancer on the preexisting state of immunosurveillance, and on the type of infections, with their ability to modulate positively or negatively cytotoxic cell activity. These elements, combined with the well-known direct inducing effect of some infections on cancer development should be taken into consideration in epidemiological studies on cancer prevalence in developing versus industrialized countries.

Data availability statement

The raw data supporting the conclusions of this article will be made available by the authors, without undue reservation.

Ethics statement

The animal study was reviewed and approved by the Comité d'Ethique facultaire pour l'Expérimentation Animale–Secteur des Sciences de la Santé–Université catholique de Louvain (ref. 2014/UCL/MD/008 and 2018/UCL/MD/007).

Author contributions

MM: investigation, data analysis, and writing. PS and A-SC: investigation and writing. JV: conceptualization and writing; J-PC: conceptualization, data analysis, and writing. All authors contributed to the article and approved the submitted version.

Funding

This work was supported by the Fonds National de la Recherche Scientifique (FNRS) and the French Community (Concerted Actions), Belgium. J-PC was a research director with the FNRS.

Acknowledgments

We thank Eman Ahmed for useful help in data analyzing and editing and Pamela Cheou for preparation of antibodies.

Conflict of interest

The authors declare that the research was conducted in the absence of any commercial or financial relationships that could be construed as a potential conflict of interest.

Publisher's note

References

1. de Martel C, Ferlay J, Franceschi S, Vignat J, Bra F, Forman D, et al. Global burden of cancers attributable to infections in 2008: a review and synthetic analysis. *Lancet Oncol.* (2012) 13:607–15. doi: 10.1016/S1470-2045(12)70137-7

2. Oikonomopoulou K, Brinc D, Kyriacou K, Diamandis EP. Infection and cancer: revaluation of the hygiene hypothesis. *Clin Cancer Res.* (2013) 19:2834–41. doi: 10.1158/1078-0432.CCR-12-3661

3. Abel U, Becker N, Angerer R, Frentzel-Beyme R, Kaufmann M, Schlag P, et al. Common infections in the history of cancer patients and controls. *J Cancer Res Clin Oncol.* (1991) 117:339–44.

4. Albonico HU, Bräker HU, Hüsler J. Febrile infectious childhood diseases in the history of cancer patients and matched controls. *Med Hypotheses.* (1998) 51:315–20. doi: 10.1016/s0306-9877(98)90055-x

5. Kölmel KF, Gefeller O, Haferkamp B. Febrile infections and malignant melanoma: results of a case-control study. *Melanoma Res.* (1992) 2:207–11.

6. Kölmel KF, Pfahlberg A, Mastrangelo G, Niin M, Botev IN, Seebacher C, et al. Infections and melanoma risk: results of a multicentre EORTC case-control study. *Melanoma Res.* (1999) 9:511–9.

7. Krone B, Kölmel KF, Grange JM, Mastrangelo G, Henz BM, Botev IN, et al. Impact of vaccinations and infectious diseases on the risk of melanoma–evaluation of an EORTC case-control study. *Eur J Cancer.* (2003) 39:2372–8. doi: 10.1016/s0959-8049(03)00625-7

8. Becker N. Epidemiology of multiple myeloma. In: Moehler T, Goldschmidt H editors. *Multiple Myeloma. Recent Results in Cancer Research*. Vol. 183. Berlin: Springer (2011). p. 25–35.

9. Thirion G, Saxena A, Hulhoven X, Markine-Goriaynoff D, Van Snick J, Coutelier J-P. Modulation of the host microenvironment by a common non-oncolytic mouse virus leads to inhibition of plasmacytoma development through NK cell activation. *J Gen Virol.* (2014) 95:504–9. doi: 10.1099/vir.0.063990-0

10. De Beule N, Menu E, Bertrand MJM, Favreau M, De Bruyne E, Maes K, et al. Experimental African trypanosome infection suppresses the development of multiple myeloma in mice by inducing intrinsic apoptosis of malignant plasma cells. *Oncotarget.* (2017) 8:52016–25.

11. Mandour M, Soe PP, Uyttenhove C, Van Snick J, Marbaix E, Coutelier J-P. Lactate dehydrogenase-elevating virus enhances natural killer cell-mediated immunosurveillance of mouse mesothelioma development. *Infect Agents Cancer.* (2020) 15:30. doi: 10.1186/s13027-020-00288-6

12. Dunn GP, Koebel CM, Schreiber RD. Interferons, immunity and cancer immunoediting. *Nat Rev Immunol.* (2006) 6:836–48.

13. Iannello A, Thompson TW, Ardolino M, Marcus A, Raulet DH. Immunosurveillance and immunotherapy of tumors by innate immune cells. *Curr Opin Immunol.* (2016) 38:52–8.

14. Berg RE, Crossley E, Murray S, Forman J. Memory CD8+ T cells provide innate immune protection agains *Listeria monocytogenes* in the absence of cognate antigen. *J Exp Med.* (2003) 198:1583–93. doi: 10.1084/jem.20031051

15. Akira S, Takeda K. Toll-like receptor signalling. *Nat Rev Immunol.* (2004) 4:499–511.

16. Paget C, Mallevaey T, Speak AO, Torres D, Fontaine J, Sheehan KCF, et al. Activation of invariant NKT cells by Toll-like receptor 9-stimulated dendritic cells requires Type I interferons and charged glycosphingolipids. *Immunity.* (2007) 27:597–609. doi: 10.1016/j.immuni.2007.08.017

17. Cancro M, Potter M. The requirement of an adherent cell substratum for the growth of developing plasmacytoma cells in vivo. *J Exp Med.* (1976) 144:1554–67. doi: 10.1084/jem.144.6.1554

18. Davis MR, Manning L, Whitaker D, Garlepp MJ, Robinson BW. Establishment of a murine model of malignant mesothelioma. *Int J Cancer.* (1992) 52:881–6.

19. Markine-Goriaynoff D, Hulhoven X, Cambiaso CL, Monteyne P, Briet T, Gonzalez M-D, et al. Natural killer cell activation after infection with lactate dehydrogenase-elevating virus. *J Gen Virol.* (2002) 83:2709–16.

20. Billiau A, Heremans H, Vandekerckhove F, Dillen C. Anti-interferon-gamma antibody protects mice against the generalized Shwartzman reaction. *Eur J Immunol.* (1987) 17:1851–4. doi: 10.1002/eji.1830171228

21. Thirion G, Coutelier J-P. Production of protective gamma-interferon by natural killer cells during early mouse hepatitis virus infection. *J Gen Virol.* (2009) 90:442–7.

22. Jones LL, Chaturvedi V, Uyttenhove C, Van Snick J, Vignali DA. Distinct subunit pairing criteria within the heterodimeric IL-12 cytokine family. *Mol Immunol.* (2012) 51:234–44. doi: 10.1016/j.molimm.2012.03.025

23. Gaignage M, Uyttenhove C, Jones LL, Bourdeaux C, Chéou P, Mandour MF, et al. Novel antibodies that selectively block mouse IL-12 enable the re-evaluation of the role of IL-12 in immune protection and pathology. *Eur J Immunol.* (2021) 51:1482–93. doi: 10.1002/eji.202048936

24. Klinman DM, Yi AK, Beaucage SL, Conover J, Krieg AM. CpG motifs present in bacteria DNA rapidly induce lymphocytes to secrete interleukin 6, interleukin 12 and interferon gamma. *Proc Natl Acad Sci U S A.* (1996) 93:2879–83. doi: 10.1073/pnas.93.7.2879

25. Rook GAW. Review series on helminths, immune modulation and the hygiene hypothesis: the broader implication of the hygiene hypothesis. *Immunology.* (2009) 126:3–11. doi: 10.1111/j.1365-2567.2008.03007.x

26. Rook GAW. Hygiene hypothesis and autoimmune diseases. *Clin Rev Allergy Immunol.* (2012) 42:5–15.

27. Korneev KV. TLR-signaling and proinflammatory cytokines as drivers of tumorigenesis. *Cytokine.* (2017) 89:127–35. doi: 10.1016/j.cyto.2016.01.021

28. De Cesare M, Sfondrini L, Pennati M, De Marco C, Motta V, Tagliabue E, et al. CpG-oligodeoxynucleotides exert remarkable antitumor activity against diffuse malignant peritoneal mesothelioma orthotopic xenografts. *J Transl Med.* (2016) 14:25. doi: 10.1186/s12967-016-0781-4

29. Okada H, Takahashi K, Yaku H, Kobiyama K, Iwaisako K, Zhao X, et al. In situ vaccination using unique TLR9 ligand K3-SPG induces long-lasting systemic immune response and Synergizes with systemic and local immunotherapy. *Sci Rep.* (2022) 12:2132. doi: 10.1038/s41598-022-05702-0

30. Zhangchi D, Jian L, Yuzhang W. Toll-like receptor-9 agonists and combination therapies: strategies to modulate the tumour immune microenvironment for systemic anti-tumour immunity. *Br J Cancer.* (2022) 127:1584–94. doi: 10.1038/s41416-022-01876-6

31. Tang K, McLeod L, Livis T, West AC, Dawson R, Yu L, et al. Toll-like receptor 9 promotes initiation of gastric tumorigenesis by augmenting inflammation and cellular proliferation. *Cell Mol Gastroenterol Hepatol.* (2022) 14:567–86. doi: 10.1016/j.jcmgh.2022.06.002

32. Xu Y, Zhao Y, Huang H, Chen G, Wu X, Wang Y, et al. Expression and function of Toll-like receptors in multiple myeloma patients: toll-like receptor ligands promote multiple myeloma cell growth and survival via activation of nuclear factor κB. *Br J Haematol.* (2010) 150:543–53. doi: 10.1111/j.1365-2141.2010.08284.x

33. Coban C, Ishii KJ, Kawai T, Hemmi H, Sato S, Uematsu S, et al. Toll-like receptor 9 mediates innate immune activation by the malaria pigment hemozoin. *J Exp Med.* (2005) 201:19–25.

34. Rossi F, Fredericks N, Snowden A, Allegrezza MJ, Moreno-Nieves UY. Next generation natural killer cells for cancer immunotherapy. *Front Immunol.* (2022) 13:886429. doi: 10.3389/fimmu.2022.886429

35. Sottile R, Tannazi M, Johansson MH, Cristiani CM, Calabro L, Ventura V, et al. NK- and T-cell subsets in malignant mesothelioma patients: baseline pattern and changes in the context of anti-CTLA-4 therapy. *Intern J Cancer.* (2019) 145:2238–48. doi: 10.1002/ijc.32363

36. Kosaka A, Wakita D, Matsubara N, Togashi Y, Nishimura S-I, Kitamura K, et al. AsialoGM1+CD8+ central memory-type T cells in unimmunized mice as novel immunomodulatory of IFN-γ-dependent type 1 immunity. *Intern Immunol.* (2007) 19:249–56. doi: 10.1093/intimm/dxl140

37. Adib-Conquy M, Scott-Algara D, Cavaillon J-M, Souza-Fonseca-Guimaraes F. TLR-mediated activation of NK cells and their role in bacterial/viral immune responses in mammals. *Immunol Cell Biol.* (2014) 92:256–62. doi: 10.1038/icb.2013.99

38. Noh JY, Yoon SR, Kim T-D, Choi I, Jung H. Toll-like receptors in natural killer cells and their application for immunotherapy. *J Immunol Res.* (2020) 2020:2045860.

39. Martinez J, Huang XP, Yang YP. Direct TLR2 signaling is critical for NK cell activation and function in response to vaccinia viral infection. *PLoS Pathog.* (2010) 6:e1000811. doi: 10.1371/journal.ppat.1000811

40. Pompei L, Jang S, Zamlynny B, Ravikumar S, McBride A, Hickman SP, et al. Disparity in IL-12 release in dendritic cells and macrophages in response to Mycobacterium tuberculosis is due to use of distinct TLRs. *J Immunol.* (2007) 178:5192–9. doi: 10.4049/jimmunol.178.8.5192

41. Prasit KK, Ferrer-Font L, Burn OK, Anderson RJ, Compton BJ, Schmidt AJ, et al. Intratumoural administration of a NKT cell agonist with CpG promotes NKT cell infiltration associated with an enhanced antitumour response and abscopal effect. *OncoImmunology.* (2022) 11:2081009. doi: 10.1080/2162402X.2022.2081009

42. Villanueva AI, Mansour Haeryfar SM, Mallard BA, Kulkarni RR, Sharif S. Functions of invariant NK T cells are modulated by TLR ligands and IFNα. *Innate Immun.* (2015) 21:275–88. doi: 10.1177/1753425914527327

43. Hammond T, Lee S, Watson MW, Flexman JP, Cheng W, Fernandez S, et al. Toll-like receptor (TLR) expression on CD4+ and CD8+ T-cells in patients chronically infected with hepatitis C virus. *Cell Immunol.* (2010) 264:150–5. doi: 10.1016/j.cellimm.2010.06.001

44. Haro MA, Dyevoich AM, Phipps JP, Haas KM. Activation of B-1 cells promotes tumor cell killing in the peritoneal cavity. *Cancer Res.* (2019) 79:159–70. doi: 10.1158/0008-5472.CAN-18-0981

45. Wang X, Feng X, Wang J, Shao N, Ji C, Ma D, et al. Bortezomib and IL-12 produce synergetic anti-multiple myeloma effects with reduced toxicity to natural killer cells. *Anticancer Drugs.* (2014) 25:282–8. doi: 10.1097/CAD.0000000000000058

Frontiers in Medicine

Translating medical research and innovation into improved patient care

A multidisciplinary journal which advances our medical knowledge. It supports the translation of scientific advances into new therapies and diagnostic tools that will improve patient care.

Discover the latest Research Topics

See more →

Frontiers

Avenue du Tribunal-Fédéral 34
1005 Lausanne, Switzerland
frontiersin.org

Contact us

+41 (0)21 510 17 00
frontiersin.org/about/contact